

Karoline Kongsrud  
NTNU  
Norwegian University of  
Science and Technology  
Faculty of Natural Sciences  
Department of Biotechnology and Food Science

Karoline Kongsrud

# Mutational study of the bifunctional mannuronan C5- epimerase and alginate lyase *AlgE7 from *Azotobacter vinelandii**

May 2020





Norwegian University of  
Science and Technology

# Mutational study of the bifunctional mannuronan C5-epimerase and alginate lyase AlgE7 from *Azotobacter vinelandii*

**Karoline Kongsrud**

Biotechnology (5 years)

Submission date: May 2020

Supervisor: Finn. L Aachmann

Co-supervisor: Margrethe Gaardløs

Norwegian University of Science and Technology  
Department of Biotechnology and Food Science





# Acknowledgements

This master project was conducted at the Department of Biotechnology and Food Science at the Norwegian University of Science and Technology (NTNU) in Trondheim. The work presented was performed during the fall of 2019 and spring 2020, and some of the experiments were completed in collaboration with SINTEF – Department of Biotechnology and Nanomedicine. During the work of this project there was a worldwide outbreak of COVID-19. This led to some changes in the planned experimental work, and so deeper analysis has only been conducted for the AlgE7 wild type and one of the mutants.

First of all, I would like to thank my supervisors Finn L. Aachmann and Margrethe Gaardløs, for their positive encouragement, excellent guidance, feedback and assistance far beyond working hours. I also genuinely appreciate your time spent completing some of laboratory work during the spring of 2020. I must also express my gratitude to Margrethe Gaardløs for training me in experimental procedures and always taking time to assist me whenever I encountered difficulties in the laboratory.

I would also like to thank Randi Aune and Anne Tøndervik at SINTEF for conducting some of the experimental work presented in this project. A special thanks to all members of the biopolymer NMR research group for providing a good learning environment and for giving technical support in the laboratory. Finally, I would like to thank my family and friends for their encouragement, support and care throughout this process.



# Abstract

Alginates are a family of linear polysaccharides composed of 1 → 4 linked β-D-mannuronic acid (M) and α-L-guluronic acid (G) monomers. The two sugar molecules are C5-epimers, meaning that they only differ in the stereochemical configuration around carbon number five. The polysaccharide is found as a constituent of the cell walls of brown algae (*Phaeophyceas*) and is also synthesised by some red algae (*Rhodophyta*) and bacteria of the *Azotobacter* and *Pseudomonas* genera.

All natural alginate is initially synthesized as long chains of mannuronic acid (poly-M). Then, some of the M-residues are converted into G-residues by mannuronan C5-epimerases. These enzymes have their unique epimerization patterns, giving rise to different amounts and distributions of G-residues in the alginate chain. In addition, alginate acetylases and alginate lyases can modify the polymer by introducing acetyl groups in the alginate chain or alter the polymer length. The relative content and distribution of G-residues, acetyl-groups and the length of the polymer determine the physiochemical properties of the final alginate. These properties include thermostable hydrogel formation, water binding and biocompatibility, which make the biopolymer useful in a variety of industrial and biomedical fields.

A family of seven extracellular calcium-dependent mannuronan C5-epimerases (AlgE1-7) has been isolated from the bacterium *Azotobacter vinelandii*. Among the seven enzymes, AlgE7 has also been found to display lyase activity. Mannuronan C5-epimerases and alginate lyases have been proposed to have a similar reaction mechanism. The dual catalytic activity of AlgE7 is therefore thought to originate from the same active site in the enzyme. Mannuronan C5-epimerases and alginate lyases can be used to tailor alginate of specific properties *in vitro*. An understanding the action of these enzymes thus allows for more controlled design of alginate.

The present work aims to get a better understanding of the bifunctional activity of the *A. vinelandii* mannuronan C5-epimerase and alginate lyase AlgE7. A mutational study was performed by design of AlgE7 mutants, introducing point mutations in different residues near the active site. A total of 42 different mutants, covering mutations in 18 different residues, were included. 31 of the mutants were constructed in previous studies at NTNU and 11 of the

mutants were designed in this study using site-directed mutagenesis. A qualitative assessment of the lyase activity in all mutants was conducted, before 25 mutants and the wild type were selected for further analysis of the epimerase and lyase activity. Finally, one of the mutants (R148G) and the AlgE7 wild type were produced and purified using recombinant protein expression. These two enzymes were characterized in terms of reaction products and the mode of action using  $^1\text{H}$ -nuclear magnetic resonance (NMR) and time-resolved  $^{13}\text{C}$ -NMR.

The result of this work supported previous findings of the AlgE7 epimerase displaying both epimerase and lyase activity. Furthermore, the action on both poly-M and alternating poly-MG substrates was confirmed, whereas no lyase activity was detected on oligomers of continuous G-residues (oligo-G). The previously proposed cleavage sites G $\downarrow$ MM, G $\downarrow$ GM, M $\downarrow$ MM and M $\downarrow$ GM for AlgE7 when acting on poly-M were also seen in this study. However, a clear preference in front of a G- or a M-residue could not be determined.

Among all mutants included in the study mutant R148G stood out as different having a strongly reduced lyase activity compared to the wild type, while still displaying epimerase activity. Based on this result, residue R148 has been hypothesized to have a role in attracting the proton at the catalytic residue Y149, due to its alkaline character. By assuming that residue Y149 acts as the proton donor in the third step of the epimerization mechanism it has been proposed that residue R148 may disrupt the donation of the proton to mannuronan, and thus lead to occasionally cleavage of the alginate chain instead of epimerization. To further investigate this theory analysis of pKa values of the residues in the active site have been suggested. In addition, mutational studies of residue 148 in the other epimerases are suggested to give more insight to the role of this residue concerning lyase activity in AlgE7.

# Sammendrag

Alginater er en familie av lineære polysakkarider som består av 1 → 4 bundet β-D-mannuronsyre (M) og α-L-guluronsyre (G). De to suktermolekylene er C5-epimerer, noe som betyr at de har ulik stereokjemiske konfigurasjonen rundt karbon nummer fem. Polysakkaridet finnes som en komponent i celleveggen til brunalger (*Phaeophyceas*) og syntetiseres også av noen rødalger (*Rhodophyta*) og bakterier fra slekten *Azotobacter* og *Pseudomonas*.

I naturen blir alginat først syntetisert som lange kjeder av bare mannuronsyre (poly-M). Deretter blir noen av M-enhetene konvertert til G-enheter av mannuronan C5-epimeraser. Disse enzymene har unike epimeriseringsmønstre, noe som fører til ulike mengder og fordelinger av G-enhetene i alginatkjeden. I tillegg kan alginat acetylaser og alginat lyaser modifisere polymeren ved å henholdsvis feste på acetylgrupper i alginatkjeden og endre kjedelengden til polymeren. Forholdet mellom mengden og fordelingen av G-enheter og acetylgrupper, samt kjedelengden til polymeren, danner grunnlaget for de fysiokjemiske egenskapene til det ferdige alginatet. Disse egenskapene innebærer blant annet dannelse av termostabile hydrogeler, binding av vann og biokompatibilitet, hvilket gjør at biopolymeren er nyttig i en rekke industrielle og biomedisinske anvendelser.

En familie av syv ekstracellulære kalsiumavhengige mannuronan C5-epimeraser (AlgE1-7) har blitt isolert fra bakterien *Azotobacter vinelandii*. Blant disse syv enzymene har AlgE7 vist seg også å ha lyase aktivitet. En lignende reaksjonsmekanisme har tidligere blitt foreslått for mannuronan C5-epimeraser og alginat lyaser. De to katalytiske aktivitetene til AlgE7 er derfor antatt å stamme fra et felles aktivt sete i enzymet. Mannuronan C5-epimeraser og alginat lyaser kan brukes til å skreddersy alginat med spesifikke egenskaper *in vitro*. En forståelse av funksjonen til disse enzymene muliggjør derfor mer kontrollert design av alginat.

Formålet med dette arbeidet er få en bedre forståelse av den bifunksjonelle aktiviteten til mannuronan C5-epimerase og alginat lyase AlgE7 fra *A. vinelandii*. Et mutasjonsstudie ble utført ved design av AlgE7 mutanter. Dette ble gjennomført ved å introdusere punktmutasjoner i ulike aminosyrer nær det aktive sete. Totalt ble 42 forskjellige mutanter, som representerer mutasjoner av 18 forskjellige aminosyrer, inkludert i studiet. 31 av disse

mutantene har blitt konstruert i tidligere studier ved NTNU, mens 11 av mutantene ble designet i dette studiet ved bruk av sete-spesifikk mutagenese. En kvalitativ analyse av lyase aktiviteten til alle mutantene ble først gjennomført. Deretter ble 25 av mutantene og villtypen tatt med til videre analyse av både epimerase og lyase aktiviteten. Til slutt ble en av mutantene (R148G) og AlgE7 villtypen produsert og rensert ved bruk av rekombinant protein uttrykk. Disse to enzymene ble karakterisert i form av reaksjonsprodukter og ”mode of action” ved å bruke  $^1\text{H}$ -kjernemagnetisk resonans (NMR) og tidsoppløst  $^{13}\text{C}$ -NMR.

Resultatene fra dette arbeidet samsvarer med tidligere studier som viser at AlgE7 både har epimerase og lyase aktivitet. Videre ble også enzymenes ”mode of action” på både poly-M og alternerende poly-MG-substrat bekreftet. Imidlertid ble det ikke observert lyase aktivitet på substratet bestående av oligomerer av kontinuerlige G-enheter (oligo-G). Kuttasetene  $\text{G}\downarrow\text{MM}$ ,  $\text{G}\downarrow\text{GM}$ ,  $\text{M}\downarrow\text{MM}$  og  $\text{M}\downarrow\text{GM}$  for AlgE7 ved reaksjon på poly-M som har blitt foreslått i tidligere studier stemmer også overens med resultatene i dette studie. Derimot kunne ikke en preferanse for lyase aktivitet foran en G- eller en M-enhet bestemmes.

Av alle mutantene som ble undersøkt i dette studiet skilte mutant R148G seg ut fra de andre mutantene ettersom den viste en sterkt redusert lyase aktivitet, samtidig som den fortsatt viste epimerase aktivitet. Basert på dette resultatet har det blitt foreslått at aminosyren R148 påvirker lyase aktivitet ved å tiltrekke seg protonet som er festet til den katalytiske aminosyren Y149, på grunn av sin basiske karakter. Ved å videre anta at aminosyren Y149 er protondonoren i det tredje trinnet av epimeriseringsmekanismen, har det blitt foreslått at aminosyren R148 kan hindre at protonet blir donert til mannuronan og dermed føre til tidvis kløyving av alginatkjeden istedenfor epimerisering. For å undersøke denne teorien nærmere, har det blitt foreslått en videre analyse av pKa verdiene til aminosyrene i det aktive setet. I tillegg er det foreslått at mutasjonsstudier av aminosyre 148 i de andre epimerasene kan gi mer innsikt i hvordan denne aminosyren bidrar til lyase aktiviteten i AlgE7.

# Symbols and abbreviations

$\alpha$	alpha
$\beta$	beta
$\Delta$	4-deoxy-L-erythro-hex-4-enepyranosyluronate
$[\eta]$	Intrinsic viscosity
A <sub>20</sub>	Absorbance measured at 230 nm
AA	Amino acid
Amp	Ampicillin
bp	Base pair
DP <sub>n</sub>	Number average degree of polymerization
dNTP	Deoxynucleoside triphosphate
DDT	1,4-dithiothreitol
E	Young's modulus
EDTA	Ethylenediaminetetraacetic acid
F <sub>G</sub>	Molar fraction of G-residues
F <sub>M</sub>	Molar fraction of M-residues
FPLC	Fast protein liquid chromatography
G	$\alpha$ -L-guluronic acid
HEPES	4-(2-hydroxyethyl)-1-piperazineethanesulfonic acid
HPEAEC-PAD	High-performance anion exchange chromatography with pulsed amperometric detection
HSQC	Heteronuclear single quantum coherence
IMPACT	Intein mediated purification with an affinity chiting binding tag
IPTG	Isopropyl- $\beta$ -D-1-thiogalactopyranoside
ITC	Isothermal titration calorimetry
M	$\beta$ -D-mannuronic acid
MOPS	3-morpholinopropane-1-sulfonic acid
MS	Mass spectrometry
MQ	Milli-Q® water
MWCO	Molecular weight cut off
NMR	Nuclear magnetic resonance
OD <sub>600</sub>	Optimal density measured at 600 nm

LA	Lysogeny broth agar plates
LB	Lysogeny broth
PDB	Protein data bank
PCR	Polymerase chain reaction
pKa	negative log of the acid dissociation constant (Ka)
PL	Polysaccharide lyase
poly-M	Poly-mannuronic acid
poly-MG	Poly-alternating (MG) <sub>n</sub>
ppm	Parts per million
RO	Reverse osmosis
rpm	Revolutions per minute
SDM	Site-directed mutagenesis
SDS-PAGE	Sodium dodecyl sulphate – polyacryl amide gel electrophoresis
SEC-MALLS	Size exclusion chromatography – multi-angle laser light scattering
SLIC	Sequence- and ligation-independent cloning
SOC	Super optimal broth
TAE	Tris-acetate-EDTA
TSP	3-(trimethylsilyl)-propionic-1,1,3,3-d <sub>4</sub> acid
TTHA	Triethylenetetraamine-hexaacetate



# Contents

<b>Acknowledgements</b>	<b>i</b>
<b>Abstract</b>	<b>iii</b>
<b>Sammendrag</b>	<b>v</b>
<b>Symbols and abbreviations</b>	<b>vii</b>
<b>1 Introduction</b>	<b>1</b>
1.1 Alginates .....	1
1.1.1 Chemical composition and structure .....	1
1.1.2 Physical properties.....	3
1.1.3 Natural sources and biological function .....	7
1.1.4 Industrial and biomedical applications .....	8
1.2 Alginate-modifying enzymes .....	11
1.2.1 Biosynthesis of alginate.....	11
1.2.2 Mannuronan C5-epimerases .....	13
1.2.3 The AlgE epimerase family of <i>Azotobacter vinelandii</i> .....	13
1.2.4 Alginate lyases.....	22
1.3 The AlgE7 epimerase of <i>Azotobacter vinelandii</i> .....	23
1.4 Aim of the research project.....	25
<b>2 Material and Methods</b>	<b>27</b>
2.1 Materials.....	27
2.1.1 Instruments .....	27
2.1.2 Chemicals .....	28
2.1.3 Kits.....	29
2.1.4 Disposable equipment.....	29
2.1.5 Primers.....	30
2.1.6 Bacteria strains and plasmids.....	31
2.1.7 Alginate substrates.....	33
2.1.8 Media, buffers and solutions.....	33
2.1.9 Bioinformatics software and online tools .....	36

2.2	Methods.....	37
2.2.1	Site-directed mutagenesis (SDM) by Polymerase chain reaction (PCR) .....	38
2.2.2	Transformation of <i>E. coli</i> DH5- $\alpha$ .....	41
2.2.3	Cultivation of AlgE7 mutants .....	41
2.2.4	Plasmid isolation.....	42
2.2.5	Measuring plasmid concentration.....	42
2.2.6	Sequencing.....	43
2.2.7	Glycerol stock.....	43
2.2.8	Transformation of <i>E. coli</i> T7 express competent.....	44
2.2.9	Sequence- and ligation-independent cloning (SLIC) .....	44
2.2.10	Agarose gel electrophoresis.....	47
2.2.11	Recombinant protein expression in <i>E. coli</i> T7 express competent.....	47
2.2.12	Sonication .....	48
2.2.13	Fast protein liquid chromatography (FPLC) .....	49
2.2.14	Sodium dodecyl sulphate-polyacrylamide gel electrophoresis (SDS-PAGE)....	50
2.2.15	Dialysis .....	52
2.2.16	Freeze-drying.....	52
2.2.17	AlgE7 lyase-activity assay.....	53
2.2.18	Proton nuclear magnetic resonance ( $^1\text{H-NMR}$ ) spectroscopy .....	55
2.2.19	Time resolved $^{13}\text{C-NMR}$ spectroscopy.....	58
<b>3</b>	<b>Results</b>	<b>62</b>
3.1	Bioinformatics analysis.....	62
3.1.1	Structural study of AlgE7 .....	62
3.1.2	Multiple sequence alignment.....	65
3.1.3	Design of mutants .....	66
3.1.4	Protein parameters .....	73
3.2	Cloning.....	73
3.2.1	Cloning and expression of AlgE7 mutants .....	73
3.2.2	SLIC cloning.....	74
3.3	Protein production.....	75
3.3.1	Protein production of AlgE7 mutants carried on the pBG27 vector .....	75
3.3.2	Protein production and purification of AlgE7wt and R148G.....	77

3.4	Characterization .....	80
3.4.1	AlgE7 lyase-activity assay.....	80
3.4.2	Proton nuclear magnetic resonance ( <sup>1</sup> H-NMR) spectroscopy .....	84
3.4.3	Time-resolved <sup>13</sup> C-NMR spectroscopy .....	91
<b>4</b>	<b>Discussion</b> .....	<b>97</b>
4.1	Cloning and protein production .....	97
4.2	Qualitative analysis of AlgE7 mutants.....	100
4.3	Analysis of the AlgE7 wild type and mutant R148G.....	109
4.4	Further work.....	114
<b>5</b>	<b>Conclusion</b> .....	<b>115</b>
	<b>References</b> .....	<b>117</b>
	<b>Appendix A. AlgE7 gene and AA sequence</b> .....	<b>I</b>
	<b>Appendix B. Plasmid maps</b> .....	<b>III</b>
	<b>Appendix C. AlgE7-lyase assay</b> .....	<b>V</b>
	<b>Appendix D. Zero-order enzyme kinetics</b> .....	<b>X</b>
	<b>Appendix E. <sup>1</sup>H-NMR spectra</b> .....	<b>XI</b>
	<b>Appendix F. <sup>1</sup>H-NMR molar fractions</b> .....	<b>XVII</b>



# 1 Introduction

## 1.1 Alginates

Alginates is used as a collective term for a family of natural polysaccharides with a variety of present and potential future applications in industrial and biomedical fields (1). The polymer is primarily found as a structural component of the cell walls of brown algae (*Phaeophyceas*), but has also been identified in certain red algae (*Rhodophyta*) and bacteria belonging to the *Azotobacter* and *Pseudomonas* genera (2–6). The presence and composition of alginate varies among different sources, giving rise to polymers with unique chemical and physical properties (7). The use of alginate modifying enzymes thus creates an opportunity for biomaterial engineering, producing alginate polymers with tailored material properties (1).

### 1.1.1 Chemical composition and structure

Alginates are linear biopolymers composed of 1 → 4 linked β-D-mannuronic acid (M) and α-L-guluronic acid (G) monomer residues (Figure 1.1) (1,8–10). The M- and G-residues are C5-epimers, which means that they only differ in stereochemical configuration of the carboxyl (-COOH) group at carbon 5 (11). The monomers are organized in patterns composed of homopolymeric sequences of M- or G-residues (M-blocks and G-blocks), and heteropolymeric sequences of alternating M- and G-residues (MG-blocks) (7,12). This arrangement is accounted for by a family of enzymes called mannuronan C5-epimerases, which determines the length and distribution of the different block structures in the alginate polymer (13).

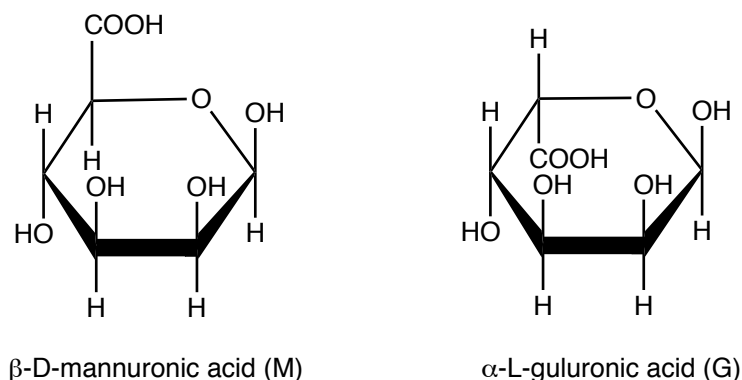


**Figure 1.1.** Molecular structure of the alginate monomers: β-D-mannuronic acid (M) and α-L-guluronic acid (G).

The different block structures give rise to different physiochemical properties of the polymer, due to the chair conformation of the two sugar monomers.  $\beta$ -D-mannuronic acid (M) and  $\alpha$ -L-guluronic acid (G) adopts a  ${}^4C_1$  and  ${}^1C_4$  conformation, respectively (Figure 1.2) (14–17). This gives significant geometric differences in the 1,4-glycosidic linkages between the monomers in the alginate chain. In M-blocks the linkages becomes diequatorial (MM), providing a ribbon-like structure where each M-residue is rotated about 180 degrees relative to the preceding monomer. In G-blocks the linkages are diaxial (GG), which gives a more rigid and buckled polymer structure. Diversely, MG-blocks have alternating equatorial-axial (MG) and axial-equatorial (GM) linkages, giving a more flexible structure compared to the homopolymeric regions. Intermolecular hydrogen bonds between alginate chains further facilitate to stabilize the chain structure (14,18).

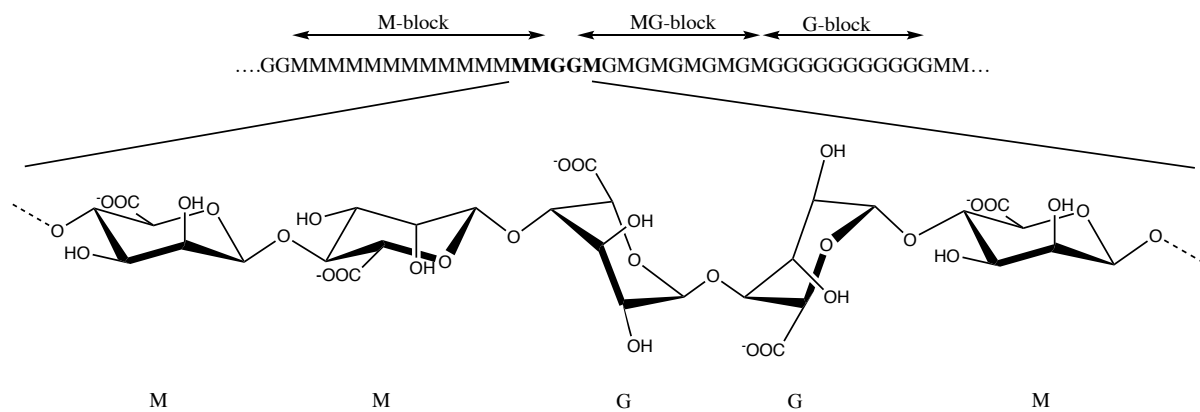


**Figure 1.2.** Alginate chain in chair conformation showing chain geometry and block structures.  ${}^4C_1$  conformation of  $\beta$ -D-mannuronic acid (M) and  ${}^1C_4$  conformation of  $\alpha$ -L-guluronic acid (G) linked by 1,4-glycosidic bonds, results in the different bond geometries: diequatorial (MM), equatorial-axial (MG), axial-equatorial (GM) and diaxial (GG).

Unlike many other polysaccharides, the sequential composition of the polymer is highly heterogenic and varies among different alginate sources, both in the relative content and distribution of the M- and G-monomers (19). Alginate is also polydisperse, which means that the polymer is composed of molecules with a wide range of molecular weight distributions (chain length distributions) (11,20). This feature is important for the physical properties of alginate and may be a result of partial degradation of the polymer during isolation and purification, biosynthesis or enzymatic modification after biosynthesis (11,21).

Different analytical techniques have been used to determine these parameters. Nuclear magnetic resonance (NMR) spectroscopy is currently the preferred method for characterizing alginate in terms of determining the frequencies of M and G monomers, as well as the dimer

(MM, MG/GM, GG) and trimer (MMM, MMG/GMM, MGM, GMG, GGM/MGG, GGG) distributions in the polymer (22–24). Other techniques such as size exclusion chromatography multi-angle laser light scattering (SEC-MALLS) and high-performance anion exchange chromatography with pulsed amperometric detection (HPAEC-PAD) permits measurements of the degree of polydispersity and block lengths in alginate samples (25,26).

## 1.1.2 Physical properties

### Ion binding and gel formation

One of the most important properties of alginate is the ability to form thermostable hydrogels (1). Efficient binding of divalent cations to alginate mediates hydrogel formation by cross-linking alginate polymers. Binding of divalent cations is highly selective with an increasing affinity in the order  $\text{Mg}^{2+} \ll \text{Mn}^{2+} < \text{Ca}^{2+} < \text{Sr}^{2+} < \text{Ba}^{2+} < \text{Cu}^{2+} < \text{Pb}^{2+}$  (27,28). The affinity for divalent cations has also been found to strongly depend on the alginate chain composition, with higher selectivity for increasing amount of G-residues in the polymer (29). This property is generally described in the so-called “egg-box” model (Figure 1.3) (29–31).

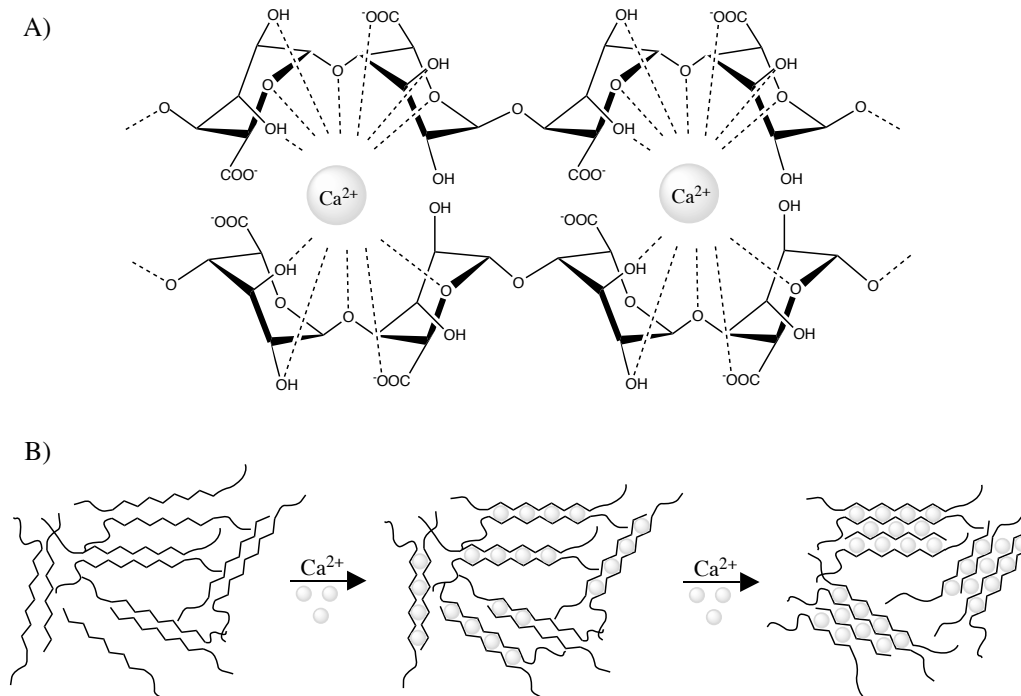


**Figure 1.3.** The “egg-box” model showing alginate gel formation. **A)** Chelation of divalent  $\text{Ca}^{2+}$  ions between sequential G-residues of two facing alginate chains, as a result of interaction with hydroxyl (-OH) and carboxyl (-COOH) groups in a cross-linking manner. **B)** Formation of inter-chain junction zones by addition of  $\text{Ca}^{2+}$  ions. The figure is reproduced from Donati and Paoletti (32).

According to the “egg-box” model, inter-chain interactions between divalent ions and G-blocks results in formation of junction zones between two alginate polymer chains (29–31). These junction zones are essential for holding the polysaccharides in a swollen network (29,30). The divalent cations are bound in cavities formed by diaxial linkages between sequential G-residues of two facing polymers (Figure 1.3.A and 1.4.A). This creates a chelate type of binding where the divalent cations interact with hydroxyl (-OH) and carboxylate (-COO<sup>-</sup>) groups of two adjacent G-residues and two G-residues in the opposing chain, which leads to cross-linking in a structure that resembles an “egg-box” (30,33–35). The formation of alginate junction zones is a cooperative mechanism, in that binding of the first ion is thermodynamically less favourable than binding of the successive ions (36,37). This process requires a certain length of G-blocks to form stable junction zones. In the case of divalent calcium ions (Ca<sup>2+</sup>) a minimum length of eight G-residues have been reported, but the minimum length of a G-block required decreases with increasing affinity for the ion (38–40).

MG-blocks can also bind calcium ions (Ca<sup>2+</sup>), eventually leading to gel formation of alginate polymers as mixed GG/MG junctions (Figure 1.4.B) and pure MG/MG junctions (Figure 1.4.C) (41). However, these gels are usually weaker, more elastic (higher Young’s modulus) and has a higher degree of syneresis than G-rich alginate gels (42). Gels prepared from G-rich alginate are generally stiffer and more brittle hydrogels, and are more resistant to rupture than M-rich alginate gels (42,43).



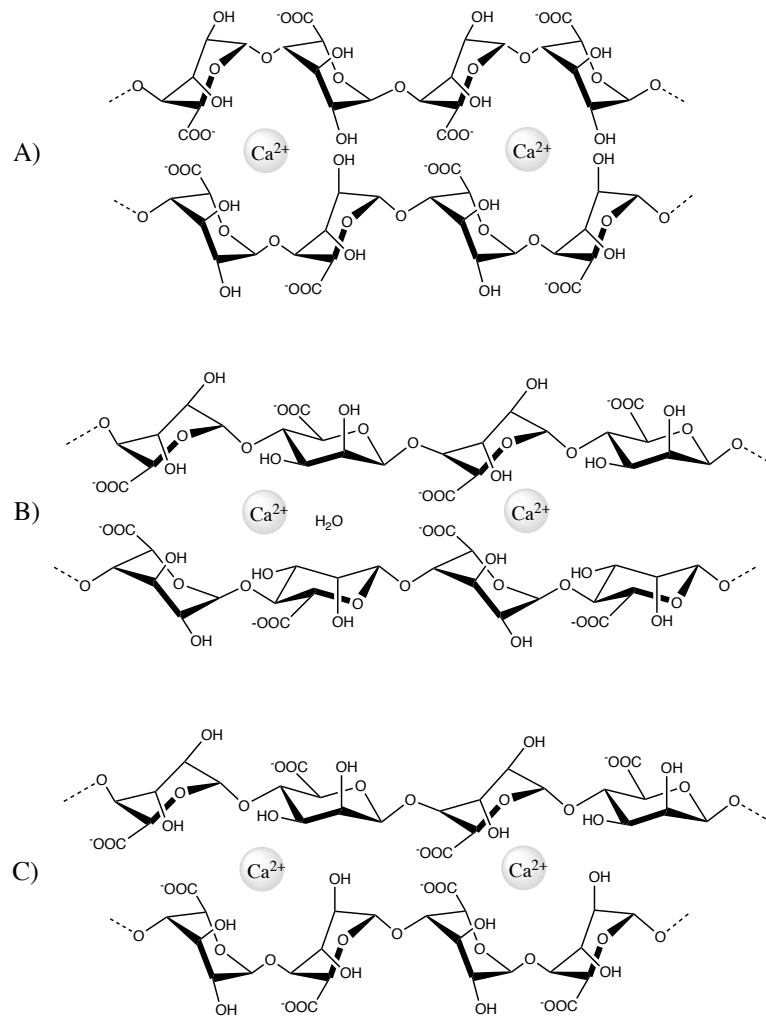


**Figure 1.4.** The three possible types of junction zones in alginate gels: **A)** GG/GG junctions, **B)** MG/MG junctions and **C)** MG/GG junctions. The figure is reproduced from Skjåk-Bræk et al. (36).

### Solubility

The solubility of alginate is highly dependent on the pH of the solvent. The measured  $\text{pK}_a$  values for  $\beta$ -D-mannuronic acid (M) and  $\alpha$ -L-guluronic acid (G) are 3.38 and 3.65, respectively (7). This means that alginate is an anionic polymer at physiological pH, in which the carboxyl groups of all monomers are fully deprotonated (11). Alginate is soluble at  $\text{pH} > 3.5$ , while an abrupt lowering in pH below the  $\text{pK}_a$  values results in precipitation of alginic acid (44). A slower and controlled decrease of pH will lead to formation of an alginic acid gel (45). Molecular weight and chain composition also affects solubility, where homopolymeric block structures (GG-blocks and MM-blocks) appear to be less soluble at acidic conditions compared to MG-blocks (44,46). The increased solubility for alginate rich in MG-blocks is likely due to conformational disorder of the glycosidic bonds (47).

Other factors limiting solubility of alginate are ionic strength and the content of the gelling ions present in the solution (20,21). When dissolving alginate salts in water, the positively charged counterions become hydrated and dissociate from the polymer (11). This gives a positive contribution to the entropy of mixing. By increasing ionic strength, the entropic gain will level off and eventually cause a salting-out effect – the solubility decreases with increasing ionic strength (32,48,49). If high salt concentrations are required, alginate should therefore be dissolved in pure water before addition of salt (50). Generally, alginate salts of monovalent cations are soluble, whereas most divalent metal ions tend to reduce solubility and to cause gel formation (32,51).

### **Stability**

The stability of alginate polymers depends on several parameters such as temperature, pH, presence of free radicals and microorganisms (32). The glycosidic linkage between the monomers are prone to cleavage in both acidic and alkaline conditions and to oxidation by free radicals (32,50). Alginate can also be degraded by alginate lyases isolated from species of alginate-producing bacteria and marine algae, and a variety of organisms that uses alginate as a carbon and energy source (e.g. marine algae and marine molluscs) (52,53). Alginate lyases catalyses the cleavage of the glycosidic linkages by a  $\beta$ -elimination reaction (see section 1.2.3) (52,54,55). This leads to degradation (depolymerisation) of the alginate polymer, causing a decrease in chain length (degree of polymerisation, DP), which in turn affects the physical properties of alginate (11). When analysing degraded alginate by NMR, the number average degree of polymerization (DP<sub>n</sub>) can be calculated. This is a measure of the average number of monomers per polymer chain (11).

### **Viscosity and chain extension**

The intrinsic viscosity  $[\eta]$  of a polymer can be explained as the ability of the polymer to cause viscosity in a solution (50). It is dependent on the length of the polymer chain, and thus on its molecular weight (56). Alginate solutions are usually highly viscous as a consequence of the extended shape of the polymer chain (57,58). In general, the relative extension (stiffness) of alginate chains rich in G-blocks is higher, due to less flexibility in the molecule caused by hindrance to rotate around the diaxial glycosidic linkages (15). The other block types have a lower degree of rotational hindrance around the glycosidic linkage, and so the chain extension of the different block types has been found to increase in the order MG<MM<GG (15).

In aqueous solution, alginate chains adapt a random coil shape as a result their inflexibility and inherent chain extension (11,57,58). However, the total expansion of the alginate polymer is also influenced by the ionic strength (11,32). Low ionic strengths cause intermolecular charge repulsion, leading to expansion of the polymer chain and hence increased hydrodynamic volume (59,60). Other factors affecting viscosity of alginate in solution are pH and the monomer sequence (15,57,58).

### 1.1.3 Natural sources and biological function

Alginate is primarily found in the cell wall of marine brown algae (*Phaeophyceas*), where it constitute up to 40 % of the dry weight (50,61,62). It is located in the intercellular matrix and algal cell wall where it forms an insoluble gel with  $\text{Na}^+$ ,  $\text{Mg}^{2+}$ ,  $\text{Ca}^{2+}$ ,  $\text{Sr}^{2+}$  and  $\text{Ba}^{2+}$  ions (27,32). This gel is considered to serve as a skeletal material, providing strength and flexibility to the algal tissue (61,63). The chemical composition and sequential structure of algae alginate varies with different species, tissues, ages of the algae, and seasonal and growth conditions (19,56,62). In general, the G/M ratio in different types of algal tissue appears to be adapted to the biological requirements of the specific parts of the algae plant (19,21,64). The amount of G-blocks is higher in rigid stipe and holdfasts than in flexible fronds (leaves), and the G-content has been found to increase with age of the algae (19,64). Alginate have also been identified as a calcium binding component in the cell wall of certain red algae (*Rhodophyta*) (3,4).

Bacterial alginate are synthesized as an extracellular polysaccharide by some species of the *Azotobacter* and *Pseudomonas* genera (5,65–67). In the soil bacterium *A. vinelandii*, alginate have been found to form a capsule around the cell while in vegetative state, as well as being an essential part of a protective G-block rich cyst coat during metabolic dormancy (68,69). The latter is a mechanism the bacterium uses to survive under adverse environmental conditions such as drought and lack of nutrients (68). Unlike algal alginate and alginate from species of *Azotobacter*, alginate produced by species of the *Pseudomonas* genera do not contain G-blocks (70). They were first isolated from the opportunistic human pathogen *Pseudomonas aeruginosa*, which causes respiratory infections in patients suffering from cystic fibrosis (6,71,72). The secreted alginate forms a biofilm that mediates bacterial adhesion and colonization of the lung epithelium (73). It also protects against phagocytosis by the host immune system and increases resistance to antibiotics (74,75).

In contrast to algal alginate, some bacterial alginates are partially acetylated in the O2 and/or O3 position on M-residues (70). Presence of these O-acetyl groups changes the physical properties of the polysaccharide, giving enhanced solubility, water-binding capacity, viscosity and chain expansion (1,76). O-acetylation has been found to inhibit the action of mannuronan C5-epimerases, which affects the amount and distribution of G-residues in bacterial alginate (77,78). O-acetylation can also make the polymer inaccessible for enzymatic degradation by alginate lyases, and are therefore thought to be involved in control of chain length (52,76,79).

### **1.1.4 Industrial and biomedical applications**

Alginate was first discovered as alginic acid in 1881 by the English chemist Edward C. C. Stanford, and have since been used in a wide range of industrial and biomedical fields (1,2,80). Most applications of alginate are based on its unique physiochemical properties, e.g. the solution, viscosity, water-binding and gelling properties (32). These properties vary among different alginates due to their natural variability in chemical structure and molecular weight, and hence determine their use in a diversity of applications (1,32). In addition, alginate has been shown to be biodegradable and biocompatible, i.e. the biopolymer does not create immunogenic responses in the biological system of the host organism (1,20,81). This makes alginate particularly suitable in medical and biotechnological industries (1,81).

In the present day, commercially available alginate is extracted from brown algae and has a world annual production of about 38,000 tonnes (82). Applications of algae alginate includes use within foods, cosmetics, pharmaceutical and biomedical products (1,21,32). Alginate is also utilized as a thickener in textile printing, surface treatment of paper, welding rods and as a water-binding agent in the production of ceramics (1,83–86).

Within the food industry, alginate is frequently used as additives. Currently, alginic acid (E400), sodium- potassium-, ammonium- and calcium alginate (E401-E404) as well as propylene glycol alginate (E405) are approved as food additives in Europe (87,88). Alginate is also used as a thickener and stabilizer in beverages, sauces and ice cream, and as a gel forming agent in jams, jellies and restructured food products such as onion rings, pimento olive fillings and pet foods (50,83). In addition, the gel forming properties of alginate are exploited in alginate encapsulation and immobilization technologies within food processing

(89). A typical example is immobilization of various types of lactic acid bacteria to produce starter cultures for the dairy industry (89,90).

Other important utilizations of alginate are in pharmaceutical products such as in formulations for treatment of heartburn and acid reflux (91). An alginate solution containing sodium bicarbonate creates an acid gel foam that serves as a protective barrier to prevent regurgitation of gastric reflux into the oesophagus (91,92). Alginate is also used to prepare materials for wound dressings such as hydrogels, biofilms and foams, in which the alginate-based material absorbs exudate and facilitate a physiological moist environment for wound healing (93).

Over the last 50 years, bacterial alginate has been shown to have a great potential in biomedical applications where high level of compositional homogeneity and more defined physical properties are important (86,94). Studies of alginate biosynthesis in bacteria and the associated alginate-modifying enzymes (e.g. epimerases and lyases), has opened the possibility of producing alginate with tailor-made properties for use in advanced biomedical applications such as drug delivery systems and tissue engineering (86,95).

Methods for drug delivery and tissue engineering are often based on immobilization and encapsulation of living cells, proteins or other chemical agents in an alginate gel (96–99). This is especially promising for use in cell transplantation, enabling *in vivo* production of therapeutically active biomolecules deficient in the body (98,100,101). The purpose of cell encapsulation is to protect the transplanted cells from the host immune system by preventing passage of immune cells, antibodies and cytokines into the alginate microcapsule, while allowing diffusion of nutrients, oxygen and biomolecules over the semipermeable capsule membrane (98). Alginate cell encapsulation also requires accurate surface coating, as alginate gels have been shown to be too porous for immunoprotection (102,103). The most studied system using alginate microcapsules is encapsulation of human insulin producing islets of Langerhans for treatment of diabetes 1, and so far clinical trials have evaluated the procedure as safe (104,105). However, there are limitations in regards to long-term efficacy and graft function as a consequence of fibrosis on the capsules, which affects the access of oxygen and nutrients into the encapsulated islets (105).

In recent years, there has been a growing interest in alginate oligomers and their potential use as active pharmaceutical drugs (106,107). The term “alginate oligomers” is here considered as molecules with molecular weights in the range 2000-5000 g/mol, whereas commercially available alginate usually have molecular weights of 30,000 to 4000,000 g/mol (106).

Alginate oligomers retain most of the physiochemical properties of high molecular weight alginates, but lose the ability to form gels with divalent cations (106,108). This allows use of high alginate concentrations without a significant increase in viscosity. The oligomers are also easy to tailor to a precisely defined chemical composition, as opposed to longer alginate chains that typically are polydisperse and may have a mixture of molecular weights (106).

Studies have shown several biological effects of alginate oligomers, e.g. control of multidrug-resistant bacterial and fungal infections, anti-inflammatory and immunosuppressive agents, inhibition of biofilm formation and disruption of already established multidrug-resistant biofilms (106,107,109–111). These properties are valuable for many medical applications, and one of the most researched utilization is in treatment of chronic lung diseases such as cystic fibrosis (CF) (106). Clinical trials have demonstrated that G-block oligomers are able to reduce the viscosity in CF-mucus by competing with packed mucins for binding of calcium (112,113). It is also shown to potentiate the efficacy of some antibiotics against multidrug-resistant pathogens up to a 512-fold (109,114). Currently, the AlgiPharma drug candidate OligoG CF-5/20 for treatment of CF has completed phase 2b clinical trials (Identifier NCT02157922; NCT02453789) and is so far considered to be safe (106,115).

Future research is now also investigating the potential use of alginate oligomers in treatment of HIV and hepatitis B virus (116). The new marine polysaccharide drug 911 derived from alginate is going through clinical investigations as a new candidate for preventing HIV-virus attachment and action of the viral reverse transcriptase (117,118). The drug has also been reported to have an inhibitory effect on the DNA polymerase of hepatitis B virus, adding a second potential use of 911 (119,120).

## 1.2 Alginate-modifying enzymes

Alginate is initially synthesized as a homopolymer of mannuronic acid (poly-M) by polymerization of GDP-mannuronic acid. Poly-M is then modified at the polymer level by different alginate-modifying enzymes: alginate acetylases, alginate deacetylases, C5-epimerases and alginate lyases (79). This results in alginate polymers with different structural and functional properties (79). The action of mannuronan C5-epimerases and alginate lyases are further discussed in section 1.2.2-1.2.4.

### 1.2.1 Biosynthesis of alginate

Biosynthesis of alginate was first studied in the brown algae *Fucus garneri*, but most of the present knowledge about the alginate biosynthetic pathway and its regulatory mechanisms comes from studies of the bacteria *P. aeruginosa* and *A. vinelandii* (1,121,122). In general, these bacteria species share a similar pathway. This is because they have a similar biosynthesis gene cluster that encodes several enzymes organized in a multiprotein complex, as well as other regulatory proteins (94,123,124). The multiprotein complex facilitates efficient coupling of the enzymatic reactions during alginate biosynthesis (124,125). However, some differences in regulation and epimerisation have been reported for different bacteria species (94,122). The biosynthetic pathway for *A. vinelandii* is described in the two following paragraphs.

Alginate can be synthesized from various carbon sources that are assimilated through different pathways, entering the alginate biosynthesis as fructose-6-phosphate (Figure 1.5) (126–128). The biosynthetic pathway starts with synthesis of the alginate precursor molecule GDP-mannuronic acid (128). This requires conversion of fructose-6-phosphate through a four-step pathway, which is catalysed by three cytosolic enzymes (AlgA, AlgC and AlgD) (129–133). GDP-mannuronic acid molecules are then polymerized into long chains of M-residues (poly-M) by an enzyme complex (Alg8-Alg44) anchored in the cytoplasmic membrane (127,134,135).

In the periplasmic space, poly-M is subjected to modification at the polymer level by the multiprotein complex (79,124). Several of the proteins (AlgI, AlgV, AlgF, AlgX) are involved in O-acetylation of bacterial alginate (124,136–139). As described in section 1.1.3,

acetylated M-residues cannot be enzymatically modified by mannuronan C5-epimerases (77). Nevertheless, a mannuronan C5-epimerase found in *Pseudomonas syringae* have shown to display deacetylase activity and is able to remove acetyl groups from acetylated alginate prior to epimerizing the polymer (140). In the periplasm is also a calcium-independent mannuronan C5-epimerase (AlgG) that can epimerize single non-acetylated M-residues into G-residues (123,124). Alginate lyases (AlgL, AlyA1, AlyA2) facilitate  $\beta$ -elimination cleavage of glycosidic bonds – AlgL cleaves M-M and M-G bonds, while AlyA1 and AlyA2 cleave M-G and G-M bonds (133,141,142). Alginate lyases found in the periplasmic space are important for controlling the molecular weight of alginate chains produced and the degradation of polymer chains that failed to be exported out of the cell (26). The alginate chain is secreted out of the cell through a membrane bound porin protein (AlgJ), and can further be modified by seven secreted calcium-dependent mannuronan C5-epimerases (AlgE1-7) depending on the needs of the bacteria (124,143–146). The polymer can also be altered by an extracellular alginate lyase (AlyA3), which is able to cleave G-M, M-G, M-M and G-G bonds, but at different rates (142).

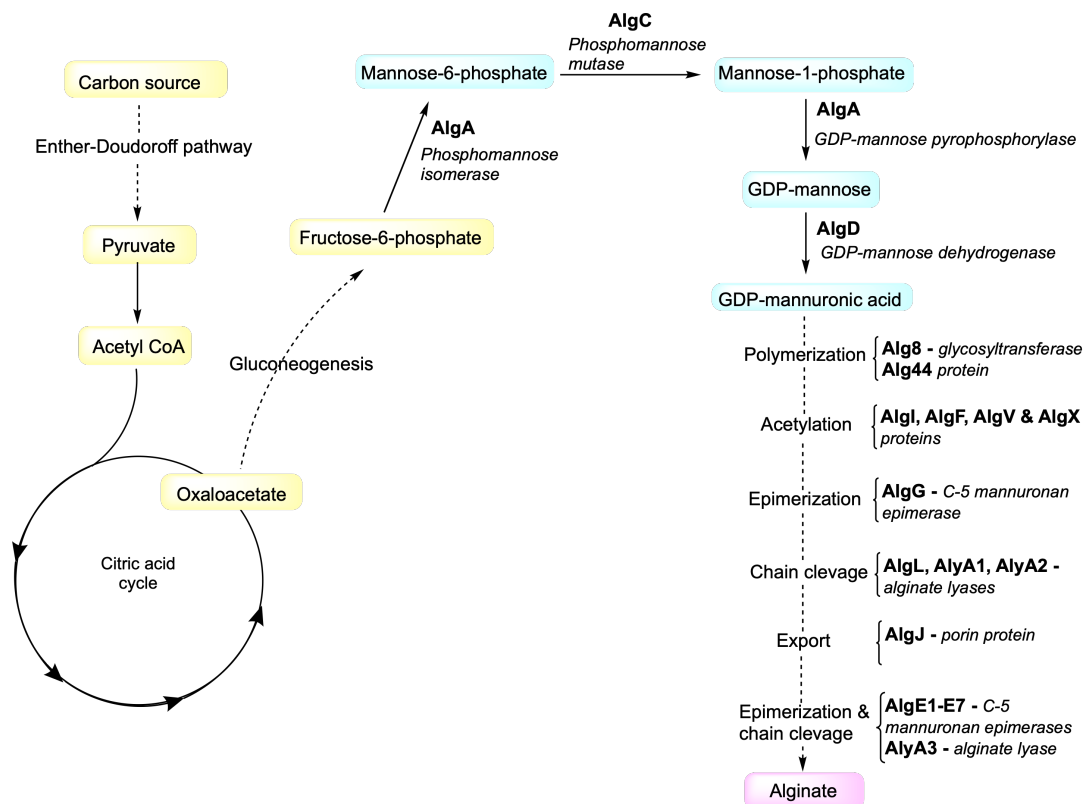


**Figure 1.5.** Biosynthesis of alginate in the bacterium *Azotobacter vinelandii*. Carbon sources are assimilated through different pathways (intermediate products shown in yellow), before entering the pathway of alginate biosynthesis (intermediate products shown in blue). Different alginate-modifying enzymes are then acting on the polymer, generating a specific sequential composition in the final polymer (purple). The figure is based on a similar figure for *Pseudomonas* presented in Hay et al. (94), but shows the enzymes and proteins identified in *A. vinelandii*.



## 1.2.2 Mannuronan C5-epimerases

Mannuronan C5-epimerases are enzymes that catalyse the inversion of the stereochemical configuration at carbon number 5 of some the  $\beta$ -D-mannuronic acid (M) residues in poly-M alginate, converting them into  $\alpha$ -L-guluronic acid (G) (11,147). Mannuronan C5-epimerase was first discovered in *A. vinelandii* in 1969, as the first enzyme reported to have epimerase activity on polymer level (148). Mannuronan C5-epimerase activity has later been observed in several species of brown algae and bacteria belonging to the *Pseudomonas* genera (149–155). In *A. vinelandii*, these epimerases are thought to have a crucial role in synthesizing alginate with a variety of physical properties, required at different life stages and under varying environmental conditions such as cyst formation (144,145,156,157). These enzymes may also be used for *in vitro* epimerization of poly-M, which makes it possible to design alginate with tailored properties for use in a variety of biotechnological and medical applications (13,158).

Two types of mannuronan C5-epimerases have been identified in alginate-producing organisms: calcium-independent (AlgG-type) and calcium-dependent (AlgE-type, see section 2.2.3) (79). All alginate-producing bacteria have shown to encode a periplasmic and calcium-independent mannuronan C5-epimerase (AlgG) that introduces single G-residues in stretches of mannuronan (79,124). Previous studies on *P. fluorescens* have reported that the AlgG protein, but not its epimerase activity, is required for alginate biosynthesis (159). It was further suggested that the presence of AlgG epimerase as a part of the multiprotein complex has a role in protecting newly synthesized alginate polymers from degradation by periplasmic alginate lyases (159,160). AlgG-mutants lacking epimerization activity have shown to produce pure poly-M alginate, which is commonly used as substrate for *in vitro* epimerization studies on alginate (159,161,162). Algal epimerases encode mannuronan C5-epimerases structural related to the AlgG-epimerase found in bacteria. However, these enzymes are difficult to extract and have therefore been less studied (152).

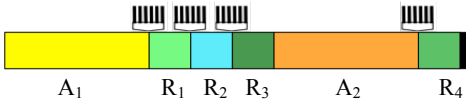
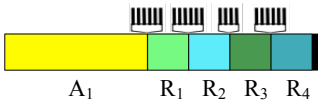
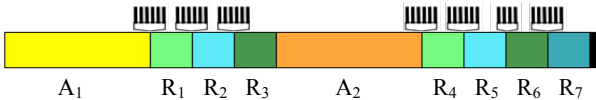
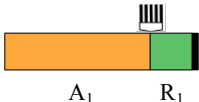
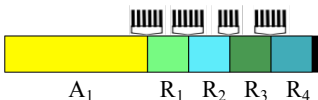
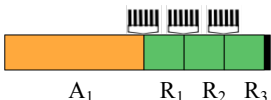
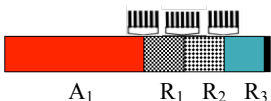
## 1.2.3 The AlgE epimerase family of *Azotobacter vinelandii*

A family of seven extracellular calcium-dependent mannuronan C5-epimerases (AlgE1-7) have been identified in *A. vinelandii* (162). These enzymes have all been cloned and expressed in *Escherichia coli* (144,145,156). *A. vinelandii* also encodes a protein (AlgY) homologous to the AlgE epimerases, which has no epimerase activity or other known function (156).

## Modular structure of AlgE epimerases

The AlgE epimerases are modular enzymes (Table 1.1) consisting of one or two catalytically active A-modules (385 amino acids) and one to seven R-modules (155 amino acids) (145). The sequence homology of each module type is between 50-100 % (145,156). Studies have demonstrated that the A-modules are catalytically active without the associated R-modules, showing that this module carries the active site (162,163). However, the enzyme activity is significantly increased in presence of at least one R-module (163). R-modules contain four to seven repeats of calcium-binding motifs, in which binding of  $\text{Ca}^{2+}$  ions is important for their structural stability (163–165). Calcium-binding sites have also been identified in A-modules and are thought to be involved in structural stability, substrate interaction by neutralization of charge and/or gel formation after epimerization (166,167).

**Table 1.1.** The modular structure of the AlgE mannuronan C5-epimerases from *A. vinelandii* and their epimerization pattern (which is dependent on the A-modules). The AlgE epimerases consists of one or two catalytically active A-modules and one to seven R-modules. Same colour illustrates the sequence homology between individual modules. The calcium-binding motifs are shown as vertical lines above the modules. Illustrations of the modular structures are reproduced from Ertesvåg et al. (13)

Enzyme	Modular structure	Epimerization pattern
AlgE1		A <sub>1</sub> : G-blocks (long) A <sub>2</sub> : MG-blocks
AlgE2		A <sub>1</sub> : G-blocks (short)
AlgE3		A <sub>1</sub> : G-blocks (short) A <sub>2</sub> : MG-blocks
AlgE4		A <sub>1</sub> : MG-blocks
AlgE5		A <sub>1</sub> : G-blocks (short)
AlgE6		A <sub>1</sub> : G-blocks (long)
AlgE7*		A <sub>1</sub> : Single G-residues and G-blocks

\* Lyase activity with preference for G-GM and G-MM bonds (168)

### Molecular structure of AlgE epimerases

The three-dimensional structure of a full-length AlgE epimerase has not been determined, but the structure of the AlgE4 modules has been elucidated (Figure 1.6). The crystal structure of the A-module from AlgE4 was determined by X-ray crystallography at 2.1 Å resolution, while the structure of the R-module was solved by NMR spectroscopy (164,166). No secondary structure of the proline-rich linker region connecting the two modules is solved, but studies of the overall structure of AlgE4 have suggested that it is unstructured and flexible (164,169).

The AlgE4 A-module shows a single-stranded, right-handed parallel  $\beta$ -helix fold, consisting of 12 complete turns (20-40 amino acids) organized in 4  $\beta$ -sheets (PB1 PB2a, PB2b, PB3), with an amphipathic  $\alpha$ -helix that caps the N-terminal end (Figure 1.6 A) (166). Protruding from the  $\beta$ -helix fold are three flexible turns (T1-3, consisting of 1-9 amino acids) connecting the  $\beta$ -strands in adjacent  $\beta$ -sheets. The active site of AlgE4 is situated in a positively charged cleft between the T1 and T3 loops at the centre of the A-module. The bottom of this cleft is made up by PB1, forming an extended binding groove where the alginate substrate can bind (166). The crystal structure of the AlgE6 A-module has later been elucidated at 1.19 Å resolution, revealing an almost identical structure (Protein data bank code 5LW3).

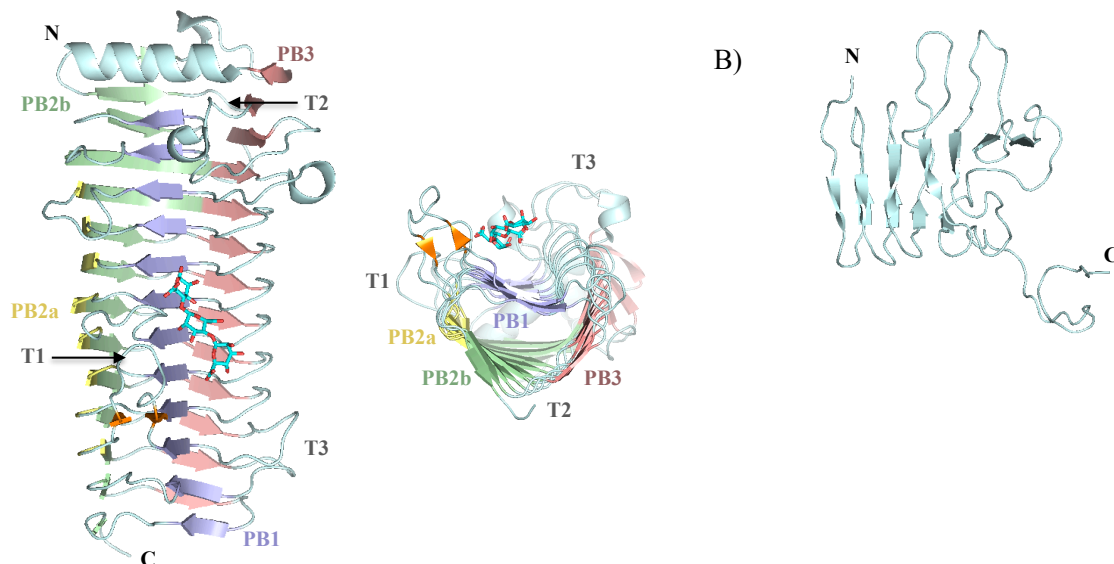


**Figure 1.6.** Structure of AlgE4. **A)**  $\beta$ -helix structure of the AlgE4 A-module, organized in 4  $\beta$ -sheets (PB1 PB2a, PB2b, PB3), with an  $\alpha$ -helix (grey) that caps the N-terminal end. The three flexible turns (T1-T3) connect the  $\beta$ -strands in adjacent  $\beta$ -sheets. PB1 (purple) shows the substrate-binding groove, with a mannuronan trisaccharide (cyan stick model) bound at the active site cleft. **B)**  $\beta$ -roll structure of the AlgE4 R-module with an unstructured C-terminal end (residues 145-167). The figure is based on the structures presented in Rozeboom et al. **(A)** and Aachmann et al. **(B)** (164,166).

Similar to the A-module, the N-terminal end of the AlgE4 R-module folds into a right-handed parallel  $\beta$ -roll (Figure 1.6 B) (164). The C-terminal end consists of an unstructured stretch of 22 amino acids (residues 145-167). This region is present at the end of the last R-module in all AlgE epimerases, and is thought to function as a secretion signal for transporting the enzyme to the out of the cell (144,145,164). Overall, the R-module has an elongated shape with a small groove on one side (164). This groove has a positively charged patch that has been shown to interact with a negatively charged M-pentamer and poly-M substrate, and to a less extent with poly-MG alginate (164,165). However, affinity studies of the three AlgE6 R-modules detected no interaction with poly-M, poly-MG or poly-G substrates when examined independently of the A-module (165). This suggests that R-modules have a role in modulating the enzyme activity by facilitating binding and positioning of the substrate (164,165).

An alignment of the amino acid sequence of A-modules of all known mannuronan C5-epimerases from algae and bacteria shows that they share a Y(G/A)(F/I)DPH(D/E) motif (residues 149-155 in AlgE4) located in subsite +1 (152,166,168,170). According to the nomenclature of sugar-binding enzymes, the catalytic site is situated within this subsite (171). The catalytic residues have been identified as the four essential amino acids Y149, D152, H154 and D178, where residue D178 seems to be conserved in AlgE epimerases only (Figure 1.7) (166). The residue D152 has been shown to be important for both the epimerase and the lyase activity in AlgE7 (168). However, the role of each catalytic residue in the reaction mechanism (described in later paragraphs) is not fully established. Nevertheless, studies have suggested that Y149 act as the catalytic base (AA2) and H154 as the catalytic acid (AA3) (166).

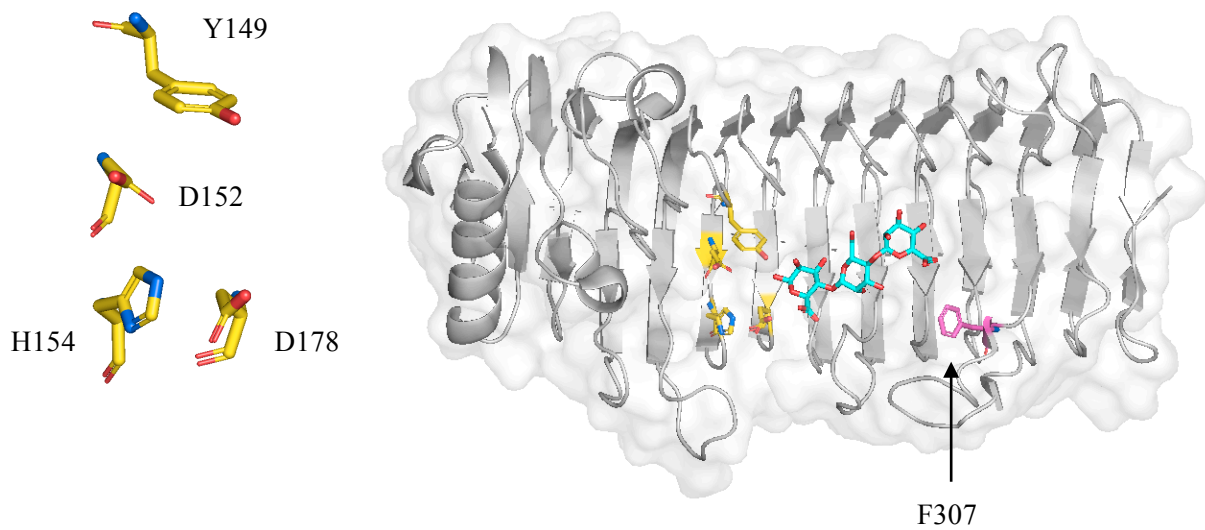


**Figure 1.7.** The catalytic residues (yellow) of the AlgE4 active site have been identified as Y149A, D152, H154 and D178, and are conserved among all seven AlgE epimerases. A bound mannuronan trisaccharide is shown in stick representation (cyan). Residue number 307 (pink) is also shown as it has been shown to be important for determining the epimerization pattern of AlgE epimerases (172). The structure is adapted from Rozeboom et al. and visualized in PyMOL (166,173).

Another interesting discovery is the significance of residue number 307 of either tyrosine (Y) or phenylalanine (F), located in a long loop in the A-module (Figure 1.7). In epimerases producing G-blocks this residue is a Y, while in epimerases creating MG-blocks it is a F (158). Recently, this residue has been demonstrated to be essential for defining the epimerisation pattern of AlgE epimerases, possibly by modulating binding of the substrate (172).

### Epimerization patterns

The seven AlgE epimerases of *A. vinelandii* all have their unique catalytic properties, resulting in different amounts and distributions of G-residues in the alginate produced (145). This gives specific non-random epimerization patterns, which are determined by the A-modules (Table 1.1) (163). The AlgE A-modules can be divided into two main groups based on their sequence homology, shown by similar colours in Table 1.1 (162). AlgE2 and AlgE5 belong to the first homology group, both creating short G-blocks (145,174). In the second homology group are AlgE4 and AlgE6. However, they generate different block structures – AlgE4 creates MG-blocks, while AlgE6 creates long G-blocks (13,146,175). Studies using hybrid A-modules indicates that only certain parts of the A-module is essential for the epimerization pattern (residue 307 is of particular importance, as described in the previous

paragraph) (172). AlgE1 and AlgE3 are composite enzymes meaning they both contain two A-modules, one of each homology group (13,162). AlgE1 and AlgE3 creates G-blocks and presumably some MG-blocks between them (13), but when the two A-modules are expressed separately, the A<sub>1</sub>-modules create G-blocks and the A<sub>2</sub>-modules create MG-blocks (163,176). AlgE7 has been identified as a bifunctional lyase/epimerase, generating short G-block oligomers (168). The lyase activity is thought to originate from the same active site as the epimerase activity, occasionally cleaving the alginate polymer instead of epimerizing it (55,168). Studies conducted with AlgE2 and AlgE5 have also shown weak lyase activity (1-3 chain breaks per 1000 epimerised M-residues), but this is probably caused by failed epimerase reaction due to gelling of alginate during G-block formation (162,174).

### **Reaction mechanism**

A unified three-step reaction mechanism has been proposed for mannuronan C5-epimerases and alginate lyases. (Figure 1.8) (55). In the first step, a positively charged amino acid (AA1) neutralizes the negatively charged carboxylate group (-COO<sup>-</sup>) of the M-residue. In the second step, a different amino acid residue (AA2) acts as a catalytic base and abstracts the proton at C5, forming an enolate anion that is stabilized by resonance. The final step has three possible outcomes, depending where the proton is donated. In the epimerase reaction, a catalytic acid (AA3) protonate the C5-carbanion from the opposite side of the sugar ring. This results in an inversion of the stereochemistry of the residue. In the lyase reaction, the proton is donated to the oxygen at C1 in the leaving group. This leads to a β-elimination of the 4-O-glycosidic bond, creating a double bond between C4 and C5 at the non-reducing end. This gives an unsaturated uronic acid residue (4-deoxy-L-erythro-hex-4-enepyranosyluronate, Δ) (55).

Studies have shown that the second step of the reaction can be reversible (175). This yields a third possible outcome, where re-protonation of the C5-carbanion by the catalytic base (AA2) or solvent from the same side it was abstracted results in the initial M-residue (55,175).

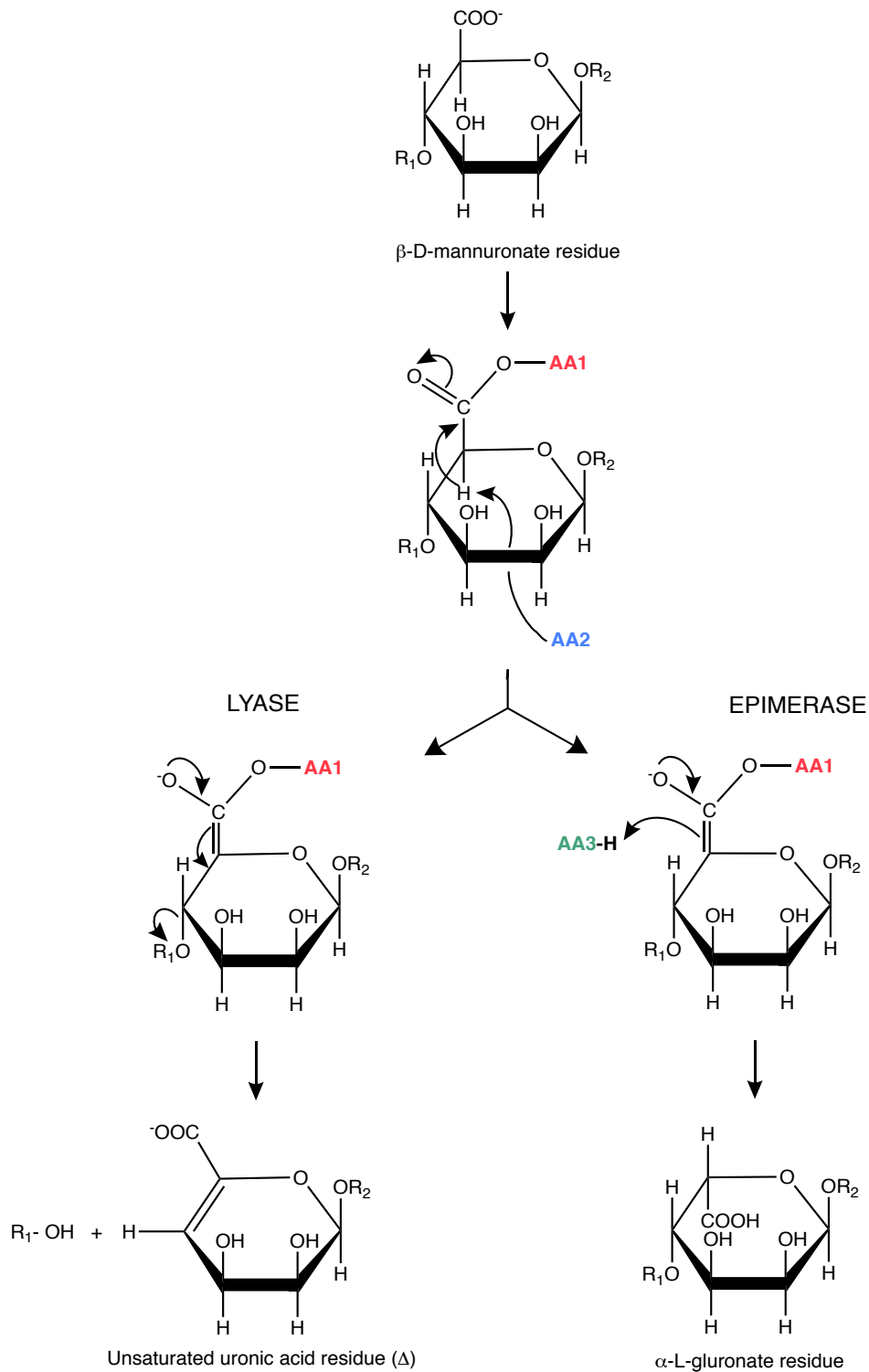


**Figure 1.8.** A unified three-step reaction mechanism proposed for mannuronan C5-epimerases and alginate lyases: AA1 refers to the amino acid residue on the enzymes that neutralizes the negative charged carboxylate ion ( $\text{COO}^-$ ), and amino acid residue AA2 abstracts the proton at C5. In the lyase reaction, the proton is donated to the oxygen at C-1 in the leaving group ( $\text{R}_1\text{-OH}$ ), which gives  $\beta$ -elimination of the 4-O-glycosidic bond. In the epimerase reaction, a proton from amino acid residue AA3 is donated to the opposite side, which changes stereochemistry and conformation of the hexose from  $\beta$ -D-mannuronic acid (M) to  $\alpha$ -L-guluronic acid (G) (55).

### Mode of action

There are four main epimerase features that can be said to define the alginate product (177):

1. Product specificity, which determines whether the enzyme generates a G-block or MG-block pattern (Table 1.1).
2. Enzyme processivity, which controls generation of single G-residues or long blocks.
3. Substrate selectivity, which is defined by individual binding constants for different sequences.
4. Reaction rate for each enzyme.

As described earlier, mannuronan C5-epimerases generate distinctive epimerization patterns (Table 1.1). After epimerisation of the first G-residue, epimerases are able to progressively epimerize the neighbouring or the second neighbouring M-residue without dissociating from the substrate, generating successive block structures along the alginate chain (175,178).

Another outcome is that the enzyme randomly dissociates from the substrate after epimerization of some residues, before initiates a new binding event with the substrate (175,178). These modes of actions can be described as the enzyme processivity – the average number of residues epimerized per binding event between the substrate and enzyme (179,180). A processive enzyme must be able to recognize and bind the substrate in more than one site (162,181). This holds true for AlgE epimerases, in which several residues surrounding the active site have been found to accommodate binding of the alginate substrate (164,166,178). In alginate, the formation of long G-blocks could be due to a high degree of processivity. However, the distinct epimerization patterns may also arise from the epimerase preferring a specific substrate depending on the distribution of pre-existing G-residues. This mode of action is also known as the “preferred attack” mechanism, where the enzyme substrate specificity depends on the affinity of a specific monomer sequence (162).

Different approaches such as time-resolved NMR spectroscopy, mass spectrometry (MS) and chromatography techniques have been used to determine if the AlgE epimerases have a processive or preferred attack mode of action (178,181–184). For the smallest epimerase AlgE4, studies have supported a processive mode of action where the enzyme epimerizes every other M-residue, creating a pattern of alternating M- and G-residues (poly-MG) (175,178,181). The  $\beta$ -1,4 linkage in poly-M substrate implies that each M-residues is rotated about 180° with respect to its neighbouring residues. This allow allows the enzyme to slide along the polymer in a processive manner without rotating the substrate (178). The minimum substrate required for activity of AlgE4 has been found to be six residues ( $M_6$ ), where the third residue from the non-reducing end is the first to be epimerized (178). For longer chains,



AlgE4 acts in the direction of the non-reducing end, epimerizing an average of 10 residues per binding event (178).

A processive mode of action has also been proposed for AlgE1 and AlgE6, which both predominantly generates G-blocks (184,185). Kinetic experiments have, however, shown a higher reaction rate for these enzymes when acting on substrate with pre-existing G-residues, and they seem to favour G-block containing substrates over poly-MG and poly-M (184). AlgE1 and AlgE6 also have the capacity to epimerize M-residues flanked by G-residues and thus merge G-blocks. These results support an initial preferred attack mechanism, but whether the enzymes continue along the substrate in a processive and/or preferred mode of action is not fully understood (184). Nevertheless, it is likely that both enzymes are processive when acting on poly-MG substrate, similar to the processive mode of AlgE4 (184). AlgE1 and AlgE6 require a minimum substrate of ten and eight residues, respectively, when acting on poly-MG. On poly-M substrates, the minimum substrate is an octamer for AlgE1 and a heptamer for AlgE6. At these minimum chain lengths, epimerization is initiated at the third (on poly-M) and fourth (on poly-MG) M-residue from the non-reducing end (184).

The similar epimerization patterns seen for AlgE1 and AlgE3 suggest that they share similar properties. However, comparison of the measured initial activity required to obtain high degrees of epimerization shows that a lower initial activity is required for AlgE3 than for AlgE1 (13). For the AlgE2, AlgE5 and AlgE7 epimerases, a preferred attack mechanism or a combination of both mechanisms has been suggested (162,168,174,184). Although AlgE2 and AlgE5 have similar epimerization patterns and a high degree of sequence identity (95 %), their substrate specificity differ (145,174,184). Kinetic data of AlgE5 indicates that this epimerase has a preference for poly-MG substrate, while epimerization experiments with AlgE2 shows that it is unable to epimerize poly-MG substrates and to merge G-block sequences (174,181,184). The mode of action for AlgE7 is described in section 1.3.

The reaction rate of AlgE epimerases is characteristic for each enzyme, and is especially important when several epimerases are acting on the alginate simultaneously, competing for the substrate (145,177). For AlgE2 and AlgE4 the reaction rate has been found to increase with increasing chain length of poly-M substrate for lengths in the range DP<sub>n</sub> 10-2000 (181). The enzyme efficiency of all epimerases is also shown to depend on calcium concentration,

the type of alginate substrate, pH and temperature, and the optimum conditions vary for the different epimerases (13,174,175,184).

### 1.2.4 Alginate lyases

Alginate lyases are enzymes that catalyse the degradation of alginate by cleaving the glycosidic linkages between the monomers by a  $\beta$ -elimination reaction (see section 1.2.3) (52,54,55). As briefly mentioned in section 1.1.2, their occurrence in nature is widely distributed, isolated from organisms that use alginate as a carbon source, as well as a variety of alginate-producing bacteria and some bacteriophages (52,53). The biological function of alginate lyases in alginate-producing bacteria may be to control the length of newly synthesized alginate (52,125). They also appear to have a role in degradation of the cyst coat during germination in *A. vinelandii* and cell detachment from the alginate biofilm produced by *P. aeruginosa* (52,186,187). In bacteriophages, lyases are important for destroying the acetylated poly-M-rich extracellular polysaccharide layer surrounding the bacteria, thereby helping the phage to penetrate this layer (52,188,189).

An alginate molecule may contain four different types of bonds: M-M, M-G, G-M and G-G. Most alginate lyases are able to cleavage more than one of these bonds, but at different reaction rates (52,190). Indeed, alginate lyases can be classified in two groups based on their substrate specificities: G-block specific (EC 4.2.2.11) and M-block specific (EC.4.2.2.3) lyases. However, this classification does not differentiate between lyases that also are able to cleave M-G or G-M bonds. O-acetylation of M-residues further complicates the study of alginate lyases, as not all alginate lyases are able to act on acetylated substrates (52). Alginate lyase can also be classified according to their mode of action as endolytic or exolytic enzymes (52,79). Most studied lyases act endolytically, cleaving glycosidic bonds inside long alginate chains, and releasing unsaturated oligosaccharides (2-5 monomers) as main products (79,191). However, some exolytic alginate lyases have been reported, removing single residues from the end of the alginate polymers (192,193).

A third type of classification is based on the sequence similarities of the enzymes (194). Alginate lyases are found in the polysaccharide lyase (PL) families PL5, PL6, PL7, PL14, PL15, PL17 and PL18 of the carbohydrate-active enzyme (CAZy) database. In addition, some lyases are grouped as unclassified polysaccharide lyases (79,194). Families PL5, PL15 and

PL17 have been found to have an  $(\alpha/\alpha)_n$  toroid fold structure, while PL7, PL14, and PL18 are folded as  $\beta$ -jelly rolls (195,196). However, enzymes belonging to the PL6 family show a similar right-handed  $\beta$ -helix fold as identified in AlgE epimerases (195,197,198). For many of the studied alginate lyases, the key amino acids tyrosine and/or histidine facilitate the catalytic  $\beta$ -elimination reaction, whereas alginate lyases of the PL6 family follow another scheme (79,196). They have been found to use  $\text{Ca}^{2+}$  ions as a neutralizing agent, a lysine as the catalytic base (AA2) and an arginine as the catalytic acid (AA3) (196,197). Thus, the PL6 family have different catalytic residues than found for the AlgE epimerases, despite their similar structures.

Most applications of alginate lyases lie in basic and applied research. A convenient application is their use in measurement of alginate concentration or epimerase activity, where the absorbance at 230 nm or the resulting unsaturated  $\Delta$  residue is measured (158,199,200). Studies of block structures in alginate utilize different cleavage specificities of lyases by degrading parts of the polymer (25,201,202). This makes it possible to analyse the remaining block structures using NMR or HPAEC-PAD (25,201,202). Alginate lyases might also be applied for tailoring alginate polymers with defined lengths *in vitro* (190).

### 1.3 The AlgE7 epimerase of *Azotobacter vinelandii*

The AlgE7 epimerase was first identified in 1999, as a member of the *A. vinelandii* AlgE epimerase family (156). Surprisingly, the AlgE7 enzyme was found to display both epimerase and lyase activity. As previously mentioned in section 1.2.3, weak lyase activity has also been identified in AlgE2 and AlgE5 (162,174). However, AlgE7 is the only epimerase reported to have lyase activity at rates comparable to other alginate lyases (52,168). The biological significance of the dual catalytic activity in AlgE7 is not fully established, but a study of an AlgE7 knock-out mutant showed that the enzyme is not required for cyst germination (142). The same study also suggests that AlgE7 mediated the release of synthesized alginate associated at the cell surface. Still, it is possible that enzyme also contributes in cyst formation in *A. vinelandii*, generating a smaller fraction of alginate oligomers (156).

### Structure and catalytic residues

The molecular structure of AlgE7 has not yet been determined, but high degree of sequence homology with the A-modules of structurally characterized AlgE4 and AlgE6 indicates a similar right-handed parallel  $\beta$ -helix structure for the AlgE7 A-module (156,166). In the same amino acid sequence alignment study, it was observed that the AlgE7 and AlgY proteins deviated the most from the rest of the AlgE1-6 A-modules (156). The three AlgE7 R-modules were also significantly homologous to the R-modules of AlgE1-E6. However, the R1 and R2 modules of AlgE7 seem to be less homologous than all the other R-modules identified in AlgE epimerases.

As explained in section 1.2.3, the active site for the epimerase activity in all AlgE epimerases contains the four catalytic residues Y149, D152, H154 and D178 (166). Studies of the lyase activity in AlgE7 also suggest that the same catalytic residues are responsible for cleavage of the alginate substrate (168). A common active site for both activities of AlgE7 coincides with the proposed reaction mechanism for epimerases and lyases, as this mechanism only differ in the last reaction step (55,168). However, as described in section 1.2.4, a similar parallel  $\beta$ -helix fold is seen in several lyases, such as members of the PL6 family (195,197,198). This might suggest that the lyase activity of AlgE7 is located at a different site than the epimerase activity. Nevertheless, current research strongly indicates a common site for both activities (168).

### Substrate specificity and mode of action

NMR spectroscopy analyses have shown that the AlgE7 enzyme creates an epimerization pattern of both single G-residues and G-blocks, whereas the AlgE7 lyase activity generates unsaturated uronic acid residues neighbouring an M-residue ( $\Delta$ M) and G- and M residues with reducing ends ( $G_{\text{red}}$  and  $M_{\text{red}}$ ) (156,168). Moreover,  $G_{\text{red}}$  residues were found in a larger amount than  $M_{\text{red}}$  residues. Based on these findings, four potential cleavage sites have been proposed for the AlgE7 enzyme:  $G\downarrow MM$ ,  $G\downarrow GM$ ,  $M\downarrow MM$  and  $M\downarrow GM$ , with clear preference for the two first mentioned (168). AlgE7 thus seems to favour cleavage at the end of G-blocks.

When acting on poly-M substrate, the initial reaction rate has been found to be higher for the epimerase reaction than for the lyase reaction, up to a point where the substrate is highly

degraded ( $DP_n < 11$ ), after which lyase activity predominates (168). This indicates that AlgE7 is able to bind small oligomers, but that longer chain lengths are required for epimerase activity. AlgE7 has also shown capable of epimerizing poly-MG substrate. NMR analysis of this reaction product also identified  $G\downarrow MG$  as a more favorable cleavage site in MG-alginate, but cleavage in this site was much less efficient. Epimerization data on different alginate substrates has also indicated that AlgE7 prefers epimerization of M-residues neighboring pre-existing G-residues (preferred attack mechanism), and that the initial degradation is higher in alginate already containing some G-residues than in pure mannuronan substrate. The latter may be explained by a need for a specific monomer sequence in order to stimulate lyase activity. Regardless, it is fair to say that there is a complex relationship between substrate composition and lyase activity.

Similar to the epimerase activity in all AlgE enzymes,  $Ca^{2+}$  ions were also found to be an absolute requirement for the lyase activity in AlgE7 (168). Experiments of the AlgE7 lyase activity have shown that acetylation of the alginate substrate inhibits the lyase activity. The same was also seen with increased ionic strength (NaCl). In addition, the highest AlgE7 lyase activity was around pH 6.9-7.3 in the presence of 2.5 mM  $Ca^{2+}$  and temperatures close to 37 °C. The optimum conditions for the epimerase activity have not been determined (168).

## 1.4 Aim of the research project

The main objective of this project has been to get a better understanding of the molecular mechanisms that contributes to the bifunctional activity of the mannuronan C5-epimerase and alginate lyase AlgE7. With that, the project also aims to get more insight into both the epimerase and lyase mechanism. This was achieved by studying and mutating amino acid residues surrounding the active site of AlgE7 that differ in relation to the other six AlgE epimerases.

Mannuronan C5-epimerases enable enzymatic modification of alginate *in vitro*, and an understanding of the action of AlgE7 can therefore be useful in specific design of alginate for biotechnological applications. A mechanistic understanding of AlgE7 may provide the ability to control which of the two activities that will occur or to abort the lyase activity. This research may also contribute to a better understanding of other enzymes with dual catalytic activity.



## 2 Material and Methods

### 2.1 Materials

#### 2.1.1 Instruments

**Table 2.1.** The instruments used in this study, listed with their product model number and the manufacturer.

<b>Instrument</b>	<b>Product model</b>	<b>Manufacturer</b>
Analytical valance	AB204-S	Mettler Toledo
	MT-5	Mettler Toledo
Block heater	QBD2	Grant Instruments
Centrifuge, rotor	Centrifuge 5430R (F-35-8-30)	Eppendorf AG
	MiniSpin® (F-45-12-11)	Eppendorf AG
	Sorvall LYNX 6000 (F14-6x250y)	Thermo Fisher Scientific
Electrophoresis	PowerPac Basic™ 300V	Bio-Rad
FPLC	ÅKTA FPLC	GE Healthcare Life Sciences
	- P-920 (pump)	
	- UPC-900 (detector)	
	- INV-907 (injector)	
	- FRAC-950 (fraction collector)	
Freeze-dryer	Beta 1-8 LDplus	Martin Christ GmbH
Gel imager	ChemiDoc™ XRS+	Bio-Rad
Incubator	Multitron CH-4103 Incubator Shaker	Infors AG
Microcentrifuge	Galaxy MiniStar C1413-VWR230	VWR
Magnetic stirrer	MR-3001-384	Heidolph Instruments GmbH
NMR	Ascend 400 MHz, AVIIIHD, 5 mm SmartProbe	Bruker Biospin
	Ascend 800 MHz, AVIIIHD,	Bruker Biospin
	5 mm cryogenic TCI probe	
PCR	Mastercycler® Gradient	Eppendorf AG
pH meter	Orion Star™ A111	Thermo Fisher Scientific
Pipettes	10 µL, 100 µL, 1000 µL	Eppendorf Research
	1000 µL, 12000 µL,	Sartorius
Sonicator	Sonifer-250	Branson Ultrasonic
Spectrophotometer	NanoDrop™ One	Thermo Fisher Scientific
	Unicam Helios Epsilon	Thermo fisher Scientific
Sterile bench	SAFE 2020	Thermo Fisher Scientific
Vortex	Classic Vortex Mixer	Fisher Scientific Ltd
Water bath	GD-100	Grant Instruments™

## 2.1.2 Chemicals

**Table 2.2** The chemicals used in this study, listed with their chemical abstracts service (CAS) registry number and the manufacturer.

<b>Chemical</b>	<b>CAS number</b>	<b>Manufacturer</b>
1,4-dithiothreitol (DTT)	3483-12-3	VWR Chemicals
3-morpholinopropane-1-sulfonic acid (MOPS)	1132-61-2	Fisher BioReagents
4-(2-hydroxyethyl)-1-piperazineethanesulfonic acid (HEPES)	7365-45-9	PanReac AppliCem
Acetic acid	64-19-7	Sigma-Aldrich
Agar bacteriological (Agar No.1)	9002-18-0	Oxoid Ltd
Ampicillin	69-52-3	PanReac AppliCem
Bromophenol	115-39-9	Merck KGaA
Calcium chloride (CaCl <sub>2</sub> )	10043-52-4	Sigma-Aldrich
D(+)-Glucose anhydrous	50-99-7	VWR Chemicals
Deuterium oxide (D <sub>2</sub> O, 99.9%)	7789-20-0	Sigma-Aldrich
DNA gel loading dye (6X)	-	Thermo Fisher Scientific
EDTA-free protease inhibitor	-	cOmplete™
Ethanol (EtOH) absolute ≥ 99.8 %	64-17-5	VWR Chemicals BDH
Ethylenediaminetetraacetic acid (EDTA)	6381-92-6	VWR Chemicals BDH
GelRed®	-	Biotium Inc
GeneRuler 1 kb DNA ladder	SM0311	Sigma-Aldrich
Glycerol bidistilled 99.5 % (C <sub>3</sub> H <sub>8</sub> O <sub>3</sub> )	56-81-5	VWR Chemicals BDH
InstantBlue™ protein stain	-	Expedeon
Isopropyl-B-D-1-thiogalactopyranoside (IPTG)	367-93-1	Sigma-Aldrich
Magnesium chloride (MgCl <sub>2</sub> )	7791-18-6	VWR Chemicals BHD
Magnesium chloride hexahydrate (MgCl <sub>2</sub> ·6H <sub>2</sub> O)	7791-8-6	VWR Chemicals BDH
Nitrogen (N <sub>2</sub> , (l))	7727-37-9	Praxair Norge AS
Potassium chloride (KCl)	7447-40-7	Merck KGaA
Precision plus protein™ all blue standards	-	Bio-Rad
RunBlue 20x SDS run buffer	-	Expedeon
Sodium chloride (NaCl)	7647-14-5	VWR Chemicals BDH
Sodium dodecyl sulphate (SDS)	151-21-3	Sigma-Aldrich
Sodium hydroxide (NaOH)	1310-73-2	Merck KGaA
Tris(2-carboxyethyl) phosphine (TCEP)	51805-45-9	Sigma-Aldrich
Triethylenetetranitrihexaacetic acid (TTHA)	869-52-3	Sigma-Aldrich
Trimethylsilylpropanoic acid (TSP)	5683-30-7	Sigma-Aldrich
Tris(hydroxymethyl)aminomethane hydrochlorid (Tris-HCl)	1185-53-1	Sigma-Aldrich
Trizma® tris base	77-86-1	Sigma-Aldrich
Triton X-100	9002-93-1	Sigma-Aldrich
Tryptone	91079-40-2	Oxoid Ltd
Yeast extract	8013-01-2	Oxoid Ltd



### 2.1.3 Kits

**Table 2.3.** The kits used in this study, listed with the components included and the manufacturer.

<b>Kit</b>	<b>Components</b>	<b>Manufacturer</b>
Monarch® Miniprep Kit Protocol	Plasmid miniprep column tubes Plasmid miniprep collection tubes Plasmid resuspension buffer Plasmid lysis buffer Plasmid neutralization buffer Plasmid wash buffer 1 Plasmid wash buffer 2	New England BioLabs Inc
Q5® Site-Directed Mutagenesis Kit	Q5 hot start high-fidelity master mix (2X) KLD reaction buffer (2X) KLD enzyme mix (10X)	New England BioLabs Inc
DNA Clean & Concentrator™-5 kit	Zymo-Spin collection tube Zymo-Spin column DNA binding buffer DNA wash buffer DNA elution buffer	Zymo Research

### 2.1.4 Disposable equipment

**Table 2.4.** List of disposable and other equipment used in this study.

<b>Disposable equipment</b>	<b>Description (product number)</b>	<b>Manufacturer</b>
Centrifuge tubes	13 mL (62.515.006)	Sarstedt AG & Co. KG
	15 mL (62.554.502)	Sarstedt AG & Co. KG
	50 mL (62.547.254)	Sarstedt AG & Co. KG
Column packing material	Chitin resin (S6651S)	New England BioLabs Inc
Cryotubes	2 mL (126263)	Cryo.S™
Dialysis membrane tubings	MWCO 6-8 kD	Spectra/Por®
Lens cleaning tissue, grade 451	0.0 4 mm (111-5003)	VWR International
Microcentrifuge tubes	1.5 mL (72.690.001)	Sarstedt AG & Co. KG
NMR sample tubes	5 mm OD (WG-1000-7)	Wilmad LabGlass
PCR tubes	0.2 mL (732-0548)	VWR International LLC
Petri dishes	55 x 14 mm (391-0611)	VWR International LLC
	90 × 16 mm (391-0459)	VWR International LLC
	140 × 21 mm (391-1501)	VWR International LLC
SDS-PAGE gels	12 % polyacrylamide	ClarePAGE™
Serological pipettes	5 mL (612-3704)	VWR International LLC
	10 mL (612-3700)	VWR International LLC
	25 mL (612-3698)	VWR International LLC
Spin columns (Amicon Ultra)	0.5 mL, membrane Ultracel® low-binding regenerated cellulose, MWCO 3kDa	Merck Norge
Sterile filters	0.22 µm (83.1826.001)	Sarstedt AG & Co. KG
	0.22 µm, 50 mL receiver bottle (564-0020)	Thermo Fischer Scientific
	0.22 µm, 1000 mL receiver bottle	Merck Millipore
Syringes	5 ml (309050)	BD Medical Technology
	10 mL (309110)	BD Medical Technology

## 2.1.5 Primers

All primers used for PCR (Table 2.5 and 2.6) and sequencing (Table 2.7) was ordered from Sigma-Aldrich. Primers used for site-directed mutagenesis (SDM) by PCR were designed with 5' ends annealing back-to-back using the NEBaseChanger (Table 2.5). Primers used for SLIC by PCR were designed with the assembly tool NEBuilder (Table 2.6). In some cases, the proposed primers from NEBaseChanger and NEBuilder were manually edited to remove the primers ability to anneal to multiple sites in the template or to create hairpin structures.

**Table 2.5.** PCR primers pairs used for SDM, designed using NEBaseChanger. The oligonucleotide sequence (5'→3), primer length (bp), GC content (%) and melting and annealing temperatures (C°) are listed as stated by NEBase Changer. Uppercase and lowercase letters in the oligonucleotide sequence illustrates the specific primer target and the point mutation respectively.

Mutation	Direction	Oligonucleotide sequence (5'→3)	Length (bp)	GC (%)	Tm (C°)	Ta (C°)
R90A	Forward	CGGCATCATCgcCTCGGCCAAC	22	68	61	62
	Reverse	GTGAGCTTTTCGTCCCAC	18	56	63	
E117L	Forward	CACCGAAGGctGGTCGACGGC	22	68	65	66
	Reverse	TTGTCCTGGTTACCGTCGATG	21	52	67	
E117K	Forward	CACCGAAGGCaAGGTCGACGGC	22	68	65	66
	Reverse	TTGTCCTGGTTACCGTCGATG	21	52	67	
Y122A	Forward	CGACGGCTTcgcTACCGGCTATATTCC	27	59	63	64
	Reverse	ACCTCGCCTTCGGTGTTG	18	61	69	
F122Y*	Forward	GACGGCTTctatACCGGCTATATTC	25	48	63	64
	Reverse	TACCTTGCCTTCGGTGTT	18	50	64	
H154A	Forward	CTTCGATCCCgcCGAGCAGACCATCAAC	28	61	64	65
	Reverse	GCGTAGCCTGATACCTCG	18	61	69	
D173A	Forward	AACGGCAAGGcCGGGTTCGTC	21	67	69	70
	Reverse	GTCGTGGGCGACGCTGTC	18	72	72	
R195A	Forward	CAACAACGGCgcCCACGGCTTC	22	68	62	62
	Reverse	TACGAGACGTTGTTCTCG	18	50	61	
H196A	Forward	CAACGGCCGCgcCGGCTTCAAC	22	73	64	63
	Reverse	TTGTACGAGACGTTGTTC	18	44	59	
R231L	Forward	GGCTCGGAAGACctGGACTTCGTCTACAAC	30	57	75	72
	Reverse	GCGCTGGACCACCAGGCCGTTG	22	73	79	
Y307L	Forward	GTGGAATCCTcCGACGACCGC	21	62	72	68
	Reverse	GATGACTTCCGCGTTGGC	18	61	67	

\* Used to remove a mutation in the algE7 gene carried by the pTB111 plasmid (Table 2.9)

**Table 2.6.** Primers used for SLIC cloning, designed using NEBuilder. The oligonucleotide sequence (5'→3), primer length (bp), GC content (%) and melting temperature (C°) are listed as stated by NEBuilder®. Uppercase and lowercase letters in the oligonucleotide sequence illustrates the annealing and the 5' extension segments respectively.

Primer name	Direction	Oligonucleotide sequence (5'→3)	Length (bp)	GC (%)	Tm (C°)
pTYB1 backbone primers	Forward	CTCGAGGGCTCTTCCTGCT	19	63	62
	Reverse	ATGTATATCTCCTTCTTAAAGTTAAACAAAA	31	23	52
algE7 insert primers	Forward	ttttgttaactttaagaaggagatatacatATGGAATACAACGTTAAG GATTTTG	56	27	61
	Reverse	aagcaggaagagccctcgagGGCAGCCTGCGAGCTGCTG	39	67	80

**Table 2.7.** Primers used for sequencing. The oligonucleotide sequence (5'→3), primer length (bp), GC content (%) and melting temperature (C°) are listed as stated by Sigma-Aldrich.

Primer name	Direction	Oligonucleotide sequence (5'→3)	Length (bp)	GC (%)	Tm (C°)
T7 promoter primer	Forward	TAATACGACTCACTATAGGG	20	40	58
pTYB intein primer	Reverse	ACCCATGACCTTATTACCAACCTC	24	46	65
pBG27 seq.primer	Forward	TGTGGAATTGTGAGCGGATAAC	22	45	66
	Reverse	TTCGAGGTTGGTGAAGATGAAGTC	24	46	67

## 2.1.6 Bacteria strains and plasmids

Bacteria strains (Table 2.8) and plasmids (Table 2.9) used in this study.

**Table 2.8.** *Escherichia coli* strains used for cloning and protein expression.

<i>Escherichia coli</i> strain	Description	Reference
NEB® 5-alpha competent	Cloning	New England BioLabs Inc
T7 express competent (ER2566)	Protein expression	New England BioLabs Inc

**Table 2.9.** Plasmids used for cloning and protein expression. All plasmids carry an ampicillin resistant gene (Amp<sup>R</sup>). Plasmid maps of pTYB1 and pBG27 are shown in Appendix B.

Numbering	Plasmids	Description	Reference or producer
-	pTYB1	Cloning and protein expression vector, T7 promoter, lac repressor, C-terminal <i>Sec</i> intein tag /chitin binding domain, ori M13, Amp <sup>R</sup>	New England BioLabs Inc
		IMPACT-CN fusion vector pTYB1 derivative containing the <i>algE7</i> gene	
1	pBG27*	Cloning and protein expression vector, <i>trc</i> promoter, lac repressor, Amp <sup>R</sup>	Published in Svanem <i>et al.</i> 1999 (146)
		pTrc99a derivative containing the <i>algE7</i> gene	
2	pKK1	pBG27 with <i>algE7</i> -R90A	This study
3	pKK2	pBG27 with <i>algE7</i> -E117L	This study
4	pRS16	pBG27 with <i>algE7</i> -E117K	Unpublished, Rannveig Skrede
5	pRS38	pBG27 with <i>algE7</i> -D119A	Unpublished, Rannveig Skrede
6	pRS39	pBG27 with <i>algE7</i> -D119E	Unpublished, Rannveig Skrede
7	pRS40	pBG27 with <i>algE7</i> -D119N	Unpublished, Rannveig Skrede
8	pKK3	pBG27 with <i>algE7</i> -Y122A	This study
9	pRS17	pBG27 with <i>algE7</i> -Y122F	Unpublished, Rannveig Skrede
10	pTB95*	pBG27 with <i>algE7</i> -R148G	Unpublished, Tonje Bjerkan
11	pJR4	pBG27 with <i>algE7</i> -R148K	I Unpublished, Jan Riedl
12	pJR3	pBG27 with <i>algE7</i> -Y149A	Unpublished, Jan Riedl
13	pRS18	pBG27 with <i>algE7</i> -Y149F	Unpublished, Rannveig Skrede
14	pRS19	pBG27 with <i>algE7</i> -D152E	Unpublished, Rannveig Skrede
15	pRS20	pBG27 with <i>algE7</i> -D152N	Unpublished, Rannveig Skrede
16	pRS36	pBG27 with <i>algE7</i> -P153A	Unpublished, Rannveig Skrede
17	pKK4	pBG27 with <i>algE7</i> -H154A	This study
18	pRS22	pBG27 with <i>algE7</i> -H154F	Unpublished, Rannveig Skrede
18	pRS21	pBG27 with <i>algE7</i> -H154Y	Unpublished, Rannveig Skrede
20	pJR1	pBG27 with <i>algE7</i> -K172L	Unpublished, Jan Riedl
21	pJR2	pBG27 with <i>algE7</i> -K172R	Unpublished, Jan Riedl
22	pKK5	pBG27 with <i>algE7</i> -D173A	This study
23	pRS23	pBG27 with <i>algE7</i> -D178E	Unpublished, Rannveig Skrede
24	pRS24	pBG27 with <i>algE7</i> -D178N	Unpublished, Rannveig Skrede
25	pRS25	pBG27 with <i>algE7</i> -D178R	Unpublished, Rannveig Skrede
26	pKK6	pBG27 with <i>algE7</i> -R195A	This study
27	pRS26	pBG27 with <i>algE7</i> -R195L	Unpublished, Rannveig Skrede
28	pKK7	pBG27 with <i>algE7</i> -H196A	This study
29	pRS37	pBG27 with <i>algE7</i> -V201L	Unpublished, Rannveig Skrede
30	pKK8	pBG27 with <i>algE7</i> -R231L	This study
31	pRS27	pBG27 with <i>algE7</i> -K255E	Unpublished, Rannveig Skrede
32	pRS28	pBG27 with <i>algE7</i> -K255L	Unpublished, Rannveig Skrede
33	pKK9	pBG27 with <i>algE7</i> -Y307F	This study
34	pKK10	pBG27 with <i>algE7</i> -E117K-R148G	This study
35	pKK11	pBG27 with <i>algE7</i> -E117K-R148G-K172L	This study
36	pJR5	pBG27 with <i>algE7</i> -R148K-K172L	Unpublished, Jan Riedl
37	pJR6	pBG27 with <i>algE7</i> -R148K-K172R	Unpublished, Jan Riedl
38	pTB113	pBG27 with <i>algE7</i> -E117K-Y122F-R148G	Unpublished, Tonje Bjerkan
39	pTB118	pBG27 with <i>algE7</i> -E117K-Y122F-K172L	Unpublished, Tonje Bjerkan
40	pTB119	pBG27 with <i>algE7</i> -E117K-Y122F-K172R	Unpublished, Tonje Bjerkan
41	pTB111*	pBG27 with <i>algE7</i> -E117K-Y122F-R148G-K172L	Unpublished, Tonje Bjerkan
42	pTB112	pBG27 with <i>algE7</i> -E117K-Y122F-R148G-K172R	Unpublished, Tonje Bjerkan
43	pTB116	pBG27 with <i>algE7</i> -E117K-Y122F-Y149A	Unpublished, Tonje Bjerkan

\* Plasmids used as DNA templates for site-directed mutagenesis by PCR in this study

## 2.1.7 Alginate substrates

Substrates for the epimerase and lyase reaction by AlgE7 that were used in this study are listed in Table 2.10.

**Table 2.10.** Alginate substrates used for the epimerase/lyase reaction. Origin, fraction of M-residues ( $F_M$ ), DPn and the producer of the substrates are listed. n.d=not determined

Alginate substrate	Origin	$F_M$	DPn	Producer
Poly-mannuronan (poly-M)	AlgG-deficient mutant of <i>Pseudomonas fluorescens</i>	1.00	~ 370	SINTEF Industry, Trondheim (183)
Poly-MG	Mannuronan epimerized by AlgE4 epimerase (produced in <i>E. coli</i> )	0.54	n.d	Wenche I. Strand, NTNU, Trondheim (178,183)
$^{13}\text{C}1$ -enriched poly-M	AlgG-deficient mutant of <i>P. fluorescens</i>	1.00	~ 70	SINTEF Industry, Trondheim (159)
$^{13}\text{C}1$ -enriched poly-MG	$^{13}\text{C}1$ -enriched poly-M epimerized by AlgE4 epimerase (produced in <i>E. coli</i> )	0.52	n.d	Wenche I. Strand, NTNU, Trondheim (25)
$^{13}\text{C}1$ -enriched G-oligomers	$^{13}\text{C}1$ -enriched poly-M epimerized by AlgE1 epimerase and hydrolysed to oligomers	0.02	~ 22	SINTEF Industry

## 2.1.8 Media, buffers and solutions

All media, buffer and solutions were sterilized by autoclaving (120 °C, 20 minutes) or sterile filtration (0.22 µm filter) before use. The pH of buffers and solutions were checked with a pH meter and adjusted to the desired pH when necessary.

### Growth media

All growth media were prepared in reverse osmosis (RO) water. The lysogeny broth agar (LA) medium was used to make agar plates. After autoclaving and partial cooling of the LA medium, the media was poured into sterile Petri dishes and solidified to agar by cooling.

#### Lysogeny broth (LB) medium

10 g/L tryptone

5 g/L yeast extract

5 g/L NaCl

Autoclaved, stored at room temperature

#### Lysogeny broth agar (LA) medium

10 g/L tryptone

5 g/L yeast extract

5 g/L NaCl

15 g/L agar bacteriological

Autoclaved, stored at 4 °C

Super optimal broth (SOC) medium

20 g/L tryptone

5 g/L yeast extract

3.6 g/L D-glucose

0.186 g/L KCl

0.5 g/L NaCl

0.952 g/L MgCl<sub>2</sub>

Adjusted to pH 7 with NaOH

Sterile filtrated, stored at -20 °C

**Buffer and agarose solution used in agarose gel electrophoresis**

The 50x Tris-acetate-EDTA (TAE) buffer was prepared in RO water.

0.8 % (w/v) agarose was dissolved in 1xTAE buffer. The agarose solution was then heated prior to adding 20 µL Gel Red®.

50X Tris-acetate-EDTA (TAE) buffer

24.2 g/L tris-base

57.1 mL/L acetic acid

100 mL 0.5 M EDTA, pH 8

Autoclaved, stored in room temperature

**Buffers for protein production and purification**

The buffers used in the protein purification IMPACT™-CN protocol were prepared in Milli-Q® (MQ) water. The cleavage buffer was first prepared without 1,4-dithiotheritol (DTT). DTT was kept on ice and added to the cleavage buffer just before use.

Lysis buffer

20 mM HEPES

5 mM CaCl<sub>2</sub>

500 mM NaCl

Adjusted to pH 6.9 with NaOH

0.05 % (v/v) Triton X-100

Sterile filtrated, stored at 4 °C

IPTG solution

0.5 M IPTG

Sterile filtrated, stored at -20 °C

Column buffer

20 mM HEPES  
 5 mM CaCl<sub>2</sub>  
 500 mM NaCl  
 Adjusted to pH 6.9 with NaOH  
 Sterile filtrated, stored at room temperature

Regeneration buffer

300 mM NaOH  
 Sterile filtrated, stored at room temperature

Cleavage buffer

100 mL column buffer  
 50 mM DTT  
 Sterile filtrated, stored at room temperature

Dialysis buffer

5mM HEPES  
 5mM CaCl<sub>2</sub>  
 Adjusted to pH 6.9 with NaOH  
 Sterile filtrated, stored at room temperature

**Buffers for SDS-PAGE**

Buffers used for SDS-PAGE was prepared in MQ water.

SDS sample buffer

150 mM tris pH 6.8  
 1.2 % (w/v) SDS  
 25 % (w/v) glycerol  
 15 % (v/v) TCEP  
 0.0269 mM bromophenol blue  
 Sterile filtrated, stored at -20 °C

SDS running buffer

0.5 % (v/v) RunBlue 20x SDS Run Buffer  
 Stored at room temperature

**Buffer for epimerase and lyase reaction**<sup>1</sup>H-NMR epimerization buffer (5x)

25 mM HEPES  
 12.5 mM CaCl<sub>2</sub>  
 Adjusted to pH 6.9 with NaOH  
 Sterile filtrated, stored at room temperature  
 Prepared in MQ-water

Time resolved <sup>13</sup>C-NMR

10 mM MOPS  
 75 mM NaCl  
 2.5 mM CaCl<sub>2</sub>  
 Adjusted to pH 6.9 with NaOH  
 Prepared in (d-99.9%) D<sub>2</sub>O

## 2.1.9 Bioinformatics software and online tools

**Table 2.11.** List of bioinformatics software and online tools used for bioinformatics analyses or other means.

<b>Bioinformatics tools</b>	<b>Reference</b>	<b>Usage</b>
Benchling	Benchling Inc.	Verification of designed PCR oligonucleotides, analysis of sequencing results, making plasmid maps
Clustal Omega	EMBL-EBI, Cambridge	Alignments of AlgE1-7 A modules
NEBaseChanger 1.2.9	New England BioLabs Inc.	Design of PCR oligonucleotides for SDM
NEBuilder 2.2.7	New England BioLabs Inc.	Design of PCR oligonucleotides for SLIC
ProtParam	ExPASy	Theoretical protein parameters: number of amino acids, molecular mass, extinction coefficient
PyMOL 2.3.2	Schrödinger LLC	Visualizing 3D protein structure and substrate, structural alignment of protein models
SWISS-MODEL	Biozentrum, University of Basel	Homology modelling of a 3D protein structure
Topspin 4.0.7	Bruker BioSpin	Analysing <sup>1</sup> H-NMR and <sup>13</sup> C-NMR spectra
WHATIF web server	CMBI, Radboud University	Mutation of residues in the amino acid sequence
YASARA Energy Minimization Server	YASARA Biosciences	Performing energy minimization of homology models
<b>Other software</b>	<b>Reference</b>	<b>Usage</b>
ChemDraw Pro 17.0	PerkinElmer Informatics	Draw chemical structures and reaction mechanisms
ImageLab 6.0.1	BioRad Laboratories	Visualizing gels
PowerPoint® 14.5.8	Microsoft ®	Making figures
Unicorn 5.01	GE Healthcare Life Sciences	Conduction FPLC experiments



## 2.2 Methods

The overall methodology for this project consists of an experimental set-up that can be divided into three main parts: cloning, protein production and characterization (Figure 2.1). All AlgE7 mutants followed the blue and orange pathway shown in the flowchart. In order to purify the AlgE7 proteins by affinity chromatography using the IMPACT™-CN system, the *algE7* gene had to be transferred to a vector containing a *Sec* VMA intein tag/chitin-binding domain (Appendix B). This is shown by the purple pathway, which only was performed for some AlgE7 mutants.

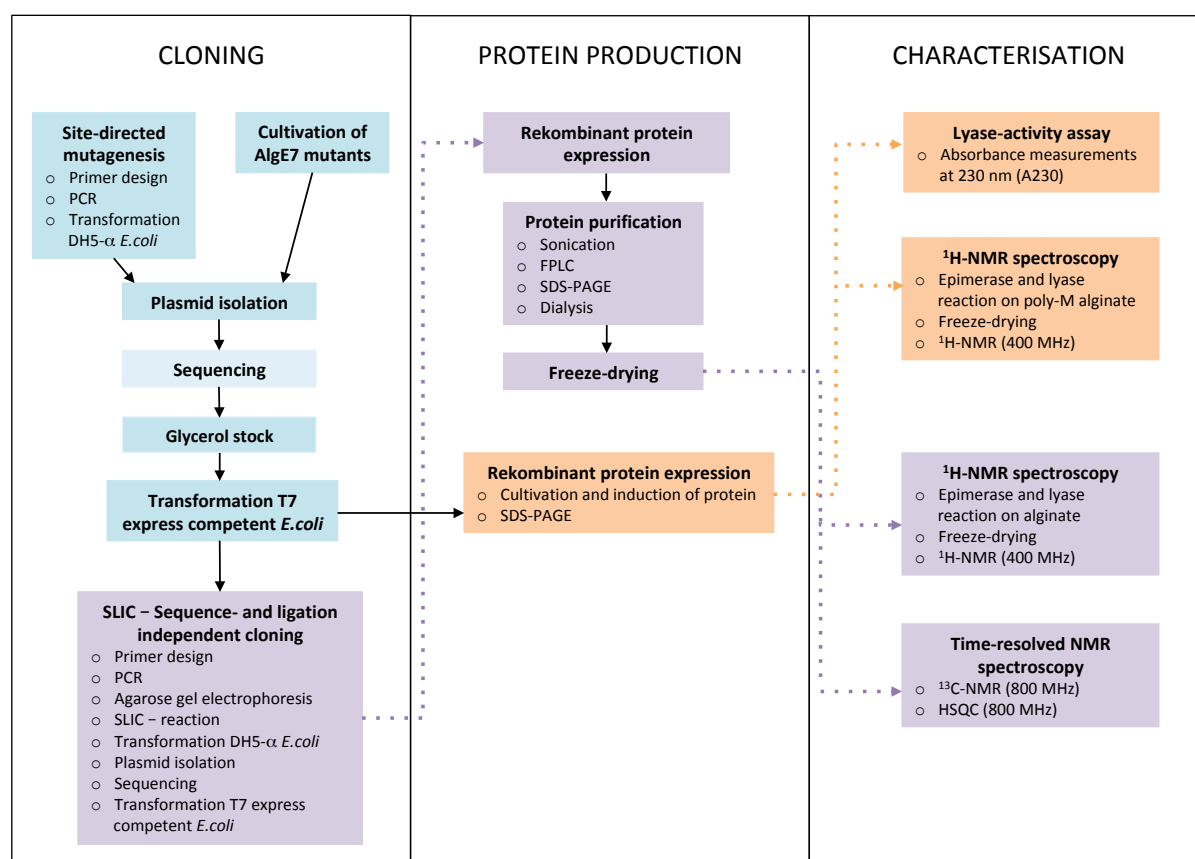


**Figure 2.1.** Flowchart showing the overall methodology for this study, consisting of three main experimental parts: cloning, protein production and characterization. **Site-directed mutagenesis** was used to create some AlgE7 mutants, and in addition several AlgE7 mutants were **cultivated** from DH5- $\alpha$  glycerol stocks made in other studies, followed by **plasmid isolation, sequencing, glycerol stock** and **transformation** (blue pathway). **Recombinant protein production** and characterization: **Lyase-activity assay** and **<sup>1</sup>H-NMR spectroscopy** were performed for almost all AlgE7 mutants (orange pathway). **Sequence- and ligation independent cloning** was used transfer some AlgE7 mutants into a vector containing *Sec* VMA intein tag/chitin-binding domain, needed for protein purification using affinity chromatography. This was followed by protein production: **recombinant protein expression, protein purification** and **freeze-drying**, and characterization: **<sup>1</sup>H-NMR spectroscopy** and **Time-resolved NMR spectroscopy** (purple pathway).

### 2.2.1 Site-directed mutagenesis (SDM) by Polymerase chain reaction (PCR)

Site-directed mutagenesis (SDM) is a technique for creating specific targeted changes in the nucleotide sequence of double-stranded plasmid DNA (point mutations: substitution, insertion or deletion). This method is widely used in molecular biology for engineering of genes and novel proteins. It is also used as a tool to study the function of specific nucleotides in DNA sequences or amino acids in proteins (203,204).

One strategy for SDM is based on polymerase chain reaction (PCR) – a technique for exponential amplification of specific sequences in a DNA molecule (Figure 2.2) (205,206). SDM by PCR utilizes custom designed oligonucleotide primers for *in vitro* replication. PCR primers comprise short nucleotide sequences complementary to opposite strands of the target DNA in the template. In order to limit non-specific primer hybridization and formation of internal hairpin structures (loops), PCR primers should be designed with a length of 18-30 nucleotides (bp) and relative low guanine and cytosine (GC) content (40-60 %). This ensures a sufficiently lower annealing temperature than the extension temperature. Primer pairs are usually designed to overlap or anneal with their 5' ends back-to-back. In the case of substitution, the forward primer carries a point mutation that creates a change in the nucleotide sequence, which subsequently leads to a change at the amino acid level (arginine: CGC → glycine: GGC). This results in all new copies of amplified target DNA carrying the substitution (204,205,207,208).

When performing PCR, a master mix of all reaction components is added to a thermocycler. Components required in the PCR master mix are a pair of PCR primers, a double-stranded template DNA, a thermostable *Taq* DNA polymerase I (originating from the bacterium *Thermus aquaticus*), four types of deoxyribonucleoside triphosphates (dNTP) and a buffer containing the co-factor  $Mg^{2+}$  and optimal pH for *Taq* DNA polymerase I. The cyclic process can be divided into three steps, which usually are repeated 25-30 times (205,209):

1. Denaturation – separation of double-stranded DNA by heating, usually 95-98 °C
2. Annealing – hybridization of oligonucleotide primers to the target DNA, usually 45-65 °C
3. DNA synthesis – *Taq* DNA polymerase I replicate the target DNA from the dNTPs in a 5' to 3' direction, thereby extending the primers, usually 70-72 °C

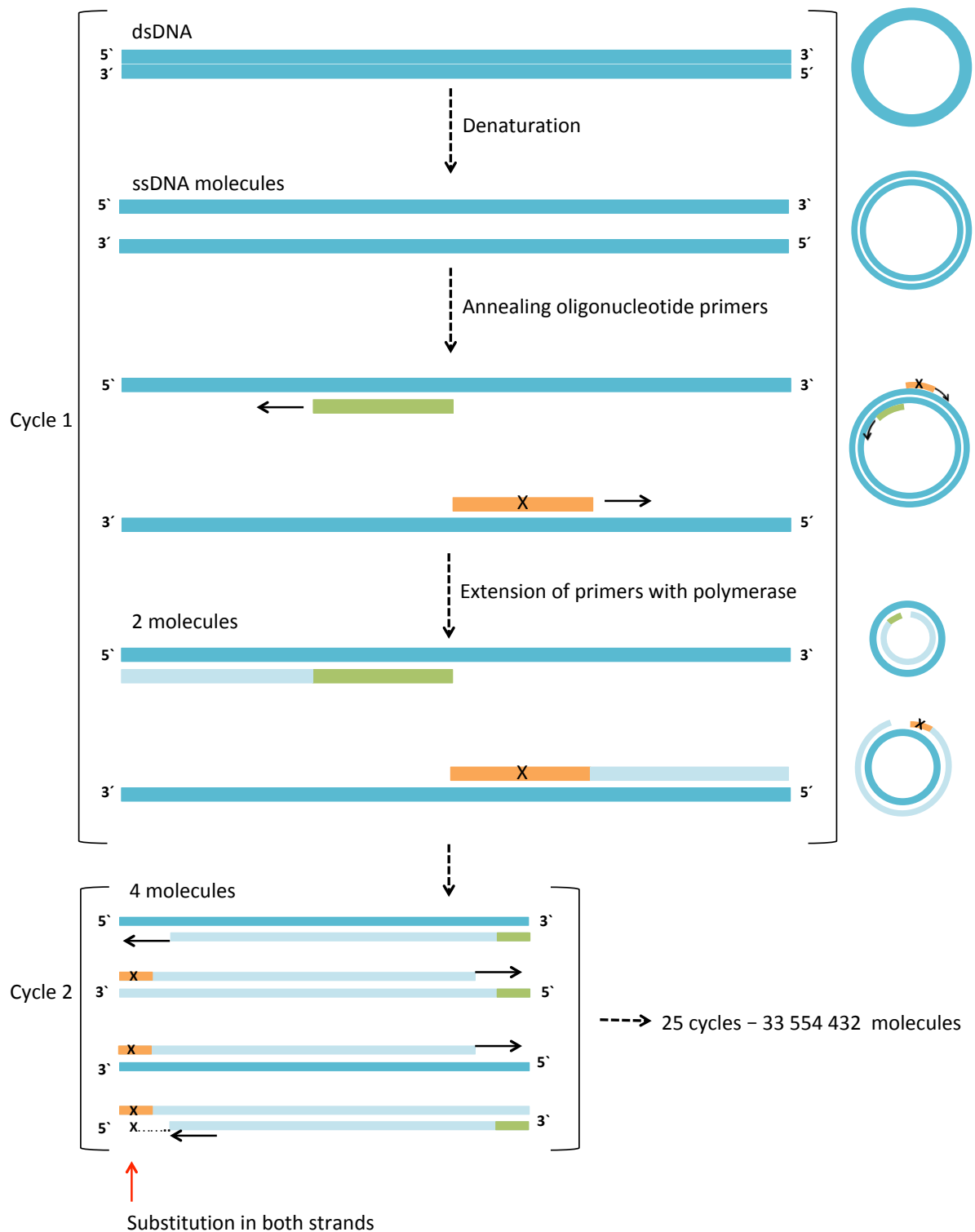


**Figure 2.2:** *In vitro* amplification of DNA using polymerase chain reaction (PCR). The cyclic three-step process is shown: denaturation of dsDNA into two ssDNA, annealing of oligonucleotide primers to the template DNA and DNA synthesis of the target sequence by thermostable *Taq* DNA polymerase I. The case of substitution is also shown, where the forward primer (orange) carries a point mutation (X). When a strand that carries the substitution is used as template, the substitution will be created in both strands (red arrow) (207,208).

The PCR products resulting from each cycle are linear, double-stranded and blunt-ended DNA molecules. These products are further treated with an enzyme mix containing a kinase, a ligase and endonuclease DpnI. The kinase phosphorylates the 5'-ends of linear DNA molecules, which then are recircularized by the ligase through an intermolecular blunt-end ligation. Simultaneously, the endonuclease DpnI will recognise and digest methylated DNA, and thus remove template DNA (methylated) from the recircularized PCR products (not methylated) (207).

### **Procedure for Site-directed mutagenesis (SDM) by Polymerase chain reaction (PCR)**

PCR oligonucleotide primers were designed using NEBase Changer and checked for non-specific hybridization, hairpin structures and mismatches in Benchling (Table 2.5). Site-directed mutagenesis (SDM) was performed according to the NEB Q5® Site-Directed Mutagenesis Kit protocol (207). The reagents for PCR (12.5 µL Q5 hot start high-fidelity, 1.25 µL forward primer (10 µM), 1.25 µL reverse primer (10 µM), 1 µL DNA template (Table 2.9) and 9 µL nuclease-free water) were assembled in a PCR tube, mixed on a vortex and transferred to a PCR thermocycler. PCR was run using the thermocycling conditions as stated in the protocol (Table 2.12). The amplified PCR product was then subjected for enzymatic treatment by mixing 1 µL PCR product, 5 µL KLD reaction buffer, 1 µL KLD enzyme mix and 3 µL nuclease-free water in a new PCR tube. The samples were incubated at room temperature for 5 minutes before transformation.

**Table 2.12.** Thermocycling conditions used for polymerase chain reaction (PCR) for exponential DNA amplification, as described in the NEB 5Q® Site-Directed Mutagenesis Kit protocol (207).

<b>Reaction step</b>	<b>Temperature (°C)</b>	<b>Time (sec)</b>
Initial denaturation	<b>98</b>	<b>30</b>
25 cycles	98	10
	68-72*	30
	72	210-300**
Final extension	72	120
Hold	4	

\*Calculated using the NEB T<sub>m</sub> calculator from New England BioLabs Inc.

\*\*30 sec/kb. Plasmid size: 6.866kb and 10.009kb (Appendix B).

### 2.2.2 Transformation of *E. coli* DH5- $\alpha$

Transformation is a process where competent cells take up foreign genetic material from the environment and pass it on in following generations, either by incorporation in the cell genome or by existing as a plasmid in the cell cytoplasm. Competent cells are in a state where they can take up and utilize extracellular DNA from their surroundings. Competence can be achieved by artificial transformation in the laboratory, e.g. by chemical treating the cells with divalent cations before exposing them to a brief increase in temperature (heat-shock). This is thought to create pores in the plasma membrane, which transiently increase the membrane permeability by opening gated membrane channel proteins, allowing uptake of extracellular DNA into the cell (207,210–213).

#### Procedure for transformation and inoculation of *E. coli* DH5- $\alpha$

A 1,5 mL tube of 50  $\mu$ L NEB® 5-alpha competent *E. coli* cells was thawed on ice. 5  $\mu$ L KLD mix was added to the cells, gently mixed by flicking the tube and incubated on ice for 30 minutes. The cells were heat-shocked (42°C) in a water bath for 30 seconds and instantly transferred back on ice for 5 minutes. 950  $\mu$ L of room tempered SOC medium was added to the tube, before the tube was incubated at 37°C with shaking (250 rpm) for 60 minutes. 100  $\mu$ L of culture was plated onto ampicillin LA selection plates and incubated at 37°C over night. It was also made a concentrated culture, by centrifuging the cells into a pellet, pouring off the medium and resuspending in 100  $\mu$ L LB medium. The concentrated culture was then plated in the same manner as the original culture. The plated cultures were checked the next day, and 2-4 colonies from each LA plate were transferred to 13 mL tubes together with 6 mL of LB medium and 6  $\mu$ L ampicillin (100 mg/mL). The cultures were incubated (37°C) with shaking (250 rpm) over night, for subsequent plasmid isolation.

### 2.2.3 Cultivation of AlgE7 mutants

The AlgE7 wild type and 31 different AlgE7 mutants in the pBG27 plasmids (Table 2.9) were collected from DH5- $\alpha$  glycerol stocks stored at - 80 °C. A sample from each glycerol stock were plated onto ampicillin LA selection plates using a toothpick, and incubated at 37°C over night. One colony from each plate was picked and transferred to liquid cultures for incubation at 37°C with shaking (250 rpm) over night, before plasmid isolation. This was done in the same manner as described in section 2.2.2.

### 2.2.4 Plasmid isolation

Plasmid isolation was performed by alkaline lysis of cells, where cells break open and release their content, from which plasmid DNA can be separated from other cell components (214). Cells grown in a liquid media (broth culture) were harvested by centrifugation and resuspended in a solution containing Tris-HCl and EDTA. Upon cell lysis, these components inhibits cellular enzymes that can damage DNA and binds metal ions essential for preserving the cell wall structure (208). An alkaline lysis solution containing the detergent sodium dodecylsulfate (SDS) and sodium hydroxide (NaOH) results in dissolution of the phospholipid membrane and denaturation of most cell proteins and double-stranded DNA (dsDNA) into single strands (ssDNA). Unlike genomic ssDNA, plasmid ssDNA will not tangle with other denatured molecules because their intertwined strands keep them supercoiled. The neutralization solution ensures reannealing of plasmid ssDNA into dsDNA that dissolves in the solution. Genomic ssDNA is too large for reannealing and will form a complex with SDS, lipids and denatured proteins, resulting in a precipitate removed by centrifugation. In the Monarch® Miniprep Kit, RNase is also added to the neutralization buffer, which acts by degrading cellular RNA. Further isolation and purification of plasmid DNA was done by column chromatography. Plasmid DNA from the cell extract binds the silica matrix in the column. Washing solutions was then added to remove salts, RNA and residual cellular debris, which allows elution of purified plasmid DNA with nuclease-free water (208,215).

#### Procedure for plasmid isolation

Plasmid DNA was isolated from DH5- $\alpha$  and T7 Express Competent *E. coli* cells using the Monarch® Miniprep Kit (215). This procedure contains six main steps: cell resuspension of the cell pellet, cell lysis, neutralization of lysate, binding of plasmid DNA, washing and elution of plasmid DNA. Details are specified in the protocol (215)

### 2.2.5 Measuring plasmid concentration

The concentration and quality of purified plasmid DNA was determined by using a spectrophotometer (NanoDrop™ One). 2  $\mu$ l DNA sample was placed on the pedestal and the absorbance was measured at 260 nm, reporting nucleic acid concentration (ng/ $\mu$ L) and two

absorbance ratios (A260/A280 and A260/A230). The latter was used to determine the quality of purified plasmid DNA, where ratios less than 1.8 indicates contamination (208).

### 2.2.6 Sequencing

DNA sequencing is a technique for determining the nucleotide sequence of a DNA molecule. In Sanger sequencing, multiple copies of the template DNA are produced *in vitro* by DNA replication. Each new DNA strand is terminated with a specific chain-termination nucleotide (dideoxynucleotide (dNTP) – missing the 3' reactive hydroxyl and thus prevents further elongation of the chain), which is incorporated at random by DNA polymerase. This results in fragments of varying lengths, separated based on size on a polyacrylamide gel. The dNTPs can be labelled with fluorescent tags, used to identify the nucleotides at each position in the sequence (208,216).

#### Procedure for preparation of sequencing samples

8  $\mu\text{L}$  purified plasmid DNA (40-60 ng/ $\mu\text{L}$ ) and 2  $\mu\text{L}$  sequencing primer (10 $\mu\text{M}$ ) (Table 2.7) were assembled in a 1.5 mL tube and sent to Eurofins GATC Biotech GmbH for automated Sanger sequencing with their LightRun service. The sequencing results were analysed using Benchling.

### 2.2.7 Glycerol stock

Glycerol stocks are used for long-term storage of bacteria and plasmids. Glycerol is added to the bacteria cultures in order to disrupt hydrogen bonding between water molecules, thereby reducing the formation of ice crystals that can damage the cells during freezing (217).

#### Procedure for glycerol stocks

DH5- $\alpha$  and T7 Express Competent *E. coli* cells were transformed with 1  $\mu\text{L}$  verified plasmid DNA. One colony from each LA plate was inoculated in 1 mL LB medium and 1  $\mu\text{L}$  ampicillin (100 mg/mL) over night (37°C, 250 rpm). The next day, 1 mL overnight culture and 1 mL glycerol (50%) was added to cryotubes and stored at - 80 °C.

### 2.2.8 Transformation of *E. coli* T7 express competent

Transformation and inoculation of T7 express competent *E. coli* cells was performed in the same manner as described for NEB® 5-alpha competent *E. coli* cells in section 2.2.2.

Differences to this description are that T7 Express competent *E. coli* cells were transformed with 1  $\mu$ L of verified plasmid DNA (40-60 ng), and the cells were heat-shocked for 15 seconds.

### 2.2.9 Sequence- and ligation-independent cloning (SLIC)

Sequence- and ligation-independent cloning (SLIC) is a method for assembling two or multiple DNA fragments in a single reaction based on *in vitro* homologous recombination and single-strand annealing. This method relies on an exonuclease (T4 DNA polymerase), which generates ssDNA 5' overhangs in vector and insert fragments, followed by homologous recombination *in vitro* (218).

One approach to SLIC is based on PCR amplification (see section 2.2.1) of the vector backbone and the gene of interest, generating linear dsDNA fragments (219) (Figure 2.3). The oligonucleotide primers used for amplification of the insert fragments must be custom designed with 5' extensions (20 base pairs or longer) that are complementary to the ends of the linearized vector backbone. Amplified linear products of the vector backbone and insert are then assembled and treated with 3' exonuclease T4 DNA polymerase to generate 5' overhangs. In order to stop the action of T4 DNA polymerase, the reaction mixture is placed on ice, which allows annealing of the vector and insert at complementary sequences. This creates a recombined intermediate that is transformed into competent *E. coli* cells, where the cell endogenous repair system fills in missing nucleotides and thus generates covalently closed double-stranded recombinant plasmids *in vivo* (218,219).



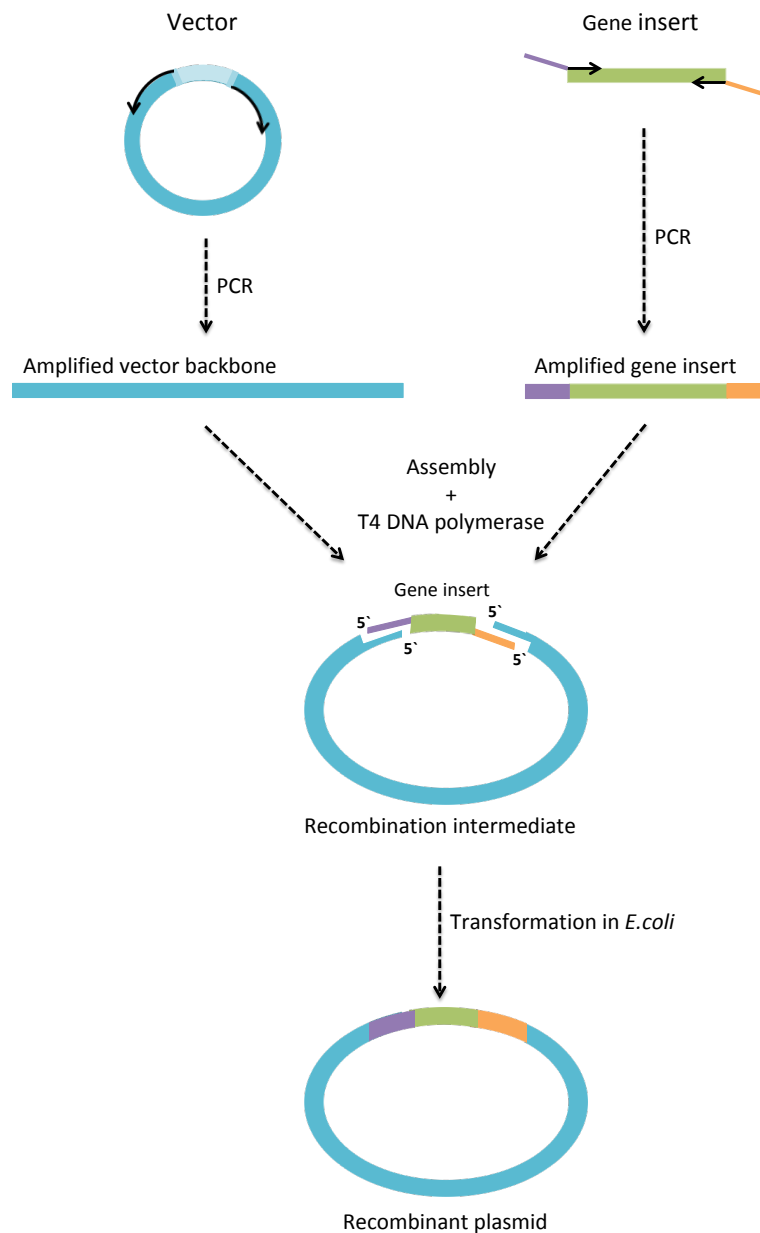


**Figure 2.3.** Production of recombinant plasmid using *in vitro* homologous recombination and single-strand annealing (SLIC). PCR is first used to amplify the vector backbone and gene insert (with 5' extensions), generating linearized PCR products. Amplified products are assembled and treated with T4 DNA polymerase, resulting in complementary 5' overhangs annealing together, before transformation of the recombination intermediate into *E. coli*. The figure is reproduced from Jeong et al. (219), and shows the procedure used in this study.

### Procedure for sequence and sequence independent cloning (SLIC) by PCR

Prior to the SLIC reaction, the pTYB1 vector backbone and *algE7* gene insert were amplified by PCR. The insert PCR reaction was conducted for the five *AlgE7* point mutants: E117K, Y122F, R148G, K172L and K172R in the pBG27 plasmids (Table 2.9).

PCR oligonucleotide primers (Table 2.6) were designed using the NEBuilder assembly tool and checked for non-specific hybridization, hairpin structures and mismatches in Benchling. 12.5  $\mu\text{L}$  Premix Taq<sup>TM</sup> DNA Polymerase (Takara Taq<sup>TM</sup> Version 2.0) (220), 1.25  $\mu\text{L}$  forward primer 1.25  $\mu\text{L}$  forward primer (10  $\mu\text{M}$ ), 1.25  $\mu\text{L}$  reverse primer (10  $\mu\text{M}$ ), 1  $\mu\text{L}$  DNA template and 10  $\mu\text{L}$  DNA template nuclease-free water were assembled in a PCR tube, mixed on a vortex and transferred to a PCR thermocycler. PCR was run using the thermocycling conditions as stated by Takara Bio Inc for using Premix Taq<sup>TM</sup>, and by adding a final extension step (Table 2.13).

**Table 2.13.** Thermocycling conditions used for polymerase chain reaction (PCR) for exponential DNA amplification, as described in the protocol for using Premix Taq<sup>TM</sup> (Takara Taq<sup>TM</sup> Version 2.2)(220). In addition, a final extension step was added to this protocol.

Reaction step	Temperature (°C)	Time (sec)
Initial denaturation	<b>98</b>	<b>30</b>
30 cycles	98	10
	55	5
	72	13-38*
Final extension	72	120
Hold	4	

\*5 sec/kb. Vector backbone: 7.442kb. Insert: 2.567kb

Following amplification, the PCR product was subjected for enzymatic treatment by adding 1  $\mu\text{L}$  DpnI and 2  $\mu\text{L}$  Cutsmart buffer and incubating the PCR tube at 37 °C over night. Gel electrophoresis was used to verify amplification of the linear PCR product (section 2.2.10). The PCR product was purified using the DNA Clean & Concentrator<sup>TM</sup>-5 kit and concentration of the purified DNA was measured as described in section 2.2.5 (221).

The SLIC reaction was performed according to the SLIC protocol proposed in Jeong et al. (219), using a vector to insert molar ratio of 1:2. 1  $\mu\text{L}$  purified backbone PCR product, 1  $\mu\text{L}$  purified insert PCR product, 2  $\mu\text{L}$  10x NEB 2.1 buffer, 1  $\mu\text{L}$  T4 DNA polymerase (NEB, 3u/ $\mu\text{L}$ ) and 15  $\mu\text{L}$  nuclease-free water were assembled in a new PCR tube. The sample was incubated at room temperature for 5 minutes and on ice for another 10 minutes. 10  $\mu\text{L}$  SLIC reaction product was then transformed into DH5- $\alpha$  *E. coli* cells, followed by plasmid isolation, sequencing and transformation of T7 express competent *E. coli* cells (procedures described in sections 2.2.2, 2.2.4-2.2.8).

### 2.2.10 Agarose gel electrophoresis

Gel electrophoresis is a biochemical method for separating molecules of different charge and size by passing an electric current through a gel made of agarose or polyacrylamide. The gel solidifies into a molecular matrix through hydrogen bonding and hydrophobic interactions. This creates pores that allow passage of molecules through the gel when applying an electric field. Charged molecules are deposited at one electrode and migrate in the field toward the oppositely charged electrode. The rate of migration for each molecule depends on its charge, size and shape, the type of gel and the electrophoretic effect – movement of counterions reduce the electrophoretic mobility of the molecules to be separated (208,213).

For separation of DNA molecules, an agarose gel is usually used and negatively charged DNA fragments is separated based on size. Large fragments move slower and a shorter distance than small fragments, due to more friction between the larger DNA fragments and the gel matrix. DNA is a colourless molecule that has to be stained with a nucleic acid stain for visualization. Stained DNA fragments separated on the gel are visualized under ultraviolet (UV) light and identified by comparing to a DNA ladder, consisting of DNA fragments of known sizes (208,213).

#### Procedure for agarose gel electrophoresis

0.8 % agarose with Gel red® was solved in 1xTAE buffer and poured in a casting tray with a well comb to solidify for 20 minutes. The gel was placed in a gelbox filled with 1xTAE buffer. 1µL of 6x DNA gel loading dye (0.7 % v/v) was added to 3 µL of PCR product, before 4µL sample and 0.75 µL GeneRuler 1kb DNA were loaded into separate wells. The gels were run at 90 V for 45 minutes. DNA fragments were photographed in a gel imager and visualized in ImageLab.

### 2.2.11 Recombinant protein expression in *E. coli* T7 express competent

A transcriptional control system is often used to regulate expression of cloned genes. One common strategy is using the lac (lactose) operon, which regulates transcription of enzymes for digestion of lactose. Lactose is used as an alternative carbon source to glucose in *E. coli*, and in order to save energy the lac operon is turned off when glucose is present in the cell. The lac operon is controlled by the regulator gene lacI, encoding a repressor protein that binds to the operator (lacO), which in turn inhibits RNA polymerase from binding to the lac

promoter and transcribing the associated genes. When glucose levels are low and lactose is present in the cell, the lactose metabolite allolactose allosterically binds the lac repressor. This causes it to dissociate from lacO, allowing transcription of genes under lac operon control. IPTG is a molecule that mimics allolactose, and is often used to induce expression of T7 RNA polymerase, which is required for transcription of the target gene (213,222).

### **Procedure for recombinant protein expression**

Expression and purification of recombinant proteins were performed according to the NEB IMPACT<sup>TM</sup> (intein mediated purification with an affinity chitin-binding tag)-CN system (223).

A preculture of T7 Express Competent *E. coli* cells with sequence verified recombinant plasmid was made in a 250 mL Erlenmeyer flask by inoculating 25 mL LB medium containing ampicillin (100 µg/mL), and incubating at 37 °C with shaking (250 rpm) over night. The next day, 500 mL 2xLB medium was inoculated with 5 mL overnight culture and 500 µL ampicillin in a 2 L baffled flask, and incubated at 37 °C with shaking (250 rpm) for 2 hours. After 2 hours of incubation, OD<sub>600</sub> was measured with a spectrophotometer and incubation was continued until OD<sub>600</sub> reached 0.8-1.0. The culture was placed on ice for 5 minutes, induced by adding 500 µL IPTG (0.5M) and incubated (16 °C) with shaking (250 rpm) for 16-20 hours. The culture was transferred to two 250 mL sterile centrifuge tubes and centrifuged (4 °C, 5500 g) for 5 minutes. The supernatant was discarded, and the pellet was immediately used for protein purification or stored at -20 °C for later use.

### **2.2.12 Sonication**

Sonication is a method of disrupting cell membranes and macromolecules by applying ultrasonic pressure waves to agitate particles in a sample. A metal probe is commonly used to produce the pulse, which is also called a sonicator. The effect of heating during sonication can be reduced by using short pulses (10-30 seconds) with 30-60 seconds of break in between as well as keeping the sample on ice bath (20,224,225).

### **Procedure for sonication**

The pellet from the recombinant protein expression procedure (section 2.2.11) was transferred to a 50 mL tube, placed on ice and resuspended in 25 mL protein purification lysis buffer with

¼ EDTA-free protease inhibitor tablet. The resuspended cells were kept on ice bath and sonicated in 3 cycles of 3 minutes each, using a 12 mm flat tip immersed in the cell suspension. The sonication was performed with the following conditions: 40 % amplitude, 50 % duty cycle for 20 seconds, 30 seconds break and changing the ice between each cycle. The lysate was centrifuged (23 000 g) for 30-45 minutes to remove cell debris, before the supernatant was sterile filtrated (0.22 µm) and subjected to protein purification.

### 2.2.13 Fast protein liquid chromatography (FPLC)

Column chromatography is a technique for separating a mixture of components through a column, based on the components affinity toward a porous stationary phase and a fluid mobile phase. For purification and analysis of proteins, fast protein liquid chromatography (FPLC) is widely used (20,226). One approach to FPLC is using a column matrix covered with a ligand that specifically binds to an affinity tag fused to the protein of interest, thus separating the protein from the mixture. The NEB IMPACT<sup>TM</sup>-CN system utilizes an inducible self-cleavable splicing element (intein) combined with a chitin-binding domain (CBD) as the affinity tag (Figure 2.4). On the chitin resin column, the CBD will bind and immobilize the proteins containing the CBD-intein tag to the column, allowing other proteins and cellular debris to be washed out. Addition of thiol reagents such as 1,4-dithiotheritol (DTT) is then used to induce on-column cleavage, releasing the target protein from the CBD-intein tag. This allows elution of the target protein from the column (223).

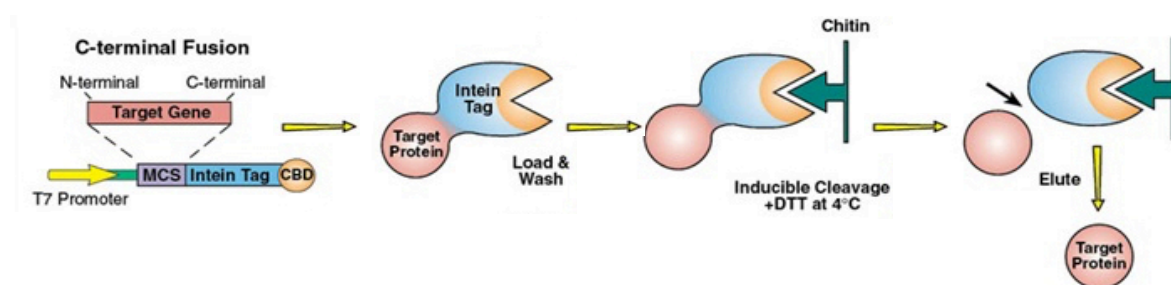


**Figure 2.4.** Illustration of affinity purification of proteins, as described in the IMPACT<sup>TM</sup>-CN system protocol with C-terminal fusion. The C-terminal of the target gene is fused to the N-terminal of an inducible self-cleavable splicing element (intein) containing a chitin-binding domain (CBD). The CBD binds to the chitin resin column, separating the target protein from other proteins and cellular debris, which is washed out. Induction of on-column cleavage by adding 1,4-dithiotheritol (DTT), releases the target protein from affinity CBD-intein tag, allowing elution of the target protein from the to be eluted from the column (223).

**Procedure for affinity purification and on-column cleavage**

The chitin column was prepared by letting the chitin beads (resin) set for 30 minutes and washing with 10 column volumes of column buffer (2 mL/min). Water cooling was turned on, before loading the clarified cell extract onto the column (1 mL/min). The column was washed with 10 column volumes of column buffer (2 mL/min) and further with 3 column volumes of freshly prepared cleavage buffer (2 mL/min), placed on ice. After flushing with the cleavage buffer, water cooling and column flow was turned off, and the column was left in room temperature for 16-40 hours. The target protein was eluted from the column in six 5 mL fractions using the column buffer (2 mL/min).

After elution of protein, the chitin column was regenerated with regeneration buffer (2 mL/min) for 30 minutes. The resin was then allowed to soak for 30 minutes by turning of the column flow. The column was further washed with regeneration buffer (2 mL/min) for 60 minutes, then with MQ® water (2 mL/min) for 60-100 min and finally with 20 % Ethanol (2 mL/min) for 45 minutes. The column was stored at 4 °C. FPLC experiments were conducted by using the Unicorn 5.01 software.

**2.2.14 Sodium dodecyl sulphate-polyacrylamide gel electrophoresis (SDS-PAGE)**

Sodium dodecyl sulphate-polyacrylamide gel electrophoresis (SDS-PAGE) is a gel electrophoresis technique for separating proteins based on molecular weights. It is used to verify a target protein and evaluate sample purity after protein purification. Polyacrylamide gels have smaller pore size compared to agarose gels and are therefore better suited to separate proteins, which usually are too small to be separated in an agarose gel. Samples for PAGE are prepared with the anionic detergent SDS that binds to and denatures proteins, giving them a uniform negative charge proportional to their length. For complete denaturation, samples are also treated with reducing agents such as  $\beta$ -mercaptoethanol and tris(2-carboxyethyl) phosphine (TCEP), which breaks disulfide bonds in the protein structure (20,216,226).

### **Procedure for Sodium dodecyl sulphate-polyacrylamid gel electrophoresis (SDS-PAGE)**

Samples for SDS-PAGE were collected at different stages during the protein expression and purification procedure (purple pathway, Figure 2.1). The following samples were obtained:

- Uninduced sample: 1 mL culture was transferred to a 1.5 mL tube prior to protein induction (Section 2.2.11), centrifuged (16 000 g) for 10 minutes, before resuspending the pellet in 50  $\mu$ L SDS sample buffer.
- Induced sample: 1 mL culture was transferred to a 1.5 mL tube after protein induction (Section 2.2.11), centrifuged (16 000 g) for 10 minutes, before resuspending the pellet in 50  $\mu$ L SDS sample buffer.
- Cell lysate sample: 10  $\mu$ L sterile filtrated (0.22 $\mu$ m) cell lysate (Section 2.2.12) was transferred to a 1.5 mL tube mixed with 10  $\mu$ L SDS sample buffer.
- Cell debris sample: A small piece of cell pellet (Section 2.2.12) was transferred to a 1.5 mL tube and resuspended in 50  $\mu$ L SDS sample buffer.
- Eluted FPLC fractions: 10  $\mu$ L of each eluted protein fraction (Section 2.2.13) were transferred to a 1.5 mL tube and mixed with 10  $\mu$ L SDS sample buffer.

Prior to running the gel, all samples were heated on a block heater (95 °C) for 10 minutes and centrifuged (16 000 g) for 10 minutes. The samples was then loaded to a ready-made polyacrylamide gel (12 %, ClearPAGE™) in the specified amount and order:

- Gel well number 1-4: 10  $\mu$ L of uninduced sample (no.1), induced sample (no.2), cell lysate sample (no.3) and cell debris sample (no.4).
- Gel well number 5: 5  $\mu$ L of Precision plus protein™ all blue standards
- Gel well number 6-12: 10  $\mu$ L of each purified protein fractions applied in the eluted order

The gel was run in SDS running buffer at 130 V for 85 minutes, gently rinsed in RO water and transferred to a large Petri dish. Then, the gel was stained with InstantBlue™ and placed on an orbital shaker for 1 hour. The purified protein was photographed in a gel imager and visualized in ImageLab.

### 2.2.15 Dialysis

Dialysis is a laboratory technique for separating molecules in a solution by diffusion over a semipermeable membrane driven by a concentration gradient. The technique is often used to remove small unwanted molecules such as dyes, reducing agents and salts from a solution of macromolecules. Dialysis membrane tubes have a specific molecular weight cut off (MWCO), allowing passage of molecules below the cut-off size limit, while retaining larger molecules. This causes smaller molecules to equilibrate between the buffer solution and the dialysis membrane tubing containing the macromolecules. The dialysis process is more efficient by using a high buffer to sample volume ratio and changing the dialysate at least twice (20,222,225).

#### Procedure for dialysis

Assessment of the SDS-PAGE was used to combine the purified protein fractions that had approximately same amount of protein. This resulted in three dialysis tubes for each protein sample.

Dialysis membrane tubing (Spectra/Por®, MWCO 6-8 kDa) was placed in RO water for 30 minutes. The membrane was rinsed on the inside and the outside with RO water, and closed in one end by tying a knot and attaching a dialysis tubing closure clip. The purified protein sample was then transferred to the tubing by using a pipette, before closing the other end in the same manner as the first. The sealed tubing was immersed in a dialysis buffer with a buffer to sample volume ratio of 1:100. The buffer was changed six times. The dialysed sample was then transferred to a 50 mL tube and subjected for freeze-drying.

### 2.2.16 Freeze-drying

Freeze-drying (lyophilisation) is a dehydration process in which frozen solvent and water molecules are removed from a material by sublimation. Sublimation denotes the phase change of a substance from a solid state to gas, without passing through an intermediate liquid phase (Figure 2.5.A). Freeze-drying is an effective method used for preserving variety of heat-sensitive materials such as foods, pharmaceuticals and other biotechnological products. The materials are first crystallized at low temperature under atmospheric pressure, before they are transferred to a freeze-dryer chamber and maintained in a frozen state under vacuum conditions. When the pressure inside the drying chamber is lowered to a value corresponding



to the vapour pressure curve (sublimation curve) (Figure 2.5.B), the sublimation process takes place and vapour released condenses on the ice condenser coils. Finally, residual water molecules adsorbed to the material is removed at a higher temperature and the lowest possible pressure through a process called desorption (227–229).

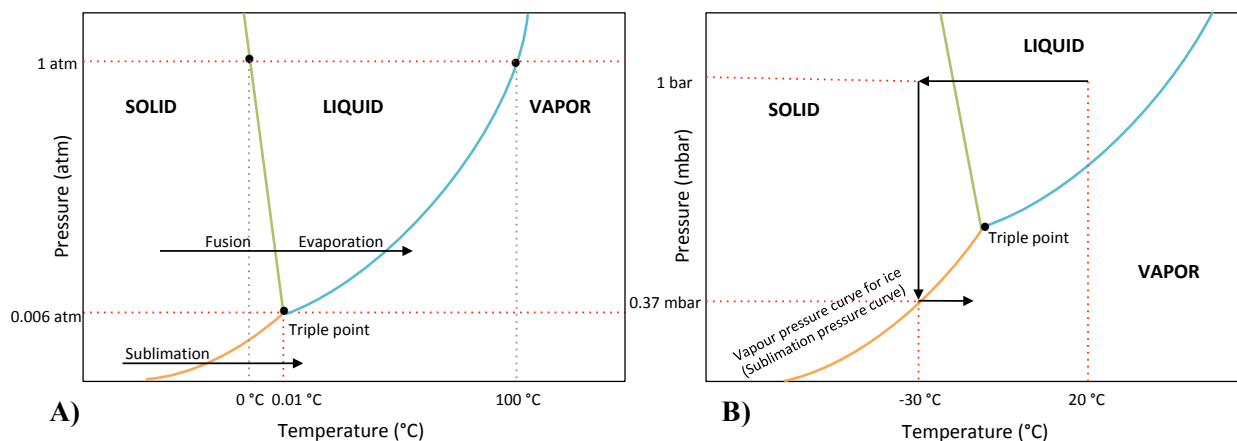


**Figure 2.5.** Phase diagram for water showing the three phases (solid, liquid and vapour) and under which conditions the phases coexist at equilibrium (A). The fusion curve (green), evaporation curve (blue) and the sublimation curve (orange) signify the pressure of at equilibrium for solid and liquid, liquid and vapour, and solid and vapour, respectively. Under freeze-drying, the pressure is lowered to a value corresponding to the sublimation curve, enabling sublimation to take place. The figure is reproduced from Christ (228).

### Procedure for freeze-drying

The 50 mL tube containing the dialysed protein sample or the 1.5 mL tube containing the alginate product after epimerase and lyase reaction (section 2.2.19) was frozen in liquid nitrogen. The lid of the tube was removed and the opening was covered with parafilm, in which small holes were made with a needle. The sample tube was then placed in a Fast-Freeze® flask, which was attached to the drying chamber on the freeze-dryer and freeze-dried for 1-3 days.

### 2.2.17 AlgE7 lyase-activity assay

As mentioned in sections 1.2.3-1.3, alginate lyase activity generates unsaturated uronic acid residues ( $\Delta M$  in AlgE7) upon cleavages of glycosidic linkages in polymer chain (13,55). The unsaturated residue has a strong absorbance peak at 230 nm ( $A_{230}$ ) and measurements of this parameter have therefore been used as a measure of the lyase activity in all AlgE7 mutants in made in this and previous studies (Table 2.9) (199).

**Procedure for protein expression, SDS-PAGE and AlgE7 lyase-activity assay**

The following experimental procedures were conducted by Randi Aune at SINTEF - Department of Biotechnology and Nanomedicine.

Preculture of T7 Express Competent *E. coli* glycerol stocks (75  $\mu$ L) were made in greiner 96-FB-well plates by inoculating the cells in 75  $\mu$ L LB-medium containing ampicillin (100  $\mu$ g/mL), and incubated at 30 °C, 850 rpm) and 75 % relative humidity over night. The next day, 510  $\mu$ L reduced Hi-Ye medium containing ampicillin (100  $\mu$ g/mL) was inoculated with 10  $\mu$ L overnight culture on new 96-DB-wellplates, and incubated at 30 °C, 850 rpm and 80 % relative humidity. After 6-8 hours of incubation, 260  $\mu$ L Glycerol-Ye-induction medium was added to the each well in the 96-FB-wellplates, before incubation at 16 °C and 850 rpm for 16 hours. 10 $\mu$ L of culture was transferred to new 96-FB-wellplates for measuring OD<sub>600</sub> (the culture was diluted with 90  $\mu$ L 0.9% NaCl), before the microplates were centrifuged (3500 g) for 10 minutes. The supernatant was discarded, and 700  $\mu$ L B-per II solution containing benzonase (2  $\mu$ L/mL) was added to each well. The microplates were sealed using aluminium Costar sealing tape and the plates were shaken (3000 rpm) for 1 minute before incubation in room temperature for 1 hour. After incubation, the microplates were shaken (3000 rpm) for 1 minute and centrifuged (3200 g) for 10 minutes. The resulting B-per II enzyme extracts were transferred to new 96-FB-well plates.

In order to verify protein production in the B-per II enzyme extract, SDS-PAGE was performed using a similar procedure as described in section 2.2.14. Exceptions to this procedure was that Precision Plus Protein<sup>TM</sup> Dual Color standard were used as molecular weight standard and the gels were run at 150 V for 1 hour.

The AlgE7 lyase-activity assay was set up by adding 180  $\mu$ L Tris-HCL buffer (50 mM) containing 2.5 mM CaCl<sub>2</sub> (concentration in well), 50  $\mu$ L poly-M alginate (1 mg/mL) and 20 $\mu$ L B-per II enzyme extract to each well on a Costar UV-transparent microplate. The plates were shaken at 800 rpm for 1 minute and placed on a Spectrax ABS Plus microplate reader. The absorbance at 230 nm (A<sub>230</sub>) was measured every 5 minute for 18 hours. The measured absorbance was used to evaluate the degree of lyase activity in the different AlgE7 mutants.

### 2.2.18 Proton nuclear magnetic resonance ( $^1\text{H-NMR}$ ) spectroscopy

Nuclear magnetic resonance (NMR) spectroscopy is a method that measures nuclei absorption of electromagnetic radiation in the radiofrequency region when the molecules are placed in a strong magnetic field. This is a widely used analytical tool for elucidating the chemical composition and molecular structure of organic molecules (230).

All atomic nuclei carry a charge due to positively charged protons and will generate a magnetic dipole if the charge “spins” around the nuclear axis. The resulting nuclear spin is called the angular momentum of the atomic nucleus and is characterized by a nuclear spin quantum number ( $I$ ). This number depends on both the atomic mass and the atomic number of the nuclei, and can take up values of  $0, \frac{1}{2}, 1, \frac{3}{2}$  etc. When atomic nuclei with  $\frac{1}{2}$  spin (e.g.  $^1\text{H}$  and  $^{13}\text{C}$ ) are placed in a magnetic field, the nuclei can take on two spin states. The gap between these spin states are called  $\Delta E$ , and by applying radiofrequency radiation pulse that equals  $\Delta E$  the nuclei will absorb energy. This changes the nuclei from a lower to a higher energy level, which in turn causes emittance of electromagnetic radiation when the excited nuclei return to its ground state. This emitted energy can be detected by a NMR instrument (230,231).

Atomic nuclei are shielded by local electrons within a molecule. This causes each nucleus in a molecule to have a characteristic resonance frequency, described by its chemical shift ( $\delta$ ). The chemical shift ( $\delta$ ) is defined as the resonance frequency of an atomic nucleus in relation to a reference compound ( $\delta=0$ ). It is a dimensionless unit independent of the strength of the magnetic field, which is expressed in parts per million (ppm) (230,231).

Usually, high molecular weight alginate samples are depolymerized by acid hydrolysis to an average chain length ( $\text{DP}_n$ ) of 30-50 monomers before NMR analysis. This is done in order to reduce the viscosity in solution, providing a sufficient resolution in the NMR spectrum (22,24,232). In this study, alginate samples epimerized by AlgE7 was analysed. The AlgE7 enzyme also has lyase activity, causing cleavage of the alginate chain (146,168). Therefore, the alginate samples were not degraded prior NMR analysis in this study.

Proton nuclear magnetic resonance ( $^1\text{H-NMR}$ ) spectroscopy can be used to determine the monomer frequencies in the alginate polymer, that is the molecular fractions of M ( $F_M$ ) and G ( $F_G$ ) residues (22). The molecular fractions of the four diads ( $F_{MM}$ ,  $F_{MG}$ ,  $F_{GM}$  and  $F_{GG}$ ) and the eight triads ( $F_{MMM}$ ,  $F_{MMG}$ ,  $F_{GGM}$ ,  $F_{MGM}$ ,  $F_{GMG}$ ,  $F_{GGM}$ ,  $F_{MGG}$  and  $F_{GGG}$ ) can also be calculated from  $^1\text{H-NMR}$  (22–24). In addition, the molar fractions of residues comprising reducing ends ( $F_{G_{red}}$ ,  $F_{M_{red}}$ ) and unsaturated non-reducing ends ( $F_{\Delta}$ ), resulting from cleavage of the alginate chain can be calculated. An example of a  $^1\text{H-NMR}$  spectrum of alginate epimerized and degraded by AlgE7 is given in Figure 2.6 (168).

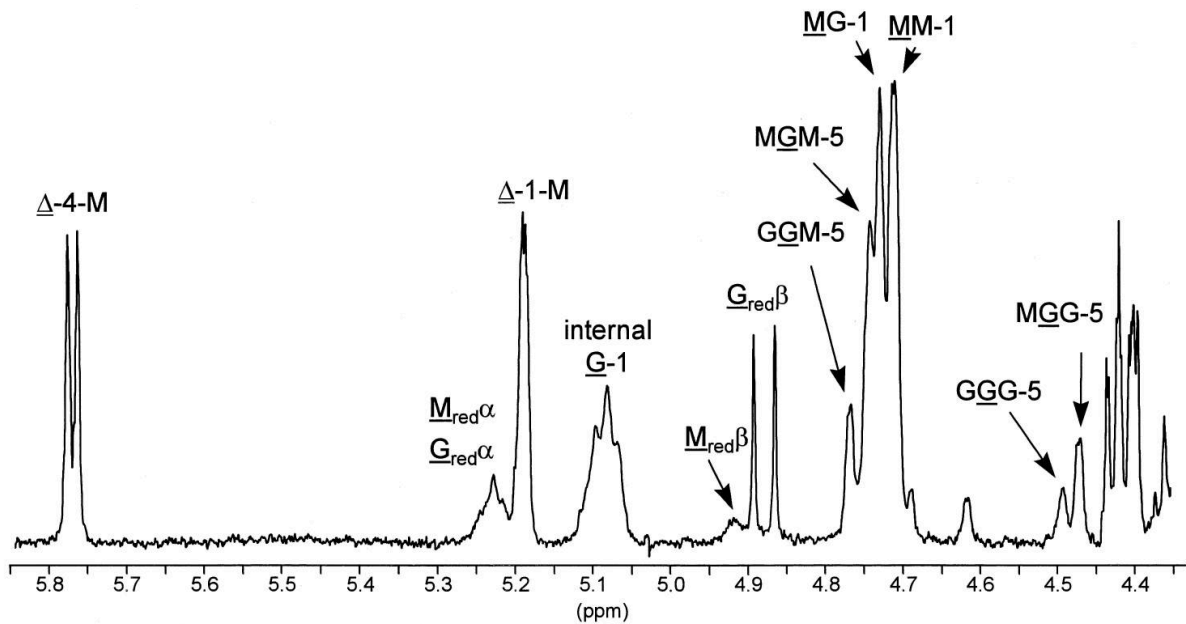


**Figure 2.6.**  $^1\text{H-NMR}$  spectrum of alginate ( $F_M=0.95$  and  $F_G=0.0$ ) epimerized and cleaved by AlgE7. The spectrum shows the anomeric region of alginate in 300 MHz. The  $\underline{G}$ ,  $\underline{M}$ ,  $\underline{G}_{red}$ ,  $\underline{M}_{red}$  and  $\underline{\Delta}$  denote internal G residues, internal M residues, G and M residues at the reducing end and the unsaturated non-reducing end (4-deoxy-L-erythro-hex-4-enopyranosyluronate), respectively. The numbers represents the position of the proton in the sugar ring (H-1 and H-5 proton) and neighbouring G and M residues are shown with no underline (146).

In this study, the molar fractions ( $F$ ) were estimated by integration of the signals intensities ( $I$ ) in the anomeric region (Figure 2.6), and calculated according to the “maximum-averaging method” using the following relations:

$$I(G) = 0.5((G1+GGG5+MGG5) + 0.5(GGM5+MGM5+MG1)) \quad (2.1)$$

$$I(M) = 0.5(GGM5+MGM5+MG1) + MM1$$

$$I(GG) = 0.5(G1+GGG5+MGG5 - 0.5(GGM5+MGM5+MG1)) \quad (2.2)$$

$$I(GM) = 0.5(GGM5+MGM5+MG1)$$

$$\begin{aligned}
I(\text{MM}) &= \text{MM1} \\
I(\text{GGM}) &= 0.05(\text{GGM5} + \text{MGM5} + \text{MG1}) \times \text{GGM5} / (\text{GGM5} + \text{MGM5}) \quad (2.3) \\
I(\text{MGM}) &= 0.05(\text{GGM5} + \text{MGM5} + \text{MG1}) \times \text{MGM5} / (\text{GGM5} + \text{MGM5}) \\
I(\text{GGG}) &= I(\text{GG}) - I(\text{GGM})
\end{aligned}$$

$$\begin{aligned}
I(\Delta) &= \Delta\text{-1-M signal} \quad (2.4) \\
I(\text{G}_{\text{red}}) &= \text{G}_{\text{red}}\beta + (\text{G}_{\text{red}}\beta \times 0.2) \\
I(\text{M}_{\text{red}}) &= \text{M}_{\text{red}}\beta + (\text{M}_{\text{red}}\beta \times 2.2)
\end{aligned}$$

$$\begin{aligned}
I(\text{total}) &= I(\text{G}) + I(\text{M}) + I(\Delta) + I(\text{M}_{\text{red}}) + I(\text{G}_{\text{red}}) \quad (2.5) \\
I(\text{Gtotal}) &= I(\text{G}) + I(\text{G}_{\text{red}}) \\
I(\text{Mtotal}) &= I(\text{M}) + I(\text{M}_{\text{red}})
\end{aligned}$$

From this, molar fractions of the parameters can be calculated as:

$$\begin{aligned}
F(\text{the specific parameter}) &= I(\text{the specific parameter}) / I(\text{total}) \quad (2.5) \\
\text{Example: } F_{\text{M}} &= I(\text{M}) / I(\text{total})
\end{aligned}$$

Reducing end signals can further be used to calculate the number average degree of polymerization ( $DP_n$ ), that is the average number of monomer residues per alginate chain in the alginate sample analysed.  $DP_n$  can be calculated by equation 2.6:

$$DP_n = \frac{I(\text{total})}{I(\text{M}_{\text{red}}) + I(\text{G}_{\text{red}})} \quad (2.6)$$

### **Procedure for epimerase and lyase reaction using enzyme extract (orange pathway)**

0.5 mg poly-M alginate substrate (Table 2.1.7) and 360  $\mu\text{L}$  RO water was added to 1.5 mL tubes, and placed on a tube rotator until the substrate was dissolved. Then, 100  $\mu\text{L}$  epimerase and lyase reaction buffer 5x containing 25 mM HEPES and 12.5 mM  $\text{CaCl}_2$  were added to the tubes, before 40  $\mu\text{L}$  B-Per II enzyme extract of unknown concentration was added. The tubes were placed on a tube rotator and incubated at room temperature for 24 hours. The enzyme reaction in were terminated by adding 120  $\mu\text{L}$  EDTA (50 mM) to the 1.5 mL tubes, before heating samples on a block heater (95  $^\circ\text{C}$ ) for 15 minutes. The samples were then frozen in liquid nitrogen and freeze-dried, before subsequent  $^1\text{H}$ -NMR spectroscopy.

### **Procedure for epimerase and lyase reaction using purified enzyme (purple pathway)**

The epimerase and lyase reaction on alginate substrate using purified enzyme was performed in almost the same manner as described in the previous paragraph. Differences to this description are that the samples were prepared in a 15 mL tube with 10 mg alginate substrate, 3.2 mL RO water, 800  $\mu$ L epimerase and lyase reaction buffer, and purified enzyme with a substrate to enzyme ratio of 1:300 (w/w). These samples were incubated at 25 °C with shaking (170 rpm) for 6, 12, 24, 36, 48 and 60 hours, by transferring 0.5 mL sample from the 15 mL tube to a 1.5 mL tube at each time point.

### **Procedure for $^1\text{H}$ -NMR spectroscopy**

Samples for characterization by NMR spectroscopy were prepared by dissolving the freeze-dried samples in 500  $\mu$ L  $\text{D}_2\text{O}$  (99.9%). 2.5  $\mu$ L TSP (1%) and 20  $\mu$ L TTHA (0.3M, pH7) was added, before transferring the samples to NMR sample tubes. The samples were analysed using a 400 MHz NMR spectrometer equipped with a 5 mm SmartProbe at 83 °C. Spectra were obtained using the following acquisition parameters: pulse program = zg30, number of scans = 64, spectral width = 10 ppm, water signal (reference to TSP) = 4.24 ppm. The spectra were analysed in Topspin 4.0.7 and the data were processed using the equation 2.1-2.6 presented above.

### **2.2.19 Time resolved $^{13}\text{C}$ -NMR spectroscopy**

Time-resolved  $^{13}\text{C}$ -NMR spectroscopy is an application of NMR to carbon, measured continuously over time. This allows chemical compounds to be monitored during a reaction that changes the chemical composition and molecular structure. The same principle as described for  $^1\text{H}$ -NMR applies for  $^{13}\text{C}$ -NMR, and instead of detecting proton nuclei, resonances from the  $^{13}\text{C}$  isotope carbon are detected by the NMR instrument. The natural abundance for  $^{13}\text{C}$  is ~1.1 %. In addition, the nuclei have a lower gyromagnetic ration. This results in the  $^{13}\text{C}$  to be less compared to  $^1\text{H}$ -NMR. This can be improved by using  $^{13}\text{C}$ -enriched substrates (233).

When studying C5-mannuronan epimerases, this method can be used to obtain detailed information about the mode of action on alginate substrates. Using  $^{13}\text{C}$ 1-labelled substrate simplifies the NMR spectrum, as it is only the anomeric signal that is followed in the reaction. In the recorded spectra for time-resolved  $^{13}\text{C}$ -NMR, signals for the triads  $\text{MMM}$ ,  $\text{MMG}$ ,

GGM, MGM, GMG GGM, MGG and GGG can be identified. For the action of Alge7 enzyme on alginate substrates, signals for reducing ends of M and G residues and unsaturated non-reducing ends can also be identified (158,183,233).

The HSQC (heteronuclear single quantum coherence) spectrum is two-dimensional (2D) with one axis for proton ( $^1\text{H}$ ) and the other for a heteronucleus – an atomic nucleus other than a proton such as  $^{13}\text{C}$ . The spectrum contains a signal for each proton attached to the carbon being considered. The HSQC can help resolve overlapping signals in the 1D spectrum (of proton or carbon) in a 2D plan, and thus facilitate a more complete assignment of all signals obtained (233).

### **Alginate substrates**

The alginate substrates used for time-resolved NMR analysis are listed in Table 2.10 and the concentration of substrates used was as follows:

$^{13}\text{C}$ 1-enriched poly-M = 11.25 mg/mL

$^{13}\text{C}$ 1-enriched poly-MG = 11.6 mg/mL

$^{13}\text{C}$ 1-enriched oligo-G = 11.4 mg/mL

### **Procedure for Time-resolved NMR spectroscopy of epimerized alginate samples**

The following experimental procedure was conducted by Professor Finn L. Aachmann at NTNU – Department of Biotechnology and Food Science.

Time-resolved NMR spectra were recorded on BRUKER Ascend 800 MHz AVIIIHD equipped with 5 mm cryogenic TCI probe at NV NMR center. The time-resolved NMR recording the epimerization reaction was performed at 25 °C.

For the time-resolved NMR analysis of epimerization reactions, a stock solution of 250-3000  $\mu\text{L}$  of  $^{13}\text{C}$ 1-enriched alginate polymers in 5 mM MOPS, pH 6.9 with 75 mM NaCl in 99.9 %  $\text{D}_2\text{O}$  was prepared. Purified enzyme fractions from ion exchange chromatography were subject to buffer exchange and concentrated (final concentration around 0.3 mg/mL) up by spin columns with MWCO 3 kDa. Samples were washed with 5 mM MOPS, pH 6.9 with 75 mM NaCl and 27.5 mM  $\text{CaCl}_2$  in 99.9%  $\text{D}_2\text{O}$ . The enzyme concentrations were determined by Nanodrop. 160  $\mu\text{L}$  of  $^{13}\text{C}$ 1-enriched polymer stock solution (in 3 mm NMR tube) was preheated in the NMR instrument and 1D proton and carbon spectra were recorded to ensure

that the sample had not undergone any degradation or contamination prior to the time-resolved NMR experiment. 16  $\mu\text{L}$  of enzyme solution was added to preheated substrate and mixed by inverting the sample four times. The sample was then immediately inserted into the preheated NMR instrument and the experiment was started.

The recorded spectrum is a pseudo-2D type experiment recording a 1D carbon NMR spectrum every 5 minutes, with a total of 200 time points (total experiment time 16h 40m). The recorded 1D carbon spectrum (using inverse gated proton decoupling) contains 16K data points and has a spectral width of 200 ppm, 48 scans with a  $30^\circ$  flip angle, and relaxation delay of 2.1 s (total recording time of 121s). The spectra were recorded, processed and analyzed using TopSpin 3.6p17 software (Bruker BioSpin).





## 3 Results

### 3.1 Bioinformatics analysis

32 single amino acid point mutants and 10 combined amino acid mutants were included in this study (Table 2.9), of which 9 single mutations and 2 combination mutants were constructed in this study. The mutant candidates designed in this study were selected based on structural analysis of a 3D homology model of AlgE7 and an multiple sequence alignment of the A-modules identified in the all AlgE epimerases.

#### 3.1.1 Structural study of AlgE7

As described in section 1.3, the structure of the AlgE7 enzyme has not yet been solved. In order to identify amino acid residues surrounding the active site, a homology model of the AlgE7 A-module was made using the SWISS-MODEL server (234,235) (Figure 3.1.). This server created two homology models using AlgE4 A-module (Protein Data Bank code 2PYG) and AlgE6 A-module (Protein Data Bank code 5LW3) as templates. The model based on the A-module of AlgE4 was chosen, because this model had slightly higher sequence identity (65.16%) than the model based on A-module of AlgE6 (62.94%). The model shows a similar right-handed parallel  $\beta$ -helix structure as identified for the AlgE4 and AlgE6 A-modules. When visualized in PyMOL, the catalytic residues were identified and (Y149, D152, H154 and D178), which are highlighted in the structure in Figure 3.1.

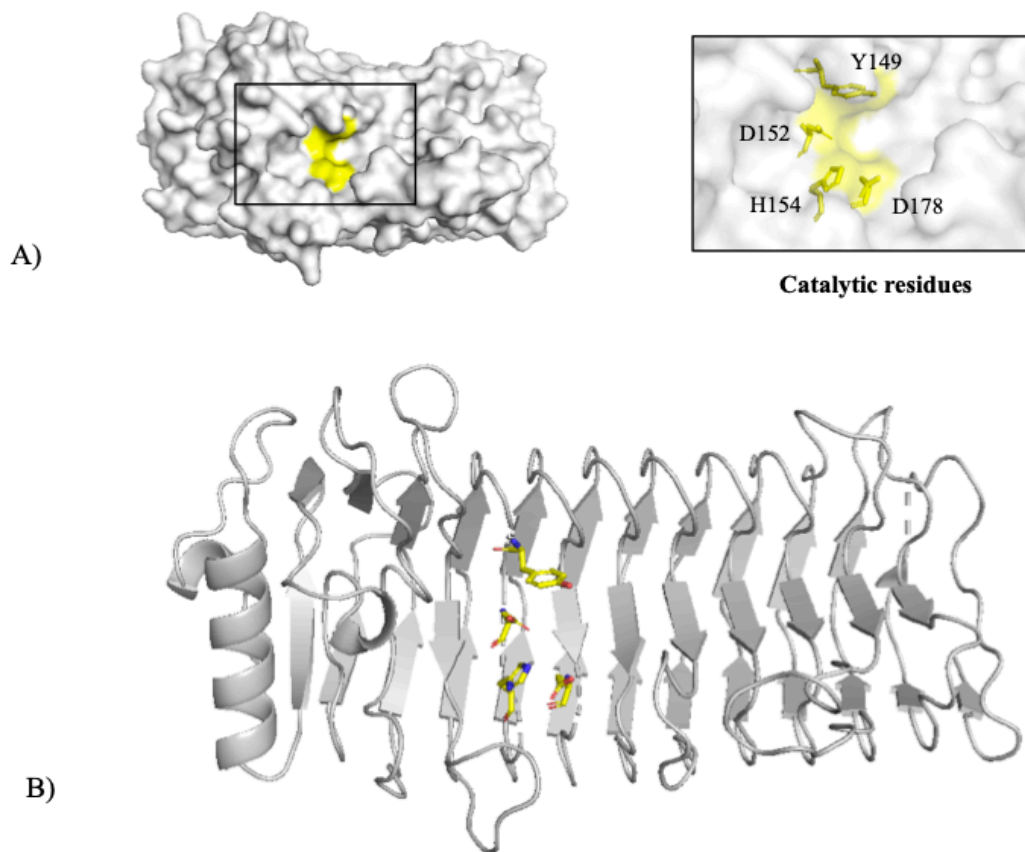


**Figure 3.1.** Homology model of the AlgE7 A-module made using the SVISS-MODEL server (234,235), using the AlgE4 A-module (Protein Data Bank code 2PYG) as template. **A)** Surface view of the homology structure with the position of the catalytic residues: Y149, D152, H154, D178 (yellow). **B)** Secondary motifs of the homology structure: the spiral represents an  $\alpha$ -helix and flat arrows represent  $\beta$ -sheets connected by loops. The structure was visualized in PyMOL.

The homology model of the AlgE7 A-module was further tested using the YASARA Energy Minimization Server (236). This server performs an energy minimization using the YASARA force field that has a stable energy minimum close to native structures, and thus moves the amino acid residues in the model into more stable conformations (236). By structurally aligning the homology model with the energy minimized model in PyMOL, it was observed very small changes of the whole model and the position of the catalytic residues (Figure 3.2.). The homology model was therefore thought to be a reliable model for studying residues surrounding the active site.

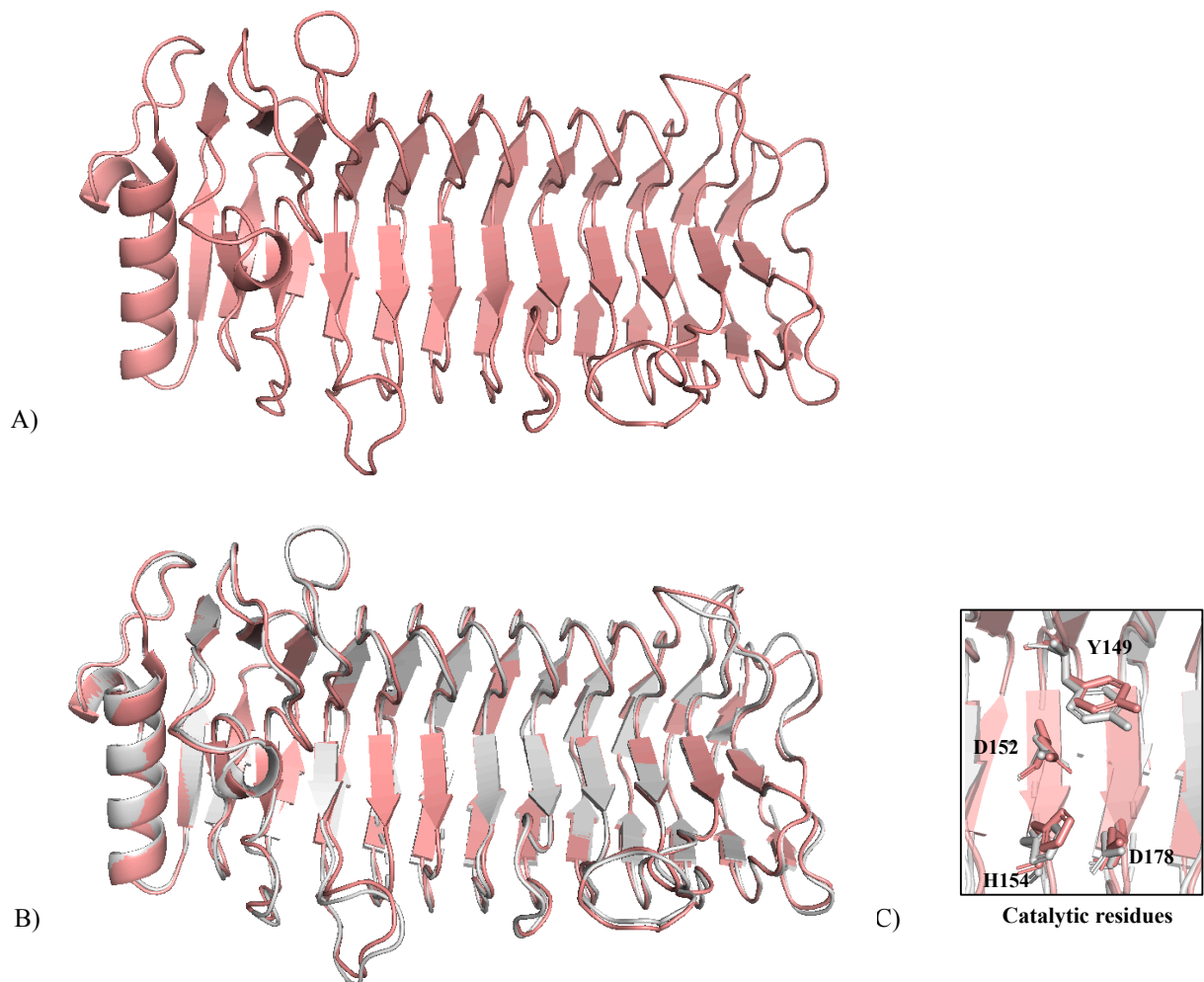


**Figure 3.2.** **A)** Energy minimized model of the AlgE7 A-module made using the YASARA Energy Minimization Server (236), shown with secondary motifs. **B)** Structural alignment of the homology model of AlgE7 (grey) and the energy minimized model (pink). **C)** Alignment of the catalytic residues (stick model). The structures was visualized and aligned in PyMOL.

As described in the following sections, mutant R148G was the only protein that was purified in addition to the AlgE7 wild type. This mutant has therefore also been tested with energy minimization. This was done by introducing the mutation in the original homology model using the WHAT IF web server, followed by energy minimization of the mutated model (236,237). The resulting energy minimization model was structurally aligned to the mutated homology model in PyMOL. Very similar changes were seen as for the wild type model shown in Figure 3.2. No change in position of the mutated residue R148G were seen in the alignment of the mutated and the energy minimalized model (Figure 3.3.A). By studying the same residue in the alignment of the homology and energy minimized model for the wild type, a larger change in position for this residue was seen (Figure 3.3.B).

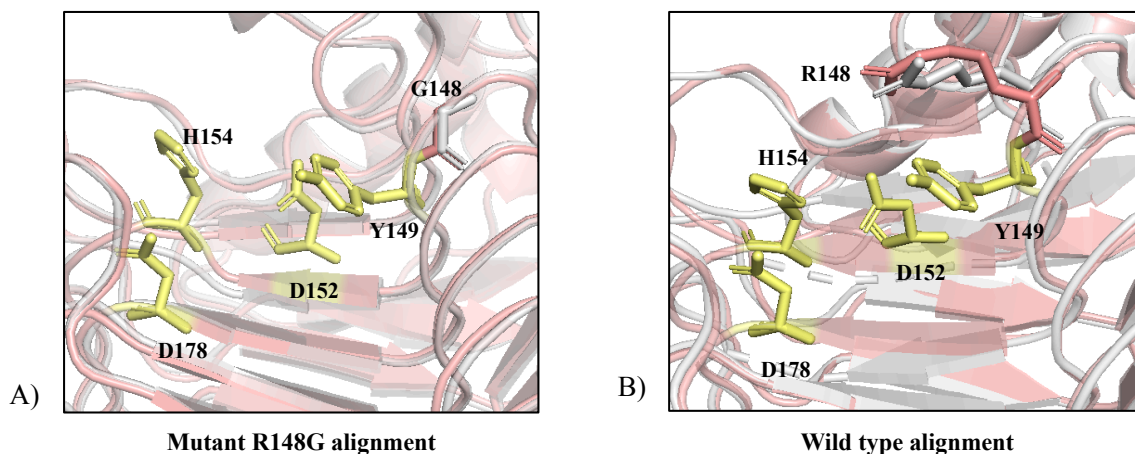


**Figure 3.3.** Structural alignment of the homology model of Alge7 (grey) and the energy minimized model (pink) for mutant R148G (A) and Alge7 wild type (B) showing the position of residue 148 and catalytic residues (yellow). The energy minimized structures was made using the YASARA Energy Minimization Server (236), and visualized and aligned with the homology models in PyMOL.

### 3.1.2 Multiple sequence alignment

In order to identify differences in amino acid residues surrounding the active site in the homology model made for Alge7, a multiple sequence alignment of the nine different A-modules identified in Alge epimerases was performed using Clustal Omega (238). The alignment is shown from residue 90 to 313 (residue 33-255 for Alge1A<sub>2</sub> and Alge3A<sub>2</sub>) in Figure 3.4. This part of the sequence was found to be most interesting when studying the homology model of Alge7, as this area comprises the residues surrounding the proposed binding cleft and catalytic residues. Residues that were chosen for mutation in this study (see section 3.1.3) and the residues that was mutated in previous studies (Table 2.9) are highlighted in colour codes, as described in Figure 3.4.

AlgE7A	90	RSANGEKTHDYGISDLTIDGNQDNTEG <b>VD</b> GFYTGYPGKNGADYNVTVERVEIRE	145
AlgE1A2	33	RSAYGEETS <sup>33</sup> NFGMSDLTLDG <sup>33</sup> NRDNTSG <b>KVD</b> GW <b>F</b> NGYIPGQDGADRNVTIERVEIRE	88
AlgE3A2	33	RSAYGEETS <sup>33</sup> NFGMSDLTLDG <sup>33</sup> NRDNTSG <b>KVD</b> GW <b>F</b> NGYIPGQDGADRNVTIERVEIRE	88
AlgE4A	90	RSAYGEETS <sup>90</sup> NFGMRDLTLDG <sup>90</sup> NRDNTSG <b>KVD</b> GW <b>F</b> NGYIPGGDGADRDVTIERVEVRE	145
AlgE6A	90	RSPFGEETS <sup>90</sup> NFGMRDLTLDG <sup>90</sup> NRANTVD <b>KVD</b> GW <b>F</b> NGYAPGQPGADRNVTIERVEVRE	145
AlgE2A	90	RSAYGEETS <sup>90</sup> NFGMSDLTLDG <sup>90</sup> NRDNTSG <b>KVD</b> GW <b>F</b> NGYIPGEDGADRDVTIERVEIRE	145
AlgE5A	90	RSAYGEETS <sup>90</sup> NFGMSDLTLDG <sup>90</sup> NRDNTSG <b>KVD</b> GW <b>F</b> NGYIPGEDGADRDVTIERVEIRE	145
AlgE1A1	90	RSAYGEETS <sup>90</sup> NFGMSDLTLDG <sup>90</sup> NRDNL <b>SAKVD</b> GW <b>F</b> NGYIPGQDGADRDVTIERVEIRE	145
AlgE3A1	90	RSAYGEETS <sup>90</sup> NFGMSDLTLDG <sup>90</sup> NRDNL <b>SAKVD</b> GW <b>F</b> NGYIPGQDGADRDVTIERVEIRE	145
AlgE7A	146	VS <b>RYAFD</b> PHEQTINLTIRDSVAHDN <b>GLD</b> GFVAD <b>FQ</b> IGAVFENNVSYN <b>NGRHGFNI</b> V	201
AlgE1A2	89	MS <b>GYGFD</b> PHEQTINLTIRDSVAHDN <b>GLD</b> GFVAD <b>YL</b> VDSVFENN <b>VAYNNGRHGFNI</b> V	144
AlgE3A2	89	MS <b>GYGFD</b> PHEQTINLTIRDSVAHDN <b>GLD</b> GFVAD <b>YL</b> VDSVFENN <b>VAYNNGRHGFNI</b> V	144
AlgE4A	146	MS <b>GYGFD</b> PHEQTINLTIRDSVAHDN <b>GLD</b> GFVAD <b>YL</b> VDSVFENN <b>VAYANDRRHGFNV</b> V	201
AlgE6A	146	MS <b>GYGFD</b> PHEQTINLVLRDSVAH <b>HNGLD</b> GFVAD <b>YQ</b> IGGTFENN <b>VAYANDRRHGFNV</b> V	201
AlgE2A	146	MS <b>GYGFD</b> PHEQTINLTIRDSVAHDN <b>GLD</b> GFVAD <b>FQ</b> IGGVFENNVSYN <b>NDRRHGFNI</b> V	201
AlgE5A	146	MS <b>GYGFD</b> PHEQTINLTIRDSVAHDN <b>GLD</b> GFVAD <b>FQ</b> IGGVFENNVSYN <b>NDRRHGFNI</b> V	201
AlgE1A1	146	MS <b>GYGFD</b> PHEQTINLTIRDSVAHDN <b>SLD</b> GFVAD <b>YQ</b> VGGVFENNVSYN <b>NDRRHGFNI</b> V	201
AlgE3A1	146	MS <b>GYGFD</b> PHEQTINLTIRDSVAHDN <b>SLD</b> GFVAD <b>YQ</b> VGGVFENNVSYN <b>NDRRHGFNI</b> V	201
AlgE7A	202	TSSHDIVFTNNVAYGNGANGLVVQR <b>GEDR</b> DFVYNVEIEGGSFHDNGQEGVLI <b>KMS</b>	257
AlgE1A2	145	TSTYDFVMTNNVAYGNGGAGLTIQR <b>GEDLA</b> QPTDILIDGGAYYDNALEGVLF <b>KMT</b>	200
AlgE3A2	145	TSTYDFTLN <b>SVAYGNGGAGLVIQR</b> GAED <b>LA</b> QPTDILIDGGAYYDNALEGVLL <b>KMT</b>	200
AlgE4A	202	TSTHDFVMTNNVAYGNGSSGLVVQR <b>GLEDL</b> ALPSNILIDGGAYYDNAREGVLL <b>KMT</b>	257
AlgE6A	202	TSTNDFVMRNNVAYGNGGGLVVQR <b>GSENLA</b> HPENILIDGGSSYYDNGLEGVLV <b>KMS</b>	257
AlgE2A	202	TSTNDFVLSNNVAYGNGGAGLVVQR <b>SSDV</b> AHPYDILIDGGAYYDNGLEGVQ <b>IKMA</b>	257
AlgE5A	202	TSTNDFVLSNNVAYGNGGAGLVVQR <b>SYDV</b> AHPYDILIDGGAYYDNGLEGVQ <b>IKMA</b>	257
AlgE1A1	202	TSTNDFVLSNNVAYGNGGAGLVVQR <b>SYDL</b> PHPYDILIDGGAYYDNALEGVQL <b>KMA</b>	257
AlgE3A1	202	TSTNDFVLSNNVAYGNGGAGLVVQR <b>SYDL</b> PHPYDILIDGGAYYDNALEGVQL <b>KMT</b>	257
AlgE7_A	258	TDVTLQ <b>GA</b> EIYGN <b>YAG</b> VRVQGV <b>ED</b> VRI <b>LD</b> NYI <b>HD</b> NAQ <b>S</b> KANA <b>EV</b> IV <b>ESY</b> DDRDGP	313
AlgE1_A2	201	NNVTLQ <b>NA</b> EIYGN <b>SSG</b> VRLYGT <b>ED</b> VQ <b>IL</b> DNQ <b>I</b> HDNSQ <b>NG</b> TY <b>PE</b> VLLQ <b>AF</b> DD-SQV	255
AlgE3_A2	201	NNITLQ <b>NA</b> EIYGN <b>SSG</b> VRLYGT <b>ED</b> VQ <b>IL</b> LNQ <b>I</b> HDNAQ <b>N</b> VAYA <b>EV</b> LLQ <b>SF</b> ND-VGV	255
AlgE4_A	258	SDITLQ <b>NA</b> DIHGN <b>SSG</b> VRVYGAQ <b>D</b> VQ <b>IL</b> DNQ <b>I</b> HDNAQ <b>AA</b> AV <b>PE</b> VLLQ <b>SF</b> DDTAGA	313
AlgE6_A	258	NNVT <b>VQ</b> NA <b>DI</b> HGN <b>SSG</b> VRVYGAQ <b>VQ</b> ILGNQ <b>I</b> HDNA <b>K</b> TAVA <b>PE</b> VLLQ <b>SY</b> DDTLGV	313
AlgE2_A	258	HDVTLQ <b>NA</b> EIYGN <b>LYG</b> VRVYGA <b>ED</b> VQ <b>IL</b> DNQ <b>I</b> HDNSQ <b>NG</b> SY <b>AE</b> ILLQ <b>SY</b> DDTAGV	313
AlgE5_A	258	HDVTLQ <b>NA</b> EIYGN <b>LYG</b> VRVYGA <b>ED</b> VQ <b>IL</b> DNQ <b>I</b> HDNSQ <b>SG</b> SY <b>AE</b> ILLQ <b>SY</b> DDTAGV	313
AlgE1_A1	258	HDVTLQ <b>NA</b> EIYGN <b>LYG</b> VRVYGAQ <b>D</b> VQ <b>IL</b> DNQ <b>I</b> HDNSQ <b>NG</b> AY <b>AE</b> VLLQ <b>SY</b> DDTAGV	313
AlgE3_A1	258	HDVTLQ <b>NA</b> EIYGN <b>LYG</b> VRVYGAQ <b>D</b> VQ <b>LL</b> DNQ <b>I</b> HDNSQ <b>NG</b> AY <b>AE</b> VLLQ <b>SY</b> DDTAGV	313

**Figure 3.4:** Multiple sequence alignment of the different A-nodes identified in AlgE epimerases (AlgE1A1, AlgE1A2, AlgE2A, AlgE3A1, AlgE3A2, AlgE4A, AlgE5A, AlgE6A and AlgE7A). The alignment is shown for residues spanning from number 90 to 313 (residue 33–255 for AlgE1A2 and AlgE3A2). All residues that have been mutated in this study or mutated in previous studies (and included in this study), are highlighted in colours. **Orange:** residues that are conserved or consensus among all the A-modules, **blue:** residues that stand out as different from all other A-modules, **green:** catalytic residues, **red:** residue 307 that either comprises a tyrosine (Y) or a phenylalanine (F). The alignment was made using Clustal Omega (238), and the order of the modules is assigned based on sequence homology.

### 3.1.3 Design of mutants

The residue differences in AlgE7 that were identified by the multiple sequence alignments were further examined by visual inspection of the homology model structure. In addition, charged residues projection toward the active site was studied. On the basis of this analysis and the mutants made in previous studies (Table 2.9), 11 new mutants were constructed by site-directed mutagenesis. All mutants included in this study are listed in Table 3.1, and the position of the residues that were mutated is shown in the energy minimized model of AlgE7 in Figure 3.5.

**Table 3.1.** Mutants constructed in this study describing the residue(s) involved, the amino acid mutation(s) made and the reason for the mutation(s). The table covers 5 pages. \* Mutants constructed in this study.

Residue(s)	Description of residue	Amino acid mutation	Proposed effect of mutation
R90	Positively charged residue projecting toward the active site	Arginine (R) → Alanine (A)*	Alanine scanning - removing the positively charged side chain may change binding of the negatively charged substrate in the binding groove, and hence affect enzyme activity
E117	Negatively charged residue projecting toward the active site, conserved as lysine (K) in all other AlgE enzymes	Glutamic acid (E) → Leucine (L)*  Glutamic acid (E) → Lysine (K)	L: Removing the negative charge changes the electrostatic interactions with neighbouring residues, this may affect the positioning of the negatively charged substrate in the active site.  K: Changing into the positively charged K may lead to stronger binding of and altered positioning of the negatively charged substrate.  For both mutations made at residue E117: Since K is conserved in the other epimerases at this residue these substitutions are thought to reduce the lyase activity.
D119	Negatively charged residue projecting toward the active site, conserved residue in all AlgE enzymes	Aspartic acid (D) → Alanine (A)  Aspartic acid (D) → Glutamic acid (E)  Aspartic acid (D) → Asparagine (N)	A: Alanine scanning - removing the negatively charged side chain may change positioning of the negatively charged substrate in the binding groove, and hence affect enzyme activity  E: Changing into the negatively charged E that has a different geometry than D, change the electrostatic interactions. This may alter positioning and binding of the negatively charged substrate, and hence affect enzyme activity  N: Removing the negative charge changes the electrostatic interactions with neighbouring residues, this may affect the positioning of the negatively charged substrate in the binding groove, and hence affect the enzyme activity

Residue(s)	Description of residue	Amino acid mutation	Proposed effect of mutation
Y122	Residue is close to catalytic residue H154 and D152, conserved as phenylalanine (F) in all other AlgE enzymes	Tyrosine (Y) → Alanine (A)* Tyrosine (Y) → Phenylalanine (F)	A: Alanine scanning – removing the aromatic side chain may remove possible interaction with the substrate, and hence affect the enzyme activity.  F: Removing the polar OH-group may remove possible interaction with the catalytic residue H154. Since F is conserved at this residue in the other epimerases this substitution is thought to reduce the lyase activity.
R148	Positively charged residue, close to catalytic residue Y149, conserved as glycine (G) in all other AlgE enzymes	Arginine (R) → Glycine (G) Arginine (R) → Lysine (K)	G: Removing the positively charged side chain changes electrostatic interactions with the catalytic residues and also the interaction with the negatively charged substrate.  K: Changing into the positively charged K that has a different geometry than R, changes the electrostatic interactions. This may alter the interaction with the catalytic residues and binding of the negatively charged substrate.  For both mutations made at residue R148: Since G is conserved in the other epimerases at this residue these substitutions are thought to reduce the lyase activity.
Y149	Catalytic residue	Tyrosine (Y) → Alanine (A) Tyrosine (Y) → Phenylalanine (F)	A: Alanine scanning – removing the aromatic side chain aborts the function of catalytic residue  F: Removing the polar OH-group removes the ability to act as a proton donor or acceptor in catalysis
D152	Catalytic residue, negatively charged	Aspartic acid (D) → Glutamic acid (E) Aspartic acid (D) → Asparagine (N)	E: Changing positioning of the negative charge may lead to loss of catalytic function  N: Removing negative charge removes the catalytic function of the residue



<b>Residue(s)</b>	<b>Description of residue</b>	<b>Amino acid mutation</b>	<b>Proposed effect of mutation</b>
P153	Residue positioned between two catalytic residues H152 and H154, conserved residue in all AlgE epimerases	Proline (P) → Alanine (A)	Alanine scanning – loss of structural integrity by altering positioning of the catalytic residue H152 and H154. This is thought to reduce enzyme activity
H154	Catalytic residue, positively charged	Histidine (H) → Alanine (A)*	A: Alanine scanning - removing the aromatic and positively charged side chain aborts the function of catalytic residue
		Histidine (H) → Phenylalanine (F)	F: Removing the nitrogen donor/acceptor atoms in the aromatic and positively charged side chain removes the ability to act as a proton donor or acceptor in catalysis.
		Histidine (H) → Tyrosine (Y)	Y: As the role of Y149 and H154 as hydrogen donor or acceptor in catalysis is not fully established, exchanging H into Y may affect catalysis
K172	Positively charged residue, close to catalytic residue Y149, conserved as leucine (L) in all other AlgE enzymes	Lysine (K) → Leucine (L)	L: Removing the positive charge may change the electrostatic interactions with the catalytic residues and also the interaction with the negatively charged substrate.
		Lysine (K) → Arginine (R)	R: Changing into the positively charged R that has a different geometry than K, changes the electrostatic interactions. This may alter the interaction with the catalytic residues and binding of the negatively charged substrate.
			For both mutations made at residue K172: Since L is conserved in the other epimerases at this residue these substitutions are thought to reduce the lyase activity.
D173	Negatively charged residue close to catalytic residue Y149, conserved residue in all AlgE epimerases	Aspartic acid (D) → Alanine (A)*	Alanine scanning – removing the negatively charged side chain may change binding of the negatively charged substrate in the binding groove, and hence affect enzyme activity

<b>Residue(s)</b>	<b>Description of residue</b>	<b>Amino acid mutation</b>	<b>Proposed effect of mutation</b>
D178	Catalytic residue, negatively charged	Aspartic acid (D) → Glutamic acid (E)	E: Changing positioning of the negative charge may lead to loss of catalytic function
		Aspartic acid (D) → Asparagine (N)	N: Removing negative charge removes the catalytic function of the residue
		Aspartic acid (D) → Arginine (R)	R: Changing to a positive charge removes the catalytic function of the residue
R195	Positively charged residue projecting toward the active site, conserved residue in all AlgE epimerases	Arginine (R) → Alanine (A)*	A: Alanine scanning - removing the positively charged side chain may affect substrate binding, and hence reduce enzyme activity
		Arginine (R) → Leucine (L)	L: Removing the positive charge may lead to weaker binding of the negatively charged substrate in the active site and hence reduce the enzyme activity.
H196	Positively charged residue projecting toward the active site, conserved residue in all AlgE epimerases	Histidine (H) → Alanine (A)*	Alanine scanning – removing the aromatic and positively charged side chain may affect substrate binding, and hence reduce enzyme activity
V201	Projecting into the binding groove, conserved residue in all AlgE epimerases	Valine (V) → Leucine (L)	Changing the residue into the slightly larger L may change interaction with the substrate, and hence affect enzyme activity
R231	Positively charged residue projecting toward substrate binding groove, Hydrophobic amino acid (Leucine or Valine) in all other AlgE enzymes	Arginine (R) → Leucine (L)*	Changing the residue into a hydrophobic L may affect the positioning of negatively substrate. Since L/V is conserved in the other epimerases at this residue this substitution is thought to reduce the lyase activity.
K255	Positively charged residue, projecting toward the substrate binding groove, conserved residue in all AlgE epimerases	Lysine (K) → Glutamic acid (E)	E: Changing to a negatively charged E might affect binding of the negatively charged substrate and hence the enzyme activity
		Lysine (K) → Leucine (L)	L: Removing the positive charge might affect binding of the negatively charge substrate, and hence the enzyme activity

<b>Residue(s)</b>	<b>Description of residue</b>	<b>Amino acid mutation</b>	<b>Proposed effect of mutation</b>
Y307	Residue shown to be essential for defining the epimerization pattern in AlgE enzymes (172), Y in G-block formers and F in MG-block formers	Tyrosine (Y) → Phenylalanine (F)*	Mutation changes the epimerization pattern to create MG-blocks (172).
E117 R148	See descriptions above	Glutamic acid (E) → Lysine (K) Arginine (R) → Glycine (G)	Changing the residues into the amino acid conserved in other AlgE enzymes is thought to affect the lyase activity. The same applies to all combination mutants that contains mutants E117K, Y122F, R148G and K172L
E117 R148 K172	See descriptions above	Glutamic acid (E) → Lysine (K) Arginine (R) → Glycine (G) Lysine (K) → Leucine (L)	
R148 K172	See descriptions above	Arginine (R) → Glycine (G) Lysine (K) → Leucine (L) or Arginine (R)	For mutant K172R in combinations: Changing into the positively charged R that has a different geometry than K, can alter the electrostatic interactions. This may change the interaction with the catalytic residues and binding of the negatively charged substrate.
E117 Y122 R148	See descriptions above	Glutamic acid (E) → Lysine (K) Tyrosine (Y) → Phenylalanine (F) Arginine (R) → Glycine (G)	
E117 Y122 K172	See descriptions above	Glutamic acid (E) → Lysine (K) Tyrosine (Y) → Phenylalanine (F) Lysine (K) → Leucine (L) or Arginine (R)	
E117 Y122 R148 K127	See descriptions above	Glutamic acid (E) → Lysine (K) Tyrosine (Y) → Phenylalanine (F) Arginine (R) → Glycine (G) Lysine (K) → Leucine (L) or Arginine (R)	
E117 Y122 Y149	See descriptions above	Glutamic acid (E) → Lysine (K) Tyrosine (Y) → Phenylalanine (F) Tyrosine (Y) → Alanine (A)	The combination mutant includes mutation of a catalytic residue, the mutation of residue Y149 into A is thought to abort the function of catalytic residue

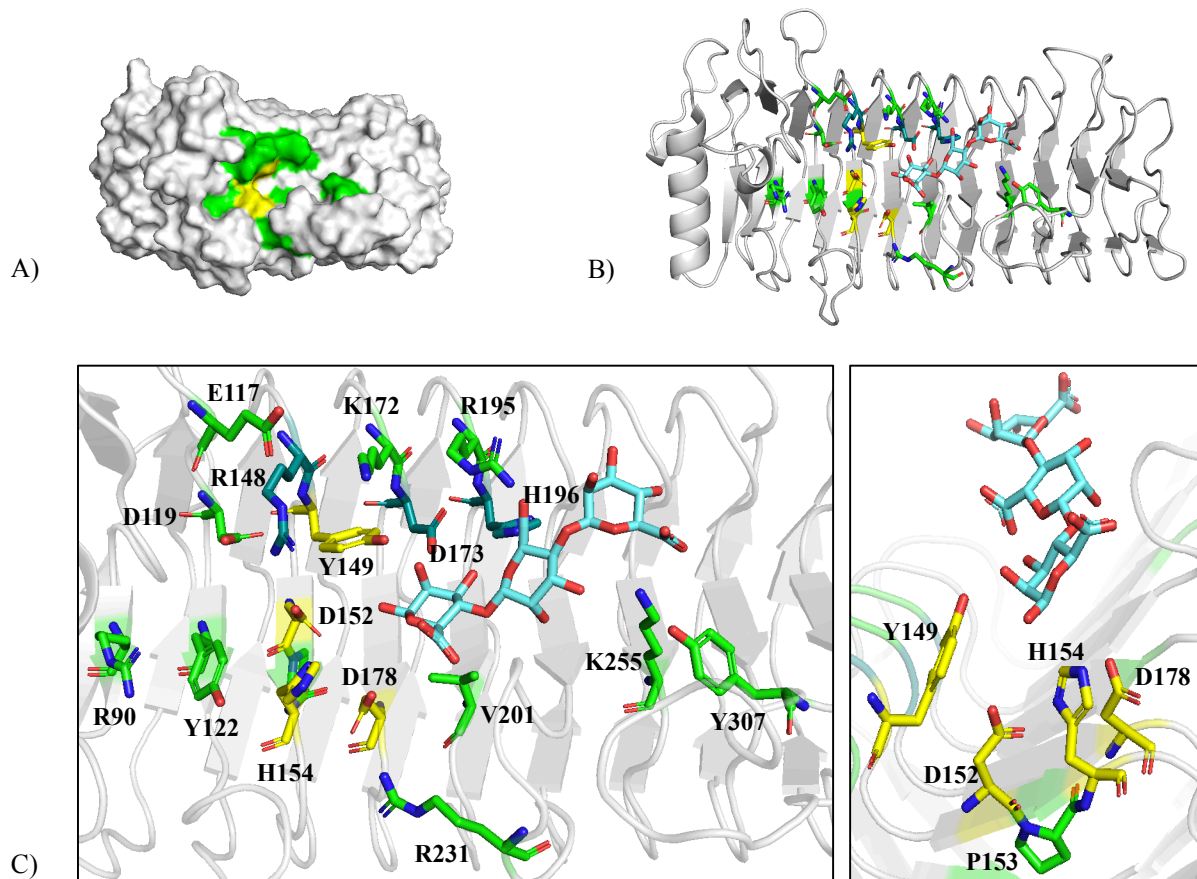


**Figure 3.5.** Visual inspection of residues surrounding the active site in the energy minimized homology model of AlgE7 A-module. **A)** Surface view of the homology structure with the position of the catalytic residues (yellow) and the residues selected for mutation in this study (green). **B)** Secondary motif of the homology structure showing the catalytic residues (yellow), the other residues mutated (green) and a mannuronan trisaccharide substrate (light blue) as stick models. The substrate is obtained from the crystal structure of AlgE4 (PDB: 2PYG) and is shown for visual reference. **C)** Closer view of the all residues mutated. To the left: catalytic residues (Y149, D152, H154 and D178) in yellow sticks and the residue R90, E117, D119, Y122, R148, K172, D173, R195, H196, V201, R231, K255 and Y307 shown in green sticks. Darker green colour is used to distinguish the amino acid residues that are close to each other. To the right: residue P153 (green) and the catalytic residues (yellow). The structure was visualized in PyMOL.

### 3.1.4 Protein parameters

Theoretical protein parameters were calculated from the AlgE7 amino acid sequence (UniProtKB: Q9ZFG9) using the ExPASy ProtParam server (Table 3.2) (239). The molecular mass (MW) and molar extinction coefficient  $\epsilon$  ( $M^{-1}cm^{-1}$ ) were used to identify protein bands in SDS-PAGE gels and to calculate protein concentrations in purified protein samples, respectively (Section 3.3.). The parameters were also calculated for mutant R148G, as this was the only mutant purified in this study.

**Table 3.2.** Theoretical protein parameters: number of amino acids, molecular weight (Da) and molar extinction coefficient ( $M^{-1}cm^{-1}$ ) for AlgE7 wild type and mutant R148G. The parameters were calculated using the ExPASy ProtParam server.

Protein	Amino acids	MW (Da)	$\epsilon$ ( $M^{-1}cm^{-1}$ )
AlgE7	856	90364.14	61660
R148G	856	90265.00	61660

## 3.2 Cloning

The experimental procedures used in the cloning and expression part are described in sections 2.2.1-2.2.11. Point mutations for 11 of the AlgE7 mutants were introduced to the *algE7* gene in the derivative expression vector pBG27, constructed by Svanem et al.1999 (156) (Appendix B, Figure B.1), using the NEB Q5® Site-Directed Mutagenesis Kit. In addition, the AlgE7 wild type and 31 AlgE7 mutants in similar plasmids (Table 2.9) were cultivated from DH5- $\alpha$  *E. coli* glycerol stocks.

### 3.2.1 Cloning and expression of AlgE7 mutants

#### Transformation and cultivation of *E. coli* DH5- $\alpha$ cells

PCR primers for SDM were designed using NEBaseChanger and checked for non-specific hybridization, hairpin structures and mismatches in Benchling. The linear PCR product was ligated and transformed into NEB® 5-alpha competent *E. coli* cells, before the culture was plated onto selection plates and incubated over night. The next day, white colonies were observed and counted, e.g. the number of colony-forming units (CFU) per mL for mutant D173A was  $\sim 2.0 \times 10^3$  CFU/mL.

For the AlgE7 mutants cultivated from DH5- $\alpha$  *E. coli* glycerol stocks, a sample from each glycerol stock was plated onto selection plates using a toothpick and incubated overnight.

### **Verification of AlgE7 point mutations**

After transformation of *E. coli* DH5- $\alpha$  cells and cultivation of AlgE7 mutants from *E. coli* DH5- $\alpha$  glycerol stocks, colonies of each mutant were inoculated in 6 mL LB medium and the plasmid was purified using the Monarch® Miniprep Kit protocol. The purified plasmid (40-60 ng/mL) was sent to Eurofins GATC Biotech GmbH for sequencing. Benchling was used to confirm the mutations in the sequencing results.

### **Transformation of *E. coli* T7 Express competent cells**

The verified plasmids were transformed into T7 express competent *E. coli* cells for later protein production. The cells were plated onto selection plates and incubated over night. The next day, white colonies were observed and counted, e.g. the number of colony-forming units (CFU) per mL for mutant D173A was  $\sim 3.0 \times 10^3$  CFU/mL.

## **3.2.2 SLIC cloning**

As described in section 2.2.9, the five single point mutants E117K, Y122F, R148G, K172L and K172R, introduced to the algE7 gene in the pBG27 vector (Appendix B, Figure B.1), were transferred to the pTYB1 vector (Appendix B, Figure B.2) by SLIC cloning. This was done in order to purify the proteins by affinity chromatography. However, it was only time to purify mutant R148G during the work of this thesis.

### **Verification of amplicons**

PCR primers for SLIC cloning were designed using NEBuilder assembly tool. Amplification of the linear PCR products, pTYB1 vector backbone (7442 bp) and algE7 gene insert (2567 bp), were confirmed by agarose gel electrophoresis (Figure 3.6). In the lane containing the algE7 gene insert for mutant R148G, less amplified PCR product was observed compared to the other mutants. This is because a small amount of sample was lost when applied on the gel, resulting in less PCR product loaded into the well.

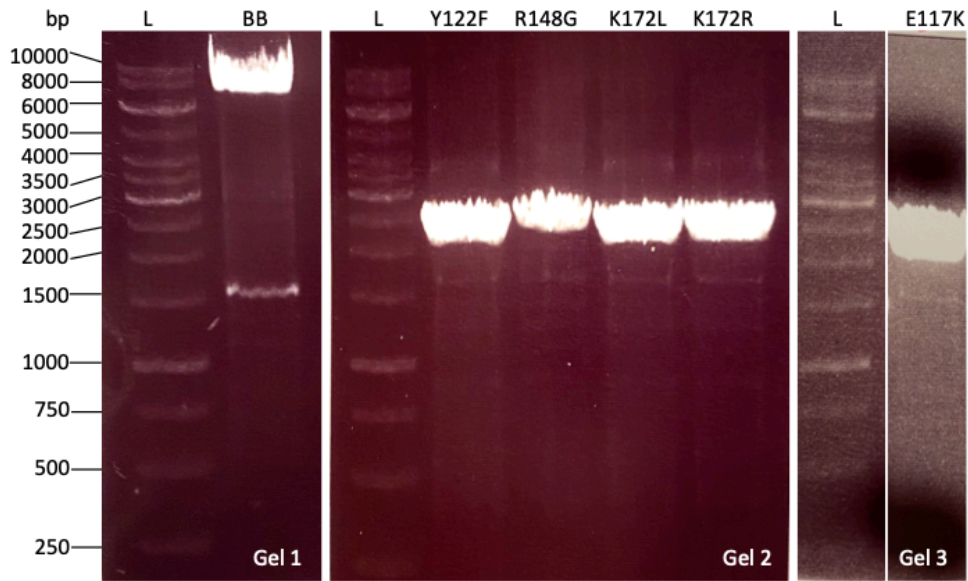


**Figure 3.6.** Verification of amplified PCR products, visualized on 0.8% agarose gels. **Gel 1:** linear PCR product (7442 bp) of the pTYB1 vector backbone (BB) (4  $\mu$ L). **Gel 2:** linear PCR products (2567 bp) of the *algE7* gene insert, shown for the point mutants Y122F, R148G, K172L and K172R. **Gel 3:** same as in gel 2, shown for point mutant E117K. L: Thermo Scientific<sup>TM</sup> Gene Ruler 1kb DNA Ladder (0.75  $\mu$ L). Side labels identify the number of base pairs (bp) of specific fragments in the DNA ladder.

### 3.3 Protein production

Protein production of the *Alge7* wild type and all *Alge7* mutants in the pBG27 vector were performed by Randi Aune at SINTEF – Department of Biotechnology and Nanomedicine, as described in section 2.2.17. Protein production and affinity purification was carried out for the *Alge7* wild type and mutant R148G in the pTYB1 vector using the NEB IMPACT<sup>TM</sup>-CN system, as described in section 2.2.11-2.2.15.

#### 3.3.1 Protein production of *Alge7* mutants carried on the pBG27 vector

As described in section 2.2.14, SDS-PAGE was used to verify production of the *Alge7* protein in the B-Per II enzyme extracts from induced cells. The *Alge7* wild type and all *Alge7* mutants analysed showed multiple bands, including a strong band at  $\sim$ 100 kDa. This band probably represents the *Alge7* protein, which has a molecular weight of  $\sim$ 90 kDa (Figure 3.7).

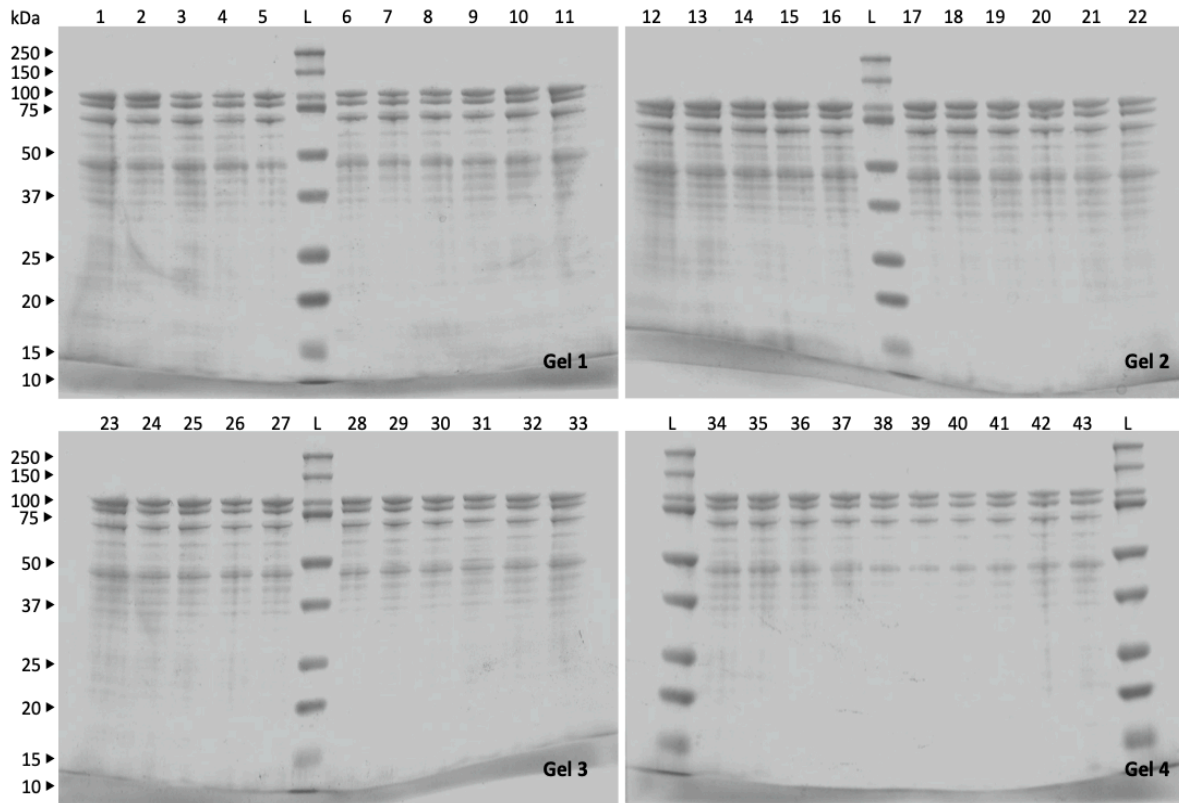


**Figure 3.7.** Images of Coomassie Brilliant Blue stained SDS-PAGE gels showing AlGE7 protein expression (100 kDa) in the B-Per II enzyme extracts. Arrow labels identify the molecular weights (kDa) according to the Precision Plus Protein™ Dual Color standard (Bio-Rad). **1:** enzyme extract containing the AlGE7 wild type (10  $\mu$ L) shown in gel 1, **2-43:** enzyme extracts containing AlGE7 mutant number 2-43 (10  $\mu$ L) shown in gel 1-4, **L:** molecular weight standard (5  $\mu$ L). Numbering of the mutants is shown in Table 2.9, Section 2.1.6

In order to verify that the band seen at  $\sim$ 100 kDa in the cell extracts corresponds to the AlGE7 protein, a gel with enzyme extracts of AlGE7 wild type and five AlGE7 mutants (mutant number 2, 3, 5, 8 and 10) were run together with samples of protein extracts from induced T7 express competent *E. coli*, not containing the pBG27 vector or containing the vector pTrc99a (Figure 3.8). The latter is an “empty vector” not containing the *algE7* gene. In lanes containing the T7 express competent *E. coli* without the pBG27 vector and in lanes containing the vector pTrc99a, no protein band was seen at  $\sim$ 100 kDa.



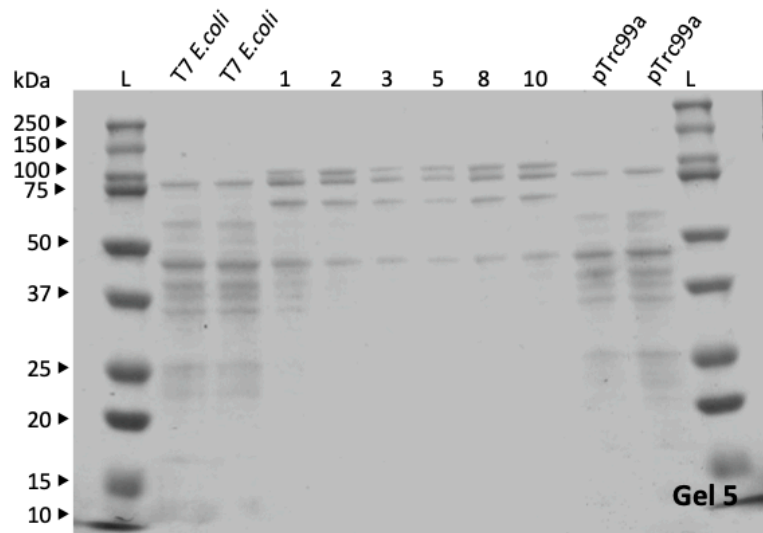


**Figure 3.8.** Image Coomassie Brilliant Blue stained SDS-PAGE gel showing no protein band at 100 kDa for protein extracts from induced T7 express competent *E. coli* without the pBG27 vector (**T7 *E. coli***, 10  $\mu$ L) and with an empty vector (**pTtrc99a**, 10  $\mu$ L). **1:** enzyme extract containing the AlgeE7 wild type (10  $\mu$ L), **2, 3, 5, 8 and 10:** enzyme extracts containing AlgeE7 mutant number 2, 3, 5, 8 and 10 (10  $\mu$ L), **L:** molecular weight standard (5  $\mu$ L). Arrow labels identify the molecular weights (kDa) according to the Precision Plus Protein™ Dual Color standard (Bio-Rad). Numbering of the mutants is shown in Table 2.9, Section 2.1.6

### 3.3.2 Protein production and purification of AlgeE7wt and R148G

#### Fast protein liquid chromatography (FPLC)

In order to purify the AlgeE7 protein, clarified cell extract was subjected to affinity purification and on-column cleavage. A chromatogram from purification of the AlgeE7 wild type is presented in Figure 3.9, showing the maximum UV absorption of 305 mAU as a function of volume (mL) eluted from the column. The fractions A1-A7 are indicated along the x-axis and the highest amount of protein was eluted in fraction 3 and 4. The chromatogram for purification of AlgeE7 mutant R148G showed a similar elution profile, but as only half of the culture was purified it had a lower UV absorption than for the wild type. This chromatogram was not recorded.

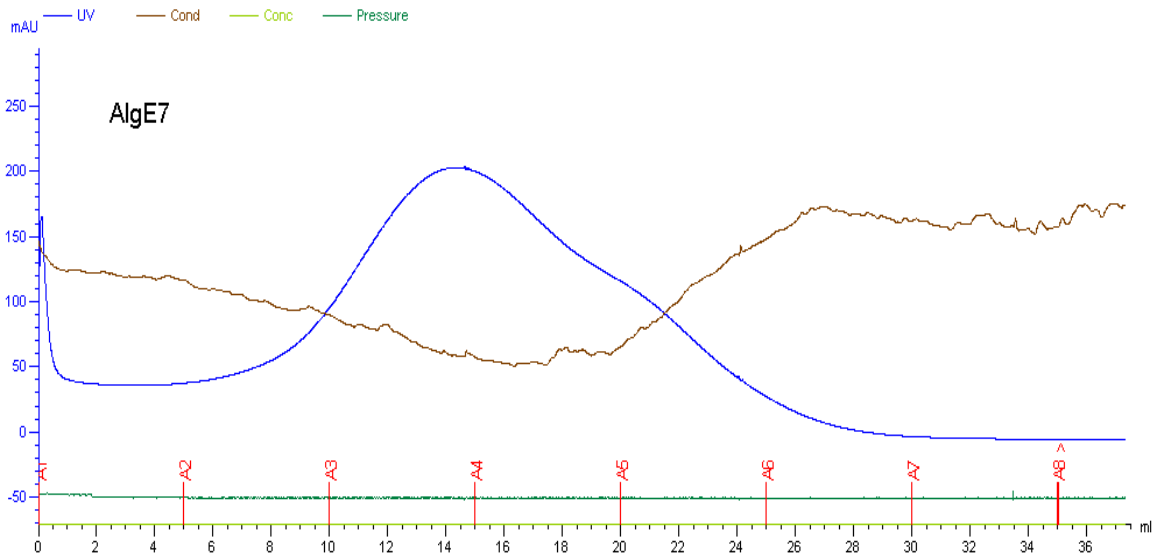


**Figure 3.9.** FPLC-chromatogram showing the elution profile (UV absorption at 305 mAU) of the AlgE7 wild type (blue). The AlgE7 protein was purified on a chitin resin column and eluted with a column buffer into seven 5 mL fractions. The seven fractions are indicated in red along the x-axis.

### Sodium dodecyl sulphate-polyacrylamide gel electrophoresis (SDS-PAGE)

After purification of the AlgE7 wild type and mutant R148G, the protein was analysed using SDS-PAGE, as described in section 2.2.14. This was done in order to verify protein expression and to assess the purity of the eluted FPLC fractions.

In lanes containing protein, a strong band was observed at  $\sim 100$  kDa (Figure 3.10). This band shows that the AlgE7 protein was purified. The largest amount of protein was visible in fraction 3 and 4 for both the AlgE7 wild type and mutant R148G. For the fractions with purified R148G, less amount of protein was visible in the SDS-PAGE gel than for the wild type. This can be best seen in lanes containing fraction 3 and 4. The reason for this is that R148G was purified from half of the culture (250 mL) after harvesting the pellet, cell lysis and sonication, whereas the wild type was purified using the whole culture (500 mL). It was also observed multiple faint bands in the lanes containing purified protein. In lanes containing cell extract from induced cells and sterile filtrated supernatant of lysed cells a strong band was observed at  $\sim 150$  kDa. This band may correspond to AlgE7 protein bound to the intein tag, which has a molecular weight of  $\sim 50$  kDa.

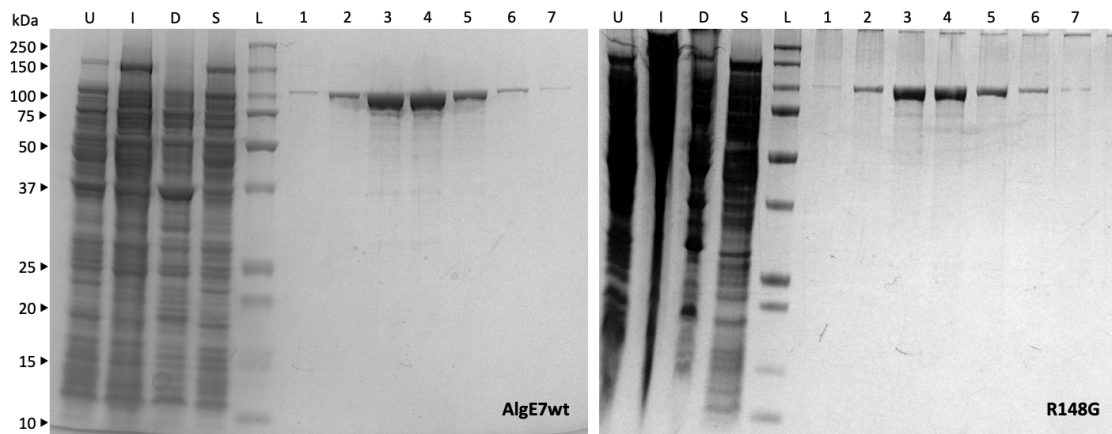


**Figure 3.10.** Image Coomassie Brilliant Blue stained SDS-PAGE gels showing expression and purification of AlgE7 wild type and mutant R148G, using the IMPACT<sup>TM</sup>-CN system. Arrow labels show the molecular weight (kDa) according to the Precision Plus Protein<sup>TM</sup> All blue Standards (BioRad). Labelling of the lanes is described as follow; **U**: extract from uninduced cells (10  $\mu$ l), **I**: extract from induced cells at 16 °C 16-20 hours (10  $\mu$ l), **D**: cell debris (10  $\mu$ l), **S**: sterile filtrated supernatant of lysed cells (10  $\mu$ l), **L**: molecular weight standard (5  $\mu$ l), **1-7**: eluted FPLC fractions containing the purified protein (20  $\mu$ l).

### Estimation of protein concentration

After assessing the SDS-PAGE gel, fraction 3 and 4, 2 and 5 and 1 and 6 were combined and transferred to three dialysis tubes. After dialysis, the protein concentrations in the combined FPLC-fractions from purification of mutant R148G were determined by measuring the absorbance at 230 nm with NanoDrop<sup>TM</sup> One (Table 3.3). From these concentrations the yield of purified protein for mutant R148G was calculated to be 4.2 mg. This calculation was not conducted for the wild type, but based on the SDS-PAGE gels (Figure 3.10) it is assumed that the yield of purified AlgE7 wild type was higher than for mutant R148G.

**Table 3.3.** Protein concentration (mg/mL) of purified mutant AlgE7-R148G, in the combined FPLC-fractions after dialysis. After dialysis, each combined FPLC-fraction had a volume of 13 mL

Enzyme	Concentration (mg/mL)			
	A1+A6	A2+A5	A3+A4	A7
AlgE7-R148G	0.015	0.07	0.24	Discarded

## 3.4 Characterization

The lyase activity of AlgE7 wild type and all AlgE7 mutants was measured by absorbance at 230 nm using a microplate reader. The lyase and epimerase activities of AlgE7 wild type and 25 of the mutants were then analysed using  $^1\text{H-NMR}$  spectroscopy. Finally,  $^1\text{H-NMR}$  and time-resolved  $^{13}\text{C-NMR}$  was used to characterize the chemical composition of poly-M and poly-MG substrates after incubation with AlgE7 wild type and mutant R148G. Methods for sample preparation and the experimental procedures used for the AlgE7-lyase activity assay,  $^1\text{H-NMR}$  and time-resolved  $^{13}\text{C-NMR}$  are described in sections 2.2.17, 2.2.18 and 2.2.19, respectively.

### 3.4.1 AlgE7 lyase-activity assay

The data from the activity assay showed that lyase activity (A230) was detected for the AlgE7 wild type and 16 of the mutants. To sort the data, absorbance plots of two parallels for all AlgE7 mutants were made, showing measured lyase activity (A230) over time (Appendix C). There were large variations between the parallels in the data, making it difficult to assess the lyase activity in the samples and to compare them. In order to determine which of the AlgE7 mutants displaying lyase activity, a qualitative assessment have been used.

A visual inspection of the absorbance plots indicates that the AlgE7 mutants can be organized in three groups of lyase activity: active lyase, less active lyase and inactive lyase. Absorbance plots of two parallels for the AlgE7 wild type, three AlgE7 mutants (R90A, E117L and H196A) representing the different groups of lyase activity, and a blank sample are presented in Figure 3.11.

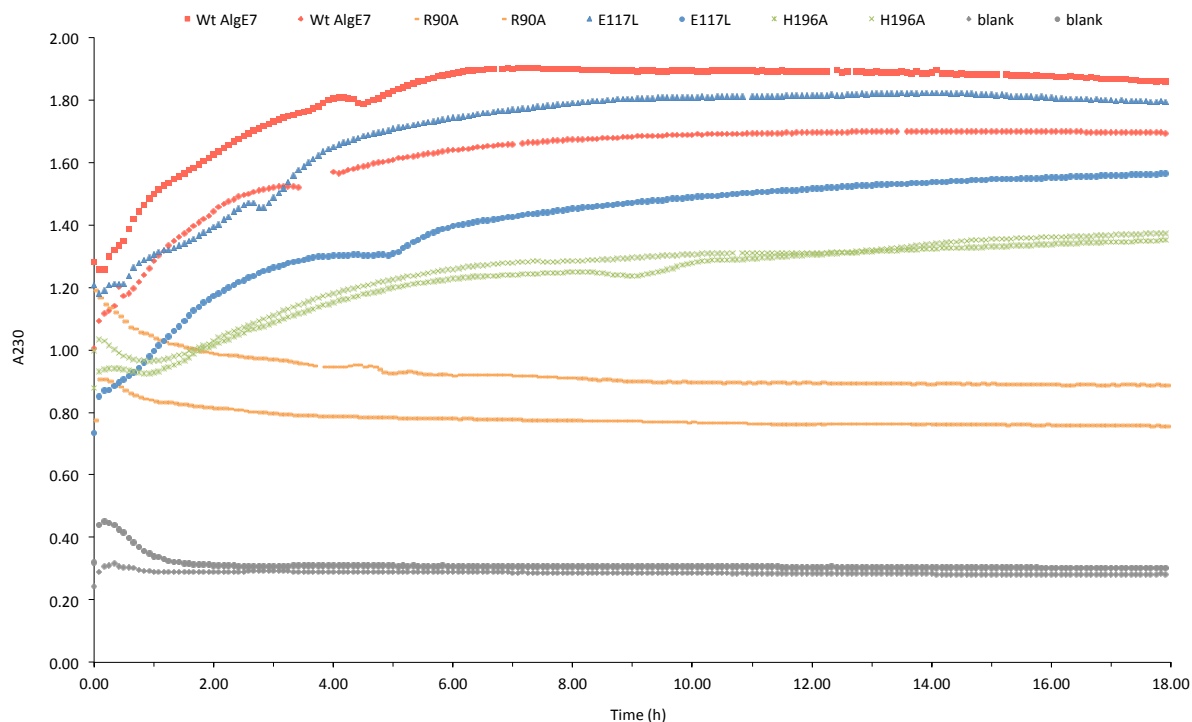


**Figure 3.11.** AlgE7 lyase activity of AlgE7 wild type (red), the mutants R90A (orange), E117L (blue) and H196A (green) and a blank sample (grey) measured by absorbance at 230 nm (A230) every 5 minutes for 18 hours. The AlgE7 lyase activity was assessed using poly-M alginate (1mg/mL) and B-Per II enzyme extract. Two parallels for each mutant are shown. Missing points is a result of failed measurements.

In order to classify the AlgE7 mutants in the three groups mentioned above, the initial activity for all samples was investigated. At the beginning of the reaction, there is a significantly larger amount of substrate relative to enzyme concentration. This means that there is an unlimited amount of substrate in the initial reaction. Consequently, it can be assumed that the initial rate of reaction product formation is independent of the substrate concentration. This gives a constant reaction rate for the initial activity, i. e., the initial measured lyase activity follows a zero-order reaction, meaning that there is a linear relationship between measured absorbance (A230) and time (h). Equations explaining the zero-order enzyme kinetics are shown in Appendix D.

Assuming a zero-order reaction, the slope of a linear regression curve for the initial activity can be used as a qualitative measure of the lyase activity. The slope will only depend on the ability of the enzyme to act on the substrate, and can therefore be used to compare the lyase activity for different AlgE7 mutants. Linear regressions of the first 4 hours of measured lyase activity (A230) were performed for all samples. The slope values obtained were used to classify the AlgE7 mutants in the three groups: active lyase (slope > 0.07), less active lyase

(slope: 0.07-0.01) and inactive lyase (slope < 0.01). As an example, the linear regression of AlgE7 wild type (active lyase), the AlgE7 mutants R90A (inactive lyase), E117L (active lyase) and H196A (less active lyase), and a blank sample is shown in Figure 3.12.

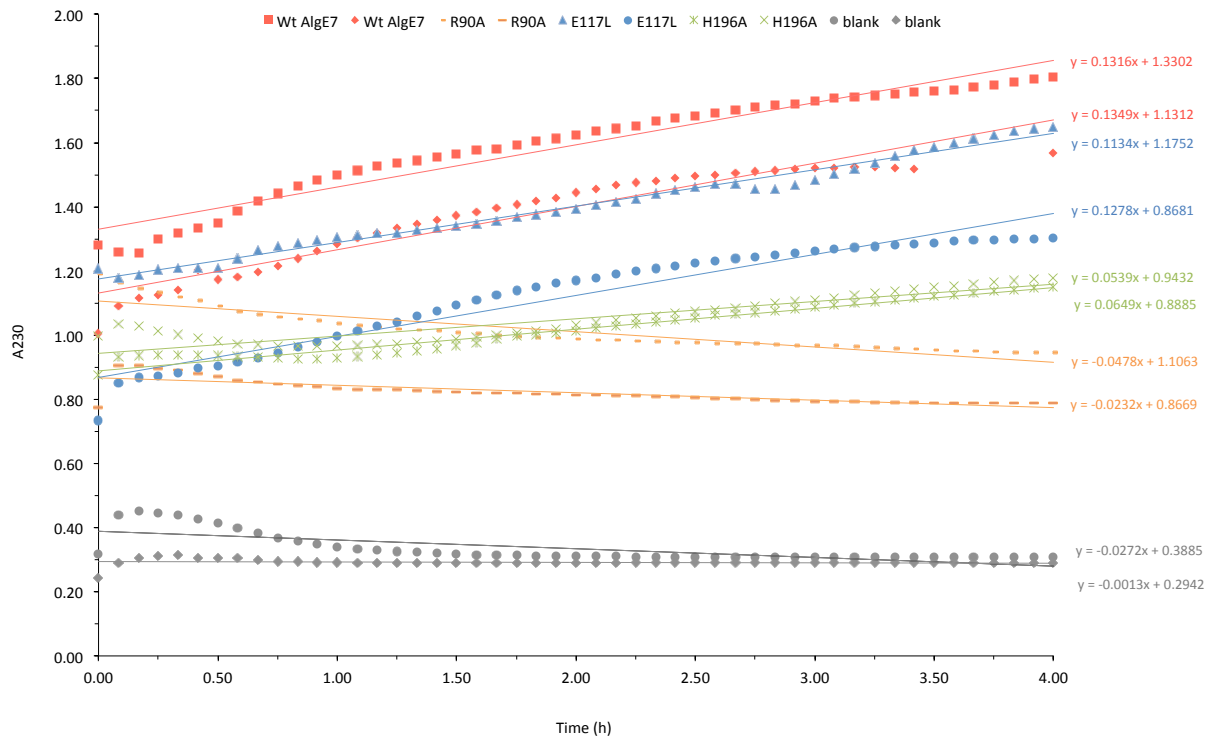


**Figure 3.12.** Linear regression of the initial AlgE7 lyase activity (first 4 hours) of AlgE7 wild type (red), the mutants R90A (orange), E117L (blue) and H196A (green), and a blank sample (grey). The lyase activity was measured by absorbance at 230 nm (A230) every 5 minutes, using poly-M alginate (1mg/mL) and B-Per II enzyme extract. Missing points is a result of failed measurements. The linear regression line and its formula are shown for both parallels. The lyase activity is divided into three groups based on the slope of the linear regression line: active lyase (slope > 0.7), less active lyase (slope: 0.07-0.01), inactive lyase (slope < 0.01). Therefore, the grouping of the samples shown is: active lyase – Wt AlgE7 and E117L, less active lyase – H196A, inactive lyase – R90A and blank.

A qualitative representation of AlgE7 lyase activity for all AlgE7 mutants is presented in Table 3.4. The classification of lyase activity is based on the slope the linear regression lines of the two parallels, as explained in the previous paragraph. The results of linear regression showed that the two parallels for each mutant belong to the same group (Table 3.4). Exceptions are the two combination mutants (mutant number C.39 and C.40), which have slopes classified in two different groups (inactive/less active). This may indicate very weak lyase activity, as shown by the colour code in the table.

For several of the mutants, there was a drop in the absorbance measurements during the first hour (Figure 3.11, Appendix C). For mutant number 16 (P153A) this drop is causing the mutant to be grouped as an inactive lyase, but the absorbance measured beyond 4-5 hours shows a slow increase that may indicate low lyase activity (Appendix C, Figure C.3). This was not seen for any of the other mutants.

**Table 3.4.** Results of the AlgE7-lyase assay using poly-M (1mg/mL) and the B-Per II enzyme extract containing the AlgE7 enzyme (unknown concentration). The AlgE7 lyase assay was performed for the AlgE7 wild type and 42 AlgE7 mutants. The lyase activity is divided into three groups based on the slope of a linear regression line of the first 4 hours. The slope of the linear regression line and a qualitative representation of measured lyase activity are shown in the table. The qualitative representation is presented by an orange colour code – dark orange represents active lyase (slope > 0.7), lighter orange colour represents less active lyase (slope: 0.7-0.01) and no colour represents inactive lyase (slope < 0.01).

Numbering	AlgE7 mutant	Slope		Lyase activity
		Parallel 1	Parallel 2	
1	AlgE7wt	0.13	0.13	
2	R90A	-0.05	-0.02	
3	E117L	0.11	0.13	
4	E117K	0.12	0.08	
5	D119A	-0.05	-0.03	
6	D119E	0.05	0.03	
7	D119N	-0.04	-0.03	
8	Y122A	-0.04	-0.03	
9	Y122F	0.10	0.07	
10	R148G	-0.03	-0.02	
11	R148K	0.01	0.01	
12	Y149A	-0.03	-0.03	
13	Y149F	-0.02	-0.03	
14	D152E	-0.03	-0.01	
15	D152N	-0.04	-0.02	
16	P153A	-0.03	-0.05	*
17	H154A	-0.04	-0.05	
18	H154F	-0.01	-0.07	
19	H154Y	-0.01	-0.06	
20	K172L	0.08	0.13	
21	K172R	0.17	0.18	
22	D173A	-0.05	-0.08	
23	D178E	-0.02	-0.03	
24	D178N	-0.05	-0.01	
25	D178R	-0.01	-0.01	
26	R195A	-0.01	-0.01	
27	R195L	-0.04	-0.02	
28	H196A	0.06	0.05	
29	V201L	0.01	0.03	
30	R231L	0.08	0.08	
31	K255E	0.02	0.03	
32	K255L	0.02	0.03	
33	Y307F	0.12	0.10	

Numbering	AlGE7 mutant	Slope		Lyase activity
		Parallel 1	Parallel 2	
C.34	E117K + R148G	-0.01	-0.09	
C.35	E117K + R148G + K172L	-0.02	-0.07	
C.36	R148G + K172L	-0.05	-0.06	
C.37	R148G + K172R	-0.04	-0.02	
C.38	E117K + Y122F + R148G	-0.05	-0.02	
C.39	E117K + Y122F + K172L	-0.01	0.01	♣
C.40	E117K + Y122F + K172R	-0.01	0.01	♣
C.41	E117K + Y122F + R148G + K172L	-0.06	-0.02	
C.42	E117K + Y122F + R148G + K172R	-0.07	-0.02	
C.43	E117K + Y122F + Y149F	-0.1	-0.04	

\* A slow increase in absorbance (A230) can be observed after 4-5 hours (Appendix C, Figure C.3). This may indicate weak lyase activity, shown by the colour code.

♣ The slope of parallel 1 and 2 are classified in different levels of lyase activity, inactive and less active, respectively. This may indicate very weak lyase activity, as shown by the colour code.

### 3.4.2 Proton nuclear magnetic resonance ( $^1\text{H-NMR}$ ) spectroscopy

#### $^1\text{H-NMR}$ of epimerized and degraded poly-M using B-Per II enzyme extract

The AlGE7 wild type and 25 of the mutants were selected for  $^1\text{H-NMR}$  based on analysis of the AlGE7 lyase-activity assay. Because it was used enzyme extracts and not purified enzymes for epimerization and degradation of poly-M, these  $^1\text{H-NMR}$  results have been assessed qualitatively.

In the  $^1\text{H-NMR}$  spectra, signals of both lyase and epimerase activity on poly-M substrate were identified for half of the AlGE7 mutants, while for 5 of the mutants no signals were detected for either activities. For mutant number 10 (R148G), signals for only epimerase activity were identified. This was also found for several of the combination mutants containing R148G (mutant number C.36-38, C.41 and C.42). As an example, the recorded  $^1\text{H-NMR}$  spectra showing the three different outcomes of analysed poly-M samples after reaction with the AlGE7 mutants are presented in Figure 3.13. The figure shows the spectra of the AlGE7 wild type and the following mutants: R90A (inactive lyase and epimerase), E117K (active lyase and epimerase) and R148G (active epimerase).  $^1\text{H-NMR}$  spectra for all 25 mutants are shown in Appendix E.

All spectra contain a doublet at approximately 4.5 ppm. This signal refers to non-alginate protons that have not been identified, and for simplicity this signal is labelled “unknown”.



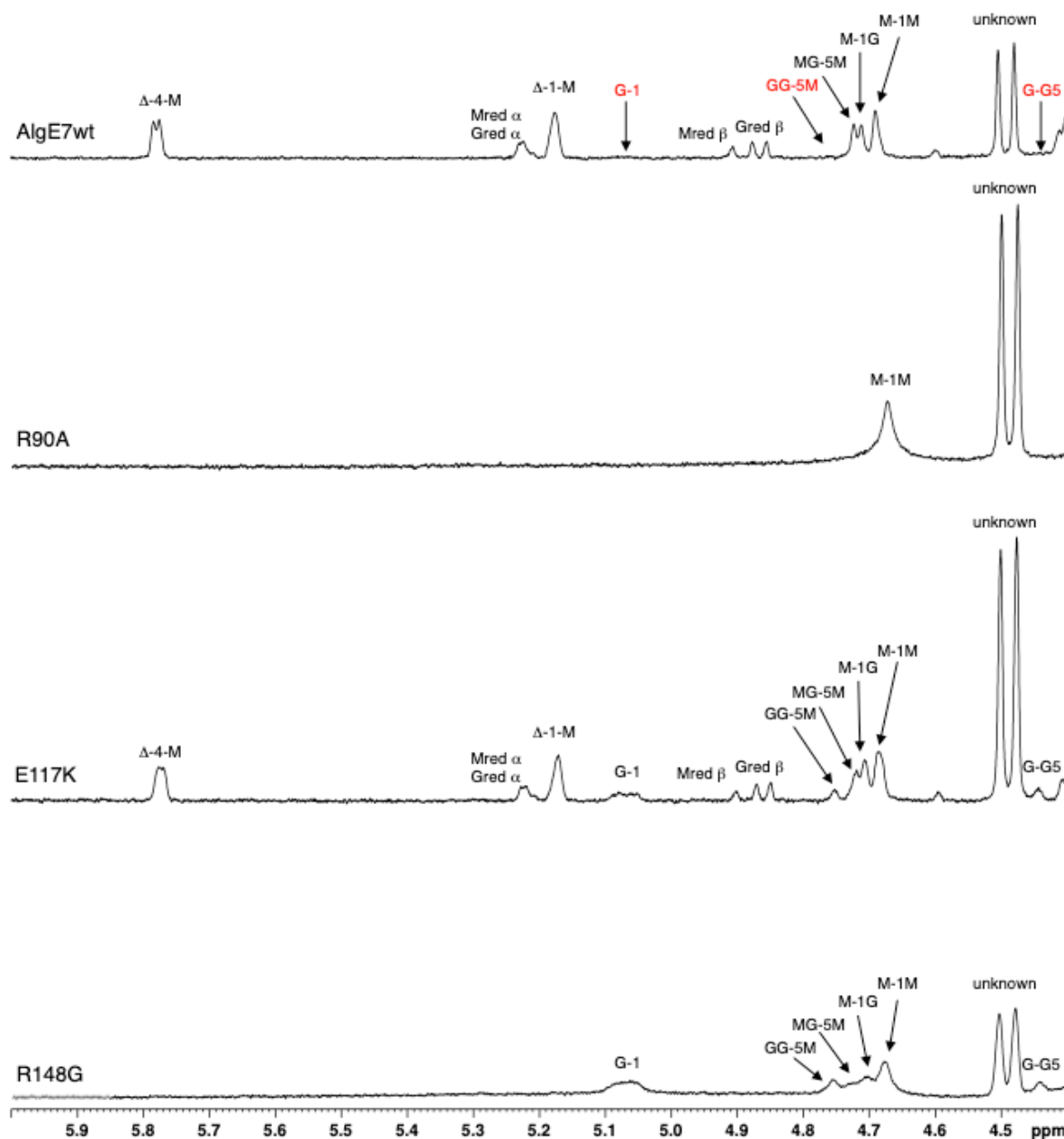


**Figure 3.13.**  $^1\text{H-NMR}$  spectra (400 MHz) showing the anomeric region of poly-M after epimerization and degradation by AlgE7 wild type and three AlgE7 point mutants (R90A, E117K and R148G) for 24 hours. The spectra were recorded at 83 °C and samples contained 1 mg/mL alginate dissolved in  $\text{D}_2\text{O}$ . The concentration of enzyme extract is not known. Missing signals from internal G-residues (G-1) and G-block signals (GG-5M, G-G5) in the AlgE7 wild type spectrum is labelled in red. The signal labelled “unknown” refers to non-alginate protons that have not been identified.

The signals from internal G-residues (G-1) and G-block signals (GG-5 and GGM-5) could not be observed in the  $^1\text{H}$ -NMR spectrum recorded for AlgE7 wild type epimerized and degraded poly-M sample (Figure 3.13). These signals were also not observed for mutant number 3 (E117L) and 21 (K172R) (Appendix E, Figure E.1 and E.3).

By integrating the  $^1\text{H}$ -NMR spectra of all samples, sequential parameters of epimerized and degraded poly-M samples were calculated using the equations from section 2.2.18 (Appendix F, Table F.1). In order to compare the AlgE7 mutants, the molar fractions  $F_{\text{Gtotal}}$ ,  $F_{\Delta}$  and  $F_{\text{Mtotal}}$  were further used as a measure of epimerase activity, lyase activity and remaining fraction of substrate monomers, respectively. These three molar fractions are presented in bar charts for all AlgE7 mutants (Figure 3.14). The mutants are sorted in three diagrams based on similar results: mutants showing similar activity as the AlgE7 wild type (Figure 3.14.A), mutants showing a lower lyase activity (Figure 3.14.B) and mutants showing only epimerase activity or no activity (Figure 3.14.C).

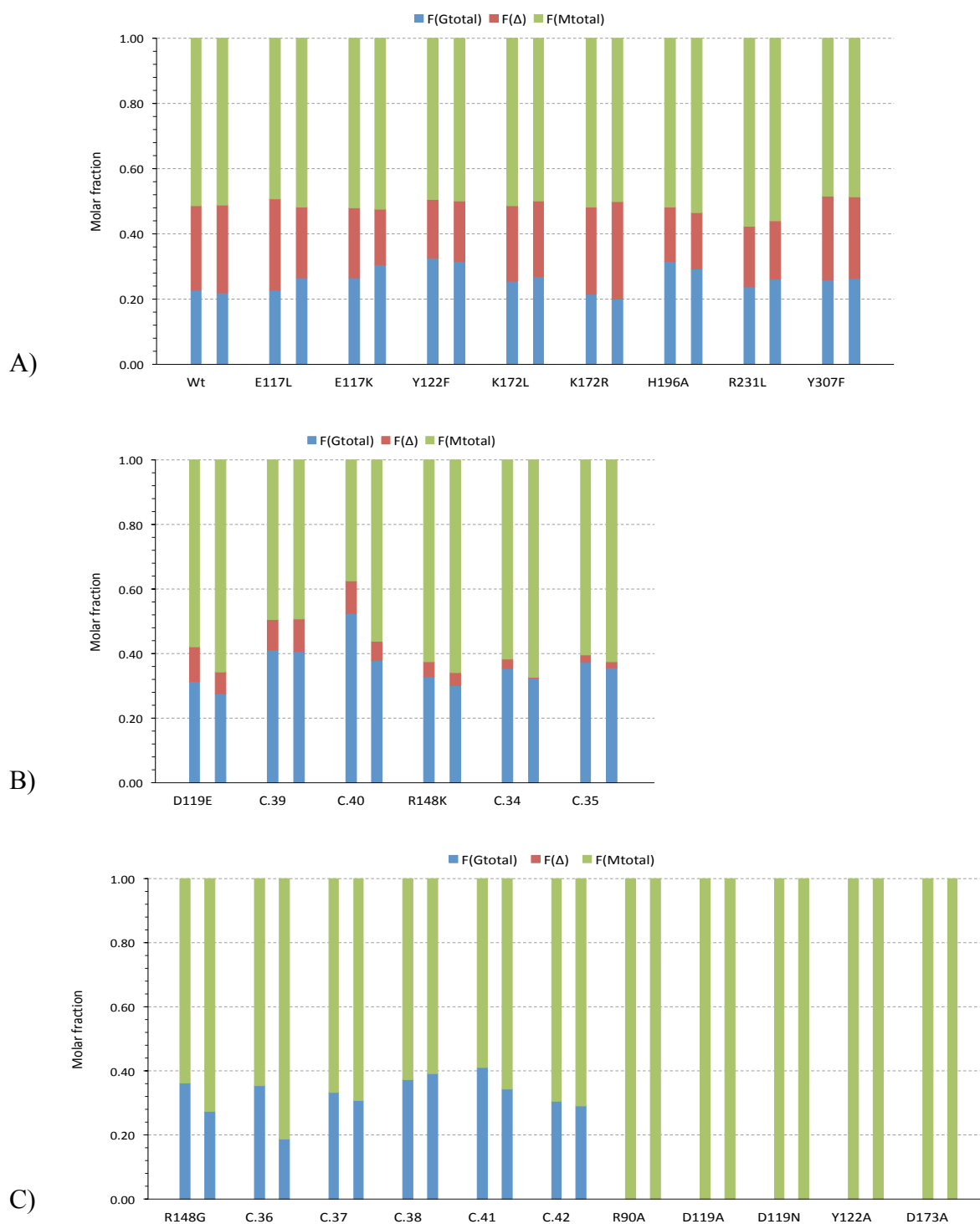


**Figure 3.14.** Molar fractions of residues epimerized ( $F_{Gtotal}$ ), bonds cleaved ( $F_{\Delta}$ ) and residues not epimerized ( $F_{Mtotal}$ ) in poly-M alginate after reaction with the AlgE7 mutants. The molar fractions are calculated from  $^1H$ -NMR data and two parallels are shown for each mutant. **A)** Epimerase (blue) and lyase (red) active mutants: AlgE7 wild type and the point mutant E117L, E117K, Y122F, K172L, K172R, H196A, R131L and Y307F. **B)** Epimerase (blue) and lower lyase (red) active mutants: point mutant D119E and R148K, and the AlgE7 combination mutants E117K+Y122F+K172L (C.39), E117K+Y122F+K172R (C.40), E117K+R148G (C.34) and E117K+R148G+K172L (C.35). **C)** Epimerase (red) active mutants: point mutants R148G, E117K+K172L (C.36), E117K+K172R (C.37), E117K+Y122F+R148G (No.38), E117K+Y122F+R148G+K172L (C.41) and E117K+Y122F+R148G+K172R (C.42). Inactive (green) mutants: R90, D119A, D119N, Y122A and D173A.

### **<sup>1</sup>H-NMR of epimerized and degraded alginate substrates using purified enzymes**

The action of AlgE7 wild type and mutant R148G on alginate substrates were monitored by <sup>1</sup>H-NMR over time after incubating poly-M (Figure 3.15) and poly-MG (Figure 3.16) alginate samples with the enzymes for 6, 12, 24, 48 and 60 hours.

In the recorded <sup>1</sup>H-NMR spectra, signals of both lyase and epimerase activity on poly-M substrate were identified for AlgE7 wild type, whereas signals for only the epimerase activity were identified for mutant R148G (Figure 3.15). Traces of lyase signals ( $\Delta$ -1-M and  $\Delta$ -4-M) were visible after 24 hours, but they were too low to integrate. When acting on poly-MG, lower signals of both lyase and epimerase activity were identified for AlgE7 wild type, while no signals for either activity were detected for mutant R148G (Figure 3.15).

The signals in the <sup>1</sup>H-NMR spectra were integrated and the sequential parameters for the epimerized and degraded alginate samples were calculated according to the equations in section 2.2.18 (Appendix F, Table F.2). By plotting the resulting molar fractions of residues epimerized ( $F_{Gtotal}$ ), bonds cleaved ( $F_{\Delta}$ ) and  $DP_n$ , against time, a more quantitative relationship of the epimerase and lyase activity could be obtained. This is shown for both enzymes acting on poly-M (Figure 3.15) and poly-MG (Figure 3.16). The plots show that for samples where both activities are detected (AlgE7 wild type), the epimerase activity is higher than the lyase activity.

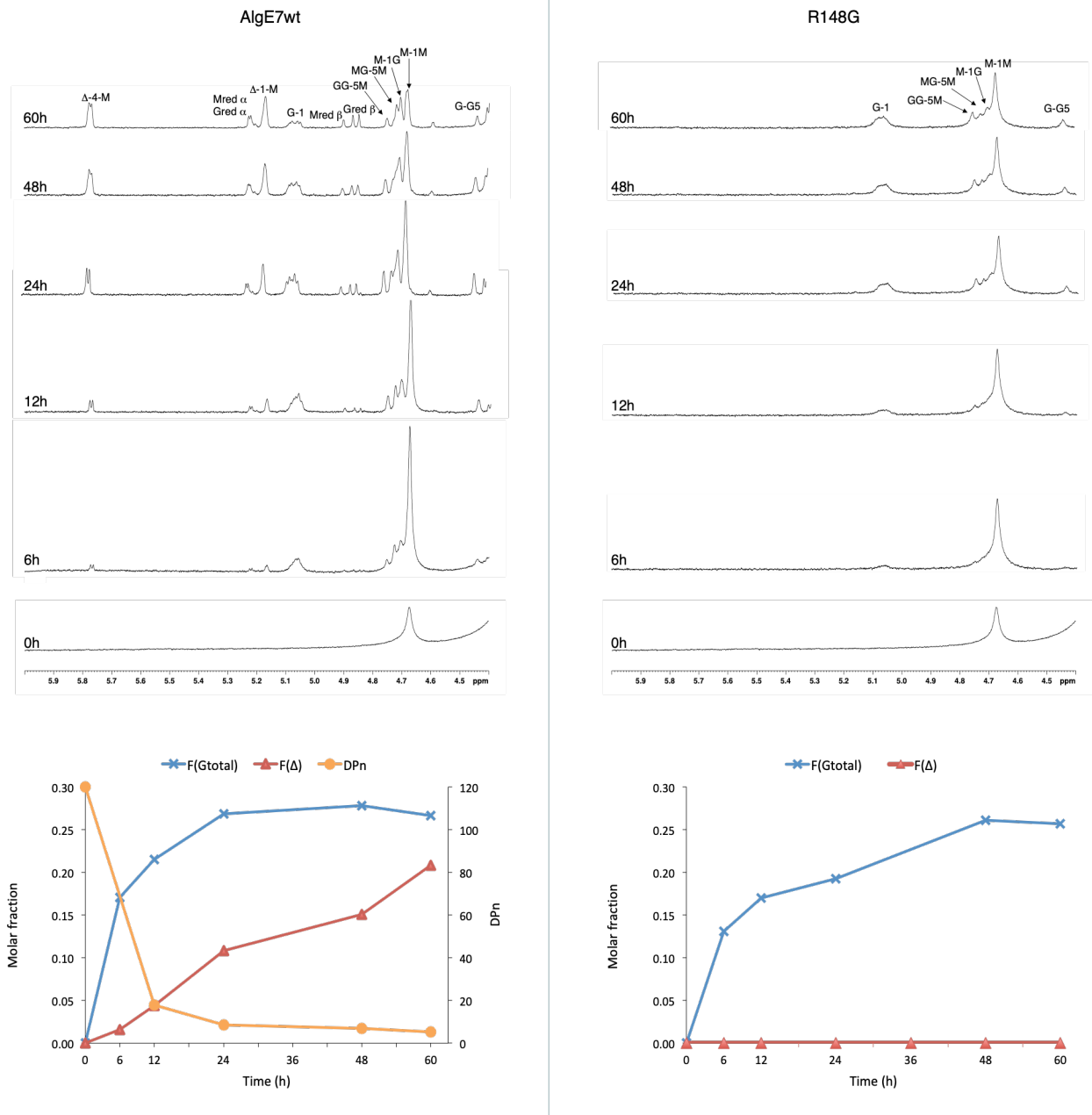


**Figure 3.15** Epimerized and degraded poly-M alginate samples after incubation with AlgE7 wild type (left) and mutant R148G (right) for 6, 12, 24, 48 and 60 hours. Enzyme to substrate ratio 1:300 w:w. At the top: the <sup>1</sup>H-NMR spectra (400 MHz) of the anomeric region of alginate are shown. The spectra were recorded at 83 °C and the samples contained 1 mg/mL poly-M alginate ( $F_M=1.0$ ) dissolved in D<sub>2</sub>O. At the bottom: the molar fractions of residues epimerized ( $F_{G_{total}}$ ), bonds cleaved ( $F_{\Delta}$ ) and DP<sub>n</sub> (only shown for AlgE7wt) plotted as a function of incubation time with the enzyme. The three molar fractions were calculated by integration of the spectra shown in the figure.

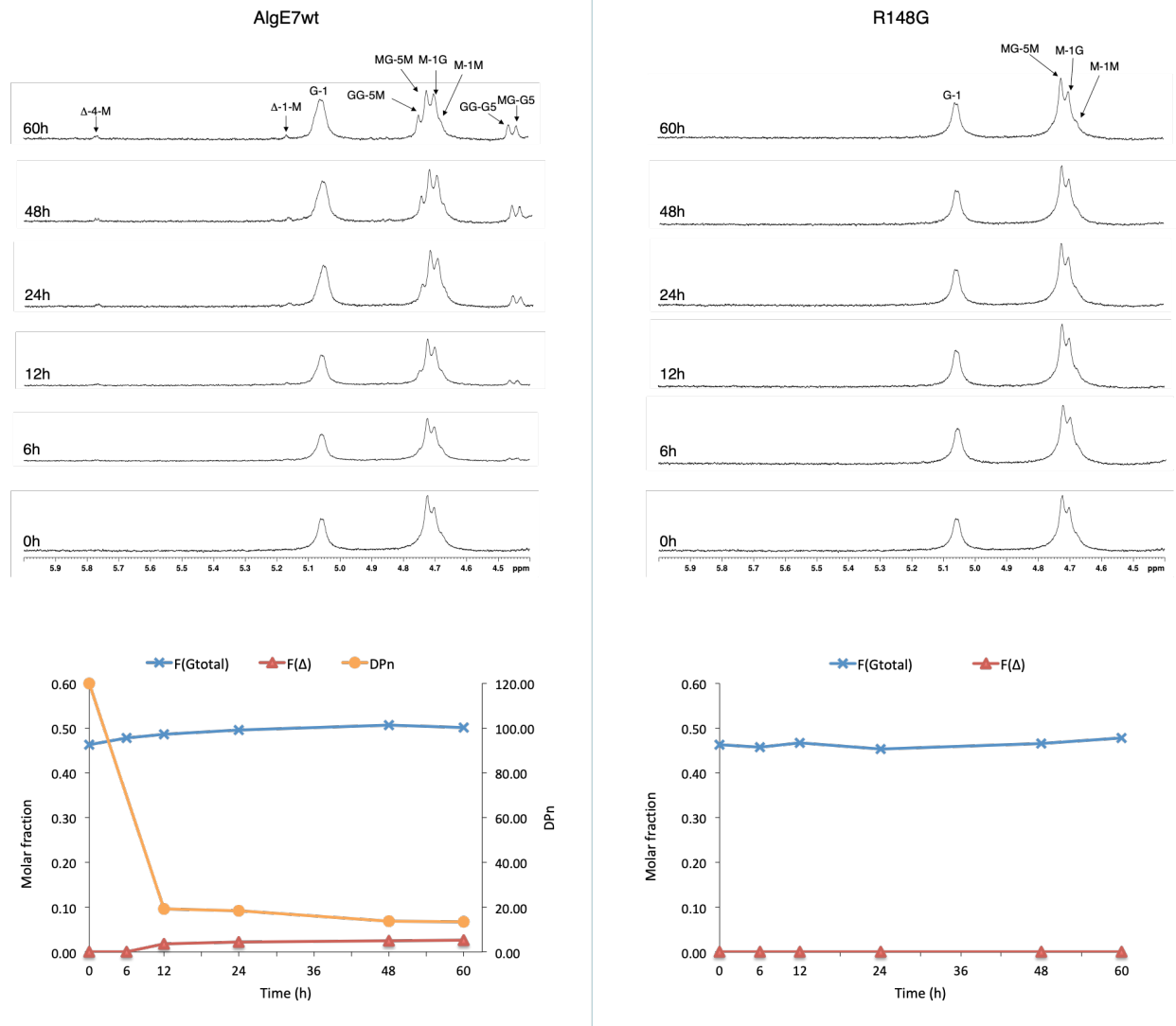


**Figure 3.16.** Epimerized and degraded **poly-MG alginate** samples after incubation with AlgE7 wild type (left) and mutant R148G (right) for 6, 12, 24, 48 and 60 hours. Enzyme to substrate ratio 1:300 w:w. At the top: the  $^1\text{H-NMR}$  spectra (400 MHz) of the anomeric region of alginate are shown. The spectra were recorded at  $83\text{ }^\circ\text{C}$  and the samples contained  $1\text{ mg/mL}$  poly-MG alginate ( $F_M=0.54$ ) dissolved in  $\text{D}_2\text{O}$ . At the bottom: the molar fractions of residues epimerized ( $F_{\text{Gtotal}}$ ), bonds cleaved ( $F_{\Delta}$ ) and  $\text{DP}_n$  (only shown for AlgE7wt) plotted as a function of incubation time with the enzyme. The three molar fractions were calculated by integration of the spectra shown in the figure.

### 3.4.3 Time-resolved $^{13}\text{C}$ -NMR spectroscopy

The bifunctional activity of AlgE7 wild type and mutant R148G in terms of epimerase and lyase activity could not directly be probed from the  $^1\text{H}$ -NMR time course. Therefore, time-resolved NMR spectra were recorded on  $^{13}\text{C}$ -enriched alginate substrates (Table 2.10) to provide detailed information of the mode of action. Further, the analysis of the data is simplified using  $^{13}\text{C}$ -enriched alginate, where only the anomeric signal for the sugar residues is followed.

For  $^{13}\text{C}$ -labeled poly-M substrate a decrease in the content of M-blocks (MMM) and an increasing signal from MGM and GMG as well as initial GGG formation were observed for both enzymes, confirming their epimerase activities (Figure 3.17 A, B). For AlgE7 wild type increasing signal from unsaturated residues next to an M residue ( $\Delta\text{M}$ ) were observed and a subsequent decrease in MGM and GGG signals, confirming lyase activity. This is also supported by an increase in the reducing end signal for M and G, which indicate that AlgE7 wild type prefer to cleave  $\text{G}\downarrow\text{MM}$ ,  $\text{G}\downarrow\text{GM}$ ,  $\text{M}\downarrow\text{MM}$  and  $\text{M}\downarrow\text{GM}$ . For mutant R148G the lyase activity are nearly abolished as only a weak increase are detected for the reducing end signal of M and G.

In addition, the end products from the reaction were analysed using a 2D  $^{13}\text{C}$  HSQC spectra. In the HSQC spectrum the correlation between the carbon and the proton directly attached to it are observed in 2D plan enhancing the resolution. For AlgE7 wild type signals for GGG, GGM and MGM are not observed in the HSQC spectrum compared to mutant R148G (Figure 3.17.C). Further, the AlgE7 wild type has clearly a strong lyase activity, as also intense signals for unsaturated residues  $\Delta\text{M}$  and reducing ends are present compared to weaker signals for mutant R148G. This confirmed that mutant R148G has very reduced overall lyase activity, while there are no indication of change in substrate performance compared to AlgE7 wild type.

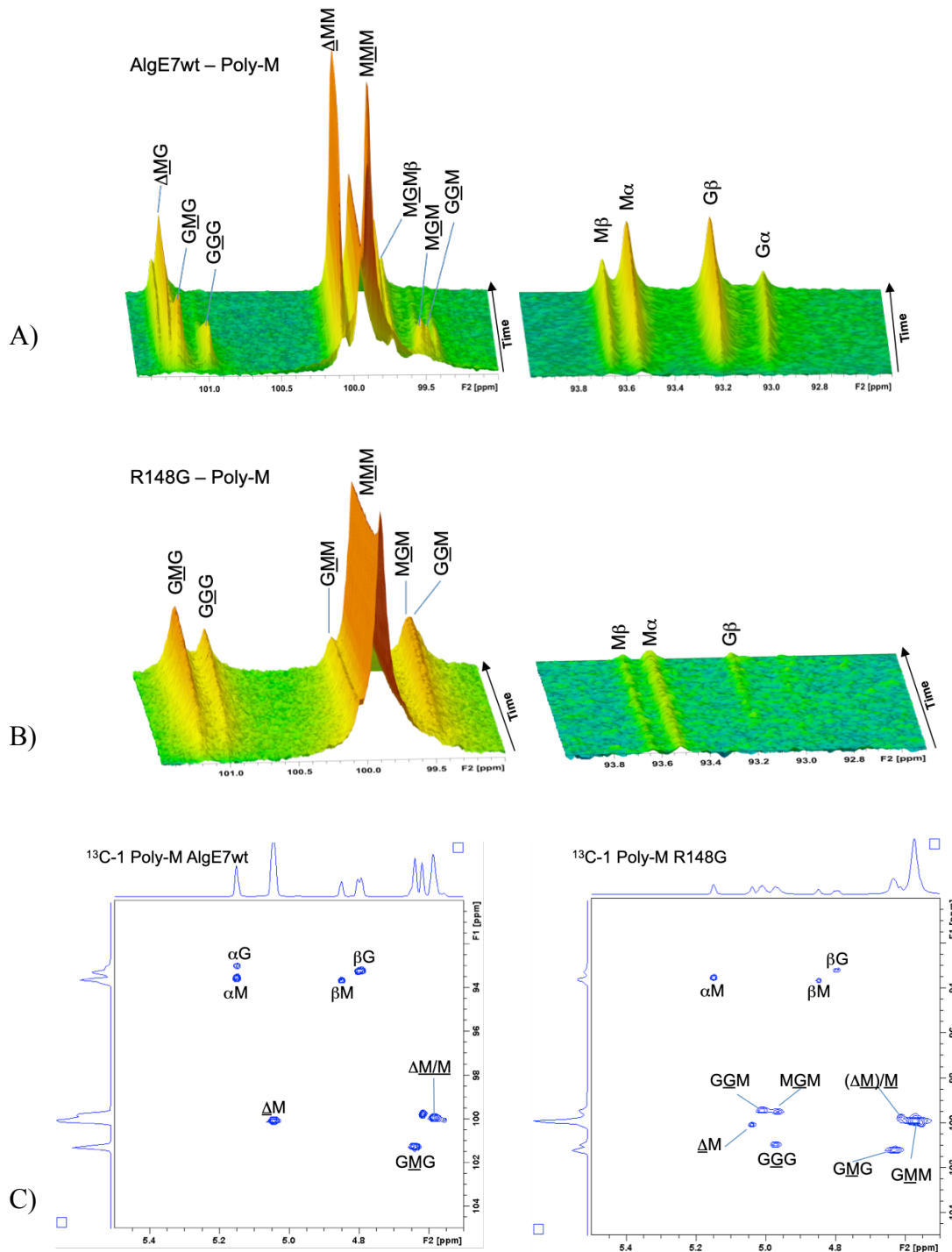


**Figure 3.17.** Time-resolved  $^{13}\text{C}$ -NMR spectra (800 MHz) showing the C1 signals of  $^{13}\text{C}$ -labeled poly-M measured over time while incubated with AlgE7 wild type (A) or mutant R148G (B). The spectra were recorded at 25 °C, and the enzyme reactions were performed in 10 mM MOPS, pH 6.9 with 75 mM NaCl, 2.5 mM  $\text{CaCl}_2$  in 99.9%  $\text{D}_2\text{O}$ . C) 2D HSQC spectra of the end products from the time-resolved reactions of poly-M for the AlgE7 wild type (right) and mutant R148G (left), recorded at 800 MHz and 25°C. The spectra show the correlation between the C1 carbon (vertically) and the proton (horizontally) directly attached. A, B and C) The position of the triads in the spectra is indicated, and the M and G monomer generating the signal is underlined. Signals marked with symbols indicate unsaturated end from the  $\beta$ -elimination reaction ( $\Delta$ ), and  $\alpha$ - or  $\beta$ -reducing end.



In the time-resolved spectra using  $^{13}\text{C}$ -labeled poly-MG substrate, a decrease in the content of MG-blocks ( $\text{MGM}$ ) and an increase in signal for  $\text{GMG}$ ,  $\text{GGM}$  and  $\text{GGG}$  were observed for both AlgE7 wild type and mutant R148G (Figure 3.18.A, B). This shows that the enzymes are able to epimerise alternating alginate substrate by filling in G-residues to form G-blocks. For AlgE7 wild type, increasing weak signals for the reducing end of M and G, and unsaturated residues next to an M as well as G were observed in the HSQC spectrum (Figure 3.18.C). This confirms presence of lyase activity and indicates that AlgE7 wild type able to cleave  $\text{G}\downarrow\text{MG}$  and  $\text{M}\downarrow\text{GG}$  (generating  $\Delta\text{G}$ ), in addition to  $\text{G}\downarrow\text{GM}$  and  $\text{M}\downarrow\text{GM}$  (generating  $\Delta\text{M}$ ).

For mutant R148G almost no lyase activity was detected in the time-resolved spectra, as only a weak increase for the reducing end signal  $\text{G}\beta$  was observed (Figure 3.18.B). However, in HSQC spectrum signals for unsaturated residues  $\Delta\text{M}$  were present for mutant R148G. This confirmed that mutant R148G display a very low lyase activity (Figure 3.18.C).

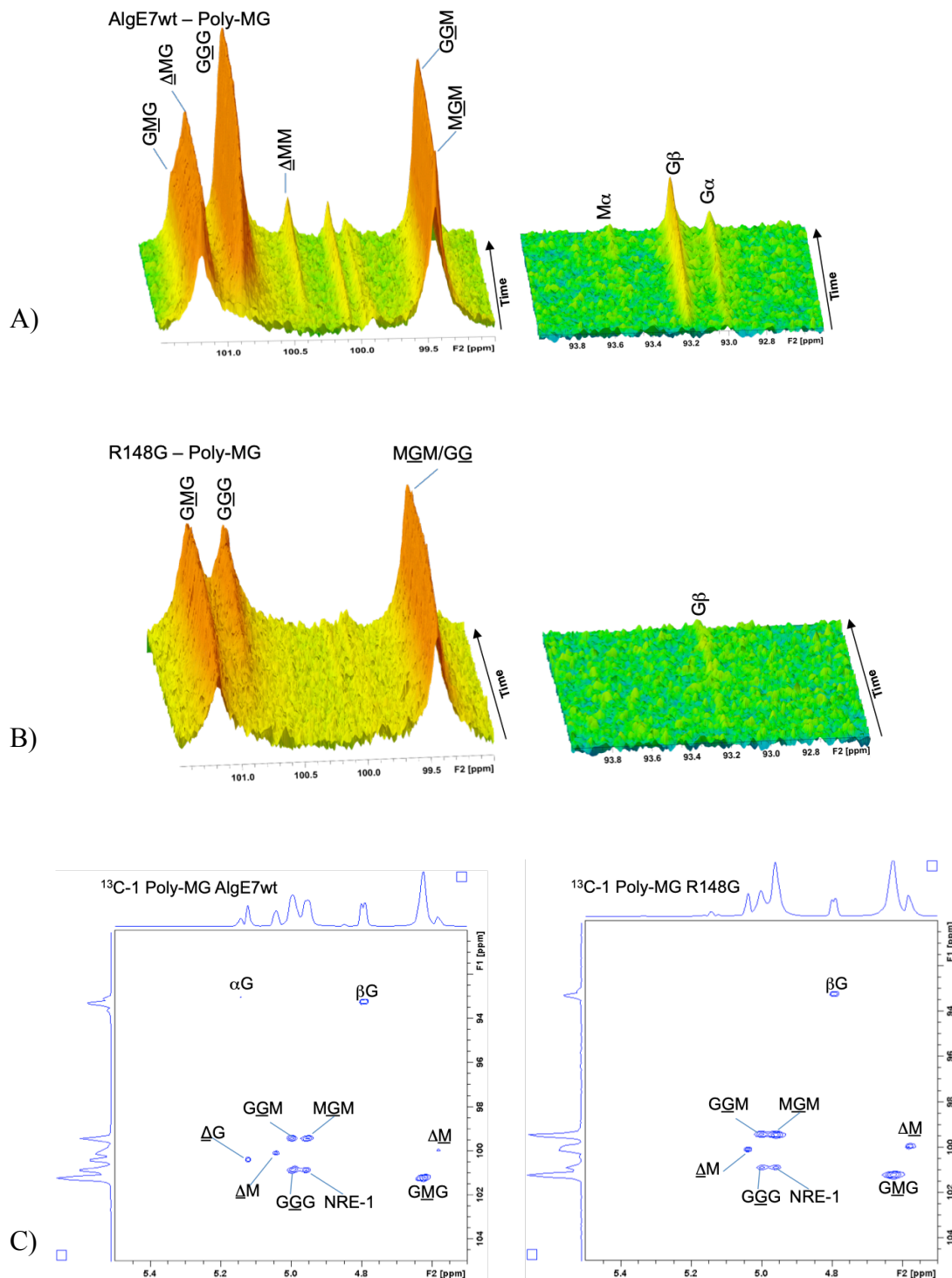


**Figure 3.18.** Time-resolved  $^{13}\text{C}$ -NMR spectra (800 MHz) showing the C-1 signals of  $^{13}\text{C}$ -labeled poly-MG measured over time while incubated with AlgE7 wild type (A) or mutant R148G (B). The spectra were recorded at 25 °C, and the enzyme reactions were performed in 10 mM MOPS, pH 6.9 with 75 mM NaCl, 2.5 mM  $\text{CaCl}_2$  in 99.9%  $\text{D}_2\text{O}$ . C) 2D HSQC spectra of the end products from the time-resolved reactions of poly-MG for the AlgE7 wild type (right) and mutant R148G (left), recorded at 800 MHz and 25°C. The spectra show the correlation between the C1 carbon (vertically) and the proton (horizontally) directly attached. A, B and C) The position of the triads in the spectra is indicated, and the M and G monomer generating the signal is underlined. Signals marked with symbols indicate unsaturated end from the  $\beta$ -elimination reaction ( $\Delta$ ), and  $\alpha$ - or  $\beta$ -reducing end. The NER-1 signal represents the C1 signal from the non-reducing end.

For  $^{13}\text{C}$ -labeled oligo-G substrate, no change were observed in terms of decrease in  $\text{GGG}$  and increase in reducing ends for either AlgE7 wild type or mutant R148G (Figure 3.19). This shows that the enzymes are not able to cleave pure G-blocks.

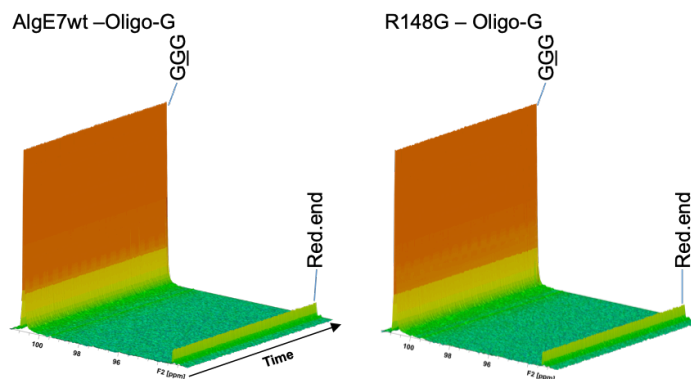


**Figure 3.19.** Time-resolved NMR spectra (800 MHz) showing the C1 signals of  $^{13}\text{C}$ -labeled oligo-G measured over time while incubated with AlgE7 wild type (left) or mutant R148G (right). The spectra were recorded at 25 °C, and the enzyme reactions were performed in 10 mM MOPS, pH 6.9 with 75 mM NaCl, 2.5 mM  $\text{CaCl}_2$  in 99.9%  $\text{D}_2\text{O}$ . The position of the triad  $\text{GGG}$  and the reducing end are labelled in the spectra.



## 4 Discussion

In the beginning of this study, the AlgE7 wild type and 42 mutants were produced and tested in a lyase-activity assay. Based on these results, 25 mutants were selected for a qualitative  $^1\text{H}$ -NMR analysis of the lyase and the epimerase activity on poly-M substrate. Finally, one mutant (R148G) and the wild type were selected for characterization of the enzyme reaction products and mode of action on different alginate substrates, using  $^1\text{H}$ -NMR and time-resolved  $^{13}\text{C}$ -NMR spectroscopy.

### 4.1 Cloning and protein production

All AlgE7 mutants investigated in this study were successfully cloned in *E. coli* DH5- $\alpha$ , of which 11 mutants were designed by using site-directed mutagenesis before subsequent transformation (Table 3.1, Table 2.9). The 31 other mutants and the wild type were cultivated from pre-existing glycerol stocks. Sanger sequencing of the isolated plasmid DNA verified the correct gene sequence for all mutants, and verified plasmids were successfully transformed into T7 express competent *E. coli*. The methods used for transformation of both DH5- $\alpha$  and T7 competent *E. coli* cells were proven to be efficient as about  $2.0\text{-}3.0 \times 10^3$  CFU/mL were obtained for each mutant.

In the first part of the cloning process, AlgE7 point mutations were introduced in the pBG27 vector (Appendix B, Figure B.1). This vector contains the necessary gene sequences for ampicillin selection of transformed cells and induction of protein expression. In order to produce pure protein with one step purification, the algE7 gene was transferred to the pTYB1 vector containing a *Sec* VMA intein tag/chitin-binding domain used for affinity chromatography with the NEB IMPACT<sup>TM</sup>-CN system (223). This was done by SLIC cloning, with which the algE7 gene in the pBG27 vector and the pTYB1 backbone were amplified and assembled. This resulted in fusion of the intein tag to the C-terminal of the algE7 gene. Based on the results from the AlgE7 lyase-activity assay and  $^1\text{H}$ -NMR using enzyme extract, five of the mutants (E117K, Y112F, R148G, K172L and K172R) were chosen for SLIC cloning.

Prior to the SLIC-reaction, amplified PCR products were verified by agarose gel electrophoresis. The agarose gels (Figure 3.6) showed expected bands for both the pTYB1 vector backbone at ~8000 bp and the algE7 gene inserts at ~2600 bp. In addition, a few faint bands representing false amplicons were seen in the gel. This may be due to factors such as insufficient stringent PCR conditions, low annealing temperature, excessive addition of primers or impurities in the PCR tube (205). False amplicons can also be a result of elevated  $Mg^{2+}$  ion concentration, which is known to inhibit the *Taq* DNA polymerase and increase the possibility of non-specific primer binding (205,209). However, Sanger sequencing of the isolated SLIC-cloned plasmid DNA verified the correct sequence for all five mutants. This confirms that the specific PCR products required for the SLIC-reaction were successfully amplified by PCR despite potential sources of error.

After transformation of T7 express competent *E. coli* cells with mutants in the pBG27 vector, the cells were cultivated on microplates and protein expression was induced. Expression of the AlgE7 proteins in the resulting B-per II enzyme extracts was confirmed by SDS-PAGE. The SDS-PAGE gels displayed multiple bands in the gels, including the expected protein bands at ~100 kDa (Figure 3.7). This band was present in similar strength for all mutants. It is therefore assumed that the production of the AlgE7 protein was very similar in all samples. This assumption is used when comparing the activity of the different mutants qualitatively (Section 4.2). Cloning and protein expression of T7 express competent *E. coli* without the pBG27 vector or containing a vector without the gene (pTrc99a) verified that the expected band at ~100 kDa corresponded to the AlgE7 protein, as these sample showed no protein band at this molecular weight (Figure 3.8). The other bands observed in the SDS-PAGE gels represents other proteins present in the enzyme extract. The experimental work discussed in this paragraph was conducted at SINTEF – Department of Biotechnology and Nanomedicine, by Randi Aune.

Protein expression and purification of the five mutants transferred to the pTYB1 vector were only performed for mutant R148G, in addition to purification of the AlgE7 wild type. As described earlier, the purification system (NEB IMPACT<sup>TM</sup>-CN system) that was used is based on fusion of an intein tag to the target protein, which in turn binds to chitin in the column resin. This system has been successfully used for purification of alginate epimerases

in previous studies, and was also shown to give pure protein in a one-step purification when used in this study (165,166,185,240).

The elution profile for AlgE7 wild type showed two absorbance peaks, with the highest absorbance seen for the first peak (Figure 3.9). As the degree of absorbance may reflect the amount of protein in each eluted fraction, this result indicates that the highest amount of protein was eluted in fraction 3 and 4. However, the amount of protein in the fractions directly eluted from the FPLC was not further evaluated, as the reducing agent DTT (used for induction of on-column cleavage) also has absorbance at 280 nm. Presence of DTT in the protein fractions would therefore affect measurements of protein concentration ( $A_{230}$ ). The chromatogram for purification of the mutant R148G was not recorded and peak intensities could therefore not be compared to the wild type. However, the elution profile for R148G showed a similar trend.

SDS-PAGE analysis showed a strong band at ~100 kDa in all lanes containing eluted protein fractions (1-7) (Figure 3.10). This band corresponds to the AlgE7 protein. However, the molecular weight shown in the gel (~100 kDa) deviates from the actual molecular weight of the protein at ~90 kDa. Previous studies of epimerases have also shown an abnormal migration when analysed by SDS-PAGE, showing that the proteins migrates to a higher molecular weight. (Ref: personal communication with Finn L. Aachmann, May 2020). The reason for this is not fully understood, but may be a result of reduced interaction with the detergent SDS that causes an incomplete denaturation of the protein. This may in turn lead to slower movement in the gel (241).

Furthermore, the SDS-PAGE gels revealed the largest amount of protein in lanes containing fraction 3 and 4, which confirms what was seen in the elution profile of the wild type. The other faint bands visible in the gels may be remnants from other proteins in the cell extracts. Strong bands were also seen at ~150 kDa in lanes with induced culture (I) and lysed cells (L). This band may correspond to the AlgE7 protein fused with the *Sec* VMA intein tag/chitin-binding domain, as this intein tag has a weight of ~50 kDa. Another possibility is presence of other proteins in the culture with weight at ~150 kDa.

In the SDS-PAGE gel for R148G, less amount of purified protein was visible than for the wild type. This was due to using half of the culture (250 mL) for purification of R148G, whereas the wild type was purified using the whole culture (500 mL). After FPLC, the fractions were combined into three samples and DDT was removed from the samples by dialysis. The protein concentration in the samples of R148G was measured (Table 3.3) and the yield of purified protein was found to be 4.2 mg per 500 mL culture. This was not determined for the wild type. However, the molecular weight standard in the SDS-PAGE gels looks relatively similar when comparing the wild type and R148G. This implies that a higher protein yield was purified for the wild type. This is also consistent with the fact that a double amount of culture was used for purification of the wild type.

## 4.2 Qualitative analysis of AlgE7 mutants

### Variation and uncertainties in the data

The lyase activity on poly-M alginate was tested for all AlgE7 mutants using an activity assay (Table 3.4). This procedure was conducted by Randi Aune at SINTEF – Department of Biotechnology and Nanomedicine. Analysis of both the lyase and epimerase activity on poly-M samples for 25 of the mutants was further done using  $^1\text{H}$ -NMR spectroscopy (Figure 3.14). All these results are regarded as qualitative, due to variation and uncertainties associated with the data. One reason for this is that the B-Per II enzyme extracts contain unknown enzyme concentrations. This makes it difficult to compare the different mutants directly. However, SDS-PAGE analysis (Figure 3.7) after protein production showed no notable difference in the amount of protein produced for the different mutants, as previously discussed in section 4.1. It is therefore assumed that a similar amount of enzyme was present in the enzyme extracts for all samples.

Variations between the two parallels observed in the data from the AlgE7 lyase-activity assay can also be explained by presence of other components in the enzyme extracts that may have interfered with the measurements. In addition, differences in initial absorbance values for almost all samples were seen (Appendix C). For several AlgE7 mutants, there was also a drop in the absorbance measurements during the first hour. The cause of this drop is uncertain, but could be a consequence of random error in measurements during the first hour. Another



explanation might be precipitation of components in the enzyme extract when it was added to the microplate containing buffer and poly-M substrate.

In the  $^1\text{H-NMR}$  spectra recorded for the negative control poly-M sample (mutant R90A, discussed in following paragraphs), a doublet at 4.5 ppm that refers to non-alginate protons was seen (labelled “unknown in Figure 3.13). This signal has not been identified, but is assumed to originate from components present in the B-Per II enzyme extract. The “unknown” signal was present in the spectra recorded for all samples, but at different intensities. This observation may be due to different amounts of the unknown component in the enzyme extracts. However, alginate proton signals appear to have similar intensities when comparing the two parallels for each mutant, supporting the assumption that similar amount of enzyme is present in all samples. Some variation between the two parallels is observed, but this does not affect the overall result for the mutant.

### **Reason for selection some mutants for $^1\text{H-NMR}$**

Based on analysis of the lyase-activity assay of AlgE7 mutants, the lyase and epimerase activity in 25 of the mutants were analysed by  $^1\text{H-NMR}$ . The reasons for selecting these mutants are described in the following paragraph.

Mutants E117L, E117K, Y122A, Y122F, R148G, R148K, K172L and K172R, were selected because residue E117, Y122, R148 and K172 are conserved as different amino acids in all the other AlgE enzymes (156) (Figure 3.4, Table 3.1), and thus stands out as interesting in AlgE7. Several of these mutants are also included in the combination mutants that were chosen, in which comparison may be difficult without analysis of the single mutants. Residue R231 also stands out, being a positively charged residue in AlgE7, while hydrophobic in all the other AlgE enzymes. The mutants of residue D119 (D119A, D119E and D119N) were selected to determine if the negative charge of this residue also is essential for the epimerase activity. Mutant Y307F was chosen in order to study changes in the epimerization pattern, as recent studies has proven that this residue (Y/F 307) is essential for defining the block pattern of AlgE epimerases (172). Based on the interesting findings for mutant R148G found from the activity assay, all combination mutants (C.34-C.42) except mutant E117K+Y122F+Y149A (C.43) were included for  $^1\text{H-NMR}$  analysis. Mutant C.43 was not included due to mutation of the catalytic residue Y149, which resulted in no activity. Mutant D173A and H196A were included because these residues have previously been found to be important for the epimerase

activity in AlgE4 (166), and because it was interesting to study if the mutations at these residues also would effect the epimerase activity. Finally, mutant R90A was included as a negative control in order to assess potential impurities in the anomeric region of alginate proton signals. This mutant showed no lyase activity in the activity assay, and has previously demonstrated to be an inactive epimerase when the same mutation is introduced in AlgE4 (Ref: personal communication with Margrethe Gaardl os, January 2020). It was therefore hypothesized that R90A in AlgE7 also would be an inactive epimerase. This was confirmed by the  $^1\text{H-NMR}$  results.

### Classification of mutants

In order to evaluate and compare the results for all AlgE7 mutants analysed by the activity assay and  $^1\text{H-NMR}$ , a classification of the mutants were made. When assessing the results from the lyase activity assay it was assumed that the A230 measurement followed an initial zero-order reaction. This assumption appears to hold, as there was observed a somewhat linear initial increase in absorbance that slows down over time, presumably due a decrease in substrate available for the enzyme. Further, the slope of a linear regression line of the first 4 hours was used to evaluate the lyase activity for all samples (Figure 3.12). Based on the resulting slope values, the mutants were divided into three groups of lyase activity: active lyase, less active lyase, and inactive lyase (Table 3.4). Classification in these groups seemed reasonable by assessment of the slope for the two parallels. However, a few mutants were difficult to classify, and in these cases a visual interpretation of the absorbance plots have been used.

A similar classification of lyase activity was made when assessing the  $^1\text{H-NMR}$  results. The recorded spectra of the poly-M samples after incubation with the AlgE7 mutants mainly showed three different outcomes: epimerase and lyase activity, only epimerase activity and no activity (Figure 3.13). To compare the mutants further, bar charts with three calculated molar fractions ( $F_{\text{Gtotal}}$ ,  $F_{\Delta}$ ,  $F_{\text{Mtotal}}$ ) were made to illustrate the epimerase and lyase activity in all samples (Figure 3.14). For almost all mutants included in the  $^1\text{H-NMR}$  analysis, the classification of lyase activity corresponds with the results from the activity assay. Exceptions are mutant H196A, E117K+R148G (C.34) and E117K+R148G+K172L (C.35) (Table 3.4, Figure.14.A, B). Mutant H196A was classified with lower lyase activity in the activity assay, but was included in the group with similar activity as the wild type in the  $^1\text{H-NMR}$  results. This was done because H196A showed similar total activity ( $F_{\text{Gtotal}} + F_{\Delta}$ ) as the wild type, and

not as reduced lyase activity as the other mutants with lower lyase activity. Mutants C.34 and C.35 were initially classified as inactive lyases (activity assay). However, as more information is obtained from  $^1\text{H-NMR}$  results, a low lyase activity was observed for these mutants when analysed by  $^1\text{H-NMR}$ .

### **Inactive lyase mutants**

26 of the mutants were classified as inactive lyases (Table 3.4, Figure 3.14.C). In this group there were 11 mutants that contained a mutation in one of the catalytic residues (Y149, D152, H154 and D178). No lyase activity was measured for these mutants, supporting the assumption made in previous studies that the epimerase and lyase activity originates from the same active site (156,168). As these residues also is proven to be essential for the epimerase activity in AlgE epimerases, the mutants mutated in a catalytic residue were not further investigated in this study (166,168). For the inactive lyase mutants R195A and R195L, the same mutations have showed very low epimerase activity when tested in AlgE4 (166)(Ref: personal communication with Margrethe Gaardl s, January 2020). These mutants were therefore not analysed by  $^1\text{H-NMR}$ . For mutant R90A, D119A, D119N, Y122A and D173A no epimerase activity was detected by  $^1\text{H-NMR}$ , and so these residues are thought to be important for the overall catalytic activity. The remaining inactive mutants are discussed in following paragraphs.

### **AlgE7 wild type**

The results for the wild type confirmed that the AlgE7 epimerase displays both epimerase and lyase activity (Table 3.4, Figure 3.14.A). However, no signals from internal G-residues (G-1) and the G-block signals GG-5 and GGM-5 were detected in the  $^1\text{H-NMR}$  spectra for AlgE7 wild type epimerized and degraded poly-M sample (Figure 3.13). This is not consistent with what is seen for the wild type in an earlier study (156). Nevertheless, in a previous study using time-resolved  $^1\text{H-NMR}$  might offer an explanation for the missing signals. This study showed that after some time more G-monomers were consumed by bond cleavage than formed by epimerization, resulting in a decrease in  $F_G$ , and thus lower G-block signals over time (168). A similar trend was also seen in the time-resolved  $^{13}\text{C-NMR}$  results obtained in the study presented here, as discussed in section 4.3. The G-1, GG-5 and GGM-5 signals were also not detected in the spectra for mutant E117L and K172R (Appendix E. Figure E.1 and E.3). In addition, the other signals for these mutants were also relatively similar to the wild type, indicating that the mutations made at these residues do not have a large effect on the

catalytic activity of AlgE7. This is also seen in the bar charts comparing the mutants (Figure 3.14.A).

### **Mutants with similar activity as the wild type**

Several of the mutants (E117L, E117K, Y122F, K172L, K172R, H196A, R231L, Y307F) showed epimerase and lyase activity relatively similar to the wild type (Table 3.4, Figure 3.14.A). Within this group, three of the mutants (E117K, Y122F and K172L) possess a substitution into an amino acid that is conserved at the specific residue in the other AlgE epimerases (156) (Figure 3.4, Table 3.1), neither of which display lyase activity. It could therefore be assumed that changes of residue E117, Y122 and K172 would have a significant effect on the lyase activity of AlgE7. However, the amino acid substitutions made at these residues (E117L, E117K, Y122F, K172L and K172R) seems to only lead to a small reduction of lyase activity. These residues are all positioned close to the active site (Figure 3.5), and by exchanging or removing the charge (in case of mutants E117L, E117K, K172L and K172R) the chemical environment changes. For this reason, the reduced activity seen can be thought to result from altered electrostatic interactions with other residues, which possibly changes the positioning and binding of the negatively charged substrate at the active site. This may in turn reduce the likelihood for lyase the activity to take place.

For mutant Y122F, the change of a tyrosine (Y) into the similar sized amino acid phenylalanine (F), removes the polar OH-group projecting toward the catalytic residue H154 (Figure 3.5). It is possible that the OH-group on Y122 interacts with H154. Further, it can be suggested that the lower lyase activity observed for mutant Y122F are due to loss of this potential interaction, which consequently may change the positioning of residue H154. Moreover, when residue Y122 is replaced by an alanine (A) in mutant Y122A, no epimerase or lyase activity was detected. This may suggest that the hydrophobic surface of residue Y122 has a role in regulating binding of the substrate.

Despite the reasons for the change in lyase activity observed for mutant E117L, E117K, Y122F, K172L and K172R, the results indicate that residue E117, Y122 and K172 are not key residues for aborting the lyase activity. However, the combination mutant E117K+Y122F+K172L (C.39) and E117K+Y122F+K172R (C.40) shows that mutation of these residues simultaneously has a larger effect on the lyase activity (Table 3.4, Figure 3.14.B). This suggests that residues E117, Y122 and K172 have a role facilitating lyase the

activity in AlgE7, possibly due to changes in interactions with other residues on the protein surface of the binding groove or binding of the substrate, as discussed in the previous paragraph.

Another mutant classified as an active mutant was mutant R231L. At residue 231, there is a positively charged arginine (R) in AlgE7 whereas a hydrophobic Leucine (L) or Valine (V) in all other AlgE epimerases (156) (Figure 3.4, Table 3.1). The mutant for this residue (R231L) showed only slightly lower total activity ( $F_{\text{Gtotal}} + F_{\Delta}$ ) than the wild type, indicating that the positive charge is not essential for either of the two activities in AlgE7. However, by analysing the obtained spectra for this mutant (Appendix E, Figure E.4), the intensity of the  $M_{\text{red}}\beta$  signal are stronger than  $G_{\text{red}}\beta$  signal, which is the opposite of what is observed for the wild type and the other lyase active mutants. The molar fractions of reducing ends reveal much lower amount of  $G_{\text{red}}$  ( $F_{\text{Gred}} = 0.04$ ) than  $M_{\text{red}}$  ( $F_{\text{Mred}} = 0.14$ ) residues compared to the wild type ( $F_{\text{Gred}} = 0.12$ ,  $F_{\text{Mred}} = 0.16$ ) (Appendix F, Table F.1). This may suggest that the positive charge of residue R231 have a role in binding of the negatively charged alginate substrate, so that cleavage of  $G\downarrow MM$  and  $G\downarrow GM$  bonds (generating  $G_{\text{red}}$ ) are preferred.

Studies have indicated that the wild type has preference for  $G\downarrow MM$  and  $G\downarrow GM$  bonds (168), whereas in this study the amount of  $M_{\text{red}}$  was higher than  $G_{\text{red}}$  for the wild type, indicating preference for the other two proposed cleavage sites  $M\downarrow MM$  and  $M\downarrow GM$ . Nevertheless, the reaction condition used in this study differ from the conditions in the previous study with regards to factors such as pH, temperature ionic strength and concentration of  $\text{Ca}^{2+}$  ions, which may effect the product profile obtained. For example, the temperature used for the epimerase and lyase reaction in this study was 25 °C, whereas 37°C were used in pervious study. The latter is also the temperature found to be the optimum for the lyase activity in AlgE7 (168), which thus may explain the differences seen regarding the molar fraction of reducing ends. However, as the  $^1\text{H-NMR}$  results discussed here are regarded as qualitative, no conclusion of the inconsistency seen for the wild type compared to previous studies (168) or the role for the positive charge of residue R231 can be determined.

Considering mutant Y307F, the recorded  $^1\text{H-NMR}$  spectra showed lower G-1, GG-5 and GGM-5 signals than for the other mutants (Appendix E, Figure E.4). This is thought to be a consequence of changed epimerization pattern from G-blocks to MG-blocks, as recent studies

strongly suggests that residue Y or F at position 307 influences the epimerization pattern by regulation substrate binding when studied in AlgE4 and AlgE6 (172). However, this could not be confirmed, as lower signals for G-blocks also can be a consequence of lyase activity.

### **Mutants with lower lyase activity**

Moving on to consider the mutants displaying lower lyase activity than the wild type (Table 3.4, Figure 3.14.B). This includes mutant D119E, R148K, P153A, V201L, K255E, K255L, E117K+R148G (C.34), E117K+ R148G + K172L (C.35), E117K+Y122F+K172L (C.39) and E117K+Y122F+K172R (C.40). The lower lyase activity observed suggests that the residues changed are of importance for the AlgE7 lyase activity. However, lower lyase activity may also be a consequence of decreased epimerase activity, which can result in fewer preferred cleavage sites in the alginate substrate. As mentioned earlier, the potential cleavage sites for AlgE7 are G↓MM, G↓GM, M↓MM and M↓GM. These cleavage sites were proposed in earlier studies based on only identifying  $\Delta$ M unsaturated non-reducing end signals and  $G_{\text{red}}$  than  $M_{\text{red}}$  reducing end signals, where  $G_{\text{red}}$  dominates over  $M_{\text{red}}$  (168). AlgE7 is therefore thought to prefer cleavage at end of G-blocks (G↓MM, G↓GM), which thus require efficient epimerisation of the poly-M substrate. For the mutants displaying lower lyase activity that were included for the  $^1\text{H-NMR}$  analysis (D119E, R148K, C.34, C.35, C.39 and C.40), the total activity ( $F_{\text{Gtotal}}+F_{\Delta}$ ) was lower compared to the wild type, confirming a reduced epimerase activity (Figure 3.14.B). Exceptions from this are combination mutant C.39 and C.40, which seems to have a total activity ( $F_{\text{Gtotal}}+F_{\Delta}$ ) similar to the wild type.

Analysis of the lyase activity assay initially classified mutant P153 as inactive (Table 3.4). However, analysis of the absorbance plots for this mutant revealed an increase in the A230 measurements after 4 hours of measuring (Appendix D, Figure D.3). This could be a consequence of the drop in A230 measurements seen during the first hour. Another possible explanation is that enzyme first has to create its own substrate by epimerizing poly-M before it can act as a lyase. This concept has previously been proposed in  $^1\text{H-NMR}$  experiments with AlgE7 acting on different substrates (168). Moreover, structural study of residue P153 reveals that the residue is positioned between the two catalytic residues D152 and H154, and underneath the binding groove (Figure 3.5). It is therefore likely that residue P153 (conserved among all AlgE epimerases) is important for structural stability and correct positioning of the neighbouring catalytic residues in the active site. Nevertheless, the results in this study are not

sufficient for concluding on this theory and in addition, mutant P153A was only examined in the activity assay and so the epimerase activity has not been investigated.

Two of the mutants displaying lower lyase and epimerase activity were particularly interesting (Figure 3.14.B). The first is D119E, in which the negatively charged aspartic acid (D) is changed into the slightly larger negatively charged glutamic acid (E). Being negatively charged, both amino acids are able to form electrostatic interactions with other residues on the protein surface as well as repel the negatively charged substrate. Moreover, E has one additional methylene group in its side chain, and so the position of the positive charged differs compared to D. Changing residue D119 into E, may therefore change some electrostatic interactions within the structure. This could for example lead to a translocation of the substrate in the binding groove, subsequently affecting the catalytic activity of the enzyme.

Comparing mutant D119E with the other two mutations obtained at this residue (D119A and D119N), it is evident that the negative charge is essential for both the lyase and epimerase activity as mutant D119A and D119N (not possessing a charge) displayed no enzyme activity (Table 3.4, Figure 14.B,C). By examining the homology model for AlgE7, residue D119 is positioned in the vicinity of the active site (Figure 3.5). The negative charged residue D119 can therefore be assumed to be important for correct positioning of the substrate. Moreover, residue D119 is conserved among all AlgE epimerases (156) (Figure 3.4, Table 3.1), implying that the residue is significant for the epimerization reaction. This can be supported by studies with AlgE4, which has reported that residue D119 probably are involved in determining the epimerization pattern (158).

The second mutant of interest that displayed lower lyase and epimerase activity was mutant R148K. By studying residue R148 in the homology model, it is located on the surface of the binding groove very close to the catalytic residue Y149 (Figure 3.5). Being a positively charged arginine (R), residue R148 displays several potential electrostatic interactions (222,242). It is thus likely that R148 interacts with Y149 possibly by hydrogen bonding with the OH-group on the aromatic ring in tyrosine (Y). In addition, residue R148 may also facilitate neutralization of charge and binding of the negatively charged poly-M substrate. For mutant R148K, changing R into the positively charged lysine (K) reduced the lyase activity (Table 3.4, Figure 3.14.B). This can be explained by the two amino acids different geometries, in which arginine residues on protein surfaces have been reported to facilitate

more stable electrostatic interactions than lysine residues (242). Changing into a lysine is therefore thought to alter the chemical environment near the active site and the interaction with the negatively charged substrate. This may in turn change the possible interaction with Y149 and positioning of the substrate, consequently affecting the catalytic activity.

### **Mutant R148G**

In contrast to mutant R148K, substituting residue R148 into glycine (G) appeared to abort the lyase activity completely while epimerase activity was still present (Table 3.4, Figure 3.14.C). This was the most interesting observation from the <sup>1</sup>H-NMR results, as this was not seen for any of the other single mutants. In addition, almost all combination mutants containing R148G (R148G+K172L (C.36), R148G+K172R (C.37), E117K+Y122F+R148G (C.38), E117K+Y122F+R148G+K172L (C.41), E117K+Y122F+R148G+K172R (C.42)) showed no lyase activity. However, one important difference that was not seen from the activity assay was observed by <sup>1</sup>H-NMR. For two of the combination mutants containing R148G (E117K+R148G (C.34) and E117K+R148G+K172L (C.35)) there was detected very low lyase activity ( $F_{\Delta}$ ). This may indicate that mutant R148G might display some lyase activity, even though this was not seen for the single mutant. In addition, all residues mutated in C.34 and C.35 were changed into the amino acids conserved for the other AlgE epimerases (156) (Figure 3.4, Table 3.1). This could be expected to further reduce the lyase activity, and so the result of the combination mutants indicates that more residues are involved in obtaining lyase activity in AlgE7. Still, the results from the qualitative analysis strongly suggest that R148 is a key residue for the AlgE7 lyase activity. This will be further discussed in section 4.3.

In order to further characterize mutant R148G, the mutated *algE7* gene were transferred by SLIC to the pTYB1 vector containing the *Sec* VMA intein tag/chitin-binding domain, needed for protein purification using affinity chromatography. Along with mutant R148G, mutant E117K, Y122F, K172L and K172R were also SLIC cloned into pTYB1. These mutants were chosen because residue E117, Y122F and K172 are conserved as another amino acid in all the other AlgE epimerases, and because they are included in the combination mutants with R148G. It could therefore be interesting to study these mutants, with a future perspective of also analysing the combination mutants.



### 4.3 Analysis of the AlgE7 wild type and mutant R148G

To elucidate the enzyme reaction products and mode of action of AlgE7 wild type and mutant R148G,  $^1\text{H-NMR}$  and time-resolved  $^{13}\text{C-NMR}$  were recorded on different alginate substrates. Although different reaction conditions were used for the two NMR methods, the results have been compared qualitatively.

#### Action of the AlgE7 wild type

The amount of G-residues ( $F_{\text{Gtotal}}$ ) introduced by the wild type on poly-M ( $F_{\text{G}}=0.0$ ) was found to increase with longer incubation time (Figure 3.15, left), increasing the G-content to about 28% ( $F_{\text{Gtotal}}=0.28$  at 48h). In addition, after 48 hours the lyase activity ( $F_{\Delta}=0.15$ ) had degraded the substrate ( $\text{DPn}=370$ ) to oligomers with an average length of 7 residues ( $\sim 13$  bonds cleaved per 28 residues epimerized). After this point the G-content seems to decrease, while the amount of unsaturated residues ( $F_{\Delta}$ ) continues to increase. This can also be seen by visual inspection of the  $^1\text{H-NMR}$  spectra recorded after 48 and 60 hours of incubation, as the signals for G-residues ( $\underline{\text{G}}-1$ ,  $\underline{\text{GG}}-5\text{M}$ ,  $\underline{\text{MG}}-5\text{M}$  and  $\text{G}-\underline{\text{G}}5$ ) decreases whereas signals lyase activity ( $\text{M}_{\text{red}\alpha}$ ,  $\text{G}_{\text{red}\alpha}$ ,  $\text{M}_{\text{red}\beta}$ ,  $\text{G}_{\text{red}\beta}$ ,  $\Delta-4\text{-M}$  and  $\Delta 1\text{-M}$ ) increases. By assessing the time-resolved  $^{13}\text{C-NMR}$  spectra, a similar trend was seen (Figure 3.17.A). Triads containing G-residues ( $\underline{\text{MGM}}$ ,  $\underline{\text{GMG}}$ ,  $\underline{\text{GGM}}$ ,  $\underline{\text{GGG}}$ ) initially increased followed by a rapid decrease of the same triads. Simultaneously, increasing signals of unsaturated residues  $\Delta\text{M}$  and reducing end signals of M and G residues were also observed. These findings are consistent with earlier studies, showing that the epimerase activity initially dominates over the lyase activity (168). This may indicate that the epimerization reaction of AlgE7 generates a new alginate substrate that is more favourable for cleavage than the initially poly-M substrate.

In contrast to the results obtained by  $^1\text{H-NMR}$ , the time-resolved  $^{13}\text{C-NMR}$  spectra also revealed that the signals of MG-blocks ( $\underline{\text{MGM}}$ ,  $\underline{\text{GMG}}$ ) are generated earlier than G-blocks ( $\underline{\text{GGG}}$ ) in the reaction. Then, both MG-block and G-block signals decreased. This suggests that mode of action for the AlgE7 wild type on poly-M substrates initially is introduction of alternating G-residues to create MG-blocks, followed by either cleavage of MG-blocks or generation of G-blocks, which in turn also are cleaved. For the epimerization activity, this mode of action is in line with the previous proposed mode of actions for the AlgE1, AlgE4 and AlgE6 epimerase, which suggest that the enzyme epimerizes every other residue in a

processive manner without the need for rotation (neighbouring residues are rotated about  $180^\circ$  with respect to each other) (178,184,185).

From the proposed mode of action, it seems that the AlgE7 wild has a preference for cleaving substrates containing G-residues. This is further supported by the fact that no  $\underline{MGM}$ ,  $\underline{GMG}$ ,  $\underline{GGG}$  signals were present in the HSQC spectrum for the AlgE7 wild type (Figure 3.17.C), which implies that these sequences were cleaved in the final end products from the time-resolved reactions. However, cleavage between of M-blocks can not be excluded based on the results from this study, since signals for reducing ends of M-residues as well as G-residues were observed. Furthermore, the signal for only unsaturated residue next to an M ( $\Delta M$ ) was detected. Taken together, the signals observed for the lyase activity is consistent with the proposed cleavage sites ( $G\downarrow MM$ ,  $G\downarrow GM$ ,  $M\downarrow MM$  and  $M\downarrow GM$ ) for AlgE7 (168), as discussed in section 4.2. However, a clear preference for cleavage in front G or a M-residue could not be determined based on the NMR data discussed in this section. This is due to not observing any significant difference between the amount of reducing ends for G and M residues, with regards to the molar fractions ( $G_{red}$  and  $M_{red}$ ) obtained from  $^1H$ -NMR (Appendix F, Table F.2) as well as signal the intensities observed in the time-resolved  $^{13}C$ -NMR and HSQC spectra.

When acting on poly-MG substrate ( $F_G=0.46$ ), the NMR data confirmed that the AlgE7 wild type is able to epimerise poly-MG by filling in G-residues in the alternating substrate chain, generating G-blocks (Figure 3.16.left and Figure 3.18.A,C). However, by assessing the  $^1H$ -NMR results, the epimerization of poly-MG substrate appear to be much less efficient compared to epimerization of poly-M. The increase in G-content ( $F_G=0.51$  at 48h) was much lower on poly-MG substrate (Figure 3.16. left) than on poly-M (Figure 3.15.left). In the same period of time the lyase activity also appear to be less efficient on poly-MG substrate, as the amount of unsaturated residues ( $F_\Delta=0.03$ ) were much lower and the average chain length ( $DP_n=13-14$ ) was higher than for the wild type ( $F_\Delta=0.15$ ,  $DP_n=7$ ) (Appendix F, Table F.2). However, the  $DP_n$  of the poly-MG substrate used is not determined, and so the comparison of molar fractions must be taken with caution. Despite of unknown  $DP_n$  of the substrate, the data clearly indicate lower lyase activity with poly-MG substrate. One possible explanation this might be that, because poly-MG initially possesses only one of the proposed cleavage sites ( $M\downarrow GM$ ), epimerization has to take place in order to generate more preferred cleavage sites

(G↓GM). This theory may also be strengthened by observation of weak signals for unsaturated residues next to a G ( $\Delta$ G), in addition to weak  $\Delta$ M signals (also seen for the reaction on poly-M), observed in the time-resolved  $^{13}\text{C}$ -NMR and HSQC spectra (Figure 3.18.A,C). The same  $\Delta$ G signal has previously been reported for AlgE7 acting on poly-MG substrates, indicating that the enzyme also is able to cleave G↓MG and M↓GG bonds (168). Thus, epimerization on poly-MG is thought to generate a new pattern that serves as a substrate for the lyase activity of AlgE7.

By assessing the signals for reducing ends for the action of AlgE7 on poly-MG substrate, conflicting results were observed between the  $^1\text{H}$ -NMR and  $^{13}\text{C}$ -NMR data. From  $^1\text{H}$ -NMR (Figure 3.16.left, Appendix F), the molar fraction of reducing ends of M ( $F_{\text{Mred}}=0.05$ ) was found to be higher than reducing ends of G ( $F_{\text{Gred}}=0.02$ ), which may indicate that the enzyme prefers cleavage in front of a M residue when acting on poly-MG substrate. Conversely, stronger signals were observed for reducing ends of G- than M-residues in the time-resolved  $^{13}\text{C}$ -NMR and HSQC spectra (Figure 3.18.A, C), suggesting a preference for cleavage in front of a G-residue. A possible explanation is presence or absence of salt (NaCl) in the buffers used for enzyme reaction. Salt was only used in the buffer used for the reaction in the time-resolved  $^{13}\text{C}$ -NMR data, and so it can be thought that salt affects the activity of the AlgE7 enzyme.

Considering the time-resolved results using oligo-G substrate, the results showed that neither the AlgE7 wild type nor mutant R148G were able to cleave pure G-blocks (Figure 3.19). Nevertheless, this result may indicate that for the lyase reaction to take place, epimerization is also required, and so the enzyme is thought not bind the oligo-G substrate as strong as substrates containing M-residues. Furthermore, it can be hypothesized that for each binding event of enzyme with a substrate, a processive mode of epimerization is initiated before cleavage of the polymer chain leading dissociation from the substrate. Assuming that this is true, no lyase activity of oligo-G substrate should be observed as shown in the results. However, the results presented in this study is not efficient for concluding on this theory.

### Action of mutant R148G

For mutant R148G, only strong signals for epimerase activity on poly-M were observed in the  $^1\text{H-NMR}$  spectra, while signals for the lyase activity were barely visible after 24 and 60 hours of incubation (Figure 3.15, right). The amount of G-residues was found to increase similar to the wild type, as the G-content had increased to about 26 % ( $F_{\text{Gtotal}}=0.26$ ) after 48 hours. However, during the same time period virtually no G-residues had been consumed by the lyase reaction. This indicates that the mutant also has lower epimerase activity than the wild type. Another observation, supporting the lower epimerase activity for R148G can be seen from the time-resolved  $^{13}\text{C-NMR}$  and HSQC results (Figure 17.B,C). As weak signals for both  $\alpha$  and  $\beta$  reducing ends were observed for M-residues and very weak signals for only the  $\beta$  reducing end were seen for G-residues, it can be assumed that mutant R148G cleaves in front of a M-residue (resulting in  $M_{\text{red}}$ ) more often than in front of a G-residue (resulting in  $G_{\text{red}}$ ). Further, this may indicate that the epimerase activity of mutant R148G generates more MG-blocks than G-blocks, which in turn can be explained by the previous suggested mode of action for the AlgE7 enzyme – first generating MG-blocks followed by filling in the alternating substrate to create G-blocks.

When incubating mutant R148G with poly-MG substrate, no change in the signals for the original MG-substrate were detected by  $^1\text{H-NMR}$  (Figure 3.16, right). However, the  $^{13}\text{C-NMR}$  and HSQC spectra revealed that the mutant is able to introduce G-blocks (GGG) in the substrate (Figure 3.18.B,C). In addition, weak signals for reducing ends of G-residues ( $G\beta$ ) and unsaturated  $\Delta\text{M}$  residues were observed, confirming presence of weak lyase activity. These different results may be explained by the use of different reaction conditions. As previously stated, salt (NaCl) were present in the buffer used for the time-resolved  $^{13}\text{C-NMR}$  and not in the buffer used for the enzyme reaction prior to  $^1\text{H-NMR}$ . It can thus be possible that salt contributes to shielding of the charge, which may alter the chemical environment by interacting with charged residues on the protein surface. This may in turn change the electrostatic interactions within the enzyme structure, and hence the positioning of the catalytic residues and binding of the substrate. Salt also contributes to less intermolecular charge repulsion in the negatively charged alginate substrate, reducing the chain expansion of the polymer (11,32,60). This might affect binding of the substrate in the active site of the enzyme. Overall, it seems that salt affects the enzyme activity of mutant R148G, since no activity were seen even after 60 hours of incubation when analysed by  $^1\text{H-NMR}$ .

*Why is the lyase activity nearly abolished in mutant R148G?*

Residue R148 is alkaline, due to being a positively charged arginine (222), and as mentioned in the previous section, this residue is neighbouring and possibly hydrogen-bonding with the catalytic residue Y149 (Figure 3.5). The catalytic role of residue Y149 as a proton donor or a proton acceptor is not fully understood. By assuming that Y149 acts as a proton donor in the third step of the reaction mechanism (Section 1.2.3), it can be proposed that R148 is able to compete with the alginate substrate for the donating proton due to its ability as to act as base. When residue R148 is in its deprotonated form it may abstract the proton from Y149 so that the proton can not be donated to the alginate substrate. This may in turn cause occasional cleavage of the glycosidic bonds instead of epimerization. If this is true, changing the residue R148 into the non-polar glycine (G) will remove the ability of residue R148 to function as a proton acceptor, which thus offers an explanation for the strongly reduced lyase activity observed for mutant R148G.

However, the pKa value of the positively charged guanidinium group of arginine is usually very high (pKa ~12), and so the protonated form predominates at physiological pH (222,243). Arginine residues are therefore generally considered poor candidates for a role as a base. Nevertheless, studies have suggested that arginine residues may facilitate abstraction of protons and thus act as a base in some enzyme reactions, e.g. reactions catalysed by fumarate reductase, pectate and pectin lyases (244–246). In these studies, the proximity to other positively charged residues was proposed to be a factor in lowering the pKa value of the arginine residue. In addition, interactions with carboxylate groups in other residues and/or the substrate are suggested to lower the pKa value by limiting the ability of the NH<sub>2</sub>-groups to form hydrogen bonds with other residues. This may in turn force the guanidinium group into a non-planar conformation, which is a less favourable conformation for the protonated guanidinium group (244,247). On the basis of these studies, it can be proposed that the positively charged residue K172 and the negatively charged carboxylate groups of residues E117, D119 and D152 positioned close to residue R148 (Figure 3.5), contributes to the alkaline character of residue R148 by lowering the pKa value. Interaction with the carboxylate group at C5 in the alginate substrate may perhaps enhance this effect.

Another factor that might affect the reaction mechanism of AlgE7 is the change in substrate conformation as the enzyme progressively epimerizes the substrate. It is difficult to determine the orientation of the substrate in the binding groove and how the substrate orientation

changes during the reaction. This also makes it difficult to presume the role of the catalytic residue Y149 as a proton donor or acceptor in the reaction mechanism, and to understand the mechanism that facilitates lyase activity.

From this work, it is evident that residue R148 is significantly important for the lyase activity in AlgE7. However, no conclusion on the specific role of this residue in the lyase reaction can be established. Moreover, the lyase activity is not completely abolished by mutating residue R148. This strengthens the assumption that some of the other residues investigated in this study, or other residues not yet investigated, have a role in facilitating the lyase activity.

#### 4.4 Further work

On the basis of the work presented in this thesis, residue R148 stands out as very important residue with regard to the lyase activity of AlgE7. As this activity is not seen for any of the other AlgE epimerases, it would be very interesting to further investigate if a mutation of the same residue (G148) into the positively charged arginine (R) could make them able to cleave alginate substrates. Furthermore, prediction studies of pKa values of the residues close to the active site in AlgE7 may also give more insight into the role of residue R148 in lyase activity.

The result presented in this work also points out residue E117, Y122 and K172 as interesting candidates for future study. When these residues were collectively mutated in AlgE7, the lyase activity was strongly reduced, and so it would be noteworthy to also mutate these residues in the other AlgE epimerases to see if they will contribute to and perhaps enhance lyase activity.

To analyse whether the reduced lyase and/or epimerase activity seen for many of the AlgE7 mutants is due to altered binding interactions with the alginate substrate, Isothermal titration calorimetry (ITC) experiments could be performed (248). This method could also be used to determine the pH dependence of the interactions of charged residues, as well as the possible need of salt for correct positioning of the catalytic residues and binding of the substrate.

Investigation of the dependence of salt might also clarify why the results from  $^1\text{H-NMR}$  and  $^{13}\text{C-NMR}$  showed differences in lyase activity for the mutant R148G, and could also explain the differences seen with regards to preferred cleavage sites when examining the AlgE7 wild type using the different NMR methods

## 5 Conclusion

The aim of this project was to gain a better understanding of the dual catalytic activity of the *A. vinelandii* mannuronan C5-epimerase and alginate lyase AlgE7. This was conducted by mutating residues close to active site and substrate binding groove, followed by an analysis of the effect these mutations with the purpose of getting more insight to why AlgE7 displays lyase activity as the only one of the AlgE epimerases.

A study of 42 mutants in addition to the wild type were initially included in this project, and tested for lyase activity. Further analysis of the epimerase activity was done for 25 of the mutants, before one mutant (R148G) and the wild type were purified and characterised. In general, one residue (R148) positioned close to the catalytic site was found to be especially important for the lyase activity in AlgE7, as the single mutant R148G displayed a strongly reduced lyase activity. This is suggested to be a result of residue R148 possibly interacting with and attracting the proton on the catalytic residue Y149, due to its ability as to act as base. This proton is assumed to be donated from Y149 to the alginate substrate in the third step of the epimerisation mechanism. Interaction with residue R148 is thus proposed to occasionally disrupt the epimerization reaction and lead to cleave of the glycosidic bonds in the alginate chain. However, this proposed mechanism could not be determined based on the work presented in this study. To further investigate the role of this residue in AlgE7, experiments with mutation of residue 148 in the other AlgE epimerases and pKa analysis of residues near the active site have been suggested.

For the remaining mutants, it appears that residue E117, Y122 and K172 also has a role in facilitating the lyase activity. This was not prominent by analysis of the single mutants, but examination of the combination mutants including the same single mutations in these residues revealed a clearly reduced lyase activity compared to the wild type. These residues are therefore pointed out as interesting for future study.

In addition, the work presented for the characterization of the AlgE7 wild type confirmed that the enzyme acts as an epimerase by introducing G-blocks to the alginate chain, and as a lyase by generating unsaturated  $\Delta$ M residues as well as reducing end signals of M and G when acting on poly-M alginate. This confirms the four previously suggested cleavage sites G $\downarrow$ MM, G $\downarrow$ GM, M $\downarrow$ MM and M $\downarrow$ GM. Nevertheless, preferences for cleavage in front of a G- or a M-residue could not be determined from this study. Furthermore, it was also found that the AlgE7 are able to epimerize and cleave poly-MG alginate, but with lower efficiency. However, the enzyme displayed no lyase activity on oligo-G alginate substrate, and is therefore thought to not be able to cleave inside G-blocks.



## References

1. Moradali MF, Ghods S, Rehm BHA. Alginate biosynthesis and biotechnological production. In: Rehm BHA, Moradali MF, editors. *Alginates and Their Biomedical Applications*. Singapore: Springer Nature Singapore; 2018. p. 1–19.
2. Standford ECC. On Algin: a new substance obtained from some of the commoner species of marine algae. *Chem News*. 1883;47(1):254–69.
3. Okazaki M, Furuya K, Tsukayama K, Nisizawa K. Isolation and Identification of Alginic Acid from a Calcareous Red Alga *Serraticardia maxima*. *Botanica Marina*. 1982;25(3):123–31.
4. Usov AI, Bilan MI, Klochkova NG. Polysaccharides of algae 48. polysaccharide composition of several calcareous red algae: isolation of alginate from *Corallina pilulifera* P. et R. (Rhodophyta, Corallinaceae). *Botanica Marina*. 1995;38(1):43–51.
5. Gorin PAJ, Spencer JFT. Exocellular alginic acid from *Azotobacter vinelandii*. *Canadian Journal of Chemistry*. 1965 May;44(9):993–8.
6. Linker A, Jones R. A Polysaccharide resembling alginic acid from a *Pseudomonas* microorganism. Vol. 204, *Nature* (London U.K.). 1964.
7. Haug A. Composition and properties of alginates. *Rep Norw Inst Seaweed Res No30*. 1964;30:25–45.
8. Atsuki K, Tomoda Y. Studies on seaweeds of Japan I. The chemical constituents of *Laminara*. *J soc Chemi Ind Jpn*. 1926;29:509–17.
9. Hirst EL, Jones JKN, Jones WO. Structure of alginic acid. Part I *J Chem Soc*. 1939 May;1:1880–5.
10. Fischer FG, Dorfel H. Die Polyuronsäuren der Braunalgen (Kohlenhydrate der Algen I). *Hoppe-Seyler's Z Physiol Chem*. 1955;302(1):186–203.
11. Smidsrød O, Moe S. *Biopolymer chemistry*. Trondheim: Tapir Academic Press; 2008. 23–383 p.
12. Haug A, Larsen B, Smidsrød O. A study on the constitution of alginic acid by partial hydrolysis. *Acta Chem Scand*. 1966;20(1):183–90.
13. Ertesvåg H, Høidal HK, Schjerven H, Svanem BIG, Valla S. Mannuronan C-5-epimerases and their application for in vitro and in vivo design of new alginates useful in biotechnology. *Metabolic Engineering*. 1999 Jul;1(3):262–9.

14. Atkins EDT, Mackie W, Smolko EE. Crystalline structures of alginic acids. *Nature*. 1970;225(5233):626–8.
15. Smidsrød O, Glover RM, Whittington SG. The relative extension of alginates having different chemical composition. *Carbohydrate Research*. 1973 Mar;27(1):107–18.
16. Atkins EDT, Nieduszynski IA, Mackie W, Parker KD, Smolko EE. Structural components of alginic acid. I. The crystalline structure of poly- $\beta$ -D-mannuronic acid. Results of X-ray diffraction and polarized infrared studies. *Biopolymers*. 1973;12(8):1865–78.
17. Atkins EDT, Nieduszynski IA, Mackie W, Parker KD, Smolko EE. Structural components of alginic acid. II. The crystalline structure of poly- $\alpha$ -L-guluronic acid. Results of X-ray diffraction and polarized infrared studies. *Biopolymers*. 1973;12(8):1879–87.
18. Mackie W, Perez S, Rizzo R, Taravel F, Vignon M. Aspects of the conformation of polyguluronate in the solid state and in solution. *International Journal of Biological Macromolecules*. 1983;5:329–41.
19. Haug A, Larsen B, Smidsrød O. Uronic acid sequence in alginate from different sources. *Carbohydrate Research*. 1974 Feb 1;32(2):217–25.
20. Cammack R, Atwood T, Campbell P, Parish H, Smith A, Vella F, et al., editors. *Oxford Dictionary of Biochemistry and molecular Biology*. 2nd ed. Oxford: Oxford University Press; 2006.
21. Draget KI, Smidsrød O, Skjåk-Bræk G. Alginates from Algae. In: Steinbüchel A, Rhee S., editors. *Biopolymers Online*. Weinheim: Wiley-VCH Verlag GmbH & Co. KGaA; 2005. p. 1–25.
22. Grasdalen H, Larsen B, Smidsrød O. A P.M.R study of the composition and sequence of uronate residues in alginate. *Carbohydrate Research*. 1979;68(1):23–31.
23. Grasdalen H, Larsen B, Smidsrød O.  $^{13}\text{C}$ -NMR studies of monomeric composition and sequence in alginate. Vol. 89, *Carbohydrate Research*. 1981.
24. Grasdalen H. High-field,  $^1\text{H}$ -n.m.r. spectroscopy of alginate: sequential structure and linkage conformations. Vol. 118, *Carbohydrate Research*. 1983.
25. Aarstad OA, Tøndervik A, Sletta H, Skjåk-Bræk G. Alginate sequencing: an analysis of block distribution in alginates using specific alginate degrading enzymes. *Biomolecules*. 2011;13(1):106–16.
26. Bakkevig K, Sletta H, Gimmestad M, Aune R, Ertesvåg H, Degnes K, et al. Role of the *Pseudomonas fluorescens* alginate lyase (AlgL) in clearing the periplasm of alginates not exported to the extracellular environment. *Journal of bacteriology*. 2005 Dec;187(24):8375–84.

27. Haug A, Smidsrød O. Strontium–Calcium selectivity of alginates. *Nature*. 1967;215(5102):757.
28. Haug A, Smidsrød O. Selectivity of some anionic polymers for divalent metal ions. *Acta Chemica Scandinavia*. 1970;24:843–54.
29. Smidsrød O. Molecular basis for some physical properties of alginates in the gel state. *Faraday Discussions of the Chemical Society*. 1974;57:263–74.
30. Grant GT, Morris ER, Reese DA, Smith PJC, Thom D. Biological interactions between polysaccharides and divalent cations: The egg-box model. *FEBS Letters*. 1973;32(1):195–8.
31. Morris ER, Rees DA, Thom D. Characterization of polysaccharide structure and interaction by circular dichroism: Order-disorder transition in the calcium alginate system. *J Chem Soc Chem Commun*. 1973;0(7):245–6.
32. Donati I, Paoletti S. Material Properties of Alginates. In: Rehm BHA, editor. *Alginates: Biology and Applications*. Springer-Verlag Berlin Heidelberg; 2009. p. 2–46.
33. Braccini I, Pérez S. Molecular basis of Ca<sup>2+</sup>-induced gelation in alginates and pectins: the egg-box model revisited. *Biomacromolecules*. 2001;2(4):1089–96.
34. Sikorski P, Mo F, Skjåk-Bræk G, Stokke BT. Evidence for egg-box-compatible interactions in calcium-alginate gels from fiber X-ray diffraction. 2007;8(7):2098–103.
35. Plazinski W. Molecular basis of calcium binding by polyguluronate chains. Revising the egg-box model. *Journal of Computational Chemistry*. 2011;32(14):2988–95.
36. Skjåk-Bræk G, Donati I, Paoletti S. Alginate Hydrogels: Properties and Applications. In: Matricardi P, Alhaique F, Covirillo T, editors. *Polysaccharide Hydrogels - Characterization and Biomedical Applications*. 1st ed. New York: Jenny Stanford Publishing; 2016. p. 449–84.
37. Smidsrød O, Haug A. Dependence upon the gel-sol state of the ion-exchange properties of alginates. *Acta Chemica Scandinavia*. 1972;26(5):2063–74.
38. Stokke BT, Smidsrød O, Bruheim P, Skjåk-Bræk G. Distribution of uronate residues in alginate chains in relation to alginate gelling properties. *Macromolecules*. 1991 Aug;24(16):4637–45.
39. Stokke BT, Smidsrød O, Zanetti F, Strand W, Skjåk-Bræk G. Distribution of uronate residues in alginate chains in relation to alginate gelling properties - 2: Enrichment of  $\beta$ -D-mannuronic acid and depletion of  $\alpha$ -L-guluronic acid in sol fraction. *Carbohydrate Polymers*. 1993;21(1):39–46.
40. Bowman KA, Aarstad OA, Nakamura M, Stokke BT, Skjåk-Bræk G, Round AN. Single molecule investigation of the onset and minimum size of the calcium-mediated junction zone in alginate. *Carbohydrate Polymers*. 2016;148:52–60.

41. Donati I, Holtan S, Mørch YA, Borgogna M, Dentini M, Skjåk-Bræk G. New Hypothesis on the role of alternating sequences in calcium-alginate gels. 2005;6(2):1031–40.
42. Mørch YA, Holtan S, Donati I, Strand BL, Skjåk-Bræk G. Mechanical properties of C-5 epimerized alginates. *Biomacromolecules*. 2008;9(9):2360–8.
43. Martinsen A, Skjåk-Bræk G, Smidsrød O. Alginate as immobilization material: I. Correlation between chemical and physical properties of alginate gel beads. *Biotechnology and Bioengineering*. 1989 Jan 5;33(1):79–89.
44. Haug A, Larsen B. The solubility of alginate at low pH. *Acta Chemica Scandinavica*. 1963;17(6):1653–62.
45. Draget K., Skjåk-Bræk G, Smidsrød O. Alginic acid gels: the effect of alginate chemical composition and molecular weight. *Carbohydrate Polymers*. 1994;25(1):31–8.
46. Haug A, Myklestad S, Larsen B, Smidsrød O. Correlation between chemical structure and physical properties of alginates. *Acta Chemica Scandinavica*. 1967;21(3):768–78.
47. Hartmann M, Dentini M, Ingar Draget K, Skjåk-Bræk G. Enzymatic modification of alginates with the mannuronan C-5epimerase AlgE4 enhances their solubility at low pH. *Carbohydrate Polymers*. 2006;63(2):257–62.
48. Haug A. Fractionation of alginic acid. *Acta Chemica Scandinavica*. 1959;13:601–3.
49. Haug A. Ion exchange properties of alginate fractions. *Acta Chemica Scandinavica*. 1959;13:1250–1.
50. Draget KI, Moe ST, Skjåk-Bræk G, Smidsrød O. Alginates. In: Stephen AM, Phillips GO, Williams PA, editors. *Food polysaccharides and their applications*. 2nd ed. 2006. p. 289–334.
51. Haug A, Smidsrød O. The effect of divalent metals on the properties of alginate solutions. II. Comparison of different metal ions. *Acta Chemica Scandinavica*. 1965;19(2):341–51.
52. Yian Wong T, Preston LA, Schiller NL. Alginate lyase: review of major sources and enzyme characteristics, structure-function analysis, biological roles, and applications. *Annu Rev Microbiol*. 2000;54:289–340.
53. Suzuki H, Suzuki K, Inoue A, Ojima T. A novel oligoalginate lyase from abalone, *Haliotis discus hannai*, that releases disaccharide from alginate polymer in an exolytic manner. *Carbohydrate Research*. 2006;341(11):1809–19.
54. Gacesa P. Enzymic degradation of alginates. *International Journal of Biochemistry*. 1992 Apr;24(4):545–52.
55. Gacesa P. Alginate-modifying enzymes. *FEBS Letters*. 1987 Feb 23;212(2):199–202.

56. Smidsrød O, Draget K. Alginates: chemistry and physical properties. *Carbohydrate Europe*. 1996;47:6–13.
57. Smidsrød O, Haug A. A light scattering study of alginate. *Acta Chemica Scandinavica*. 1968;22(3):797–810.
58. Smidsrød O. Solution properties of alginate. *Carbohydrate Research*. 1970;13(3):359–72.
59. Zhang H, Wang H, Wang J, Guo R, Zhang Q. The effect of ionic strength on the viscosity of sodium alginate solution. *Polymers for Advanced Technologies*. 2001;12(11–12):740–5.
60. Smidsrød O, Haug A. Estimation of the relative stiffness of the molecular chain in polyelectrolytes from measurements of viscosity at different ionic strengths. *Biopolymers*. 1971;10(7):1213–27.
61. Painter TJ. Algal polysaccharides. *Algal polysaccharides*. 1983;2:195–258.
62. Black WAP. The seasonal variation in weight and chemical composition of the common British Laminariaceae. *Journal of the Marine Biological Association of the United Kingdom*. 1950;29:45–72.
63. Andersen I-L, Skipnes O, Smidsrød O, Ostgaard K, Hemmer PC. Some biological functions of matrix components in benthic algae in relation to their chemistry and the composition of seawater. In: *Cellulose chemistry and technology*. ACS Suposium Series; 1977. p. 361–81.
64. Indergaard M, Skjåk-Bræk G. Characteristics of alginate from *Laminaria digitata* cultivated in a high-phosphate environment. *Hydrobiologia*. 1987;151(1):541–9.
65. Linker A, Jones RS. A new polysaccharide resembling alginic acid isolated from *Pseudomonads*. *The Journal of biological Chemistry*. 1966;241(16):3845–51.
66. Cote GL, Krull LH. Characterization of the exocellular polysaccharides from *Azotobacter chroococcum*. *Carbohydrate Research*. 1988;181:143–52.
67. Govan JRW, Fyfe JAM, Jarman TR. Isolation of alginate-producing mutants of *Pseudomonas fluorescens*, *Pseudomonas putida* and *Pseudomonas mendocina*. *J Gen Microbiol*. 1981;125(1):217–20.
68. Sadoff HL. Encystment and germination in *Azotobacter vinelandii*. *Bacteriological Rev*. 1975;39(4):516–39.
69. Page WJ, Sadoff HL. Relationship between calcium and uroinic acids in the encystment of *Azotobacter vinelandii*. *Journal of bacteriology*. 1975;122(1):145–51.
70. Skjåk-Bræk G, Grasdalen H, Larsen B. Monomer sequence and acetylation pattern in some bacterial alginates. *Carbohydrate Research*. 1986;154(1):239–50.

71. Iacocca VF, Sibinga MS, Barbero GJ. Respiratory tract infections in cystic fibrosis. *Pediatr Ann.* 1963;16:315–24.
72. Stenvang Pedersen S, Kharazmi A, Espersen F, Høiby N. *Pseudomonas aeruginosa* alginate in cystic fibrosis sputum and the inflammatory response. *Infection and immunity.* 1990;58(10):3363–8.
73. Boyd A, Chakrabarty AM. *Pseudomonas aeruginosa* biofilms: role of the alginate exopolysaccharide. *Journal of industrial microbiology.* 1995;15:162–8.
74. Schwarzmann S, Boring Iii JR. Antiphagocytic effect of slime from a mucoid strain of *Pseudomonas aeruginosa*. *Infection and immunity.* 1971;3(6):762–7.
75. Pang Z, Raudonis R, Glick BR, Lin T-J, Cheng Z. Antibiotic resistance in *Pseudomonas aeruginosa*: mechanisms and alternative therapeutic strategies. *Biotechnology Advances.* 2019;37(1):177–92.
76. Skjåk-Bræk G, Zanetti F, Paoletti S. Effect of acetylation on some solution and gelling properties of alginates. *Carbohydrate Research.* 1989;185(1):131–8.
77. Skjåk-Bræk G, Larsen B, Grasdalen H. The role of O-acetyl groups in the biosynthesis of alginate by *Azotobacter vinelandii*. *Carbohydrate Research.* 1985;145:169–74.
78. Franklin MJ, Chitnis CE, Gacesa P, Sonesson A, White DC, Ohman DE. *Pseudomonas aeruginosa* AlgG is a polymer level alginate C5-mannuronan epimerase. *Journal of bacteriology.* 1994;176(7):1821–30.
79. Ertesvåg H. Alginate-modifying enzymes: Biological roles and biotechnological uses. *Front Microbiol.,* 2015;6:1–10.
80. Standford ECC. Improvements in the manufacture of useful products from seaweeds. *British patent;* 142, 1881.
81. Skaugrud Ø, Hagen A, Borgersen B, Dorhish M. Biomedical and pharmaceutical applications of alginate and chitosan. *Biotechnology and Genetic Engineering Reviews.* 1999;16(1):23–40.
82. Helgerud T, Gåserud O, Fjereide T, Andersen PO, Larsen CK. Alginates. In: Imeson A, editor. *Food stabilisers, thickeners and gelling agents.* Wiley-Blackwell Publishing Ltd.; 2009. p. 50–72.
83. Onsøyen E. Commercial applications of alginates. *Carbohydrates in Europe.* 1996;14:26–31.
84. Chen F, Long J-J. Influences of process parameters on the apparent diffusion of an acid dye in sodium alginate paste for textile printing. *Journal of Cleaner Production.* 2018;205:1139–47.

85. Kale RD, Maurya Y, Potdar T. Paper-reinforced sodium alginate/carboxyl methyl cellulose-based bio-composite films. *Journal of Plastic Film & Sheeting*. 2018;34(2):179–95.
86. Rehm BH. Biosynthesis and application of alginates. In: Wnek GE, Bowlin GL, editors. *Encyclopedia of biomaterials and biomedical engineering*. 2nd ed. CRC Press,; 2008. p. 350–8.
87. Smith J, Hong-Shum L. *Food additives data book*. 2nd ed. Wiley & Sons; 2001. 1128 p.
88. EFSA panel on Food additives and nutrition sources added to food, Younes M, Aggett P, Aguilar F, Crebelli R, Filipič M, et al. Re-evaluation of alginic acid and its sodium, potassium, ammonium and calcium salts (E400-E404) as food additives. *EFSA Journal*. 2017;15(11):1–57.
89. Brownlee IA, Seal CJ, Wilcox M, Dettmar PW, Pearson JP. Applications of alginates in food. In: Rehm B, editor. *Alginates: Biology and Applications*. Springer Berlin Heidelberg; 2009. p. 211–28.
90. Champagne CP, Lacroix C, Sodini-Gallot I. Immobilized cell technologies for the dairy industry. *Critical Reviews in Biotechnology*. 1994;14(2):109–34.
91. Mandel KG, Daggy BP, Brodie DA, Jacoby HI. Review article: alginate-raft formulations in the treatment of heartburn and acid reflux. *Alimentary Pharmacology and Therapeutics*. 2000;14(6):669–90.
92. Banning D, Craig DQM, Joliffe IG, Hampson F, Field PF, Onsoyen EJ, et al. Pourable alginate compositions. Reckitt & Colman Products Ltd, UK.; Patent number: WO1998048814A1, 1998. p. 1–49.
93. Aderibigbe BA, Buyana B. Alginate in Wound Dressings. *Pharmaceutics*. 2018;10(2):1–19.
94. Hay ID, Ur Rehman Z, Moradali MF, Wang Y, Rehm BHA. Microbial alginate production, modification and its applications. *Microbial biotechnology*. 2013;6(6):637–50.
95. Ertesvåg H, Valla S, Skjåk-Bræk G. Genetics and biosynthesis of alginates. *S.I: Carbohydrates in Europe*; 1996. 14–18 p.
96. Guarino V, Altobelli R, Sala F d., Borzacchiello A, Ambrodi L. Alginate processing routes to fabricate bioinspired platforms for tissue engineering and drug delivery. In: Rehm BHA, Moradali MF, editors. *Alginates and Their Biomedical Applications*. Singapore: Springer Nature Singapore; 2018. p. 101–20.
97. Esquisabel A, Hernández R, Igartua M, Gascóan R, Calvo B, Pedraz JL. Production of BCG alginate-PLL microcapsules by emulsification/internal gelation. *Journal of microencapsulation micro and nano carriers* . 1997;14(5):627–38.

98. Gonzalez-Pujana A, Orive G, Pedras JL, Santos-Vizcaino E, Hernandez RM. Alginate microcapsules for drug delivery. In: Rehm BHA, Moradali MF, editors. *Alginates and Their Biomedical Applications*. Singapore: Springer Nature Singapore; 2018. p. 67–100.
99. Majewski RL, Zhang W, Ma X, Cui Z, Ren W, Markel DC. Bioencapsulation technologies in tissue engineering. *Journal of applied biomaterials & functional materials*. 2016;14(4):395–403.
100. Hunt NC, Grover LM. Cell encapsulation using biopolymer gels for regenerative medicine. *Biotechnology Letters*. 2010;32(6):733–42.
101. Orive G, Santos E, Poncelet D, Hernández RM, Pedraz JL, Wahlberg LU, et al. Cell encapsulation: technical and clinical advances. *Trends in Pharmacological Sciences*. 2015;36(8):537–46.
102. Orive G, Hernández RM, Gascón AR, Calafiore R, Chang TMS, Vos P De, et al. Cell encapsulation: Promise and progress. *Nature Medicine*. 2003;9(1):104–7.
103. Demont A, Cole H, Marison IW. An understanding of potential and limitations of alginate/PLL microcapsules as a cell retention system for perfusion cultures. *Journal of Microencapsulation*. 2016;33(1):80–8.
104. Skjåk-Bræk G, Espevik T. Application of alginate gels in biotechnology and biomedicine. *Carbohydrates in Europe*. 1996;14:19–25.
105. Strand BL, Coron AE, Skjåk-Bræk G. Current and future perspectives on alginate encapsulated pancreatic islet. *Stem cells translational medicine*. 2017;6(4):1053–8.
106. Rye PD, Tøndervik A, Sletta H, Pritchard M, Kristiansen A, Dessen A, et al. Alginate oligomers and their use as active pharmaceutical drugs. In: Rhem B, Moradali M, editors. *Alginates and Their Biomedical Applications*. Singapore: Springer Nature Singapore; 2018. p. 237–56.
107. Xing M, Cao Q, Wang Y, Xiao H, Zhao J, Zhang Q, et al. Advances in research on the bioactivity of alginate oligosaccharides. *Marine Drugs*. 2020;18(3):1–25.
108. Padoł AM, Draget KI, Stokke BT. Effects of added oligoguluronate on mechanical properties of Ca - Alginate - oligoguluronate hydrogels depend on chain length of the alginate. *Carbohydrate Polymers*. 2016;147:234–42.
109. Khan S, Tøndervik A, Sletta H, Klinkenberg G, Emanuel C, Onsøyen E, et al. Overcoming drug resistance with alginate oligosaccharides able to potentiate the action of selected antibiotics. *Antimicrobial Agents and Chemotherapy*. 2012;56(10):5134–41.
110. Mirshafiey A, Rehm BHA, Sahmani AA, Naji A, Razavi A. M-2000, as a new anti-inflammatory molecule in treatment of experimental nephrosis. *Immunopharmacology and immunotoxicology*. 2004;26(4):611–9.



111. Pritchard MF, Powell LC, Jack AA, Powell K, Beck K, Florance H, et al. A low-molecular-weight alginate oligosaccharide disrupts pseudomonal microcolony formation and enhances antibiotic effectiveness. *Antimicrobial agents and chemotherapy*. 2017;61(9):1–14.
112. Ermund A, Recktenwald C V, Skjåk-Bræk G, Meiss LN, Onsøyen E, Rye PD, et al. OligoG CF-5/20 normalizes cystic fibrosis mucus by chelating calcium. *Clinical and Experimental Pharmacology and Physiology*. 2017;44(6):639–47.
113. Pritchard MF, Powell LC, Menzies GE, Lewis PD, Hawkins K, Wright C, et al. A new class of safe oligosaccharide polymer therapy to modify the mucus barrier of chronic respiratory disease. *Molecular Pharmaceutics*. 2016;13(3):863–72.
114. Tøndervik A, Sletta H, Klinkenberg G, Emanuel C, Powell LC, Pritchard MF, et al. Alginate oligosaccharides inhibit fungal cell growth and potentiate the activity of antifungals against *Candida* and *Aspergillus* spp. *PLoS ONE*. 2014;9(11):e112518.
115. ClinicalTrials.gov. AlgiPharma, clinical trials for alginate oligoG, cystic fibrosis. Identifier: NCT02157922; NCT02453789.
116. Szekalska M, Puciłowska A, Szymańska E, Ciosek P, Winnicka K. Alginate: current use and future perspectives in pharmaceutical and biomedical applications. *International Journal of Polymer Science*. 2016;2016:1–17.
117. Xin XL, Geng MY, Guan HS, Li ZL. Study on the mechanism of inhibitory action of 911 on replication of HIV-1 in vitro. *Chinese Journal of Marine Drugs*. 2000;19(4):15–8.
118. Xin XL, Ding H, Geng MY, Liang PF, Li YX, Guan HS. Studies of the anti-AIDS effects of marine polysaccharide drug 911 and its related mechanisms of action. *Chinese Journal of Marine Drugs*. 2000;19(6):4–8.
119. Jiang BF, Xu XF, Li L, Yuan W. Study on “911” anti-HBV effect in HepH2.2.15 cell culture. *Modern Preventive Medicine*. 2003;30(4):517–8.
120. Gao Y, Zhang L, Jiao W. Marine glycan-derived therapeutics in China. In: Zhang L, editor. *Progress in molecular biology and translational Science: glycans and glycosaminoglycans as clinical biomarkers and therapeutics, PART 2*. Academic Press - an imprint of Elsevier; 2019. p. 124.
121. Lin T. Pathway of alginic acid synthesis in the marine brown algae, *Fucus garneri* Silva. *The Journal of Biological Chemistry*. 1966;241(22):5284–97.
122. Rehm BHA, Valla S. Bacterial alginates: Biosynthesis and applications. *Applied Microbiology and Biotechnology*. 1997;48:281–8.
123. Rehm BH, Ertesvåg H, Valla S. A new *Azotobacter vinelandii* mannuronan C-5-epimerase gene (*algG*) is part of an alg gene cluster physically organized in a manner similar to that in *Pseudomonas aeruginosa*. *Journal of Bacteriology*. 1996;178(20):5884–9.

124. Urtuvia V, Maturana N, Acevedo F, Peña C, Díaz-Barrera A. Bacterial alginate production: an overview of its biosynthesis and potential industrial production. *World J Microbiol Biotechnol.* 2017;33(11):1–10.
125. May TB, Chakrabarty AM. *Pseudomonas aeruginosa*: genes and enzymes of alginate synthesis. *Trends in Microbiology.* 1994.
126. Anderson AJ, Hacking AJ, Dawes EA. Alternative pathways for the biosynthesis of alginate from fructose and glucose in *Pseudomonas mendocina* and *Azotobacter vinelandii*. *Journal of General Microbiology.* 1987;133(4):1045–52.
127. Beale JM, Foster JL. Carbohydrate fluxes into alginate biosynthesis in *Azotobacter Vinelandii* NCIB 8789: NMR Investigations of the triose Pools. *Biochemistry.* 1996;35(14):4492–501.
128. Pindar DF, Bucke C. The biosynthesis of alginic acid by *Azotobacter vinelandii*. *Biochem J.* 1975;152(3):617–22.
129. Shinabarger D, Berry A, May TB, Rothmel R, Fialho A, Chakrabarty AM. Purification and characterization of phosphomannose isomerase-guanosine diphospho-D-mannose pyrophosphorylase: A bifunctional enzyme in the alginate biosynthetic pathway of *Pseudomonas aeruginosa*. *Journal of Biological Chemistry.* 1991;266(4):2080–8.
130. Zielinski NA, Chakrabarty AM, Berry A. Characterization and regulation of the *Pseudomonas aeruginosa* algC gene encoding phosphomannomutase. *Journal of Biological Chemistry.* 1991;266(15):9754–63.
131. Tatnell PJ, Russell NJ, Gacesa P. GDP-mannose dehydrogenase is the key regulatory enzyme in alginate biosynthesis in *Pseudomonas aeruginosa*: Evidence from metabolite studies. *Microbiology.* 1994;140(7):1745–54.
132. Campos M, Martínez-Salazar JM, Lloret L, Moreno S, Núñez C, Espín G, et al. Characterization of the gene coding for GDP-mannose dehydrogenase (algD) from *Azotobacter vinelandii*. *Journal of Bacteriology.* 1996;178(7):1793–9.
133. Lloret L, Barreto R, León R, Moreno S, Martínez-Salazar J, Espín G, et al. Genetic analysis of the transcriptional arrangement of *Azotobacter vinelandii* alginate biosynthetic genes: identification of two independent promoters. *Molecular microbiology.* 1996;21(3):449–57.
134. Maharaj R, May TB, Shang-Kwei W, Chakrabarty AM. Sequence of the alg8 and alg44 genes involved in the synthesis of alginate by *Pseudomonas aeruginosa*. *Gene.* 1993;136(1–2):267–9.
135. Mejía-Ruíz H, Guzmán J, Moreno S, Soberón-Chávez G, Espín G. The *Azotobacter vinelandii* alg8 and alg44 genes are essential for alginate synthesis and can be transcribed from an algD-independent promoter. *Gene.* 1997;199(1–2):271–7.

136. Franklin MJ, Ohman DE. Identification of algF in the alginate biosynthetic gene cluster of *Pseudomonas aeruginosa* which is required for alginate acetylation. *Journal of Bacteriology*. 1993;175(16):5057–65.
137. Franklin MJ, Ohman DE. Identification of algI and algI in the *Pseudomonas aeruginosa* alginate biosynthetic gene cluster which are required for alginate O acetylation. *Journal of Bacteriology*. 1996;178(8):2186–95.
138. Riley LM, Weadge JT, Baker P, Robinson H, Codée JDC, Tipton PA, et al. Structural and functional characterization of *Pseudomonas aeruginosa* AlgX: role of AlgX in alginate acetylation. *The Journal of biological chemistry*. 2013;288(31):22299–314.
139. Vazquez A, Moreno S, Guzmán J, Alvarado A, Espín G. Transcriptional organization of the *Azotobacter vinelandii* algGXLVIFA genes: Characterization of algF mutants. *Gene*. 1999;232(2):217–22.
140. Bjerkan TM, Bender CL, Ertesvåg H, Drabløs F, Fakhr MK, Preston LA, et al. The *Pseudomonas syringae* genome encodes a combined mannuronan C-5-epimerase and O-acetylhydrolase, which strongly enhances the predicted gel-forming properties of alginates. 2004;279(28):28920–9.
141. Ertesvåg H, Erlien F, Skjåk-Bræk G, Rehm BH, Valla S. Biochemical properties and substrate specificities of a recombinantly produced *Azotobacter vinelandii* alginate lyase. *Journal of bacteriology*. 1998;180(15):3779–84.
142. Gimmestad M, Ertesvåg H, Heggeset TMB, Aarstad O, Svanem BIG, Valla S. Characterization of three new *Azotobacter vinelandii* alginate lyases, one of which is involved in cyst germination. *Journal of Bacteriology*. 2009;191(15):4845–53.
143. Hay ID, Rehman ZU, Ghafoor A, Rehm BHA. Bacterial biosynthesis of alginates. *Journal of Chemical Technology and Biotechnology*. 2010;85(6):752–9.
144. Ertesvåg H, Doseth B, Larsen B, Skjåk-Braek G, Valla S. Cloning and expression of an *Azotobacter vinelandii* mannuronan C-5-epimerase gene. *Journal of bacteriology*. 1994;176(10):2846–53.
145. Ertesvåg H, Høidal HK, Hals IK, Rian A, Doseth B, Valla S. A family of modular type mannuronan C-5-epimerase genes controls alginate structure in *Azotobacter vinelandii*. *Molecular microbiology*. 1995;16(4):719–31.
146. Svanem BI, Skjåk-Bræk G, Ertesvåg H, Valla S. Cloning and expression of three new *Azotobacter vinelandii* genes closely related to a previously described gene family encoding mannuronan C-5-epimerases. *Journal of bacteriology*. 1999;181(1):68–77.
147. Larsen B, Haug A. Biosynthesis of alginate : Part I. Composition and structure of alginate produced by *Azotobacter vinelandii* (Lipman). *Carbohydrate Research*. 1971 Apr 1;17(2):287–96.

148. Haug A, Larsen B. Biosynthesis of alginate. Epimerisation of D-mannuronic to L-guluronic acid residues in the polymer chain. *Biochimica et Biophysica Acta*. 1969;192(3):557–9.
149. Madgwick J, Haug A, Larsen B. Polymannuronic acid C-5-epimerase from the marine alga *pelvetia canaliculata*. *Acta Chem Scand*. 1973;27(9):3592–4.
150. Ishikawa M, Nisizawa K. Polymannuronic acid C-5-epimerase activities in several brown algae and its localization in frond. *Bulletin of the Japanese Society of Scientific Fisheries*. 1981;47(7):889–93.
151. Greene A., Madgwick J. Alginate-modifying enzymes in australian marine algae. *Botanica Marina*. 1986;29(4):329–34.
152. Nyvall P, Corre E, Boisset C, Barbeyron T, Rousvoal S, Scornet D, et al. Characterization of mannuronan C-5-epimerase genes from the brown alga *laminaria digitata*. *Plant physiology*. *Planr physiology*. 2003;133(2):726–35.
153. Franklin MJ, Chitins CE, Gacesa P, Sonesson A, White DC, Ohman DE. *Pseudomonas aeruginosa* AlgGisapolymerlevelalginateC5-mannuronan epimerase. *Journal of bacteriology*,. *Journal of Bacteriology*. 1994;176(7):1821–30.
154. Peñaloza-Vázquez A, Kidambi SP, Chakrabarty AM, Bender CL. Characterization of the alginate biosynthetic gene cluster in *pseudomonas syringae* pv. *syringae*. *Journal of Bacteriology*. 1997;179(14):4464–72.
155. Morea A, Mathee K, Franklin MJ, Giacomini A, O'Regan M, Ohman DE. Characterization of AlgG encoding C5-epimerase in the alginate biosynthetic gene cluster of *pseudomonas fluorescens*. *Gene*. 2001;278(1):107–14.
156. Svanem BIG, Skjåk-Bræk G, Ertesvåg H, Valla S. Cloning and expression of three new *Azotobacter vinelandii* genes closely related to a previously described gene family encoding mannuronan C-5- epimerases. *Journal of Bacteriology*. 1999;181(1):68–77.
157. Hoidal HK, Svanem BIG, Gimmestad M, Valla S. Mannuronan C-5 epimerases and cellular differentiation of *Azotobacter vinelandii*. *Environmental Microbiology*. 2000;2(1):27–38.
158. Tøndervik A, Klinkenberg G, Aachmann FL, Svanem BIG, Ertesvåg H, Ellingsen TE, et al. Mannuronan C-5 epimerases suited for tailoring of specific alginate structures obtained by high-throughput screening of an epimerase mutant library. *Biomacromolecules*. 2013;14(8):2657–66.
159. Gimmestad M, Sletta H, Ertesvåg H, Bakkevig K, Jain S, Suh S, et al. The *Pseudomonas fluorescens* AlgG protein, but not its mannuronan C-5-epimerase activity, is needed for alginate polymer formation. *Journal of Bacteriology*. 2003;185(12):3515–23.

160. Jain S, Franklin MJ, Ertesvåg H, Valla S, Ohman DE. The dual roles of AlgG in C-5-epimerization and secretion of alginate polymers in *Pseudomonas aeruginosa*. *Molecular microbiology*. 2003;47(4):1123–33.
161. Chitinis CE, Ohman DE. Cloning of *Pseudomonas aeruginosa* algG, which controls alginate structure. *Journal of Bacteriology*. 1990;172:2894–900.
162. Ertesvåg H, Valla S, Skjåk-Bræk G. Enzymatic Alginate Modification. In: Rhem BHA, editor. *Alginates: Biology and Applications*. Berlin: Springer-Verlag; 2009. p. 96–110.
163. Ertesvåg H, Valla S. The A modules of the *Azotobacter vinelandii* mannuronan-C-5-epimerase AlgE1 are sufficient for both epimerization and binding of Ca<sup>2+</sup>. *Journal of bacteriology*. 1999;181(10):3033–8.
164. Aachmann FL, Svanem BIG, Günter P, Petersen SB, Valla S, Wimmer R. NMR Structure of the R-module: A parallel  $\beta$ -roll subunit from an *Azotobacter vinelandii* mannuronan C-5 epimerase. *Journal of biological chemistry*. 2006;281(11):7350–6.
165. Buchinger E, Knudsen DH, Behrens MA, Pedersen JS, Aarstad OA, Tøndervik A, et al. Structural and functional characterization of the R-modules in alginate C-5 epimerases AlgE4 and AlgE6 from *Azotobacter vinelandii*. *The Journal of biological chemistry*. 2014;289(45):31382–96.
166. Rozeboom HJ, Bjerkan TM, Kalk KH, Ertesvåg H, Holtan S, Aachmann FL, et al. Structural and mutational characterization of the catalytic A-module of the mannuronan C-5-epimerase AlgE4 from *Azotobacter vinelandii*. *The Journal of biological chemistry*. 2008;283(35):23819–28.
167. Stanisci A, Rothweiler U, Tøndervik A, Sletta H, Smalås AO, Skjak-Bræk G, et al. Structural determination and computational stimulation of the catalytic mechanism of the catalytic A-module of the emannuronan C-5 epimerase AlgE6 from *Azotobacter vinelandii*. In *Development of mannuronan C5-epimerases to perform in vitro tailoring and upg*. 2017;1–12.
168. Svanem BIG, Strand WI, Ertesvåg H, Skjåk-Bræk G, Hartmann M, Barbeyron T, et al. The Catalytic Activities of the Bifunctional *Azotobacter vinelandii* Mannuronan C-5-Epimerase and Alginate Lyase AlgE7 Probably Originate from the Same Active Site in the Enzyme. *Journal of Biological Chemistry*. 2001;276(34):31542–50.
169. Buchinger E, Aachmann FL, Aranko AS, Valla S, Skjåk-Bræk G, Iwai H, et al. Use of protein trans-splicing to produce active and segmentally (<sup>2</sup>H), (<sup>15</sup>N) labeled mannuronan C5-epimerase AlgE4. *Protein science*. 2010;19(8):1534–43.
170. Douthit SA, Dlakic M, Ohman DE, Franklin MJ. Epimerase active domain of *Pseudomonas aeruginosa* AlgG, a protein that contains a right-handed beta-helix. *Journal of bacteriology*. 2005;187(13):4573–83.
171. Davies GJ, Wilson KS, Henrissat B. Nomenclature for sugar-binding subsites in glycosyl hydrolases. *Biochem J*. 1997;15(231):557–9.

172. Stanisci A, Tøndervik A, Gaardløs M, Lervik A, Skjåk-Bræk G, Sletta H, et al. Identification of a pivotal residue for determining the block structure-forming properties of alginate C-5 epimerases. *ACS Omega*. 2020;5(8):4352–61.
173. Schrödinger L. The PyMOL Molecular Graphics System v.2.3.2.
174. Ramstad MV, Ellingsen TE, Josefsen KD, Høidal HK, Valla S, Skjåk-Bræk G, et al. Properties and action pattern of the recombinant mannuronan C-5-epimerase AlgE2. *Enzyme and Microbial Technology*. 1999;24(10):636–46.
175. Høidal H. ., Ertesvåg H, Skjåk-Bræk G, Stokke B. ., Valla S. The recombinant *Azotobacter vinelandii* mannuronan C-5-epimerase AlgE4 epimerizes alginate by a nonrandom attack mechanism. *The Journal of biological chemistry*. 1999;274(18):12316–22.
176. Ertesvåg H, Høidal H. ., Skjåk-Bræk G, Valla S. The *Azotobacter vinelandii* mannuronan C-5-epimerase AlgE1 consists of two separate catalytic domains. *The Journal of biological chemistry*. 1998;273(47):30927–32.
177. Hartmann M. Enzymatic tailoring of alginate using mannuronan C-5-epimerases. 2000.
178. Campa C, Holtan S, Nilsen N, Bjerkan TM, Stokke BT, Skjåk-Bræk G. Biochemical analysis of the processive mechanism for epimerization of alginate by mannuronan C-5 epimerase AlgE4. *Biochemical Journal*. 2004;381(1):155–64.
179. Breyer WA, Matthews BW. A structural basis for processivity. *Protein Science* . 2001;10(9):1699–711.
180. Ernst S, Rhomberg AJ, Biemann K, Sasisekharan R. Direct evidence for a predominantly exolytic processive mechanism for depolymerization of heparin-like glycosaminoglycans by heparinase I. *Proceedings of the National Academy of Sciences of the United States of America*. 1998;95(8):4182–1487.
181. Hartmann M, Holm OB, Johansen GAB, Skjåk-Braek G, Stokke BT. Mode of action of recombinant *Azotobacter vinelandii* mannuronan C-5 epimerases AlgE2 and AlgE4. *Biopolymers*. 2002;63(2):77–88.
182. Høidal H. . K, Ertesvåg H, Skjåk-Bræk G, Stokke B. . T, Valla S. The recombinant *Azotobacter vinelandii* mannuronan C-5-epimerase AlgE4 epimerizes alginate by a nonrandom attack mechanism. *Journal of Biological Chemistry*. 1999;274(18):12316–22.
183. Hartmann M, Duun AS, Markussen S, Grasdalen H, Valla S, Skjåk-Bræk G. Time-resolved 1H and 13C NMR spectroscopy for detailed analyses of the *Azotobacter vinelandii* mannuronan C-5 epimerase reaction. *Biochim Biophys Acta*. 2002;1570(2):104–12.
184. Holtan S, Bruheim P, Skjåk-Bræk G. Mode of action and subsite studies of the guluronan block-forming mannuronan C-5 epimerases AlgE1 and AlgE6. *Biochemical Journal*. 2006;395(Pt 2):319–29.

185. Aarstad OA, Stanisci A, Sætrom GI, Tøndervik A, Sletta H, Aachmann FL, et al. Biosynthesis and function of long guluronic acid-blocks in alginate produced by *Azotobacter vinelandii*. *Biomacromolecules*. 2019;20(4):1613–22.
186. Kennedy L, McDowell K, Sutherland IW. Alginases from *Azotobacter* species. *Journal of General Microbiology*. 1992;138:2465–71.
187. Boyd A, Chakrabarty AM. Role of alginate lyase in cell detachment of *Pseudomonas aeruginosa*. *Applied and Environmental Microbiology*. 1994;60(7):2355–9.
188. Bartell PF, Orr TE, Lam GKH. Polysaccharide depolymerase associated with bacteriophage infection. *Journal of Bacteriology*. 1966;92(1):56–62.
189. Davidson IW, Lawson CJ, Sutherland IW. An alginate lyase from *Azotobacter vinelandii* phage. *Journal of General Microbiology*. 1977;98(1):223–9.
190. Zhu B, Yin H. Alginate lyase: review of major sources and classification, properties, structure-function analysis and applications. *Bioengineered*. 2015;6(3):125–31.
191. Kim HT, Ko H-J, Kim N, Kim D, Lee D, Choi I-G, et al. Characterization of a recombinant endo-type alginate lyase (Alg7D) from *Saccharophagus degradans*. *Biotechnology Letters*. 2012;34(6):1087–92.
192. Ochiai A, Yamasaki M, Mikami B, Hashimoto W, Murata K. Crystal structure of exotype alginate lyase Atu3025 from *Agrobacterium tumefaciens*. *The Journal of Biological Chemistry*. 2010;285(32):24519–28.
193. Park D, Jagtap S, Nair SK. Structure of a PL17 family alginate lyase demonstrates functional similarities among exotype depolymerases. *Journal of Biological Chemistry*. 2014;289(12):8645–55.
194. Lombard V, Bernard T, Rancurel C, Brumer H, Coutinho PM, Henrissat B. A hierarchical classification of polysaccharide lyases for glycogenomics. *Biochemical Journal*. 2010;432(3):437–44.
195. Garron M-L, Cygler M. Structural and mechanistic classification of uronic acid-containing polysaccharide lyases. *Glycobiology*. 2010;20(12):1547–73.
196. Garron M-L, Cygler M. Uronic polysaccharide degrading enzymes. *Current Opinion in Structural Biology*. 2014;28:87–95.
197. Xu F, Dong F, Wang P, Cao H-Y, Li C-Y, Li P-Y, et al. Novel molecular insights into the catalytic mechanism of marine bacterial alginate lyase AlyGC from polysaccharide lyase family 6. *The Journal of biological chemistry*. 2017;292(11):4457–68.
198. Lyu Q, Zhang K, Shi Y, Li W, Diao X, Liu W. Structural insights into a novel Ca<sup>2+</sup>-independent PL-6 alginate lyase from *Vibrio* OU02 identify the possible subsites responsible for product distribution. *Biochimica et Biophysica Acta (BBA) - General Subjects*. 2019;1863(7):1167–76.

199. Østgaard K. Enzymatic microassay for the determination and characterization of alginates. *Carbohydrate Polymers*. 1992;19(1):51–9.
200. Østgaard K. Determination of alginate composition by a simple enzymatic assay. *Hydrobiologia*. 1993;260/261(1):513–20.
201. Ballance S, Holtan S, Aarstad OA, Sikorski P, Skjåk-Bræk G, Christensen BE. Application of high-performance anion-exchange chromatography with pulsed amperometric detection and statistical analysis to study oligosaccharide distributions – a complementary method to investigate the structure and some properties of alginates. *Journal of Chromatography A*. 2005;1093(1–2):59–68.
202. Tøndervik A, Klinkenberg G, Aarstad OA, Drabløs F, Ertesvåg H, Ellingsen TE, et al. Isolation of mutant alginate lyases with cleavage specificity for di-guluronic acid linkages. *The Journal of Biological Chemistry*. 2010;285(46):35284–92.
203. Siloto RMP, Weselake RJ. Site saturation mutagenesis: Methods and applications in protein engineering. *Biocatalysis and Agricultural Biotechnology*. 2012;1(3):181–9.
204. Castorena-Torres F, Peñuelas-Urquides K, Bermúdez de León M. Site-Directed Mutagenesis by Polymerase Chain Reaction. In: *Polymerase Chain Reaction for Biomedical Applications*. 2016.
205. van Pelt-Verkuil E, van Belkum A, Hays JP. *Principles and Technical Aspects of PCR Amplification*. Springer Science & Business Media B.V; 2008. 1–333 p.
206. Bell J. The polymerase chain reaction. *Immunology Today*. 1989;10(10):351–5.
207. New England BioLabs Inc. Q5 ® Site-Directed Mutagenesis Kit - Instruction Manual. 2019.
208. Brown TA. *Gene cloning and DNA Analysis: An Introduction*. 7th ed. Hoboken, United states: John Wiley & Sons, Ltd; 2016. 1–294 p.
209. Ely JJ, Reeves-Daniel A, Campbell ML, Kohler S, Stone WH. Influence of magnesium ion concentration and PCR amplification conditions on cross-species PCR. *BioTechniques*. 1998;25(1):38–42.
210. Mandel M, Higa A. Calcium-dependent Bacteriophage DNA Infection. *J Mol Biol*. 1970;53:159–62.
211. Cohen SN, Chang ACY, Hsu L. Nonchromosomal Antibiotic Resistance in Bacteria: Genetic Transformation of *Escherichia coli* by R-Factor DNA. *Proceedings of the National Academy of Sciences*. 1972 Aug 1;69(8):2110–4.
212. Panja S, Saha S, Jana B, Basu T. Role of membrane potential on artificial transformation of *E. coli* with plasmid DNA. *Journal of Biotechnology*. 2006 Dec 15;127(1):14–20.



213. Madigan MT, Martinko JM, Bender KS, Buckley DH, Stahl DA. Brock biology of microorganisms. 14th ed. Oerson Education; 2015. 26–984 p.
214. Birnboim HC, Doly J. A rapid alkaline extraction procedure for screening recombinant plasmid DNA. *Nucleic Acids Research*. 1979;7(6):1513–23.
215. New England BioLabs Inc. Nucleic acid purification, Monarch Plasmid Miniprep Kit - Instruction manual. 2016.
216. Clark D, Pazdernik N. *Molecular Biology*. 2nd editio. Oxford: Academic Press Inc; 2013. 928 p.
217. Baker S, Griffiths C, Nicklin J. *Instant Notes in Microbiology*. 4th ed. Owen E, editor. Garland Sience, Taylor & Francis Group; 2011. 1–328 p.
218. Li MZ, Elledge SJ. Harnessing homologous recombination in vitro to generate recombinant DNA via SLIC. *Nature Methods*. 2007;4(3):251–6.
219. Jeong J-Y, Yim H-S, Ryu J-Y, Lee HS, Lee J-H, Seen D-S, et al. One-step sequence- and ligation-independent cloning as a rapid and versatile cloning method for functional genomics studies. *Applied and environmental microbiology*. 2012;78(15):5440–3.
220. Takara Bio Inc. Premix Taq™ (TaKaRa Taq™ Version 2.0) - User Manual. 2019.
221. Zymo Research. DNA Clean & Concentrator™-5 - Instruction Manual.
222. Nelson DL, M.Cox M. *Lehninger Principles of Biochemistry*. 6th ed. New York: W.H. Freeman and Company; 2013. 1–1195 p.
223. New England BioLabs Inc. IMPACT™ Kit - Instruction Manual (NEB #E6901S). 2019.
224. Branson Sonifer 250 user manual. Danbury, Conneticut: Branson Ultrasonic Corporation; 82 p.
225. Reed R, Holmes D, Weyers J, Jones A. *Practical skills in biomolecular sciences*. 2nd ed. Harlow: Pearson Education/Prentice Hall; 2003. 1–485 p.
226. Alberts B, Johnson A, Lewis J, Morgan D, Raff M, Roberts K, et al. *Molecular biology of the cell*. 6th ed. New York: Garland Science; 2015. 1–1342 p.
227. Cleveland C, Morris C. *Dictionary of Energy*. 2nd ed. Elsevier; 2014. 700 p.
228. Martin Christ Gefriertrocknungsanlagen GmbH. *Freeze-dryer Beta 1-8 LDplus - operating manual*. 11th ed. Osterode am Harz; 2017. 1–100 p.
229. Haseley P, Oetjen G-W. *Freeze-drying*. 3rd ed. Weinheim: Wiley-VCH Verlag GmbH & Co.KGaA; 2018. 1–396 p.

230. Silverstein RM, Webster FX, Kimle DJ, Bryce DL. Spectrometric Identification of Organic Compounds. 8th ed. New Jersey: Jhon Wiely and Sons, Inc.; 2015. 1–452 p.
231. Field L., Sternhell S, Kalman J. Organic structures from spectra. 4th ed. Chichester: John Wiley & Sons, Ltd; 2008. 34–74 p.
232. Ertesvåg H, Skjåk-Bræk G. Modification of alginate using mannuronan C-5-epimerases. In: Bucke C, editor. Methods in Biotechnology, Vol:10:Carbohydrate Biotechnology Protocols. Totowa: Humana Press Inc.; 1999. p. 71–8.
233. Friebolin H. Basic one- and two-dimensional NMR Spectroscopy. Weinheim: VCH Publishers; 1991.
234. Biasini M, Bienert S, Waterhouse A, Arnold K, Studer G, Schmidt T, et al. SWISS-MODEL: modelling protein tertiary and quaternary structure using evolutionary information. - PubMed - NCBI. Nucleic Acids Research. 2014;42:W252–8.
235. Waterhouse A, Bertoni M, Bienert S, Studer G, Tauriello G, Gumienny R, et al. SWISS-MODEL: homology modelling of protein structures and complexes. Nucleic Acids Research. 2018;46(W1):W296–303.
236. Krieger E, Joo K, Lee J, Lee J, Raman S, Thompson J, et al. Improving Physical Realism, Stereochemistry, and Side-Chain Accuracy in Homology Modeling: Four Approaches That Performed Well in CASP8. Proteins. 2009;77(Suppl 9).
237. Rodriguez R, Chinae G, Lopez N, Pons T, Vriend G. Homology modeling, model and software evaluation: three related resources. Bioinformatics. 1998;14(6):523–8.
238. Madeira F, Park YM, Lee J, Buso N, Gur T, Madhusoodanan N, et al. The EMBL-EBI search and sequence analysis tools APIs in 2019. Nucleic acids research. 2019;47(W1):W636–41.
239. Gasteiger E, Hoogland C, Gattiker A, Duvaud S, Wilkins MR, Appel RD, et al. Protein Analysis Tools on the ExPASy Server. In: In the The Proteomics Protocols Handbook. Totowas: Humana Press Inc; 2005. p. 571–607.
240. Marit Sletmoen, Gudmund Skjåk-Bræk, Bjørn T. Stokke. Single-molecular pair unbinding studies of mannuronan C-5 epimerase AlgE4 and its polymer substrate. Biomacromolecules. 2004;5(4):1288–94.
241. Rath A, Glibowicka M, Nadeau VG, Chen G, Deber CM. Detergent binding explains anomalous SDS-PAGE migration of membrane proteins. Proceedings of the National Academy of Sciences. 2009;106(6):1760–5.
242. Sokalingam S, Madan B, Raghunathan G, Lee S-G. In silico study on the effect of surface lysines and arginines on the electrostatic interactions and protein stability. Biotechnology and Bioprocess Engineering. 2013;18:18–26.

243. Fitch CA, Platzner G, Okon M, Garcia-Moreno BE, McIntosh LP. Arginine: Its pKa value revisited. *Protein science : a publication of the Protein Society*. 2015;24(5):752–61.
244. Guillén Schlippe Y V., Hedstrom L. A twisted base? The role of arginine in enzyme-catalyzed proton abstractions. *Archives of Biochemistry and Biophysics*. 2005;433(1):266–78.
245. Mowat CG, Moysey R, Miles CS, Leys D, Doherty MK, Taylor P, et al. Kinetic and crystallographic analysis of the key active site acid/base arginine in a soluble fumarate reductase. *Biochemistry*. 2001 Oct;40(41):12292–8.
246. Charnock SJ, Brown IE, Turkenburg JP, Black GW, Davies GJ. Convergent evolution sheds light on the anti- $\beta$ -elimination mechanism common to family 1 and 10 polysaccharide lyases. *Proceedings of the National Academy of Sciences*. 2002;99(19):12067–72.
247. Raczyńska ED, Cyrński MK, Gutowski M, Rak J, Gal J-F, Maria P-C, et al. Consequences of proton transfer in guanidine. *Journal of Physical Organic Chemistry*. 2003 Feb;16(2):91–106.
248. O'Brien R, Haq I. Applications of biocalorimetry: binding, stability and enzyme kinetics. In: Ladbury JE, Doyle M, editors. *Biocalorimetry 2*. Wiley & Sons; 2004. p. 1–32.
249. House J. Fundamental concepts of kinetics. In: *Principles of chemical kinetics*. 2nd ed. Amsterdam: Academic Press - an imprint of Elsevier; 2007. p. 1–35.
250. Petrucci RH, Herring GF, Madura JD, Bissonnette C. *General chemistry: principles and modern applications*. 11th ed. Pearson Canada Inc; 2016.

# Appendix A. AlgE7 gene and AA sequence

The AlgE7 gene consists of 2568 nucleotides, which corresponds to 856 amino acids. In the following gene sequence (UniProtKB: Q9ZFG9) and the amino acid sequence (Figure A.1), the A-module is marked in purple and the three R-modules are marked in red (R<sub>1</sub>), orange (R<sub>2</sub>) and yellow (R<sub>3</sub>). The mutations listed in Table 3.1 (Section 3.1.3) were introduced to the AlgE7 gene in the pBG27 vector (Appendix B, Figure B.1), a derivative of the *E. coli* expression vector pTrc99a.

## AlgE7 gene sequence

```
ATGGAATACAACGTTAAGGATTTTGGTGCCAAGGGTGATGGCAAGACGGACGACACGGATGCCATACAG
GCGGCGATAGATGCCGCCACAAGGCGGGGGGCGGGACGGTATACCTGCCGTCCGGCGAATATCGGGT
CAGCGGTGGCGACGAGGCCTCCGACGGCGCTCTGATCATCAAGAGCAACGTCTATATCGTCGGTGCCG
GCATGGGCGAGACGGTGATCAAGCTGGTTCGATGGGTGGGACGAAAAGCTCACCGGCATCATCCGCTCG
GCCAACGGCGAGAAAACCCATGATTACGGTATCAGCGACCTGACCATCGACGGTAACCAGGACAACACC
GAAGGCGAGGTCGACGGCTTCTATACCGGCTATATTCCCAGCAAGAATGGCGCGGACTACAACGTCACG
GTCGAACGGGTGGAGATCCGCGAGGTATCCCCTACGCCTTCGATCCCCACGAGCAGACCATCAACCTG
ACGATCCGCGACAGCGTTCGCCCACGACAACGGCAAGGACGGGTTTCGTCGCCGACTTCCAGATCGGGCG
CGTGTTTCGAGAACAACGTCTCGTACAACAACGGCCGCCACGGCTTCAACATCGTCACCAGCAGTCACGA
CATCGTCTTCACCAACAACGTTCGCCTACGGCAACGGCGCCAACGGCCTGGTGGTCCAGCGCGGCTCGG
AAGACCGGGACTTCGCTTACAACGTGGAGATCGAGGGCGGCTCCTTCCATGACAACGGTTCAGGAAGGC
GTGCTGATCAAGATGAGCACCAGTGTACCCTGCAGGGCGCCGAGATCTACGGCAACGGCTACGCGGG
CGTGCGCGTGCAGGGCGTCGAGGACGTGCGGATCCTCGACAACACTACATCCACGACAACGCACAGAGCA
AGGCCAACGCGGAAGTCATCGTGGAATCCTACGACGACCGCGACGGCCCGTCCGACGACTACTACGAA
ACGCAGAACGTACGGTCAAGGGCAATACCATCGTCGGTTCGGCCAATTCACCTACGGCATCCAGGAG
CGCGCCGACGGCACCAGCTACACCAGCATCGGCAACAACAGCGTTCAGCGGCACCCAGCGCGGGATCGT
GCAGCTCTCGGGGACGAACTCGACGTTCTCCGGCAGGTCGGGCGATGCCTACCAGTTCATCGACGGCA
GCACCGGCAATGACCTGCTGACCGGTACCCCGATCGCCGATCTGATCGTGGGCGGCAGCGGCAACGAC
ACCCTGAGCGGGCAGCGCGGCAACGACGTTCTCGAAGGCGGTGCCGGCAGCGATCGCCTGACCGGGCG
CGAGGGCGCCGACATCTTCCGCTTACGGCGGTGAGCGACAGCTATTACACCGCCAGCAGCAGCGTCCG
CCGACCAGATCCTCGACTTCGACGCCAGCAATGATCGCATCGACCTACCGGGCTCGGCTTACCGGGCC
TGGGCGACGGCTACGGCGGCACCCTGGCCGTGCTGGCCAACAGCGACGGCAGCCGCACCTATCTGCGC
AGCTACGAGAAGGACGCCGACGGCCGCTATTTCTCGTCTACCCTGGACGGCAACTTCGTCGGTTCGGCTC
GACGACAGCAACCTGGTCTTCAGGCACAAGACCATCGCCGGCACCGAGGGCGACGACAGCCTGACCGG
CAACGCGATGGCGGAAATCCTCGACGGCGGCAGCGGCAACGACAGCCTCGCGGGCGGTCTGGGCAACG
ACGTGCTGAGAGGCGGTGCCGGCAGCAGATCCTGAACGGCGGCCTGGGGCGCGACCAGCTCAGCGGC
GGCGAAGGCGCGGACATATTCCGCTTACCAGCGTGGCCGACAGCTACCAGAACTCGGGCGACAACCTT
CTCCGACCTGATTCTCGATTTTCGACCCGGGCGAAGACCGCATCGATCTCAGCGGCCTGGGCTTACGCGG
CCTGGGCGACGGCCACAACGGTACCCTGCTGCTCTGGACCAGCAGCGAAAACCAACCGCACCTATCTCAA
GAACTTCGACACGGATGCCGACGGCCGGCGCTTCGAGATCGCCCTGGAGGGCGTCTTCTCCGACCTGA
GCGAGAAGCAACTGGTCTTGAACGCCTGGTACTGGAGGGCACTCGCCTCGGCGACCAGCTTTCGGGC
ACCGAGCTGAACGAGGAACTGCTCGGCGGCGCGGGGCGCGACATCCTGAACGGCGGCGCCGGCGACG
ATATTCTCGATGGCGGTTCCGAACGCGACACCCTGACCGGCGGCAGCGGCGCGGACGTGTTCCGCTTCA
ACGCCACGCTGGACAGCTTCCGCAACTACGACAATGGGACGAGCCGGGTCGACGACATCACCGACTTCA
CCGTCGGCGAGGATCTGATCGACCTTCCGCCCTCGGCTATAGCGGCTGGGCAACGGCTACGACGGC
ACGCTCGCCGTGCTGCTGAATGCCGACGGCACCAAGACCTACCTCAAGGACCGCGAAAGCGATGCGGA
CGGCAACCACTTCGAGATCGCCCTGGACGGCAACTATGCCGATCAGCTCTCCAACGGCGACTTCATCTT
CACCAACCTCGAAGTGATCGGCAGCAGCTCGCAGGCTGCC
```

## AlgE7 amino acid sequence

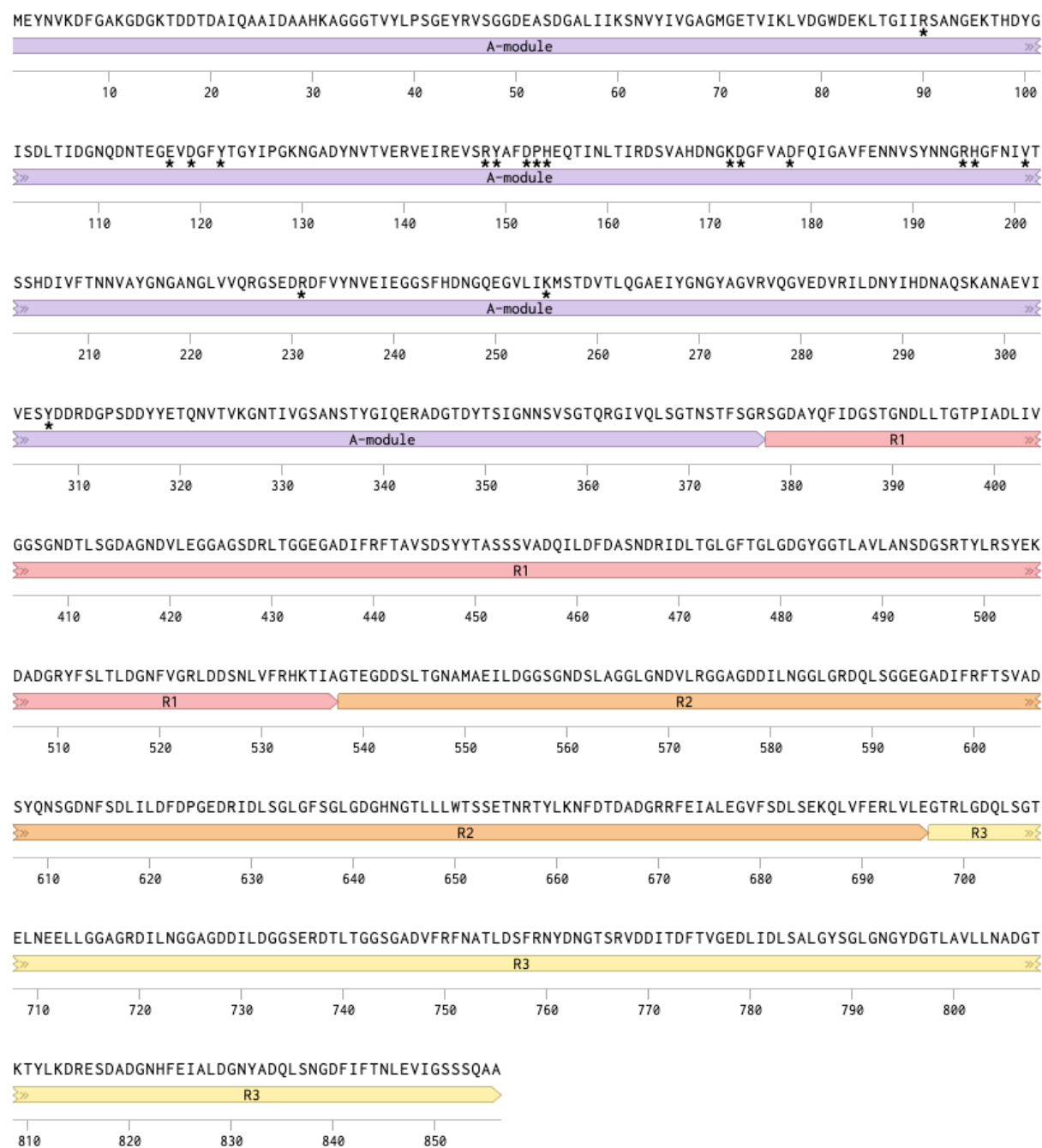


**Figure A1.** Amino acid (AA) sequence of the AlgE7 gene (UniProtKB: Q9ZFG9). A-module (purple): 1-377, R<sub>1</sub>-module (red): 378-537, R<sub>2</sub>-module (orange): 538-696, R<sub>3</sub>-module (yellow): 697-856. The residues that were mutated are marked with a star symbol (\*).

## Appendix B. Plasmid maps

### pBG27 plasmid map

The pBG27 plasmid (Figure B.1) was constructed by Svanem et al. 1999 (156) based on the backbone of the *E. coli* expression vector pTrc99A. The plasmid contains the AlgeE7 gene (UniProtKB: Q9ZFG9), trc promoter (pTrc99a promoter), rrnB terminator, ampicillin resistance (*bla*), origin of transcription and *lacI* (regulator gene).

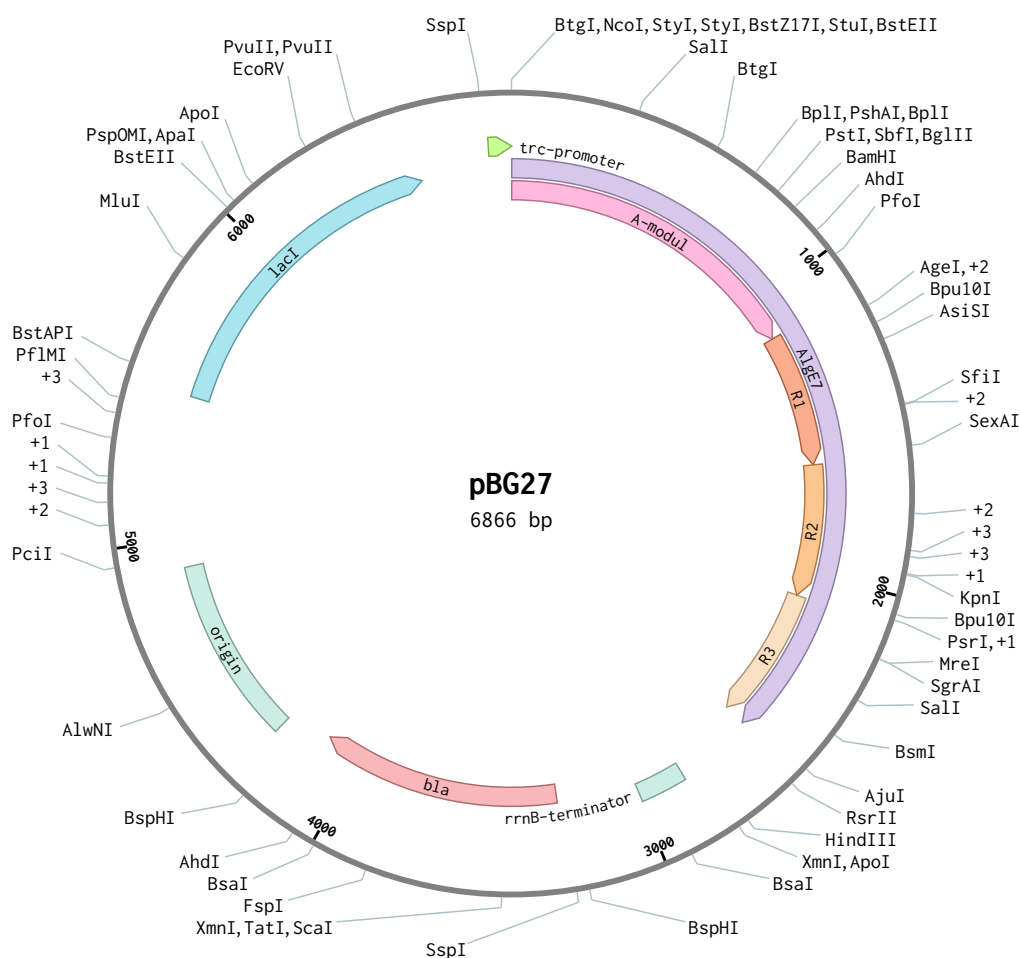
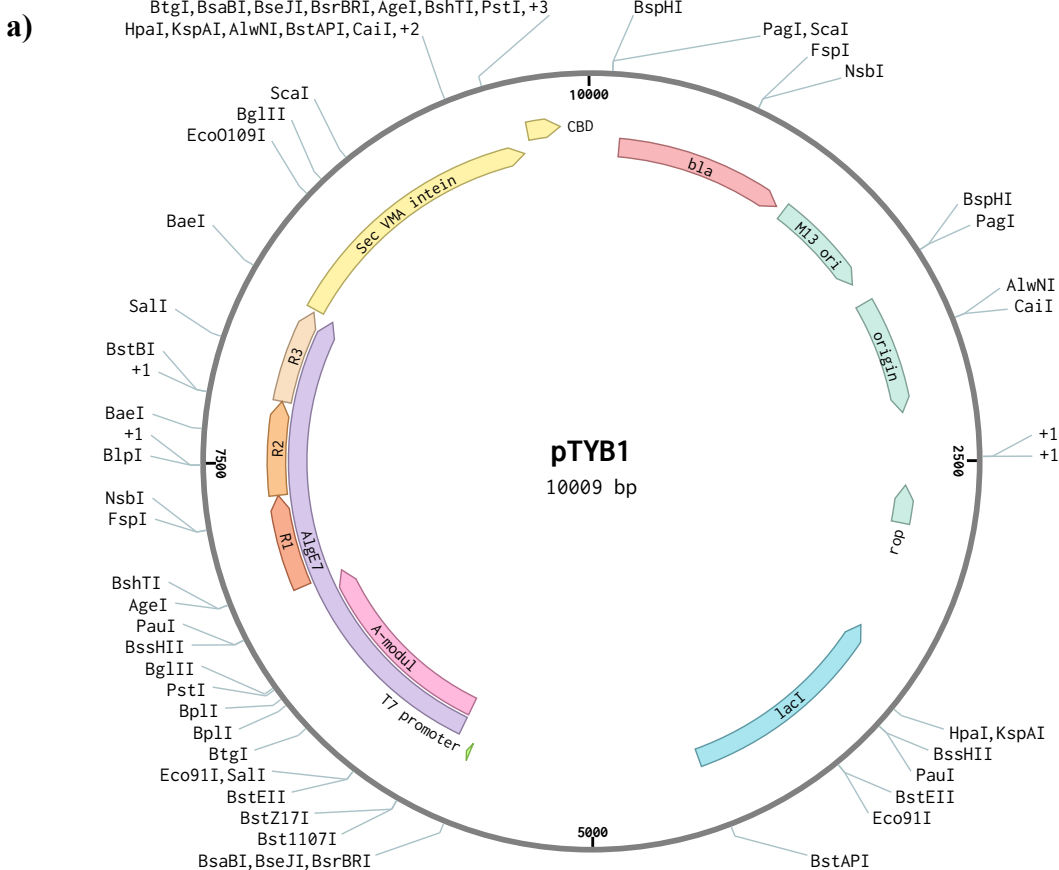


**Figure B.1.** *E. coli* cloning and expression vector pBG27 (6866bp) containing the AlgeE7 gene, trc promoter (pTrc99a promoter), rrnB terminator, ampicillin resistance (*bla*), origin of transcription and *lacI* (regulator gene). Plasmid map is exported from Benchling.

**pTYB1 plasmid map**

The *AlgeE7* gene containing the following single mutations: E117K, Y122F, R148G, K172L and K172R were transferred from the pBG27 vector to a pTYB1 vector (Figure 2.Ba). The *AlgeE7* gene is inserted in the multiple cloning site (MCS) (Figure 2.Bb) and fused with its C-terminus to the N-terminus of the *Sec* VMA intein tag/chitin binding domain (CBD).



**b)**

**Multiple Cloning Sites (MCS):**

**T7 Universal Primer →**

5'...CGG GGA TCT CGA TCC CGC GAA ATT AAT ACG ACT CAC TAT AGG GGA ATT GTG AGC  
T7 Promoter lac operator

**Intein →**

GGA TAA CAA TTC CCC TCT AGA AAT AAT TTT GTT TAA CTT TAA GAA GGA GAT ATA  
XbaI ShineDalgarno

Met	Ala	Ser	Ser	Arg	Val	Asp	Gly	Gly	Arg	Glu	Phe	Leu	Glu	Gly	Ser	Ser	Cys1	
CAT	ATG	GCT	AGC	TCG	CGA	GTC	GAC	GGC	GGC	CGC	GAA	TTC	CTC	GAG	GGC	TCT	TCC	TGC
NdeI	NheI	NruI	SallI	NotI	EcoRI	XhoI	SapI											

TTT GCC AAG GGT ACC AAT GTT TTA ATG GCG GAT GGG TCT ATT GAA TGT ATT  
KpnI

GAA AAC ATT GAG GTT GGT AAT AAG GTC ATG GGT ...3'  
← Intein Reverse Sequencing Primer

**Figure B.2. a)** *E. coli* cloning and expression vector pTYB1 (1009bp) containing the *AlgeE7* gene, T7promoter, *Sec* VMA intein tag/chitin binding domain (CBD), ampicillin resistance (*bla*), M13 ori, origin of transcription, *rop* and *lacI* (regulator gene). Plasmid map is exported from Benchling. **b)** Multiple cloning sites (MCS) region, obtained from New England Biolabs Inc.

## Appendix C. AlgE7-lyase assay

### A230 plots measuring AlgE7-lyase activity

The AlgE7 lyase-activity assay was measured by absorbance at 230 nm every 5 minutes for 18 hours. Absorbance plots of two parallels for each AlgE7 mutant is presented in Figure C.1-C.8, where Figure C.1 show AlgE7 mutants classified as active lyase, Figure C.2 and C.3 show AlgE7 mutants classified as less active lyase and Figure C.4-C.8 show AlgE7 mutants classified as inactive lyase. All plots include the AlgE7 wild type as reference.

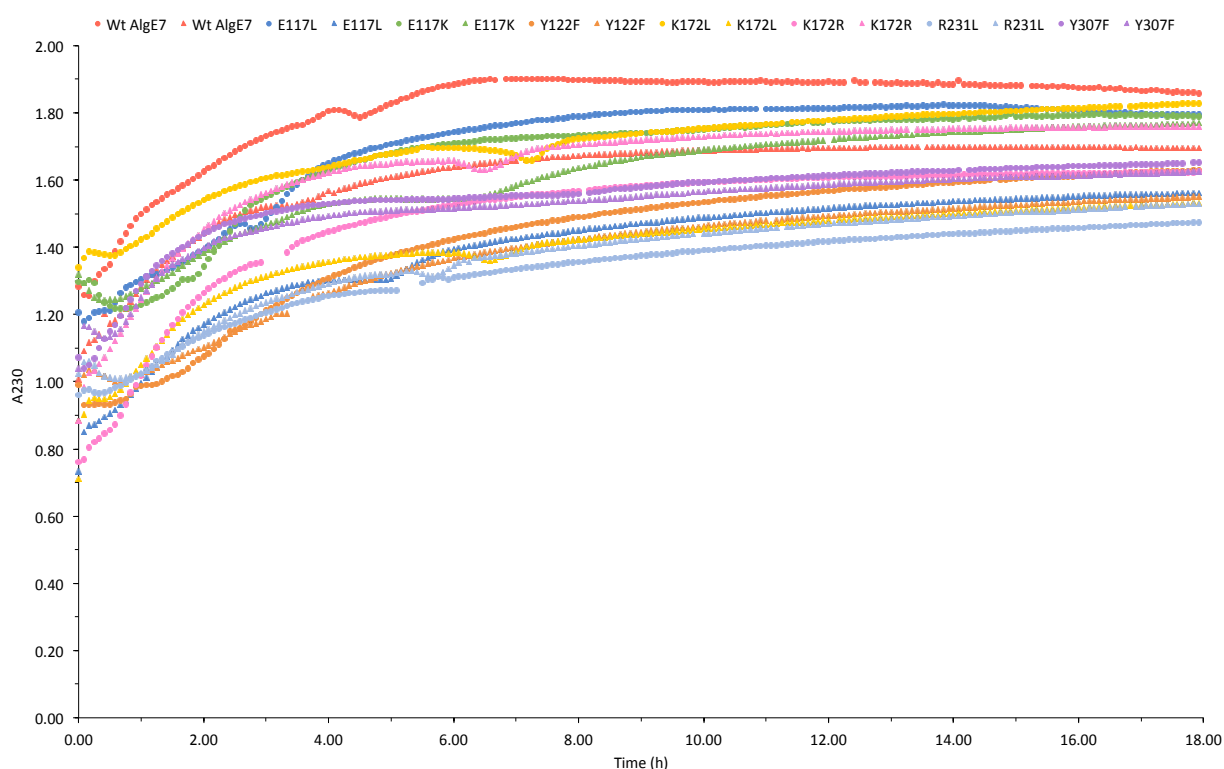


**Figure C.1.** AlgE7 lyase activity shown for AlgE7 wild type (red), and the AlgE7 mutants E117L (dark blue), E117K (green), Y122F (orange), K172L (yellow), K172R (pink), R231L (light blue) and Y307F (purple) measured by absorbance at 230 nm every 5 minutes for 18 hours. The lyase activity was observed using poly-mannuronan alginate substrate and B-PERII cell extract. Two parallels for each mutant are shown. Missing points is a result of failed measurements. Linear regression (not shown) of the first 4 hours for AlgE7 wild type and these mutants gives slope values  $> 0.07$ , which in this study is classified as active lyase.



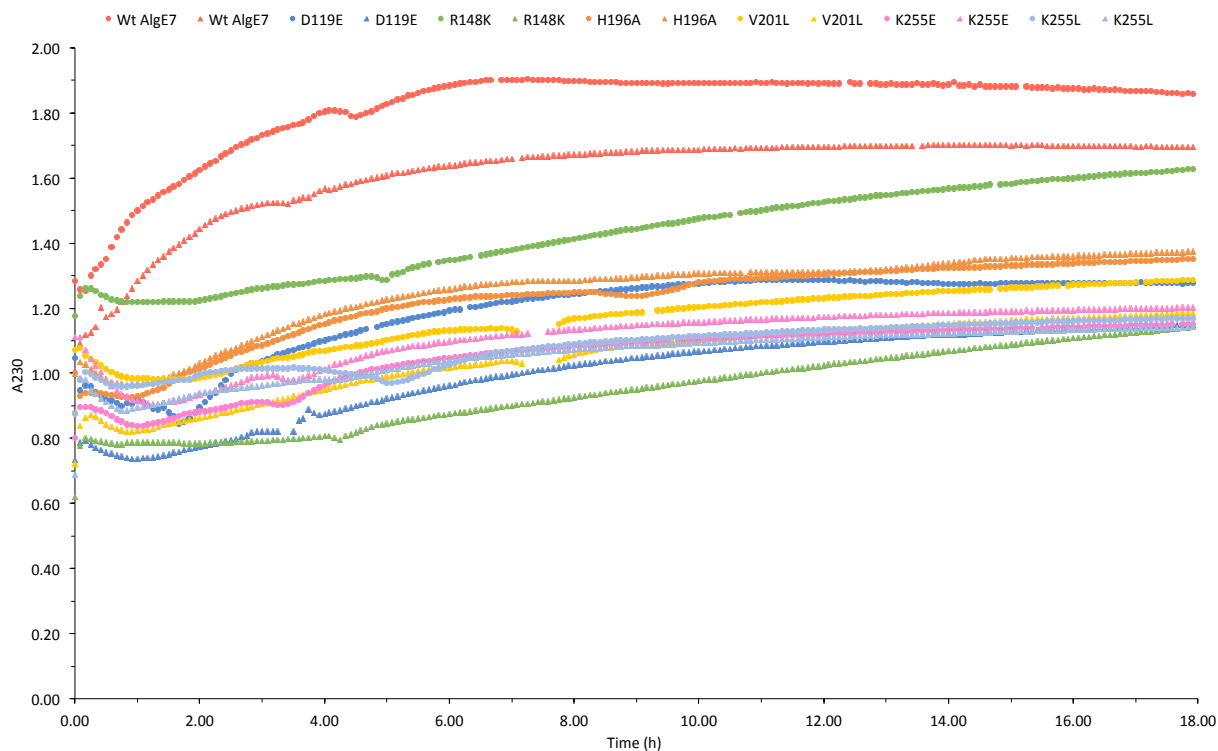


**Figure C.2.** AlgE7 lyase activity shown for AlgE7 wild type (red), and the AlgE7 mutants D119E (dark blue), R148K (green), H196A (orange), V201L (yellow), K255E (pink) and K255L (light blue), measured by absorbance at 230 nm every 5 minutes for 18 hours. The lyase activity was observed using poly-mannuronan alginate substrate and B-PERII cell extract. Two parallels for each mutant are shown. Missing points is a result of failed measurements. Linear regression (not shown) of the first 4 hours for these AlgE7 mutants gives slope values of 0.07-0.01, which in this study is classified as less active lyase.

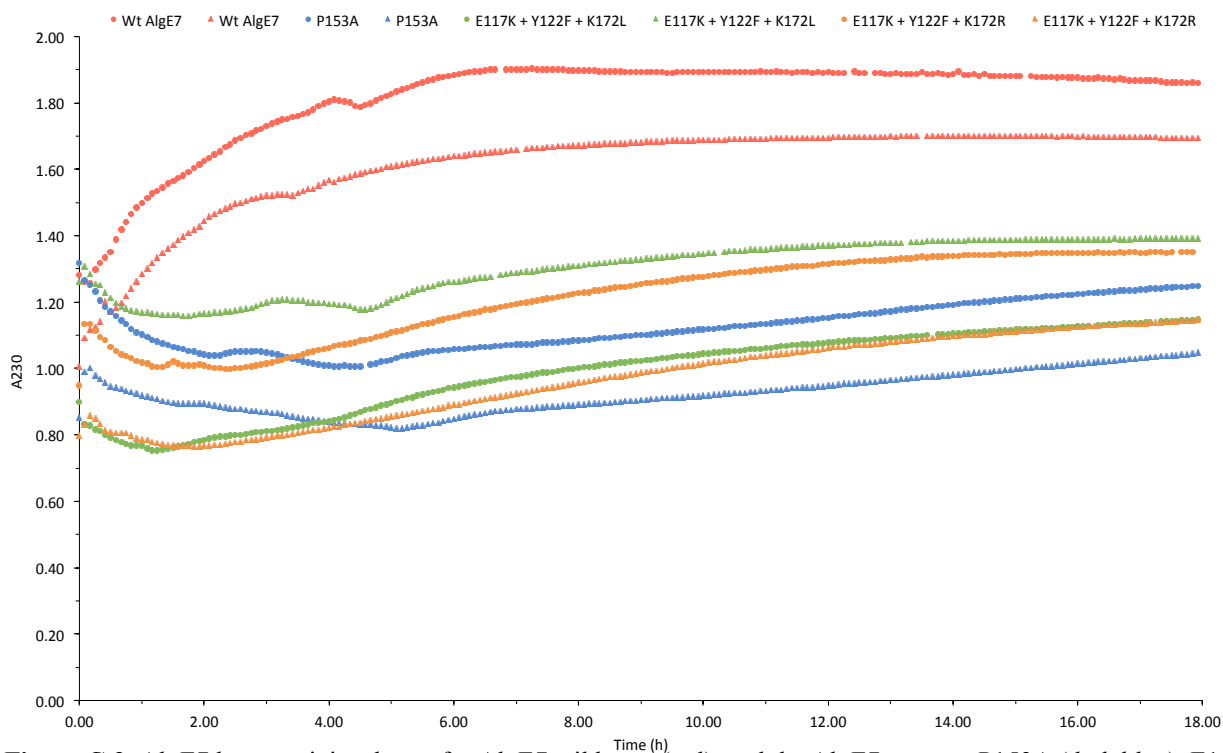


**Figure C.3.** AlgE7 lyase activity shown for AlgE7 wild type (red), and the AlgE7 mutants P153A (dark blue), E117K + Y122F + K172L (green) and E117K + Y122F + K172R (orange), measured by absorbance at 230 nm every 5 minutes for 18 hours. The lyase activity was observed using poly-mannuronan alginate substrate and B-Per II enzyme extract. Two parallels for each mutant are shown. Missing points is a result of failed measurements. Linear regression (not shown) of the first 4 hours for mutant P153A gives a slope value  $< 0.01$  (inactive lyase), while the A230 measurements show a slow increase beyond 4-5 hours that indicates low lyase activity. For the two other mutants the slope values classifies the parallels in different groups (inactive/less active), indicating very low lyase activity.

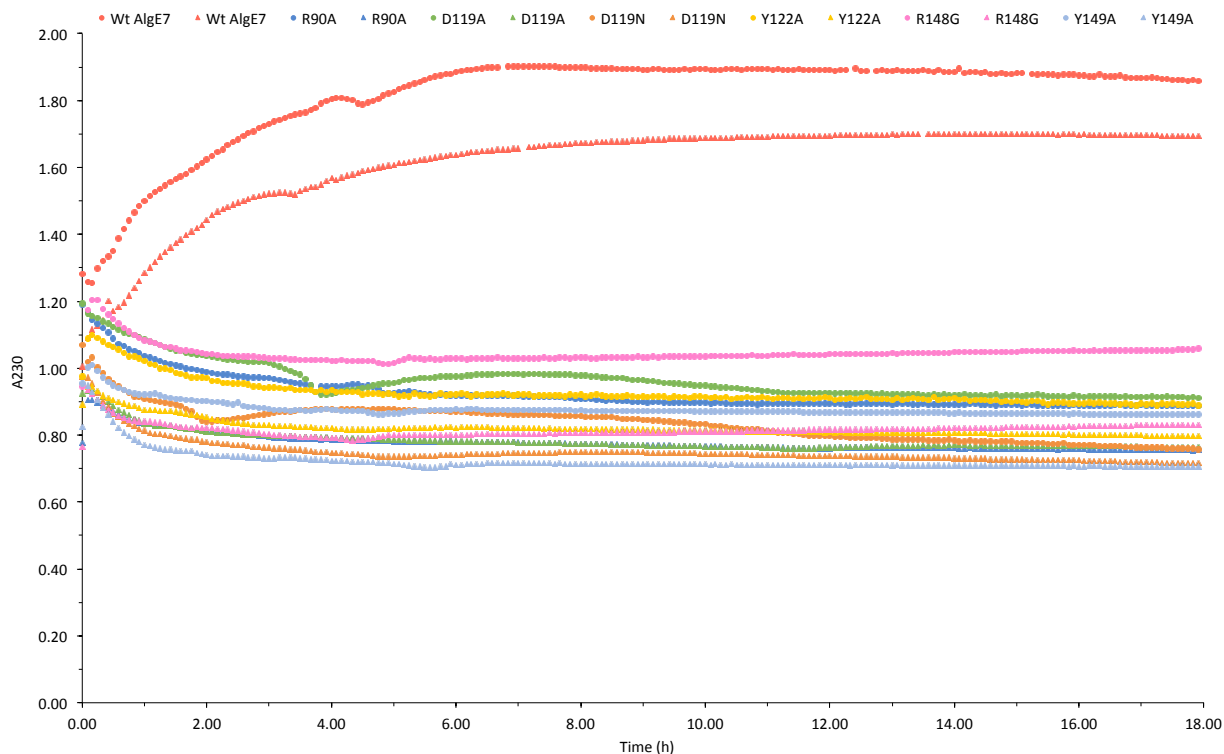


**Figure C.4.** AlgE7 lyase activity shown for AlgE7 wild type (red), and the AlgE7 mutants R90A (dark blue), D119A (green), D119N (orange), Y122A (yellow), R148G (pink) and Y149A (light blue), measured by absorbance at 230 nm every 5 minutes for 18 hours. The lyase activity was observed using poly-mannuronan alginate substrate and B-Per II enzyme extract. Two parallels for each mutant are shown. Missing points is a result of failed measurements. Linear regression (not shown) of the first 4 hours for these AlgE7 mutants gives slope values  $< 0.01$ , which in this study is classified as inactive lyase.

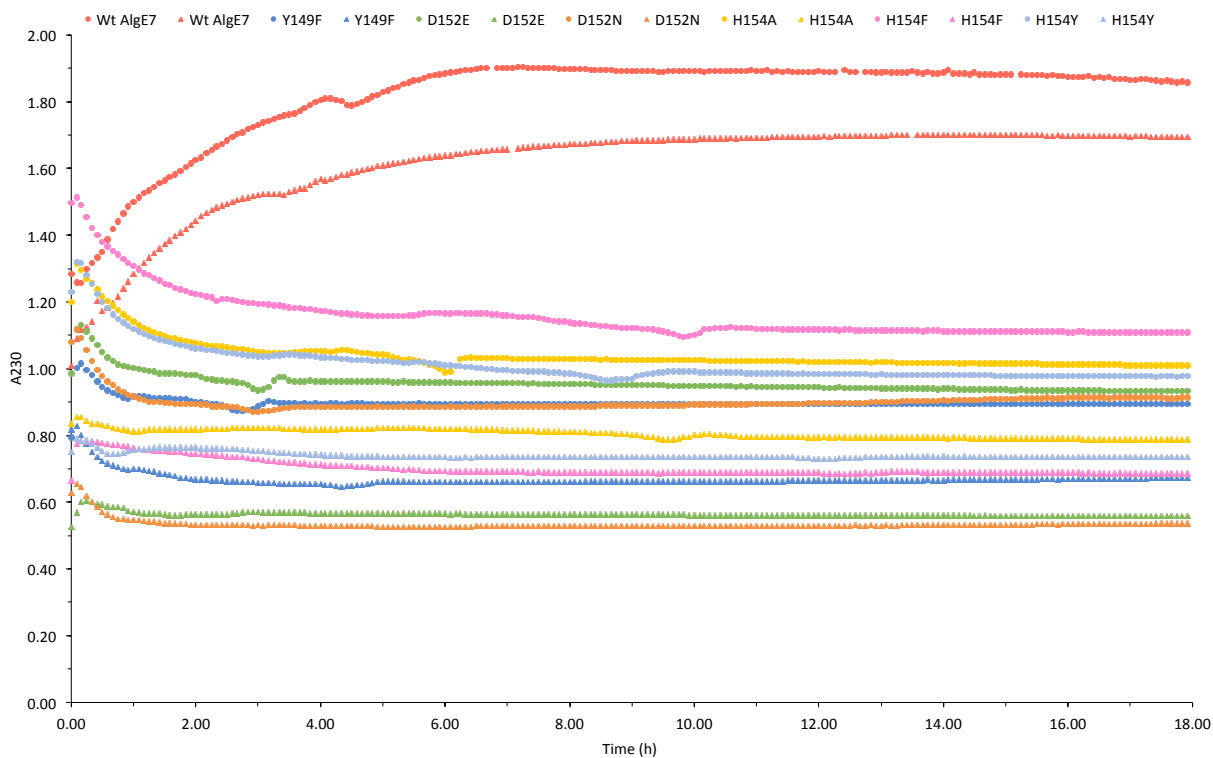


**Figure C.5.** AlgE7 lyase activity shown for AlgE7 wild type (red), and the AlgE7 mutants Y149F (dark blue), D152E (green), D152N (orange), H154A (yellow), H154F (pink) and H154Y (light blue), measured by absorbance at 230 nm every 5 minutes for 18 hours. The lyase activity was observed using poly-mannuronan alginate substrate and B-Per II enzyme extract. Two parallels for each mutant are shown. Missing points is a result of failed measurements. Linear regression (not shown) of the first 4 hours for these AlgE7 mutants gives slope values  $< 0.01$ , which in this study is classified as inactive lyase.

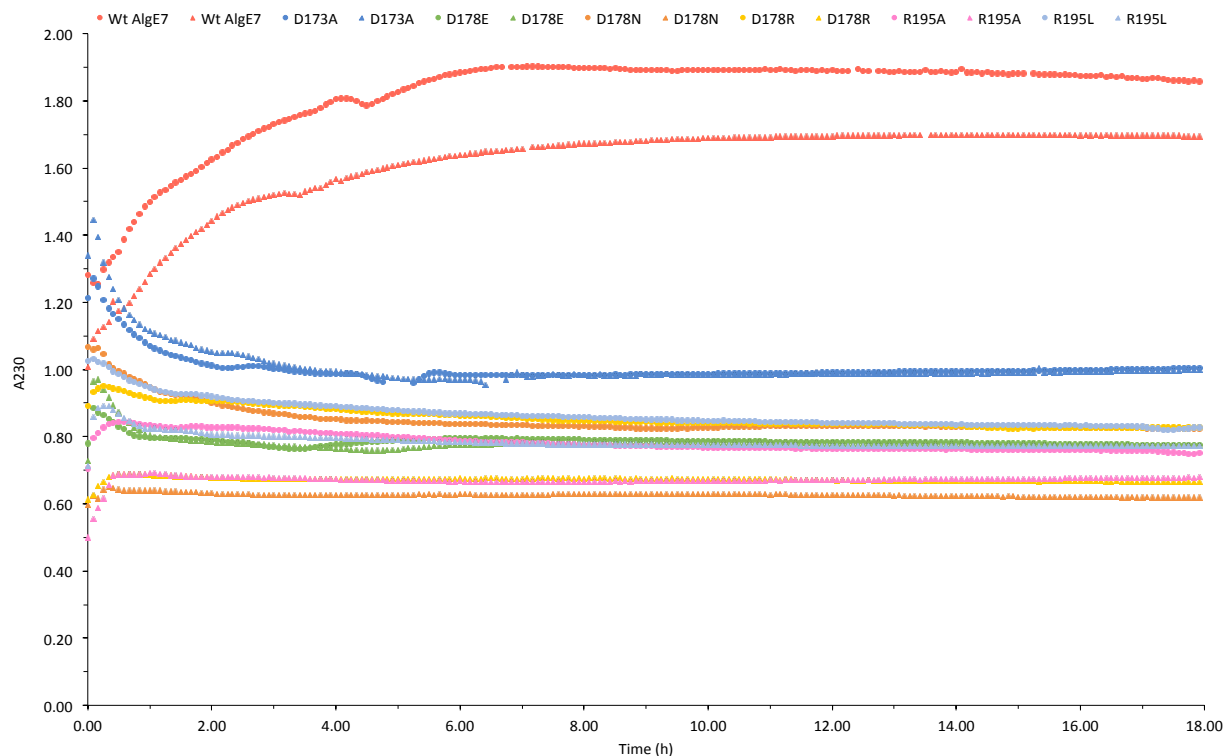


**Figure C.6.** AlgE7 lyase activity shown for AlgE7 wild type (red), and the AlgE7 mutants D173A (dark blue), D178E (green), D178N (orange), D178R (yellow), R195A (pink) and R195L (light blue), measured by absorbance at 230 nm every 5 minutes for 18 hours. The lyase activity was observed using poly-mannuronan alginate substrate and B-Per II enzyme extract. Two parallels for each mutant are shown. Missing points is a result of failed measurements. Linear regression (not shown) of the first 4 hours for these AlgE7 mutants gives slope values  $< 0.01$ , which in this study is classified as inactive lyase.

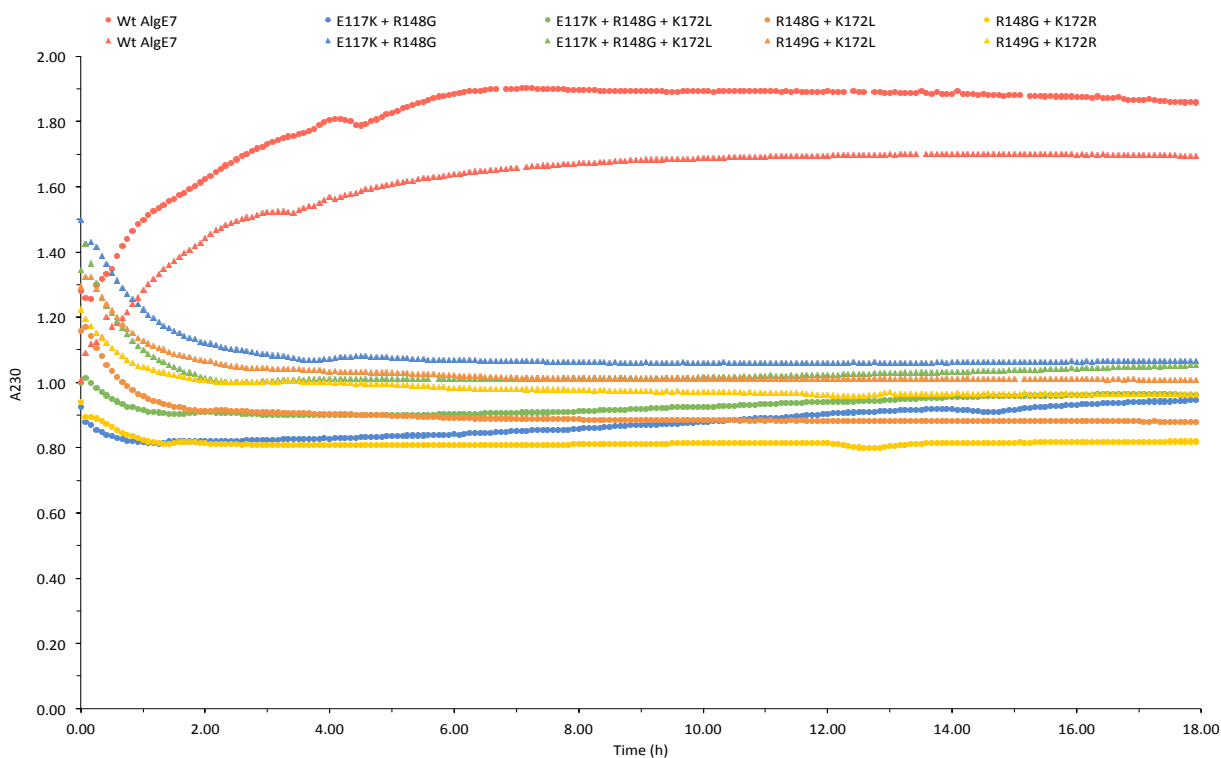


**Figure C.7.** AlgE7 lyase activity shown for AlgE7 wild type (red), and the AlgE7 mutants E117K+R148G (dark blue), E117K + R148G + K172L (green), R148G + K172L (orange) and R148G + K172R (yellow), measured by absorbance at 230 nm every 5 minutes for 18 hours. The lyase activity was observed using poly-mannuronan alginate substrate and B-Per II enzyme extract. Two parallels for each mutant are shown. Missing points is a result of failed measurements. Linear regression (not shown) of the first 4 hours for these AlgE7 mutants gives slope values  $< 0.01$ , which in this study is classified as inactive lyase.

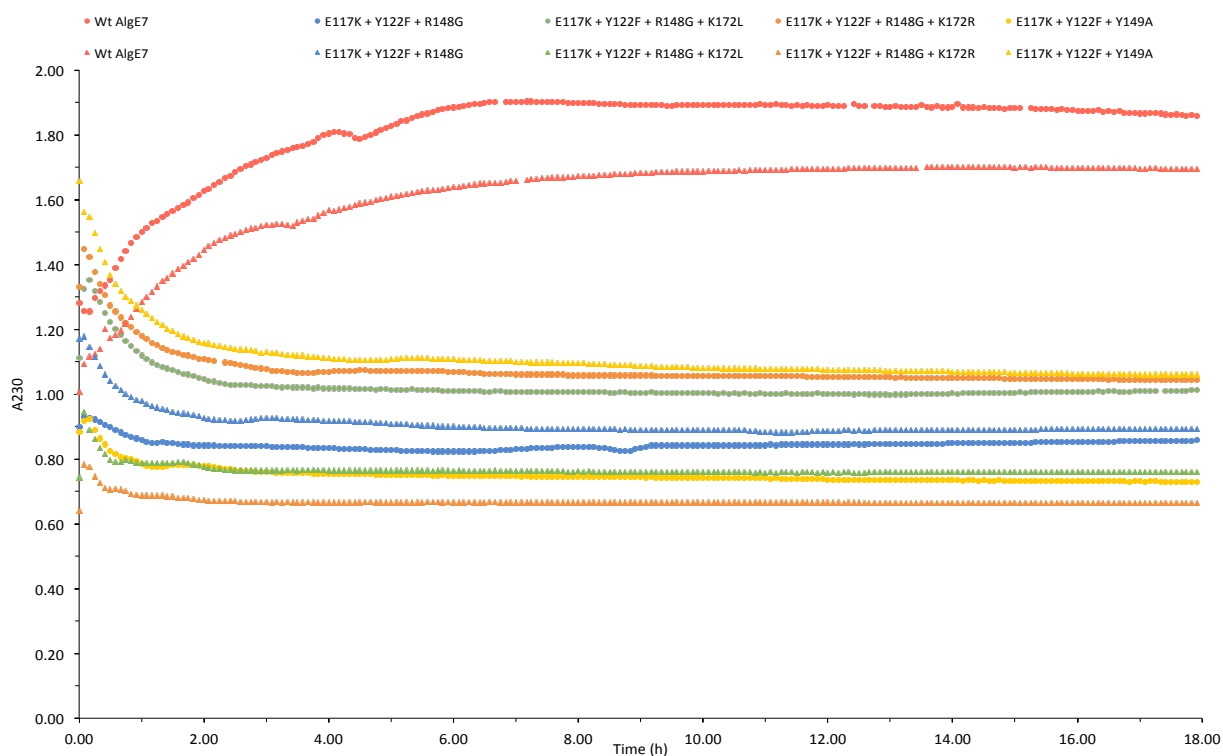


**Figure C.8.** AlgE7 lyase activity shown for AlgE7 wild type (red), and the AlgE7 mutants E117K + Y122F + R148G (dark blue), E117K + Y122F + R148G + K172L (green), E117K + Y122F + R148G + K172R (orange) and E117K + Y122F + Y149A (yellow), measured by absorbance at 230 nm every 5 minutes for 18 hours. The lyase activity was observed using poly-mannuronan alginate substrate and B-Per II enzyme extract. Two parallels for each mutant are shown. Missing points is a result of failed measurements. Linear regression (not shown) of the first 4 hours for these AlgE7 mutants gives slope values  $< 0.01$ , which in this study is classified as inactive lyase.

## Appendix D. Zero-order enzyme kinetics

### Zero-order enzyme kinetics used for analysis of the AlgE7 lyase-activity assay

Reactions catalysed by an enzyme starts with the attachment of the substrate (S) to the active site on the enzyme (E), resulting in formation of an enzyme-substrate complex (ES). In the second step the chemical reaction the product (P) is released from the enzyme, making the enzyme accessible for new substrates (Equation D.1) (222).



If amount of substrate is significantly larger in relation to the amount of enzyme, the rate of the reaction is independent of the substrate concentration over a wide range of concentrations. In this case, the reaction will follow zero-order kinetics (Equation D.2), where *rate* is the reaction rate for consumption of substrate, *k* is the reaction rate coefficient and *t* is time. Thus, the reaction rate of product formation is given by equation D.3 (249,250).

$$\text{rate} = -\frac{d[S]}{dt} = k \quad (\text{D.2})$$

$$\text{rate} = \frac{d[P]}{dt} = k \quad (\text{D.3})$$

Rearrangement and integration of equation D.2 and D.3 give rise to equation D.4 and D.5 respectively, representing the linear relationship of substrate consumption vs. time and product formation vs. time (249,250).

$$[S] = -kt \quad (\text{D.4})$$

$$[P] = kt \quad (\text{D.5})$$

In this study, the product formation is measured as an increase in A230, where the constant rate (*k*) is used as a measure of the initial lyase activity (see section 3.4.1).

## Appendix E. <sup>1</sup>H-NMR spectra

### <sup>1</sup>H-NMR spectra using enzyme extract

The <sup>1</sup>H-NMR spectra for poly-M samples after epimerization and degradation by the AlgE7 wild type and 25 of the AlgE7 mutants are presented in Figure E.1-E5. The figures shows the <sup>1</sup>H-NMR spectra recorded for one of the two parallels analysed. The signal labelled “unknown” is shown in all NMR-spectra and refers to non-alginate protons that have not been identified. The <sup>1</sup>H-NMR spectra were recorded at 83 °C and the samples contained 1 mg/mL alginate dissolved in D<sub>2</sub>O.

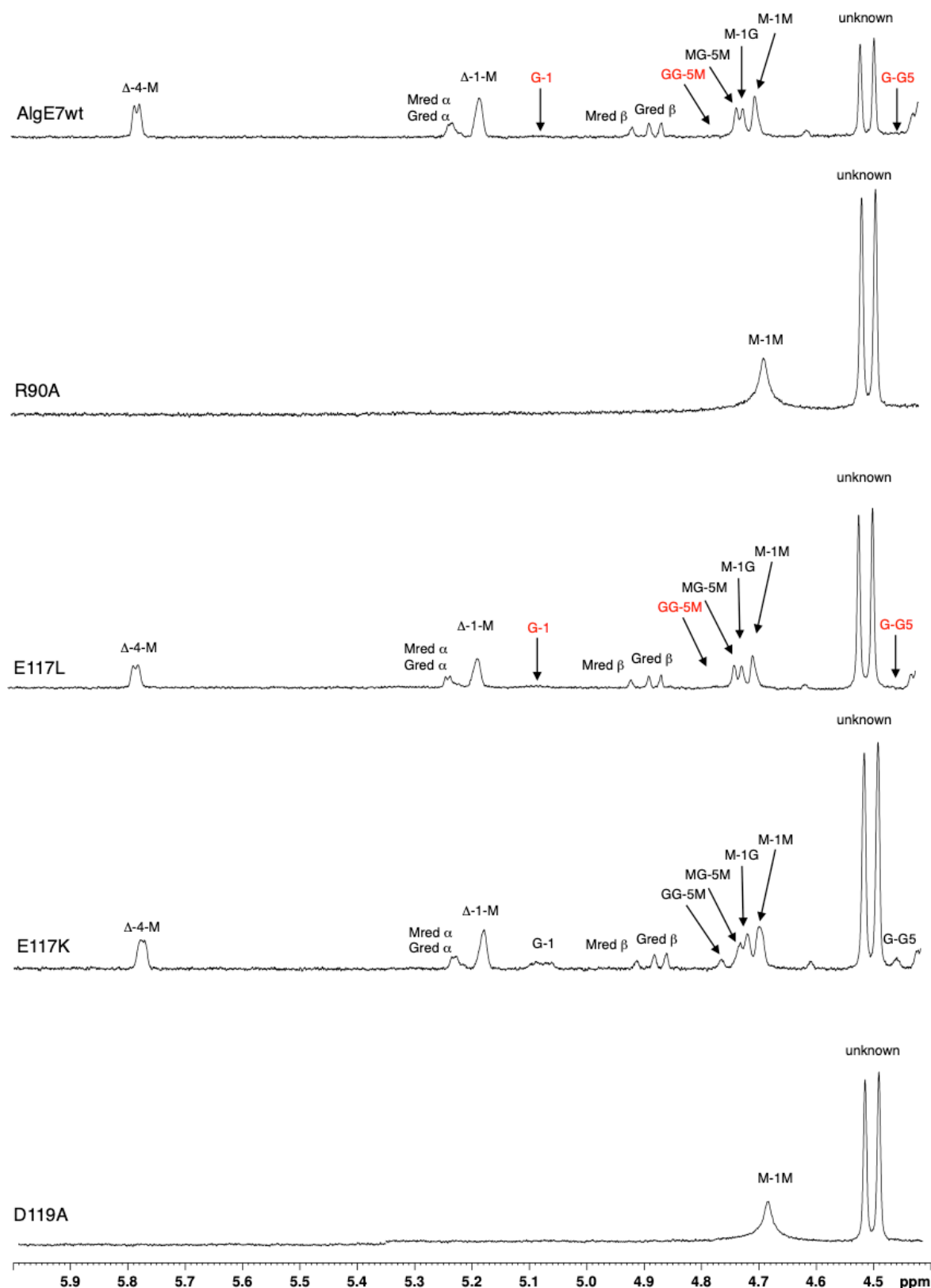


**Figure E.1.** <sup>1</sup>H-NMR spectra (400 MHz) showing the anomeric region of poly-M after epimerization and degradation by AlgE7 wild type and the AlgE7 point mutant number 2-5 (R90A, E117L, E117K and D119A) for 24 hours. The spectra were recorded at 83 °C and samples contained 1 mg/mL alginate dissolved in D<sub>2</sub>O. Missing G-1, GG-5M and G-G5 signals in the spectra recorded for AlgE7 wild type and mutant E117L is labelled in red.

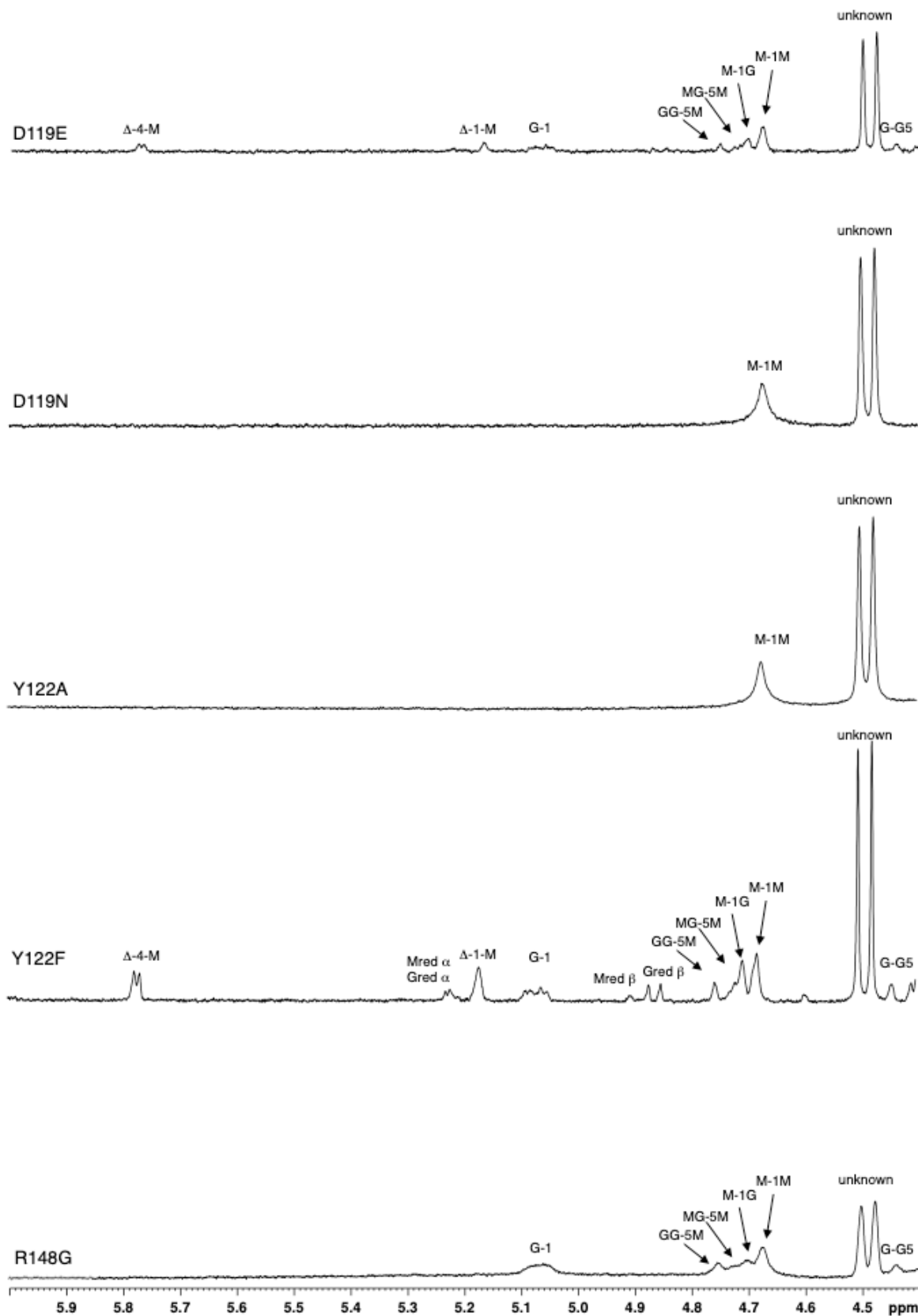


**Figure E.2.** <sup>1</sup>H-NMR spectra (400 MHz) showing the anomeric region of poly-M after epimerization and degradation by the AlgE7 point mutant number 6-10 (D119E, D119N, Y122A, Y122F and R148G) for 24 hours. The spectra were recorded at 83 °C and samples contained 1 mg/mL alginate dissolved in D<sub>2</sub>O.



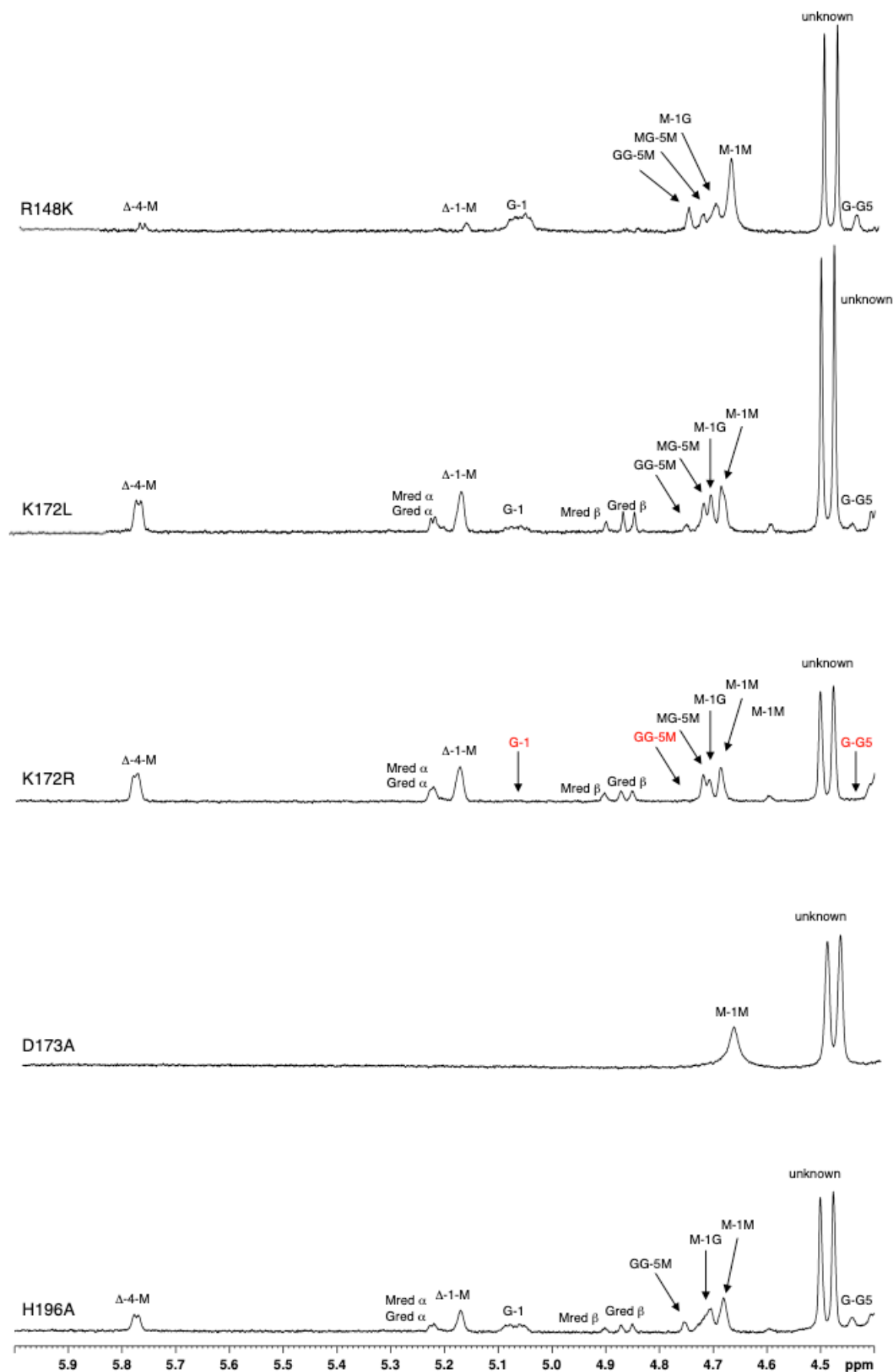


**Figure E.3.** <sup>1</sup>H-NMR spectra (400 MHz) showing the anomeric region of poly-M after epimerization and degradation by the AlgE7 point mutant number 11, 20-22 and 28 (R148K, K172L, K172R, D173A and H196A) for 24 hours. The spectra were recorded at 83 °C and samples contained 1 mg/mL alginate dissolved in D<sub>2</sub>O. Missing G-1, GG-5M and G-G5 signal in the spectrum recorded for mutant K172R is labelled in red.

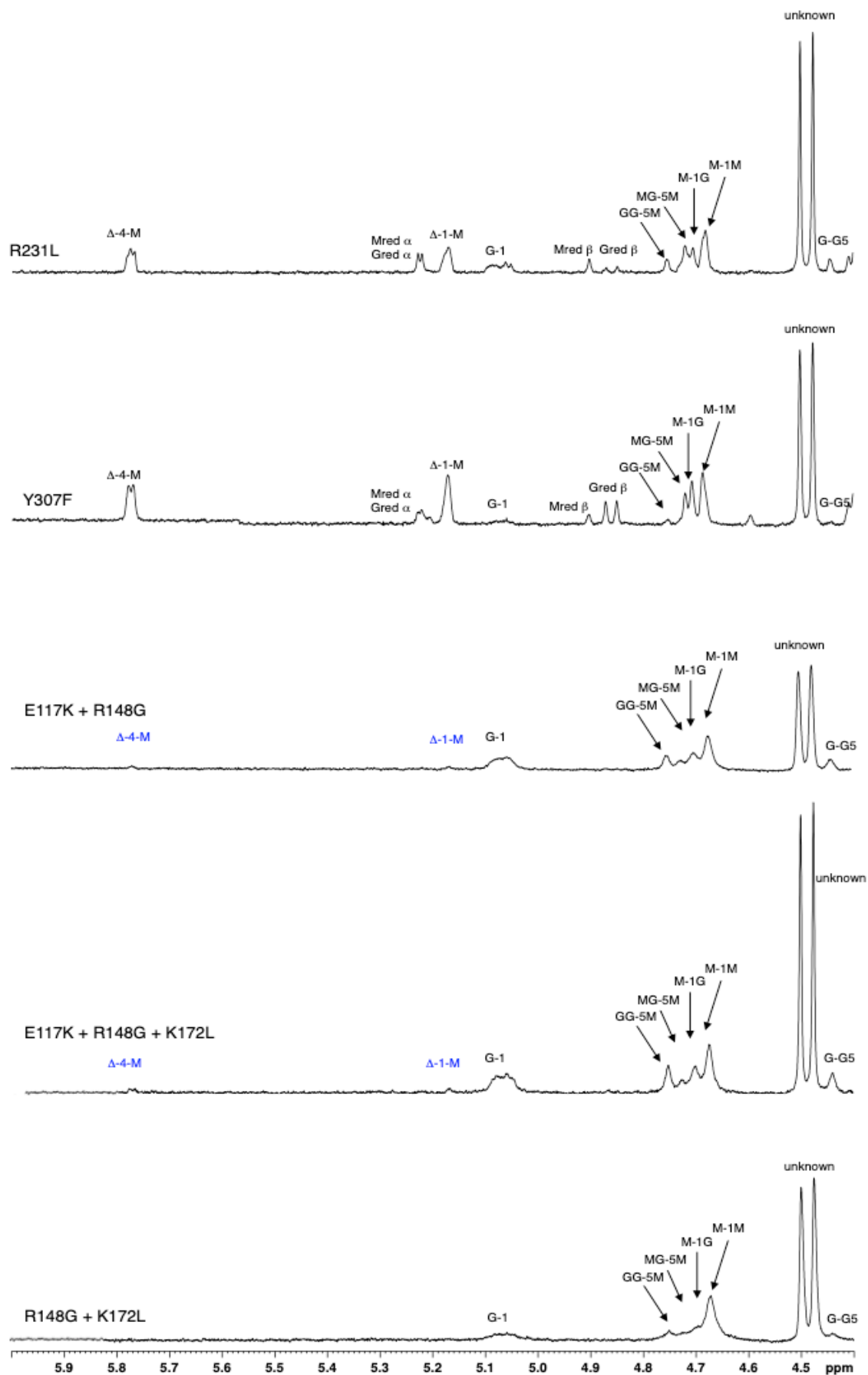


**Figure E.4.**  $^1\text{H-NMR}$  spectra (400 MHz) showing the anomeric region of poly-M after epimerization and degradation by the AlgE7 point mutant number 30 and 33 (R231L and Y307F), and the combination mutants number 34-36 (E117K+R148G, E117K+R148G+K172L and R148G+K172L) for 24 hours. The spectra were recorded at 83 °C and samples contained 1 mg/mL alginate dissolved in  $\text{D}_2\text{O}$ . Very weak lyase signals ( $\Delta$ -4-M,  $\Delta$ -1-M) observed in the spectra for mutant 34 and 35 is labelled in blue.

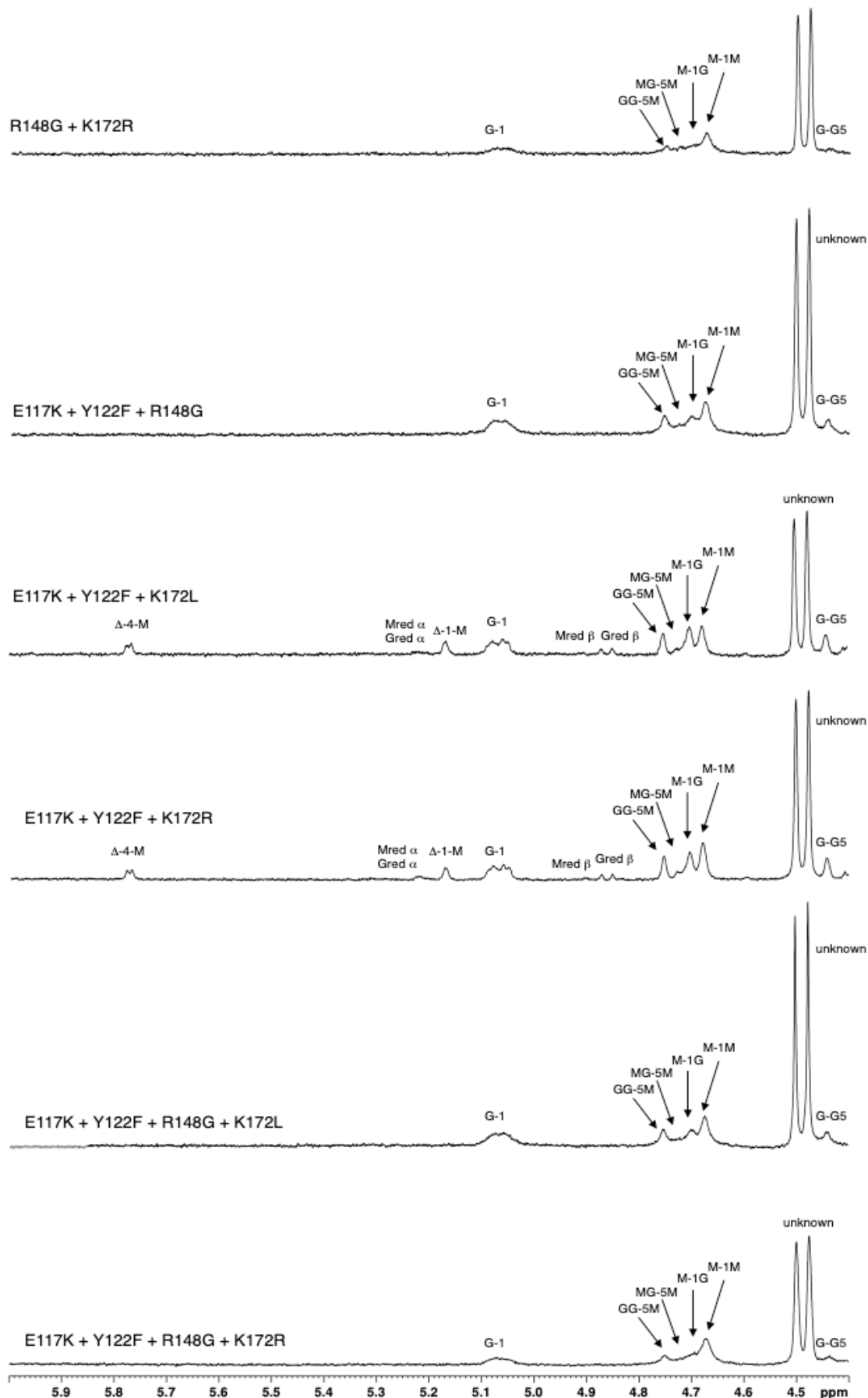


**Figure E.5.**  $^1\text{H-NMR}$  spectra (400 MHz) showing the anomeric region of poly-M after epimerization and degradation by the AlgE7 the combination mutant number 37-42 (R148G+K172R, E117K+Y122F+R148G, E117K+Y122F+K172L, E117K+Y122F+K172R, E117K+Y122F+R148G+K172L, E117K+Y122F+R148G+K172R) for 24 hours. The spectra were recorded at 83 °C and samples contained 1 mg/mL alginate dissolved in  $\text{D}_2\text{O}$ .

## Appendix F. $^1\text{H-NMR}$ molar fractions

### Sequential parameters calculated from $^1\text{H-NMR}$ spectra

By integrating the signals in the  $^1\text{H-NMR}$  spectra (Figure E.1-E.5), the sequential parameters of epimerized and degraded poly-M samples were calculated according to the equations in section 2.2.18 (Table F.1). These parameters was also calculated for the  $^1\text{H-NMR}$  spectra recorded after using purified enzyme (AlgE7 wild type or mutant R148G) for epimerization and degradation of poly-M and poly-MG substrate (Table F.2)

**Table F.1.** Monomeric composition of epimerized and degraded poly-M substrate, using B-Per II enzyme extract containing the AlgE7 protein (unknown concentration). <sup>1</sup>H-NMR analysis was done for the AlgE7 wild type and 25 of the AlgE7 mutants. The sequence parameter DP<sub>n</sub> is also shown in the table. Two parallels (P1 and P2) are shown for each AlgE7 mutant.

No.	AlgE7 mutant		F <sub>G</sub>	F <sub>M</sub>	F <sub>Δ</sub>	F <sub>Gred</sub>	F <sub>Mred</sub>	F <sub>Gtotal</sub>	F <sub>Mtotal</sub>	DP <sub>n</sub>
1	AlgE7wt	P1	0.11	0.36	0.26	0.12	0.16	0.23	0.51	3.68
		P2	0.10	0.37	0.27	0.12	0.14	0.22	0.51	3.79
2	R90A	P1	0.00	1.00	0.00	0.00	0.00	0.00	1.00	~370
		P2	0.00	1.00	0.00	0.00	0.00	0.00	1.00	~370
3	E117L	P1	0.10	0.36	0.28	0.13	0.13	0.23	0.49	3.83
		P2	0.16	0.42	0.22	0.10	0.10	0.27	0.52	4.93
4	E117K	P1	0.15	0.43	0.22	0.11	0.08	0.26	0.52	5.06
		P2	0.20	0.43	0.17	0.11	0.10	0.31	0.52	4.97
5	D119A	P1	0.00	1.00	0.00	0.00	0.00	0.00	1.00	~370
		P2	0.00	1.00	0.00	0.00	0.00	0.00	1.00	~370
6	D119E	P1	0.26	0.50	0.11	0.06	0.08	0.31	0.58	7.47
		P2	0.23	0.62	0.07	0.04	0.03	0.28	0.66	13.31
7	D119N	P1	0.00	1.00	0.00	0.00	0.00	0.00	1.00	~370
		P2	0.00	1.00	0.00	0.00	0.00	0.00	1.00	~370
8	Y122A	P1	0.00	1.00	0.00	0.00	0.00	0.00	1.00	~370
		P2	0.00	1.00	0.00	0.00	0.00	0.00	1.00	~370
9	Y122F	P1	0.21	0.42	0.18	0.12	0.08	0.33	0.49	5.09
		P2	0.21	0.44	0.19	0.11	0.06	0.31	0.50	6.03
10	R148G	P1	0.36	0.64	0.00	0.00	0.00	0.36	0.64	~370
		P2	0.27	0.73	0.00	0.00	0.00	0.27	0.73	~370
11	R148K	P1	0.30	0.61	0.04	0.02	0.03	0.32	0.63	21.59
		P2	0.28	0.65	0.04	0.02	0.01	0.30	0.66	28.32
20	K172L	P1	0.14	0.41	0.23	0.11	0.11	0.26	0.51	4.55
		P2	0.16	0.41	0.23	0.11	0.09	0.27	0.50	5.02
21	K172R	P1	0.08	0.35	0.27	0.13	0.17	0.21	0.52	3.29
		P2	0.07	0.35	0.30	0.13	0.15	0.20	0.50	3.65
22	D173A	P1	0.00	1.00	0.00	0.00	0.00	0.00	1.00	~370
		P2	0.00	1.00	0.00	0.00	0.00	0.00	1.00	~370
28	H196A	P1	0.23	0.43	0.17	0.09	0.09	0.31	0.52	5.65
		P2	0.21	0.46	0.17	0.08	0.08	0.29	0.53	6.24
30	R231L	P1	0.19	0.44	0.19	0.04	0.14	0.24	0.58	5.45
		P2	0.21	0.43	0.18	0.05	0.13	0.26	0.56	5.61
33	Y307F	P1	0.11	0.38	0.26	0.15	0.11	0.26	0.48	3.90
		P2	0.11	0.38	0.25	0.16	0.11	0.26	0.49	3.78
34	E117K + R148G	P1	0.34	0.60	0.03	0.01	0.01	0.35	0.62	42.41
		P2	0.32	0.66	0.00	0.00	0.01	0.32	0.67	77.47
35	E117K + R148G + K172L	P1	0.35	0.58	0.02	0.02	0.03	0.37	0.60	20.89
		P2	0.34	0.60	0.02	0.02	0.03	0.36	0.62	21.25
36	R148G + K172L	P1	0.35	0.65	0.00	0.00	0.00	0.35	0.65	~370
		P2	0.19	0.81	0.00	0.00	0.00	0.19	0.81	~370
37	R148G + K172R	P1	0.33	0.67	0.00	0.00	0.00	0.33	0.67	~370
		P2	0.31	0.69	0.00	0.00	0.00	0.31	0.69	~370
38	E117K + Y122F + R148G	P1	0.39	0.61	0.00	0.00	0.00	0.39	0.61	~370
		P2	0.37	0.63	0.00	0.00	0.00	0.37	0.63	~370
39	E117K + Y122F + K172L	P1	0.35	0.47	0.09	0.06	0.03	0.41	0.50	11.58
		P2	0.33	0.44	0.10	0.08	0.06	0.41	0.49	7.41
40	E117K + Y122F + K172R	P1	0.47	0.34	0.10	0.05	0.03	0.52	0.38	11.55
		P2	0.33	0.53	0.13	0.05	0.03	0.38	0.56	12.40
41	E117K + Y122F + R148G + K172L	P1	0.41	0.59	0.00	0.00	0.00	0.41	0.59	~370
		P2	0.34	0.66	0.00	0.00	0.00	0.34	0.66	~370
42	E117K + Y122F + R148G + K172R	P1	0.30	0.70	0.00	0.00	0.00	0.30	0.70	~370
		P2	0.29	0.71	0.00	0.00	0.00	0.29	0.71	~370
Poly-M alginate			0.00	1.00	0.00	0.00	0.00	0.00	1.00	~370

**Table F.2.** Monomeric composition of epimerized and degraded of poly-M and poly-MG substrate, by AlgE7 wild type and the mutant R148G. Enzyme to substrate ratio: 1:300. The sequence parameter  $DP_n$  is also shown in the table. n.d.=not determined

Enzyme and substrate	Time (h)	$F_G$	$F_M$	$F_{GG}$	$F_{GM} = F_{MG}$	$F_{MM}$	$F_{\Delta}$	$F_{Mred}$	$F_{Gred}$	$F_{Gintern}$	$F_{Gtot}$	$F_{Mtot}$	$DP_n$
AlgE7wt Poly-M alginate	0	0.00	1.00	0.00	0.00	1.00	0.00	0.00	0.00	0.00	0.00	1.00	~370
	6	0.17	0.81	0.02	0.15	0.66	0.02	0.00	0.00	0.11	0.17	0.81	118.37
	12	0.20	0.70	0.04	0.16	0.54	0.04	0.04	0.02	0.19	0.22	0.74	17.78
	24	0.22	0.56	0.04	0.18	0.38	0.11	0.07	0.05	0.20	0.27	0.62	8.66
	48	0.21	0.50	0.04	0.17	0.33	0.15	0.07	0.07	0.17	0.28	0.57	7.05
	60	0.17	0.43	0.01	0.17	0.27	0.21	0.09	0.10	0.10	0.27	0.53	5.28
R148G Poly-M alginate	0	0.00	1.00	0.00	0.00	1.00	0.00	0.00	0.00	0.00	0.00	1.00	~370
	6	0.13	0.87	0.00	0.17	0.70	0.00	0.00	0.00	0.07	0.13	0.87	~370
	12	0.17	0.83	0.00	0.19	0.64	0.00	0.00	0.00	0.13	0.17	0.83	~370
	24	0.19	0.81	0.01	0.18	0.63	0.00	0.00	0.00	0.17	0.19	0.81	~370
	48	0.26	0.74	0.06	0.20	0.54	0.00	0.00	0.00	0.25	0.26	0.74	~370
	60	0.26	0.74	0.06	0.20	0.55	0.00	0.00	0.00	0.25	0.26	0.74	~370
AlgE7wt MG-alginate	0	0.46	0.54	0.05	0.41	0.13	0.00	0.00	0.00	0.52	0.46	0.54	n.d
	6	0.48	0.52	0.09	0.39	0.13	0.00	0.00	0.00	0.53	0.48	0.53	n.d
	12	0.47	0.46	0.11	0.35	0.11	0.02	0.03	0.02	0.52	0.49	0.50	19.36
	24	0.48	0.45	0.13	0.35	0.10	0.02	0.03	0.02	0.52	0.50	0.48	18.45
	48	0.48	0.42	0.15	0.33	0.09	0.03	0.05	0.02	0.50	0.51	0.47	13.85
	60	0.48	0.42	0.16	0.32	0.11	0.03	0.05	0.02	0.52	0.50	0.47	13.40
R148G MG-alginate	0	0.46	0.54	0.05	0.41	0.13	0.00	0.00	0.00	0.52	0.46	0.54	n.d
	6	0.46	0.54	0.06	0.39	0.15	0.00	0.00	0.00	0.52	0.46	0.54	n.d
	12	0.47	0.53	0.07	0.36	0.14	0.00	0.00	0.00	0.54	0.47	0.53	n.d
	24	0.45	0.55	0.09	0.37	0.18	0.00	0.00	0.00	0.54	0.45	0.55	n.d
	48	0.47	0.53	0.06	0.40	0.13	0.00	0.00	0.00	0.53	0.47	0.53	n.d
	60	0.48	0.52	0.07	0.40	0.12	0.00	0.00	0.00	0.55	0.48	0.52	n.d